# Contributions des nanotechnologies à l'étude et à l'assemblage du Nano-Moteur flagellaire des bacteries

Jerôme Chalmeau


# THÈSE

**En vue de l'obtention du**

## DOCTORAT DE L'UNIVERSITÉ DE TOULOUSE

**Délivré par** *INSA de Toulouse*
**Discipline ou spécialité :** *Nanophysique*

---

**Présentée et soutenue par** *Chalmeau Jerome*
**Le** *24 juin 2009*

**Titre :** *Contribution from Nanotechnologies to the study and assembly of the flagellar nano-motor of bacteria*

*Contributions des nanotechnologies à l'étude et à l'assemblage du Nano-Moteur flagellaire des bacteries*

---

**JURY**
*Pr Howard Berg*
*Dr Simon Scheuring*
*Dr Christian Le Grimellec*
*Pr Jean Marie Francois*
*Dr Vincent Noireaux*
*Pr Christophe Vieu*

---

**Ecole doctorale :** *Sciences de la matiere*
**Unité de recherche :** *Laboratoire d'Analyse et d'Architecture des Systemes (LAAS)*
**Directeur(s) de Thèse :** *Christophe Vieu*
**Rapporteurs :** *Pr Howard Berg*
*Dr Simon Scheuring*

.....Block by block, Brick by Brick…….....

*Barack Obama, November the 4th 2008, Chicago, USA*

Une thèse est une aventure, scientifique d'une part et humaine dans sa globalité. Tout d'abord, une thèse c'est avant tout cela une question, un mystère de la nature à résoudre, une mécanique à comprendre, un théorème à démontrer, des expériences à inventer. C'est aussi des discussions nombreuses et variées, avec en premier lieu le directeur de thèse, qui parfois dirige, mais qui aussi laisse pleinement le talent et l'imagination voguer en dehors des sentiers balisés. Mais une thèse c'est aussi la fin d'une formation, qui peut avoir commencé longtemps avant la thèse, depuis le bac, ou même avant si on a la conviction et la passion de ce merveilleux métier qui est chercheur. Aussi loin que je me rappelle, je voulais être archéologue tout d'abord, merci Indiana Jones, mais je n'étais pas assez doué en langue donc cela ne pourrait être qu'une occupation, qui aujourd'hui encore guide mes choix de lecture et mes centres d'intérêts. Donc naturellement c'est la recherche scientifique qui m'a attiré, mais plus la recherche de temple Inca perdu dans la Jungle, mais la recherche dans la compréhension du monde dans lequel nous vivons, avec cette insatiable soif de réponses. Je veux ici remercier ma famille pour cela : ma mère pour ne pas avoir froid aux yeux, et en qui je vois l'adage « Il n'y a qu'une seule chose dont il faut avoir peur, c'est la peur elle-même », et qui m'a transmis son audace dans la vie de tous les jours ; mon père, pour avoir su me transmettre l'envie de comprendre, de poser de questions, et je veux le remercier pour ces heures passées à essuyer la vaisselle et à discuter de tout et de rien, ce qui pouvait paraitre insignifiant voir même ennuyeux à l'époque et qui aujourd'hui me paraissent comme des moments clés ; ma sœur et mon frère pour m'ont permis et me permettrent de rester, ou tout au moins, de garder les pieds sur Terre, et de tout l'amour qu'ils m'ont donné durant toutes ces années malgré des moments durs qui resteront comme nécessaire pour me permettre de devenir ce que je suis aujourd'hui. Le chemin est ouvert désormais, et vous allez lire la synthèse de 4 ans et demi de travail, multidisciplinaire mélangeant a l'échelle nanométrique la biologie, la chimie et la physique sur une formidable invention de la Nature. Comment suis-je tomber sur ce sujet ? Le hasard, comme l'évolution d'ailleurs. Une rencontre, qui succède a une autre qui est devenue ma femme michele ; un livre de biologie qui s'ouvre et un schéma du moteur, et une phrase « essayons de faire quelques choses sur ca », c'était il y a presque 6 ans, et de l'autre cote de l'océan. 6 ans après, voici le résultat dans vos mains, l'aboutissement de longues années de travail. C'est aussi la fin d'un chapitre, celui de ma vie étudiante, et le début d'un autre, celui de chercheur. Maintenant, je vais faire ce que je me suis toujours promis de faire, une recette pour une these. Ceux qui ont une culture de la Bande dessinée reconnaitront l'allusion.

Pour faire cette these, il a fallut :

-730 jours de laboratoire, 250 jours devant l'AFM, 200 jours devant la QCM, et le reste en divers….

-500 pointes AFM, 50 quartz, des litres de Liposomes, 100 mg de PllgPEG, des milliers de lamelle en verres, des centaines en mica ; des grammes de protéines pures ou non…

-Des milliers d'heures devant des écrans d'ordinateurs, des centaines de références lues et archivées, des milliers de e-m@ils, une quinzaine de réunions…

-Des litres de coca-cola, des montagnes de fromages pour récupérer, des sorties de temps en temps nécessaire pour faire baisser la pression….et de l'amour comme si c'était le soleil tout les jours…

-Environs 120000 Km parcourus en 4 ans, donc plus de 2 fois le tour de la Terre, et je veux remercier Christophe pour m'avoir permis de voyager et présenter mes résultats avec son soutien….

-Et enfin et c'est le moteur de tout, de la passion et de la patience….

Merci à tous et bonne lecture….

# Chapter I

# The Bacterial Flagellar Nano-Motor, what we know and what we do not

## Summary

# Chapter II

# Who is working with who?

# Interactions

Summary

# Chapter III
# A journey at the nano-scale
# Assembly of a part of the motor on an engineered surface

Summary

# Chapter IV
# The model strikes back
# Our vision of the Bacterial Flagellar Nano Motor

Summary

# Chapter I

# The Bacterial Flagellar Nano-Motor, what we know and what we do not

## Summary

# A) Introduction

The Bacterial Flagellar Nano-Motor (BFNM) is a nano-technological marvel, no more than 50 nm in diameter, composed of thousands of proteins perfectly organized into 20 parts. It spins a long thin external filament at a frequency close to 100 Hz, which propels the bacterium at a speed of 30 to 60 μm per second[1]. Despite its size, 20 times smaller than its host, the flagellum motor develops enough energy for moving a complex and large structure as a bacterium in the media. Compared to human for example, our legs would have to be 10 times smaller and permit us going 6 times faster than the fastest man on Earth for being comparable! This simple comparison shows how Nature developed a powerfull engine at the nano-scale. Rotating is not the only function of the flagellum nano-motor; it changes also its rotation's direction and enables bacteria to run, or to tumble. The run or tumbling behavior mainly comes from the helicity of the filament structure. The direction is controlled by a cascade of biochemical reactions within the bacterium, called "Chemotaxis"[2; 3]. Series of chemical detector are randomly dispersed on the bacterium surface, and analyze in real time the presence of molecules of interest (sugar, amino acids, dipeptides etc) in the media. The result of this multiplexed sensing is then transferred to the motor which changes the rotation from one direction to the other, depending on what kind of molecules has been found. If the detected molecules counted are "attractive", as food, the rotor spins counter clockwise (CCW) longer and the bacterium makes a longer run. When the bacterium wants to leave a region, the motor spins clockwise (CW), and the bacteria tumbles. This process leads to a non-stop random behavior of running in one direction for about a second, stopping, tumbling and running again. Using this complex process, the bacterium senses its environment and treats the chemical data in order to reach "optimized" regions. The BFNM is the key mechanical element of this perpetual search. Some species present numerous flagella, randomly dispersed on their surface. Through a mechanical phenomenon, the multiple flagella rotate in the same direction and form a bundle of flagella, allowing the bacteria to run faster through a cooperative synchronization. When the flagella rotate CW, the bundle disappears and the bacterium tumbles before choosing a new direction and so on. Other species present a single polar flagellum, some two in opposite positions. However, all of them present a similar structure and function. The flagellum is composed of 20 different proteins divided into three majors parts, and its assembly required at least 20 other proteins. The "filament" is the external part, it plays the role comparable to a helix for a submarine it is a long thin structure of several microns. This rotating

part of the flagellum propels the bacterium and its structure has been widely studied. The second part is called a “hook”, and links the filament to the inner part of the flagellum. It plays the role of a flexible link, and allows the filament to be strongly anchored to the inner part while preserving a softness and flexibility. The last part is the motor itself, called the “basal body”, which is imbedded into the bacterial membrane. The basal body is itself divided into three sub-units which together create the rotation in both directions. The flagellum structure is mainly identical between the different species, even if some additional units or small differences in the proteic structure can be encountered. Its discovery more than 30 years ago and the numerous data about the role of different genes into its assembly and function, the spatial arrangement of the motor proteins, the torque that it generates at different speeds, little is known about how does the motor really work and how the motor manages to shift abruptly from CCW to CW[4].

## B) Model

Numerous hypotheses for describing the inner mechanism of the BFNM have been proposed through the years, starting from Berg *et al.*[4], Schmitt *et al.* [5], Manson *et al.* [6], Thomas *et al.* [7] and recently Blair *et al.* [8] and Oster *et al. [9]*. All these models are mainly based on experimental well established data. In the following sections I will simplify and review them before going into further details.

The Nano-motor is divided into three parts, with a specific task for each of them, and specific interactions with the two others. Figure 1 shows a basic view of these three units and summarizes the function of the motor. The principle is similar to any motor at the macroscopic scale: a static system creates the rotation which is transferred to a rotative unit. The remaining unit plays the role of a gear and switches the rotation direction when necessary. The rotative part is called the “Rotor”, the static system, providing the necessary stroke the “Stator” and the gear the “C-ring”, each of these units is composed of proteins, which first self-assembles in order to create the bricks of the sub-unit, then assemble with other proteins to elaborate the sub-unit itself, and finally with others proteins from other sub-units for assembling the overall nano motor structure. The Nano-motor, as described here, is a very dynamic nano-machine, wherein each part is interacting strongly with others. The current hypothesis can be explained as follow: the Rotor is the internal part of the filament and is composed mainly of a protein called FliF, and rotates as a unit with the gear[7], composed of three others proteins, FliG FliM and FliN located mainly into

the cytoplasm. The FliG protein is the link between the gear and the rotor. The rotation is generated by the torque transferred between a series of stator[10], completely embedded into the inner membrane of the cell, composed of proteins MotA and MotB, and the rotor. This transfer also involves FliG protein, due to the established interaction between FliG and MotA. The torque is generated by a trans-membrane gradient of protons, which goes from the outside to the inside of the cell through the stator. This gradient creates a torque which is transferred to the rotor. When the bacterium change its direction of rotation, a chemotaxis protein called CheY swiths on its phosphorilated state through a cascade of reaction[11]. This phosphorylated protein CheY-P can binds to the gear, with the FliM proteins[12]. This binding induces a modification of the interaction between the rotor and the stator, between FliG and MotA[8; 13; 14]. The motor can rotate from clockwise to counterclockwise through a change of the concentration of the CheY-P in the cytoplasm resulting from the chemotaxis process.

Figure 1 reviews the current hypothesis about the spatial arrangement of the motor proteins element. Numerous models have been proposed through the years, but none of them have been able to be established definitely how works the motor. Blair's model summarized numerous data, mostly mutagenesis data and also cryo-Transmission Electronic Microscope (cryo-TEM) imaging analysis and computational reconstitution. We will see now in more detail what is known and don't about the motor, its assembly, structure and function and the open questions.

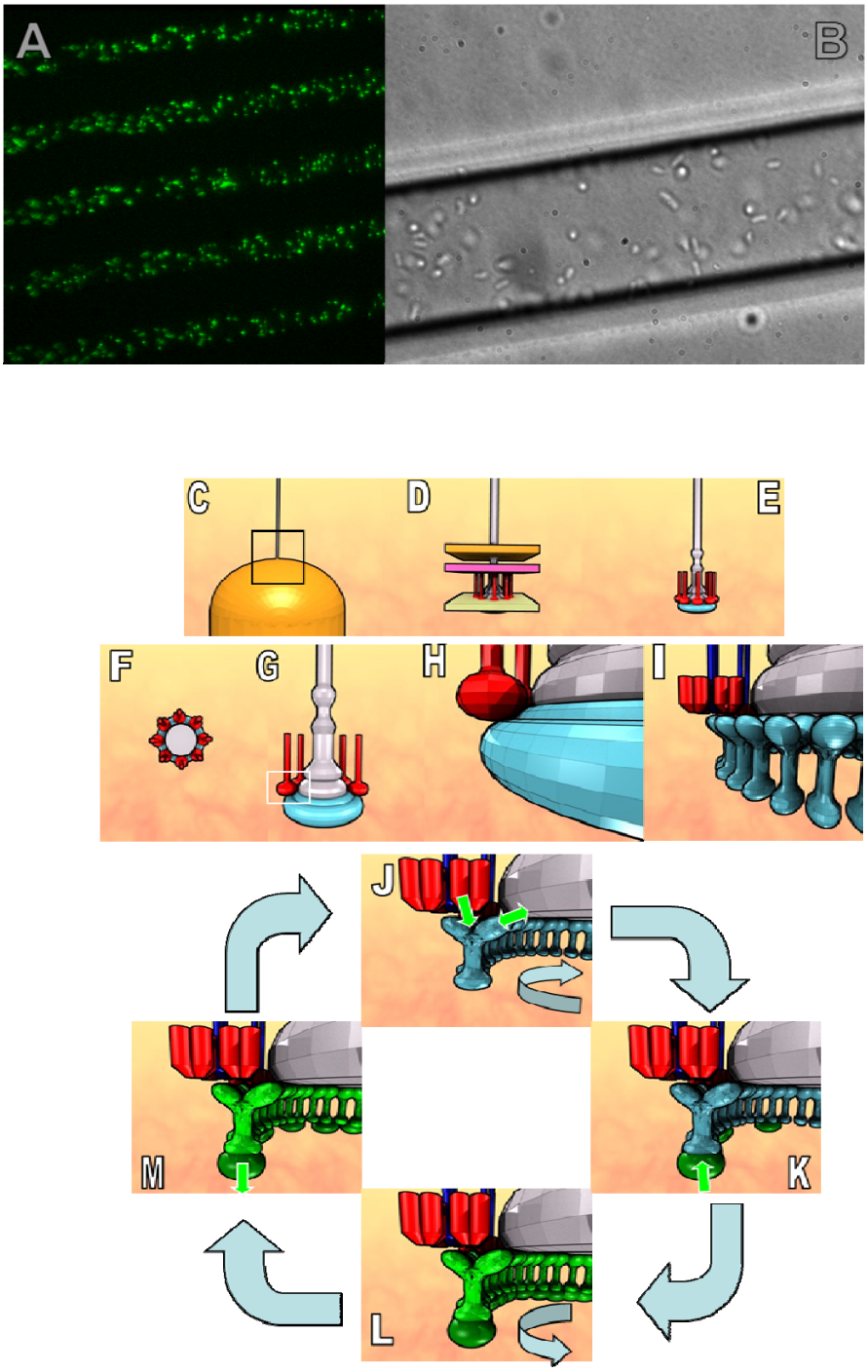


*Figure 1: The bacterial flagellum Nano-motor BFNM. A&B/view of E.coli bacteria on a surface. C/cartoon view of a polar flagellum D/ Enlarged view of the black square of C. The flagellum is embedded in several layers, starting*

*by the yellow one corresponding to the outer bacteria membrane, the pink one a periplasmic structure called the "cell wall", and finally a green one for the inner membrane. E/ The BFNM extracted from the membrane. Different units are shown, the rotor which is at the base of the filament in grey, the stators system in red and the C-ring in blue. F/ Top view of the basal body. 8 to 12 stators systems are around the rotor. 8 in this presentation, but the global assembly is possible with 12 stators. G/ Zoom in of D, we notice that The C-ring is attached to the cytoplasm side of the rotor, H/ Zoom in the white square of G. I/ Same view as G but with more realistic structure of proteins as seen by Cryo TEM and also based on genetically analysis of the motor's proteins. The C-ring is divided into Y shape units, 32 to 36, and interact with both stator and rotor, through the FliG proteins. J/ The stator transfer vertically the torque to the FliG, at the top of the C-ring. The torque is then transferred to the rotor and the filament spins CCW, the bacterium runs. K/ CheY-P, a cytoplasmic protein issued from the chemotaxis, binds to the C-ring, (to the FliM). The precise location of FliM is still unknown. L/ When a threshold number of CheY-P are attached, the C-ring moves to the CW state, and the rotor spins CW, the bacterium tumbles. M/ CheY-P start to be dephosphorilated and detaches from the FliM. When the number of bind CheY-P is below the threshold, the C-ring goes back to the CCW state.*

# C) The structure

## a. Genes and proteins

### i. Generalities

The BFNM is composed of the fundamental bricks of any form of life on Earth, proteins. The word *protein* comes from the Greek word *πρώτα* ("prota"), meaning "of primary importance", they are large organic compounds made of amino acids arranged in a linear chain and joined together by peptide bonds between the carboxyl and amino groups of adjacent amino acids. Each protein has its own unique amino acid sequence that is specified by the nucleotide sequence of the gene encoding for this protein. Proteins are always biosynthesized from N-terminus to C-terminus, which correspond to $NH_2$ terminal and COOH terminal. The size of a protein can be measured by the number of amino acids it contains and by its total molecular mass, which is normally reported in units of *daltons* (synonymous with atomic mass units), or the derivative unit kilodalton (kDa). Most proteins fold into unique 3-dimensional structures. The shape into which a protein naturally folds is known as its native state. Although many proteins can fold spontaneously and unassisted, simply through the chemical properties of their amino acids, others require the assistance of molecular chaperones to fold into their native states. When the proteins have been generated and their final folding achieved, more than one protein can be finally obtained due to an additional structure often described as the *Quaternary structure*. This structure results from the interaction of more than one protein, usually called *protein subunits* in

this context, which is a part of the larger assembly or protein complex. Indeed, proteins are not entirely rigid molecules and it has also been observed that proteins may alternate between several related structures while they perform their biological function. In the context of these functional rearrangements, the different structures are usually referred to "conformations", and transitions between them are called *conformational changes.* Such changes are often induced by the binding to an enzyme's active site. In solution all proteins also undergo variations in structure through thermal vibrations and collisions with other molecules. Our attention has been attracted by only six proteins of the flagellum basal body: proteins which are involved in the rotation and the switching. We can separate these proteins into three parts, the Stator composed of MotA and MotB, the Rotor part composed of FliF and FliG and the C-ring (gears) with FliM and FliN. Their respective names, *Mot* and *Fli*, are coming from the fact that mutagen on these proteins influence the motility (Mot) or the filament assembly or structure (Fli). This separation into three sub-units is currently under discussion but should not be problematic at this stage of the manuscript.

### ii. The Rotor, the MS-ring

The rotor is the inner part of the filament and is mainly composed of successive rings of self assembled proteins. Starting from the cytoplasm to the outer membrane, 8 proteins constitute the rotor of the flagellum: FliG, FliF, FlgI, FlgB, FlgC, FlgF, FlgH and FlgG. Early on, the basal body was thought to comprise 4 rings (M, S, P and L) and a rod, because these elements can be seen by electron microscopy when flagella are extracted, purified and negatively stained. Through the extraction procedure[15; 16; 17], flagella were fractionated in detergent by differential sedimentation [18] and those rings were named relatively to their affinity[19; 20] : with the inner membrane for the M-ring, with the Supra-membranous fractions for the S-ring, with the peptidoglycan for the P-ring and with the lipo-polysaccharide for the L-ring. Later, it appeared that the M and S rings were composed of the proteins FliF and FliG and can be fused into a single ring, called MS-ring, as proposed in figure 2. It has been established that the simplest structure found was the MS-ring, mainly composed of the FliF and FliG proteins[21] and their assembly does not require any others proteins[22]. FliF is a largest protein found in the flagellum, 61 KDa is composed of 8 different domains which apparently play different roles into the flagellum assembly and function. FliF is present into the rotor in 26 copies [23].

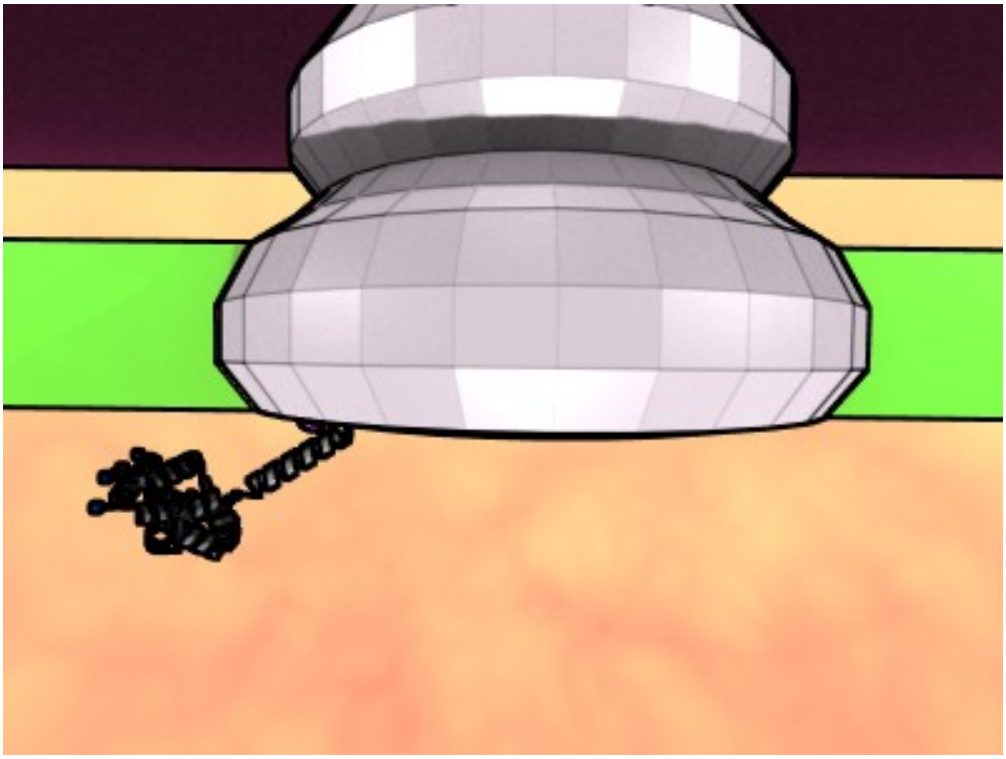

***Figure 2: the rotor****. The zone in grey represents FliF proteins, partially embedded into the inner bacterium membrane, in green. FliG is schematized in one of its hypothetical position.*

The whole assembly of the motor is mainly impossible without the FliF proteins already present in the inner membrane of the bacterium. FliF structure is unknown, but it has been established that FliF strongly interacts with FliG, through its C-terminal[16] but no others proteins from the Stator or the C-ring is apparently linked to FliF. FliG, the second MS-ring protein is present in around 26 copies in each flagellum[16; 24]. Its molecular weight has been evaluated to 37 Kda.

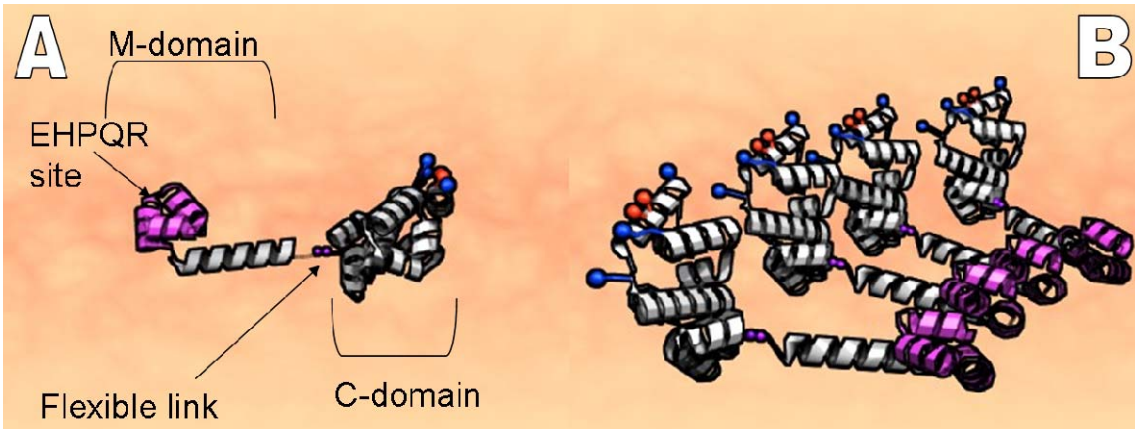


***Figure 3: FliG protein structure, based on the proposed crystal structure available on the protein data bank: http://www.rcsb.org/pdb/explore.do?structureId=1LKVDOI 10.2210/pdb1lkv/pdb.*** *A/ C and Middle domains, with the EHPQR site highlighted in purple, and also the gly-gly link. Both sites interact with FliM. B/ Lateral view of possible assembly of several FliG.*

The same number of FliF and FliG proteins lead people to position FliG at the inner side of the rotor, but its emplacement remains ambiguous. FliG structure has been partially resolved and presented in figure 3 [25]. FliG can be divided into three sub-parts, with different purposes: C-terminal appears to interact with the stator proteins[25], the middle part plays the role of flexible link and the N-termini stick FliG to the FliF through a C-N terminal interaction[26]. The presence of amino acids negatively and positively charged at the C-teminal hold an interaction with the stator MotA proteins [27]. These interactions have been supported by numerous gene and mutations analysis [27; 28; 29] and support the hypothesis that these interactions are part of the rotation origin. FliG appears also to be well organized directly into a quaternary structure called M-ring without the needs for others proteins and only one spatial organization of the FliG proteins has been proposed[30]. FliG is also crucial into the switch of the rotation. The C part and M part of the FliG interact through a patch called EHSPQR and a Glycine-Glycine link with the FliM proteins, components of the C-ring. These interactions have also been widely studied and support the idea that the switching phenomenon originates from these interactions[14]. Spatial organization has been recently proposed but remains hypothetical for the moment, due to a symmetry problem. 26 copies of FliF are present in each flagellum, 26 FliG but 34 to 36 FliM, which excludes an allosteric 1-1 interactions comparable to the FliF-FliG assembly. Hypothesis has been proposed to explain this asymmetry[6] but the questions of the emplacement of FliG, the role played by the FliM-FliG interactions remains an open question.

### iii. The Stator

The stator part of the flagellum is the most intriguing. It is mainly composed of two proteins, called MotA and MotB, and is involved into the trans-membrane gradient of protons or cations, as known as the proton motive force (PMF). An equivalent system using two proteins called PomA/PomB exists but uses a sodium motive force (SMF). However; these two proteins are deeply embedded into the inner membrane of the cell. Some species using sodium present also two other "Mot" proteins, MotX and MotY, in the periplasmic space, a space between the inner and the outer membrane of the cell. MotA has four membrane spanning α-helical segments[31; 32] and the rest of the molecule, about 2/3 lies in the cytoplasm. MotB has one membrane spanning α-helical segments near its N terminal, but most of the molecule is found in the periplasmic space [33; 34].

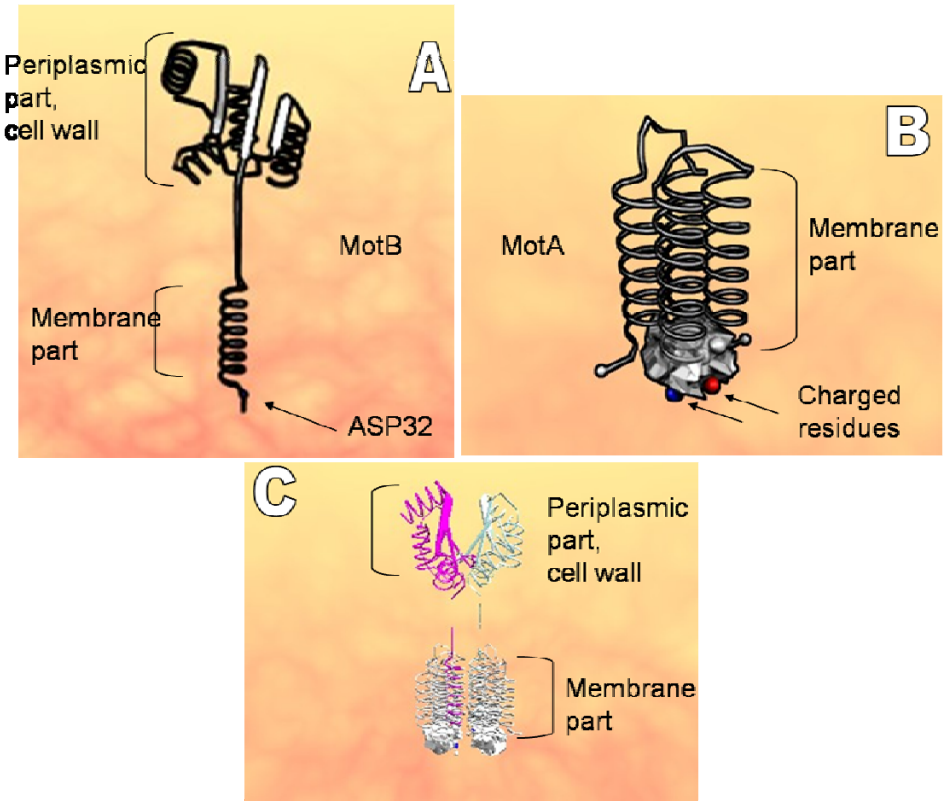


***Figure 4: Schematic view of the Stator.*** *A: MotB protein, exhibiting four domains, where only the domain which binds MotB to the cell wall has been resolved. The rest of the periplasmic domain, the hydrophobic domain (membrane part) and the cytoplasmic domain remains unknown. B: MotA proteins. 2 majors domains, the membrane part composed of 4 α-helix, and a cytoplasmic domain which counts for 2/3 of the protein. Charged amino acids on*

*the cytoplasmic domains have been identified to be part of the rotation process. C: the Stator assembly composed of 2 MotB and 4 MotA.*

Figure 4 shows their possible structure, only the periplasmic part of the MotB has been crystallized recently [35]. Their respective weight is about 32 and 34 KDa. MotA and MotB are present in 32 and 16 copies per flagellum, but it appears that MotA/MotB form a complex comprising 4 MotA and 2 MotB[36; 37],which leads a total estimation of 64 MotA and 16 MotB. Each stator can divided into two parts, composed of 2MotA/1MotB, the role of each part is not clear but it is likely that each generated a torque in opposite direction, which could be the source of the bi-direction of the rotation[34]. Genetical approachs have proposed an arrangement of the proteins [36; 37; 38], but this question remains open. The diverse protocols used for extraction of stator has failed, probably due to the trans-membrane class of both MotA and MotB[39], which lets open the question about their in vivo spatial organization. It has also been identified that the stator complex could be comparable to other inner membrane proteins complex, for example TolQ/TolR[40] or ExbBD/TonB[41] which support the current assembly hypothesis. The number of stator complex within each motor is important. Several studies have visualized some circular arrays of membranes particles ("studs") around the rotor in a freeze-fracture preparation on the inner membrane[42]. Their numbers have been evaluated in sets of 10 to 12 for E.Coli[43], but this number can change relatively to the species (14-16 for Aquaspirillum serpens, 12 for Salmonella[44]). It is therefore clear that MotA/MotB complex is playing the role of a torque generation unit. MotB anchor each complex to the cell wall[35; 45; 46], a biochemistry structure found in the periplasm, for allowing the torque to be delivered to the rotor. Genetical studies tend to show that there are two protons channels in each complex[32] and both are used at the same time[38], but the function of the complex as a proton channel remains unknown due to the lack of crystal structure of both MotA and MotB. However, the role of specific amino residues has been established, especially ASP32 of MotB wherein protons are likely to bind, but the role of the N terminus of the MotB[47], and its interaction with MotA are also unresolved[48]. R90 and E98 E150, PRO171 and PRO222 from the cytoplasmic part of MotA have been identified to interact with the C-part of FliG but their precise role remains unknown[49]. Blair proposed that each MotA interacts vertically with FliG, and because the spatial arrangement is not symmetrical, it would create the rotation of the rotor. The interaction responsible for the proton conduction between the periplasm and the cytoplasm remains unknown. It is possible to think that when MotB released a proton, the loading-torque cycle can restart and a new proton can bind and

generate a new cycle. The chemical transformation due to the passage of these protons could change the shape, structure of both MotA and MotB, but this change is still unknown.

### iv. The C-ring

This is the last sub-unit of the basal body. It is the largest ring found in the flagellum structure and is found at the base of the rotor, into the cytoplasm and is also called the "switching complex". FliM and FliN are found in 32 copies and more than 110 copies in each flagellum C-ring. Recent studies about the FliN conclude about a 1 to 4 ratio between the FliM and the FliN[4]. FliM has a molecular weight of 32kDa and FliN is the smallest proteins of the all flagellum, with a molecular weight of 14Kda. **The presence or not of FliG into the C-ring structure is one of the question about the flagellum structure**. Parts of FliM and FliN structure have been resolved recently [13; 50], Figure 5 and 6 show crystal structure of FliM and FliN and also arrangement of FliM FliN complex.

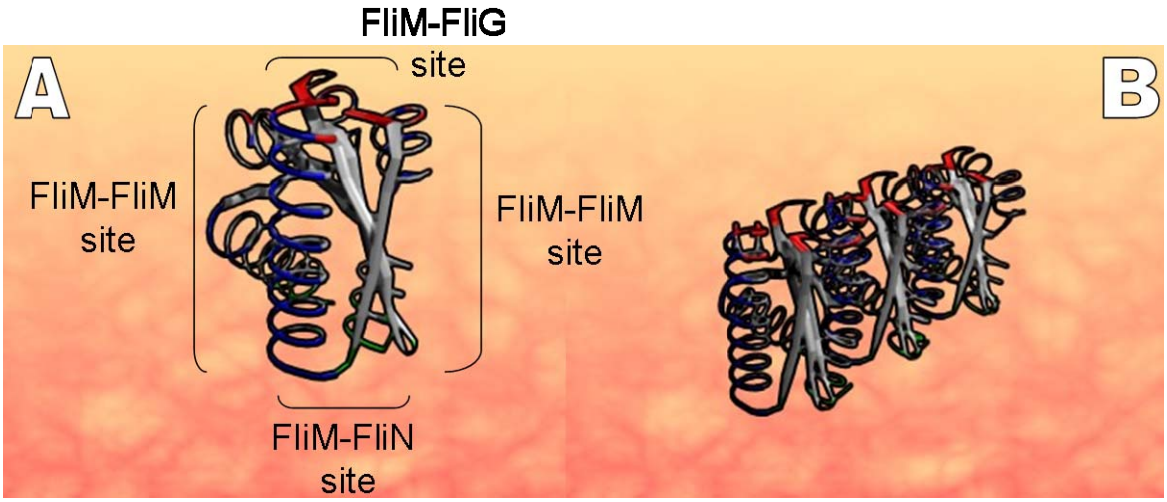


***Figure 5: FliM structure***. *A/ Interactions sites have been identified: blue for FliM-FliM interaction, corresponding to the lateral side of the proteins, the top side in red for FliM-FliG interaction and the bottom side for FliM-FliN and also for CheY-P interactions .B/ Spatial arrangement of 3 FliM, DOI 10.2210/pdb2hp7/pdb. http://www.rcsb.org/pdb/explore.do?structureId=2HP7*

Some specific sites in each protein have been identified as necessary for a proper flagellum function or assembly, and reported on these figures. Spatial arrangement of FliM/FliN complex has also been proposed [13; 14; 51] but to our knowledge no arrangement which include FliM, FliG and FliN has been published. Genetical studies have identified the sites of different interactions and some fact have been undoubtedly established: the C-ring, through the FliN has a fundamental role during the assembly phase of the flagellum [52] but its precise interactions remain unclear, the chemotactic signaling protein CheY-P binds to FliM inducing the switch which is transferred through the FliM-FliG interaction[14]. FliM is likeky to play the backbone role of the C-ring, connecting all elements together [53]. Recent data about the C-ring shape and structure have also revealed a 32 to 36 fold symmetry in good accordance with the FliM number and role[54]. However, the spatial emplacement of each protein remains subject to controversy. Due to the interaction between FliG and FliM, we admit that the C-ring rotates as a unit with the rotor, despite its presence into the cytoplasm. Structural data have identified the C-ring as a large structure bonded at the bottom of the rotor. This observation is the main and only argument that supports the rotation of the C-ring. However, direct observations in vivo could not confirm this hypothesis.


***Figure 6: FliN structure***. *A/ Dimer of the crystallized part of the FliN proteins, which corresponds to the middle and C-terminal. B/ Tetramer of the FliN domains.*

The current model proposes that FliG, FliM and FliN are part of the C-ring. Based on mutagenese experiments, one possible assembly is proposed in figure 7.

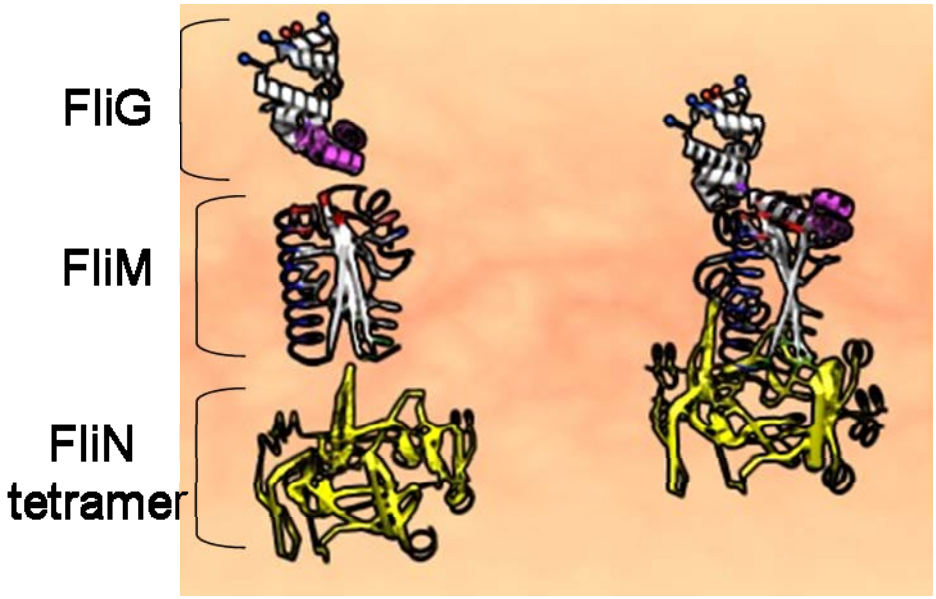


***Figure 7: Possible assembly of one unit of the C-ring****. Left, the three proteins are separated and shown assembled on the right side.*

## b. Assembly and Structure

### i. Assembly

The full flagellum is a marvelous assembly at the nanoscale; an easy calculation evaluated the numbers of elements to more than 6000. These elements are well ordered for enabling the motor to work. It has been identified that genes involved into the flagellum assembly and function are arranged in hierarchical order [21; 55; 56; 57; 58; 59; 60] in three classes, as shown in table 1. The flagellum genes are divided into three families, called class 1, 2 and 3. The role of each class is very specific: Class 1 contains the master operon. An Operon gene is a gene that regulates the production of proteins, in our case motor's proteins. Operon control is a type of gene regulation that enables organisms to regulate the expression of various genes depending on environmental conditions. Operon regulation can be either negative or positive by induction or repression. In our case, the class 1 operon is called *flhDC,* its expression is required for the two other class operon of transcription. Class 2 and 3 contains all operons needed for assembly and function of the flagellum[61]. Their respective functions, weight and copies per motor are summarized on table 2. Due to this kind of hierarchical organization, bacteria are able to control the elaboration of new flagellum or to fix part of an existing flagellum. For example, if nutriments are plentiful, chemotaxis and motility are considered useless, and cells dispense with

them[62]. However, the system which codes for the flagellum is also connected to other existing systems within the cell, for example in response to heat shock[63], cell division[64; 65] or regulation of others organelles.

| Class 1 | Class 2 | Class 3 |
|---|---|---|
| *flhDC* | *flgAMN* | *fliC* |
| | *flgBCDEFGHIJKL* | *motABcheAW* |
| | *flhBAE* | *tar tap cheRBYZ* |
| | *fliAZY* | *aer* |
| | *fliDST* | *trg* |
| | *fliE* | *tsr* |
| | *fliFGHIJK* | |
| | *fliLMNOPQR* | |

***Table 1: the three different operon and genes organization**. Each of them allows the coding for a defined element of the BFNM. The underlined genes belong to the operon shown, activated by FlhDC, but they have additional promoters activated by FliA. Thus, they are partially expressed as class 2 genes and fully as class 3 genes. Class 3 genes not mentionned in the early part of the text encodes recepetor for aspartate (tar), dipeptides (tap), ribose and galactose (trg) and serine (tsr), a sensor for redox potential (acr), enzyme involved in sensory adapation, a methyltransferase (cheR), and an enzyme that accelerates the removal of phosphate from CheY-P (cheZ)*

The motor is built from the inside out and this order was documented by Suziki and al[57] through genetical analysis. Figure 8 summarizes the different steps for the motor's construction. It starts by the simplest structure, the MS-ring, composed of the FliF and FliG proteins[21] and then the C-ring is added. No other proteins are required for these parts[22]. A supra-molecular structure called the "transport apparatus" composed of FlhA, FlhB, FliH, FliI,FliO FliP FliP and FliR self assembles at the cytoplasmic side of the MS-ring/C-ring complex[66; 67; 68; 69; 70; 71] and is the master piece for the flagellum assembly. The transport apparatus complex is responsible for the assembly of the rotor, also called the rod, followed by the hook and the filament. Most of these units are composed of self-assembled proteins which have passed one by one into a central channel within the rotor. The transport apparatus complex binds to this channel and starts to pass over rotor, hook and finally filament's proteins. This apparatus transport is used to pass components for the axial structures within a channel at the center of the MS-ring. We noted that the diameter of this channel in the center of the MS-ring does not exceed a few

nanometers. This structure is very dynamical in its process. One of the transport apparatus complex, the FliI function shows similarity into the assembly of another nano-motor, the $F_1F_O$-ATPase[72] and to components of bacterial type III secretory systems[73] and is directly involved in the assembly process.

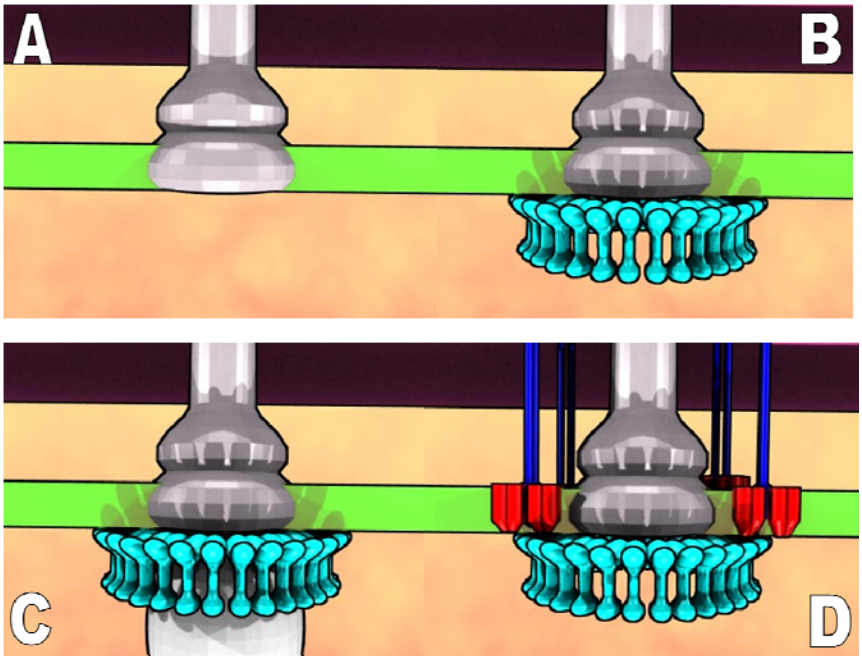


***Figure 8: Assembly of the full flagellum****. A/ First step, the FliF proteins self-assemble and form major part of the MS-ring. B/ FliG, FliM and FliN form the C-ring at the cytoplasmic side of the MS-ring. C/ The complex apparatus interacts with both rotor and C-ring and pass over all the hook and filament proteins. D/ The stators, which are apparently free to move within the inner membrane, bound to the rotor and C-ring.*

Then the proteins are assembled in a defined order, starting from the proteins above FliF, FlgG until the flagellin FliC. The process of formation of the filament has been well described by Keiichi Namba *et al* [74; 75]. Some mutations altering the C-ring structure influence the shape and size of filament elements as the hook [75] but the real influence and role played by the C-ring in the assembly process is for the moment unclear. One point is crucial in the flagellum assembly; the rotor and filament are assembled in a specific way, starting from the MS and C-ring to the filament, but the assembly of one part remains relatively independent: the Stator. The torque generating units, MotA and MotB, are apparently incorporated at any time after the class 3 genes have been expressed, which means that the full filament, rotor plus external part is completed before the incorporation of the stator. It is worth noticing that this fact has never been confirmed

by any observation in living organism. The relative independence of stator proteins reveals efficient properties: if MotA and MotB are missing or damaged, they can be replaced by new copies, which means that if some studs of stator are damaged while the rotor is spinning, the cell is able to add new copies in replacement of the damage one [76]. It can be easily compared to a man who is changing damaged part of his legs while is running without stopping his run. The assembly of the flagellum is a marvel of organization and shows how evolution through the millions of years has created an efficient process for creating a powerful self repairable organelle such as the flagellum.

| Gene product | Function or Motor component | Size (KDa) | Copies Per motor | Operon class |
|---|---|---|---|---|
| FlgA | Assembly of P-ring | 24 | XXX | 2 |
| FlgB | Proximal rod | 15 | 6 | 2 |
| FlgC | Proximal rod | 14 | 6 | 2 |
| FlgD | Assembly of hook | 24 | 6 | 2 |
| FlgE | Hook | 42 | 130 | 2 |
| FlgF | Proximal rod | 26 | 6 | 2 |
| FlgG | Distal rod | 28 | 26 | 2 |
| FlgI | P-ring | 36 | 26 | 2 |
| FlgJ | Muramidase | 34 | | 2 |
| FlgK | Hook-filament junction, at hook | 59 | 11 | 2 |
| FlgL | Hook-filament junction, at filament | 34 | 11 | 2 |
| FlgM | Anti-sigma factor | 11 | | 3a |
| FlgN | FlgK, FlgL chaperone | 16 | | 3a |
| FlhA | Protein export | 75 | | 2 |
| FlhB | Hook length control | 42 | | 2 |
| FlhC | Master regulator for Class 2 operon | 22 | | 1 |
| FlhD | Master regulator for Class 2 operon | 14 | | 1 |
| FlhE | ? | 12 | | 2 |
| FliA | Sigma factor for class 3 operon | 27 | | 2 |
| FliC | Filament, flagellin | 55 | 5340 | 3b |
| FliD | Filament cap | 50 | 10 | 3a |
| FliE | RodMSring junction | 11 | 9? | 2 |
| FliF | MS-ring | 61 | 26 | 2 |
| FliG | Rotor component | 37 | 26 | 2 |
| FliH | Protein export | 26 | | 2 |
| FliI | Protein export ATPase | 49 | | 2 |
| FliJ | Rod, hook, filament chaperone | 17 | | 2 |
| FliK | Hook length control | 39 | | 2 |
| FliL | ? | 17 | | 2 |
| FliM | Switch component | 38 | 32-36 | 2 |
| FliN | Switch component | 14 | 110-130 | 2 |
| FliO | Protein export | 11 | | 2 |

| | | | | |
|---|---|---|---|---|
| FliP | Protein export | 27 | | 2 |
| FliQ | Protein export | 10 | | 2 |
| FliR | Protein export | 29 | | 2 |
| FliS | FliC chaperone | 15 | | 3a |
| FliT | FliD chaperone | 14 | | 3a |
| MotA | Torque generating units, stator | 32 | 32? | 3b |
| MotB | Torque generating units, stator | 34 | 16? | 3b |

***Table 2: List of proteins****: All the proteins involved into the BFNM are listed, in yellow are listed the proteins involved into the external part of the flagellum, the filament and the hook, in blue the genes which are master regulator for operons family, and in red proteins directly involved into the nano-motor.*

## ii. The Global Structure

The structure of the flagellum in vivo has not been observed yet, only the external filament can be imaged while the flagellum spins. However, due to the early development of the electronic microscope techniques, especially the cryo TEM method, numerous pictures have been recorded since the first pictures by Depampilis *et al* in 1971[18] to recent Derosier *et al*[54; 77] publications. Cryo-TEM and deep etch replica allowed the observation of extracted elements, as the rotor for example, but also can be applied on frozen cell, exhibiting numerous flagellum elements. The MS-ring has been observed using deep etch replica cryo-TEM and can be seen in figure 9-10-11. Circular structures of 25 nm are clearly visible, exhibiting also a depression in the center, which sheds some light on the rotor structure.

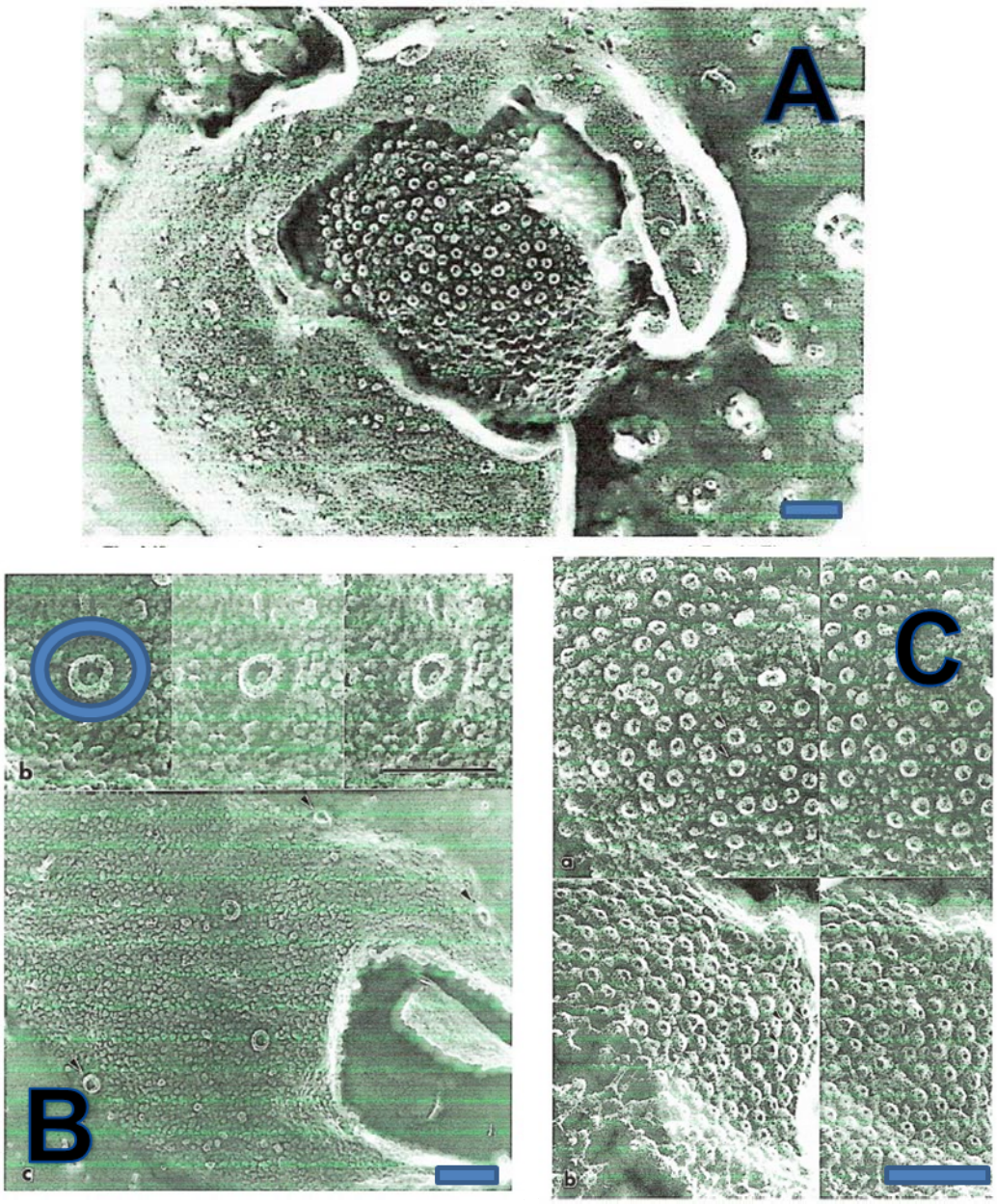


***Figure 9: Cryo-TEM picture of native Cells exhibiting numerous MS-ring structures, from reference [78].*** *A/ full cell, scale bar 100 nm; B/ Zoom on several MS-ring and some C-ring, C/ MS-ring. Scale bar 100 nm. We notice that the stator proteins are not visible on the picture.*

Other researchers have been attracted by the deep-etch replica methods, coupled to cryo-TEM. Their approach after image reconstruction allowed for the first time to visualize the flagella in 3D. Different strategy has been applied but share the same principle. Bacteria exhibiting numerous flagella are grown and through series of bio-chemical reaction coupled to centrifugation, large number of purified flagella can be obtained[18]. Several approached has

been then used to visualize these flagella using a cryo-Transmission electronic microscope (cryo-TEM) [15; 44; 79; 80]. By averaging multiple flagella images, an inside view of part of the basal body can be obtained. This picture showed in figure 10 revealed numerous aspects of the flagellum basal body shape and structure and the most recent work from Derosier *et al* [54] presents a large study about the numbers and symmetry of the different elements. It has been observed that while the flagella is extracted from the cell, the C-ring sticked to the rotor and forms a full and relatively compact structure. However, depending on the extraction protocol, the C-ring does not always stick with the rotor, which opens the question about the real in vivo arrangement and interaction of both elements. We also notice that this protocol does not give the opportunity for studying the stator part of the basal body, due its strong link with the inner cell membrane. This missing part could interfere with the full structure.

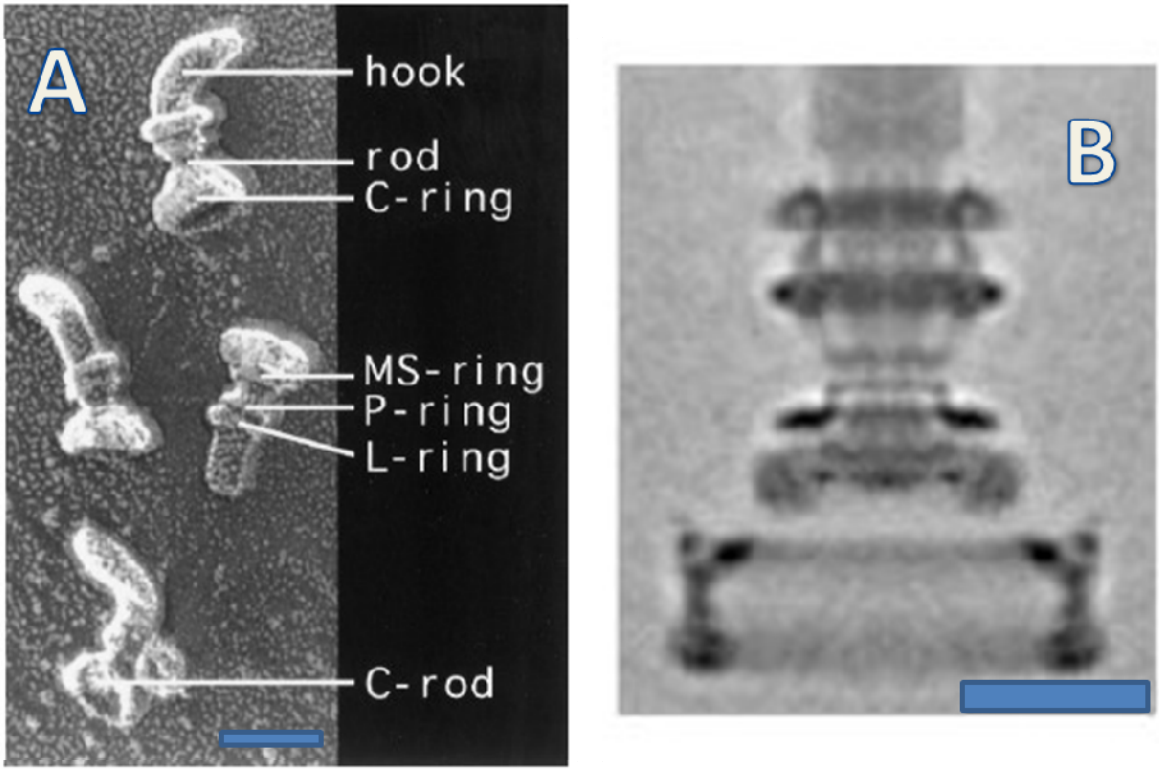


***Figure 10: Cryo-TEM images of the basal body extracted from bacterium.***

*A/ Numerous rings are clearly visible. Scale bar 50 nm. B/ Average view for a single flagellar basal body. Scale bar 20 nm. [54] [17].*

Other studies focused on the MS-ring alone[81] instead of the full flagellum. As noticed before, the MS-ring is the first and primary structure assembled during the flagella construction,

and its shape reveals numerous aspects of the flagellum global structure. By overproducing MS-rings, separation and purification, it has been possible to get images of the MS-ring entity. Such a tremendous work is briefly summarized in figure 11. It shows a typical picture of the MS ring obtained. The presence of the FliG at the inner side of the MS-ring hasn't resolved the main question of its precise localization, but the different between the MS-ring with and without the FliG brought new highlights on the FliG role in the flagella structure.

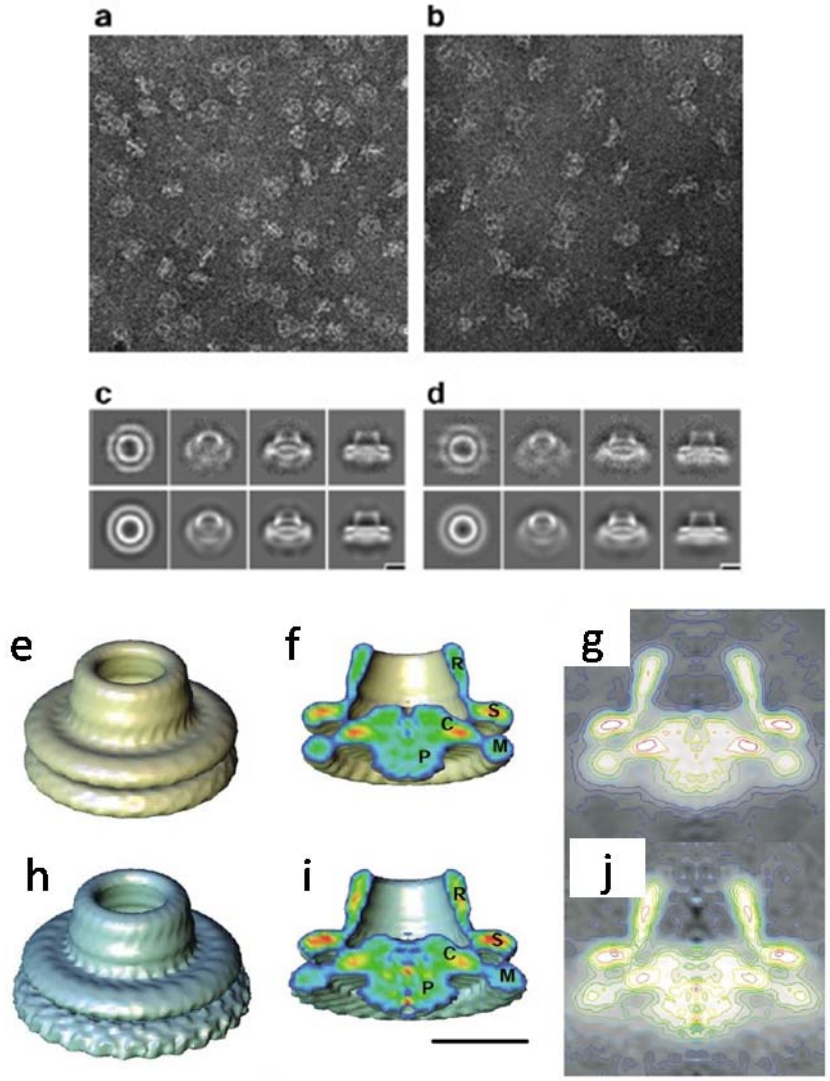


***Figure 11: CryoTEM images of the MS-ring, composed of FliF and FliG, overproduced and extracted from E.Coli***. *a and b are untreated TEM micrographs while c and d are averaged view of many compiled images showing the MS-ring from the top, or in cross section. a and c exhibit images of the MS-ring composed only of FliF while b and d MS-ring with FliF and FliG, scale bar 10nm. Images reconstruction of the MS-ring without (e,f,g) or with the FliG (h,i,j) [81]*

Other studies were also conducted through on a direct observation of elements within a full frozen cell [78]and revealed for example the presence of the stator's studs,[82]. A more recent approach consisted of a partial reconstitution of the single stator elements within an artificial structure called proteo-liposomes[77]. Briefly, proteins have been over produced and purified following an established procedure (see chapitre 2 and 3), and mixed with a phospholipidic mixture mimeting the inner bacterial membrane. Phospholipids are the main component of the cell membrane and can be manipulated in order to create 3d spherical structures called liposome, which are composed of phospholipids bilayers, or when organized on the surface in order to create a Supported Bilayer membrane (see chapter 3). We will emphasize later on this remarkable biochemical structure. However, when the lipid composition is mixed with a small amount of proteins in adequate experimental conditions, a structure called proteo-liposome can be obtained. Keiichi Namba *et al* observed using cryo-TEM the presence a proteic structure within the membrane. Figure 12 shows a typical result. They mainly work on a complex of PomA/PomB which used instead of protons sodium as an energy source, but exhibits a similar architecture than the proton nanomotor. The presence of a cylinder structure of several nano-meters and a higher density at the cylinder bottom within the membrane led them to conclude of an artificial reconstitution of a single stator. However, the experimental conditions prevented higher resolution imaging and therefore we can not conclude on the key question of the MotA/MotB in vivo organization.

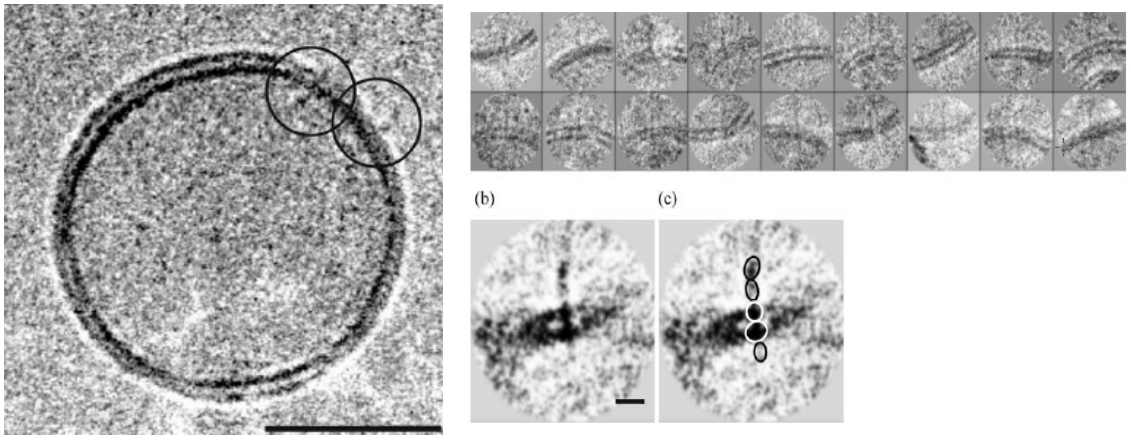


***Figure 12: Stator Proteo-liposomes****. Series of cryo-TEM images presenting the stator complex, here the PomA/PomB, reconstituted into a liposome mimicking the native E.Coli Inner membrane. A/ large view of a single proteo-liposome, scale bar 50 nm B/ series of enlarged images of the stator complex embedded into the membrane, C/ average images showing a protuberance corresponding to the MotB, scale bar 5nm [77]*

All these data were compiled for proposing a structure, summarized in figure 13. The rotor is mainly composed of the FliF and probably one part of the FliG rings, and presents a diameter between 22 and 25 nm and symmetry of 26 elements[54]. The C-ring is just under the rotor, at the cytoplasmic side, and presents numerous subunits, from 32 to 36, which corresponds to the estimated numbers of FliM[13]. Its diameter can be average to 45 nm, which represents the larger ring of the all flagellum. Successive rings are clearly visible, from the MS-ring, and to the L and P rings. We can note that the stator is missing on the picture and the full basal body was never observed, which could be the limit of this approach. However, based on these images, an attempt tried to fit the structure of the proteins previously shown into the electronic images, as shown on figure 13.

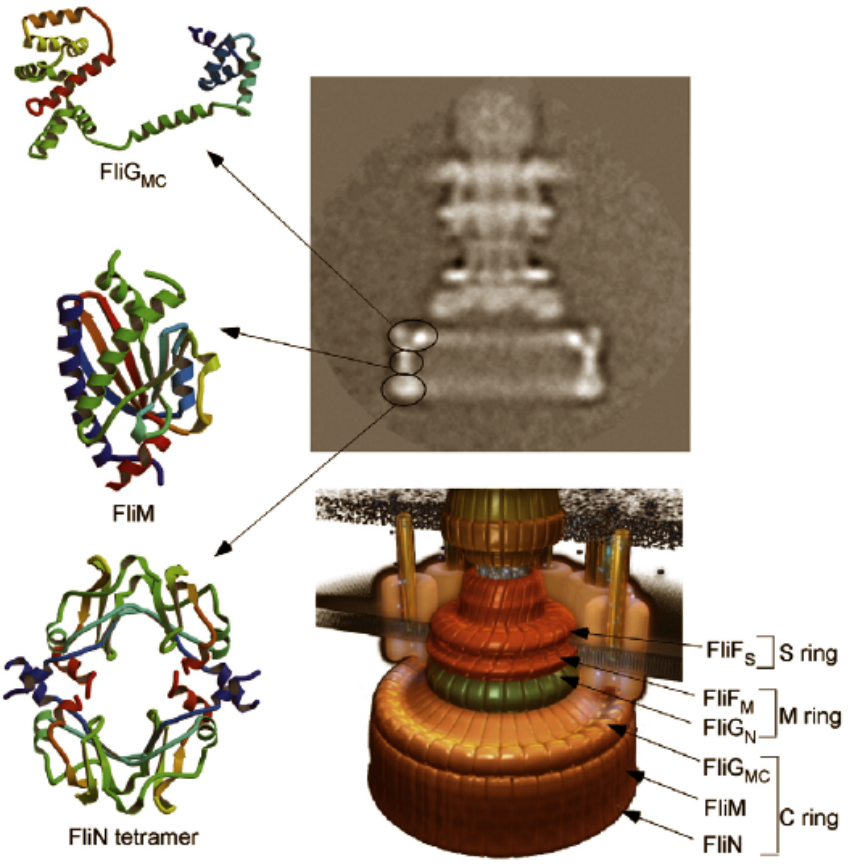


***Figure 13: Summary of a possible architecture of the different motor elements****. Crystal structure of part of FliG, FliM and tetramer FliN are fitted into the cryo-TEM images of an extracted motor. Cartoon presents the current view of the motor assembly. [53]*

## D) Mechanism

Despite the numerous questions about its internal arrangement and structure, some mechanical aspects of the flagellum motor have been obtained through different experiments. The global behavior of the flagellum, the energy which is developed, the torque and its relationship with the speed and some others data highlighted some elementary mechanism of the motor. As described by Berg[4], we can divide the mechanism into different sections: the power source, the torque generation units, the stepping, the torque relationships and the switching process. This pioneering work enabled us to highlight some crucial points about the motor function, which have to be respected by any new hypothesis describing the motor function. The work of Berg *et al,* constitutes, according to us, the solid basis on which any new proposal should rely.

### a. Power source

²Flagellar motor of *E coli* and *S.Typhimurium* for example, are powered not by ATP, but rather by a protons or ions moving down an electrochemical gradient[10; 83; 84; 85]. The work per unit charge can be described as follows:

$$\Delta P = PMF = \Delta\Psi + 2.303\ (K_B T/e)\ \Delta pH$$

Δp, also called the proton motive force (PMF) is composed of two terms:

-The membrane potential, the energy required for a charge to go through the membrane, which is by convention related to the electrostatic bias across the membrane.

-The transmembrane ion concentration gradient, wherein

ΔpH = log[H+ periplasm/H+cytoplasm] is the entropic contribution due to the ion concentration across the cytoplasmic membrane, $K_B$ the Boltzmann's constant, T the absolute temperature and e the electronic charge. *E.coli* maintains its internal pH in the range 7, 6 to 7, 8. For example, if cells grow at pH 7, Δp will be equal to -170mV ($\Delta\psi$ ~ -120mV and (-59*ΔpH) ~-50mV). In order to obtain the number of protons consumed for one rotation of the motor, it is necessary to measure experimentally:

*i. the total variation of protons in the outside medium per unit time*

*ii The pulsasion ω( rad.s$^{-1}$ )or frequency υ(Hz) of the rotation.*

This experiment is quite complex since in the medium where the variation of pH is recorded experimentally there are many cells, each containing several nano-motors. However, the numbers of protons needed for generating one rotation has been published using a high value experimental methodology where all these elements could be evaluated independently. The measurement has been made only on a bacterial species, S*treptococcus sp strain V4051* [86], which presents a peritrichously flagellated (one single flagella). It's a primarily fermentative and gram positive organism (single membrane instead of two for *E.coli*). This organism was choose instead of E coli because it's lack of energy reserve and is sensitive to ionophores and uncouplers. This organism can be also starved and artificially energized either with potassium diffusion potential or with a pH gradient (by shifthing cells to a medium of lower pH) [10; 87]. If cells are energized in this way in a medium of low buffering capacity, one can followed proton uptake by the increase in external pH. The frequency of rotation of filaments in flagellar bundles were determined by monitoring the swimming speed—the experiments were done with a smooth-swimming mutant—given the ratio of swimming speed to bundle frequency determined separately by videotaping cells under phase-contrast microscopy and measuring their vibration frequencies by power spectral analysis; see Lowe *et al[88]*. Finally, the data were normalized to single motors by counting the number of cells and the number of flagellar filaments per cell. The total proton flux into the cell was much larger than the flux through its flagellar motors. However, the two were distinguished by suddenly stopping the motors by adding an anti-filament antibody—which cross-links adjacent filaments in flagellar bundles[1]. The change was found to be directly proportional to the initial swimming speed, as would be expected if a fixed number of protons carries a motor through each revolution. This number was estimated about 1200[88]. However, this number is still under discussion, especially when compared to others biological channel such as for example those encountered in neural cells which are 100 times larger and no other experiments have confirmed or refuted this evaluation, moreover this number has been observed only on one bacterium species, and should be confirmed on other species as *E. Coli*.

## b. The torque generation units

It has been established that the proton flow through the motor is divided into at least 12 distinct protons channels (or pairs of channels) [89] . Each torque generating units is called a stator. Several stators are present around the rotor and each one of them is independent from the others. For studying the energy developed by each stator, an approach called “resurrection” has been developed since the early days of bacterial genetics. By creating a non motile mutant exhibiting no MotA or MotB proteins, a transfection method based on the use of a phage lambda factor was develop to resurrect the motility of these mutant by generating new MotA and MotB proteins[90]. Then, two set ups have been proposed: the non motile mutants were sticked to a surface though the filament and the rotation of the full body analyzed[91], or the full cell being sticked, the filament is modified such as a bead is fixed on the hook [92]. Rotation of the cell or the bead is then recorded and analyzed[93]. By this way, for each new stator added to the motor structure, the speed of the tethered cell increases in a number of equally spaced steps indicating that each additional stator created, adds the same increment of torque, i.e applied the same force at the same distance from the axis of rotation. The main argument for 8 stators around the rotor was that resurrection of this kind produced 8 equally spaced levels more than once. Figure 14 illustrates typical results of Resurrection experiments. It has been also observed that the number of studs around the rotor, evaluated to 10 to 12 for *E.Coli* for example, do not match with these data. But this stud observation can also be incomplete, and experiments with slight excess of wild type MotA MotB have given an increase of 20 % of the torque. More recently, the number of steps has been re-evaluated using the same approach, but with more accuracy reported before and 11 steps could be identified. These new data fit with more agreement with structural observations[89]. However, it should be noticed that the different observation has been made by deduction, and direct observations of the stator spatial arrangement in vivo has not been achieved yet. The role of each stator is currently under discussion, due to the lack of data about in vivo architecture, and also about a possible synchronism between the stators. The rotation speed is linearly dependent on the Proton Motive Force (pmf), by increasing the pH gradient, the rotor spins faster, which confirms the role of the protons into the rotation.

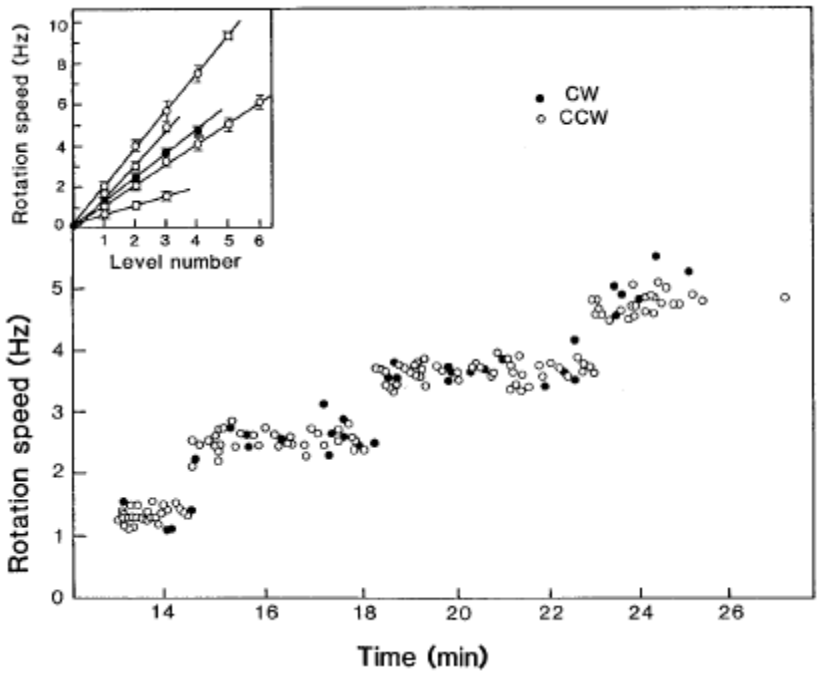


***Figure 14: Resurrection experiments****. Rotation speed of a tethered cell, showing the 4 first steps in rotation speed due to successive resurrection of stator units. [4]*

## c. Stepping

It is established that the conduction of each proton moves a stator (MotA/MotB complex) one step along the periphery of the rotor. This step is probably generated by a structural change within the stator complex, converting the electro chemical force to a torque applied on the rotor. The force is strong enough to stretch all stator components and rotate a tethered cell by a fix increment. This molecular machine behaves like a stepping motor, and the interaction between the rotor and one single stator can be easily compared to the work of two gears within a Swiss watch. Since the proton flow is likely to occur randomly, the steps will occur with exponentially distributed waiting times. Steps have been investigated since 1976[94] until recently, when Sowa *et al*[92] revealed 26 discrete steps, which could correspond to the FliG symmetry within the MS-ring. The method applied consisted in a direct observation of a rotating nano polysterene bead, fixed on single flagellum. A chimeric mutant *E.coli* has been created, exhibiting a controlled number of Sodium based nano-motor. Indeed, these authors had previously established that controlling the SMF was easier than the PMF. By adjusting the Sodium concentration, they were able to observe at low concentration the rotation of a single nano-bead generated by a single sodium stator complex. Previous studies on a full nanomotor have evaluated by a stochastic

approach the number of step around 400[95] and they concluded that the rotor was not free to execute Brownian motion, which means that the rotor and the stator are interconnected most of the time. This stochastic analysis has been pursued over the years [96]. By using the resurrection approach, it has been possible to evaluate that each "level" of resurrection increased the number of steps by 50. If we considered that there is between 8 to 11 stators around the rotor, this should create between 400 to 550 steps, which is in good agreement with reference 95. However, the difference between the steps measured by Sowa (26) and the number evaluated by stochastic approach (50) remains problematic.

## d. Torque relationship

The torque developed by the nano-motor has been widely studied through the years since the observation of the flagellum rotation. In order to evaluate the value of the torque developed by the nano-motor, the different approaches use a basic experiment of mechanics. Measuring the torque created by a motor is possible by defining the torque which will stop the rotation; this torque is sometimes called the "stall", because the rotation is stalled at this value. Studying the torque developed by the nano-motor has been made by two kinds of experiments, for low and high speed rotation regimes [97; 98] in order to define the torque/speed relationship. The main principle remained identical in both experiences: the nano-motor rotates an inert object (for example a nano-particle or the full cell body). Numerous techniques such as the electro rotation or optical trap have been used for stopping the rotation of the full bacterium cell after they were absorbed on a positively charged surface[97; 99; 100], or the rotation of a nano-particle attached on a sheared filament[101]. All these experiments, until recently [9; 89; 102; 103] gave the possibility to evaluate the torque and the rotation speed. The value of torque developed by the nano-motor has been evaluated from 2700 to 4500 pN.nm, the smaller value from estimates of the viscous drag on tethered cell, and the larger from force exerted by tethered cell on latex nano-bead held in an optical trap. It has also been identified that the speed is linearly dependent on the PMF, as described above, and also temperature dependent (see equation 1). However, it has been noticed that the actual temperature dependence (at low loads) is much higher than predicted by Eq.1.

The observed low speed and high speed regimes showed that the torque is constant until a certain speed value beyond which it declines sharply to zero. This behavior has been largely

discussed through the years and no clear structural answers have been proposed. However, George Oster *et al*[9] have recently developed a mathematical model which summarizes the different conditions of any model describing the motor function and also addresses the question of the vanishing of the torque at high speed. They proposed that a relaxation phenomenon occurred within the motor structure and this relaxation is mainly rotation speed dependent. However, no direct observation of this relaxation phenomenon has been proven or simulated within the motor structure and the structural reason of this drop is not established. By choosing a torque of 4000 pN.nm, and assuming that the torque generating units act at the periphery of the rotor of about 20nm, and considering between 8 and 12 units, we can concluded that each stator is able to develop a torque between 15 and 25 pN.nm. By calculating the energy developed by a single proton going into the cytoplasm of the bacterium through the stator, we found an equivalent torque of 27 pN nm. This value is close to the evaluated value of the torque developed by one stator. As noticed before, if we considered 52 steps (twice FliG numbers, see section Stepping), with a force and defined distance, we obtained a force of 11pN, so the passage of two protons for each step is likely. However, the real number of protons required for one step remains an open question, which could lead to other conclusions about the torque developed by each stator.

## e. Switching

Despite a role comparable to a motor of an helix, the motor is also able to rotate in both directions, ClockWise (CW) and CounterClockWise (CCW) with the same efficiency. Due to the helix shape, the bacterium is running while the rotor turns CCW and tumbles when the rotor switches to CW. However, the bacterium is not able to maintain a CCW or CW state for a long period of time but is able to bias the CCW/CW for a short period depending on its external environment [104]. Some pauses can occur during the switching process, but they never exceed 1 ms (3% of the time) and all the switching is done within that time[105].

When switching occurs, it appears to be a binary process; one does not see motor steps going on opposite direction. This observation indicates that all the force generating units act together to switch and are not independent[105; 106]. It also reveals that the conformation changes must occur synchronously in the rotor structure, probably somewhere in the C-ring/ Stator interface due to the binding of CheY-P to FliM. As described by Khan and Macnab [84] or

Macnab[107], the switching is a thermal isomerization in which the system present only two possible states for the rotor, CW and CCW state with a respective energy Gcw and Gccw, with K+ and K- representing the transition rates between both states, and Gt, the free energy needed to jump from CCW to CW. K+ and K- are characterized by a factor which represents the frequency at which the system tried to jump from one state to the other, and also a factor which represents the probability that there is enough energy to cross the activation barrier $Gt-G_{cw}$ and $Gt-G_{ccw}$. The ratio of probability $K+/K- = \exp^{(-(Gcw-Gccw)/KT)}$. This simple two states system can be represented on free energy diagram shown in figure 15.

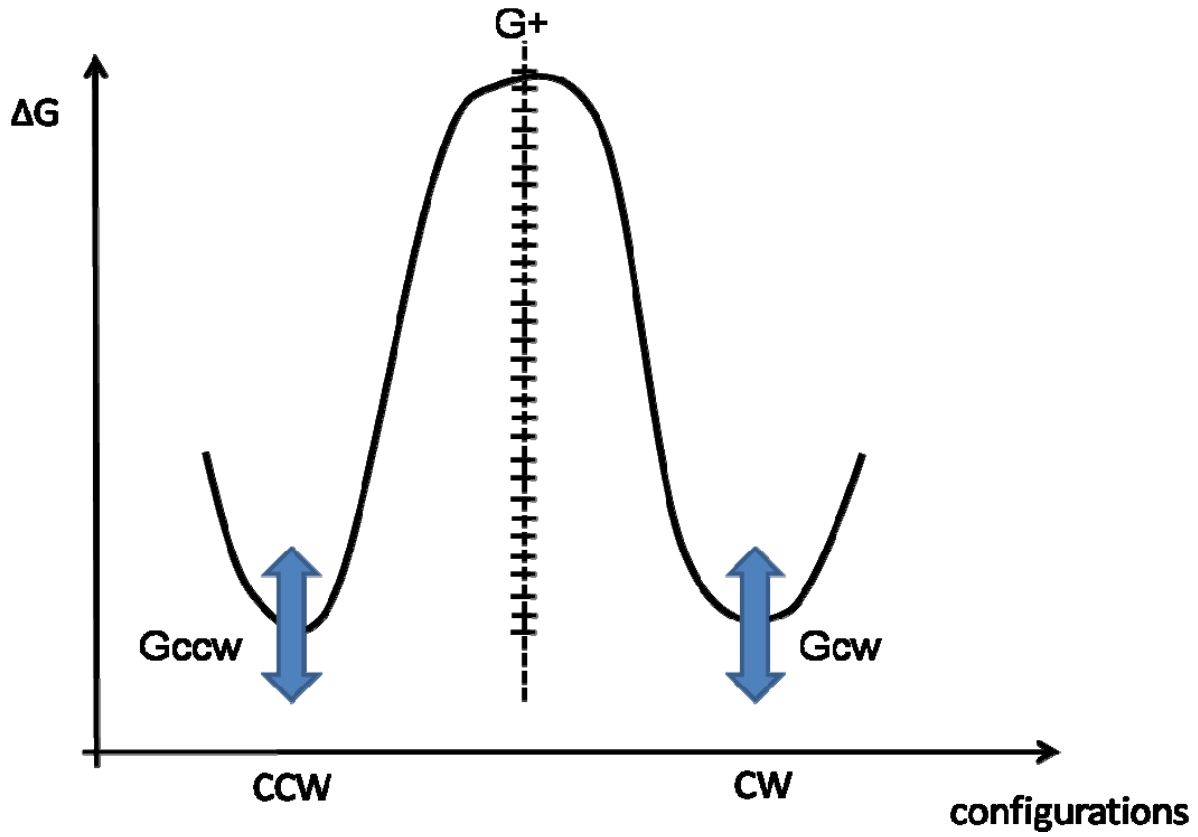


***Figure 15: Free energy diagram describing the two states corresponding to the two directions of rotation of the motor.*** *Two stables states are represented, the CCW and CW. Depending on the spatial arrangement of the proteins, the energy level of each state increases or decreases under control of interactions between CheY-P and the C-ring.*

By changing the temperature or the ratio between CheY and CheY-P in the cytoplasm, the energy level of each state can be adjusted (For example, the absence of CheY-P leads to a CCW behavior, Gccw is much smaller than Gcw)[108; 109]. Several studies addressed the question of chemotactic signaling[110] and some results are summarized in figure 16, presenting a plot of

FliM occupancy versus free cytoplasmic CheY-P. Scharf *et al* model[110] can be resumed as follow, each CheY-P/FliM binding event subtracts a small amount of energy, called "r", which was evaluated to a multiple of kT [111] to ΔG which means that Gccw increased by the same amount than Gcw decreased. When there is enough energy subtracted or added, the rotor is able to shift from one state to the other. A so-called "Allosteric model" [112] describes the switching process. The predictions of this model give similar results, based on the assumption that the probabilities of switching are affected by the stabilization of each state. This model did not explain the change which happens in the C-ring shape which is the basis of the switching mechanism; it describes only the behavior of the different elements and discusses energetically issues. Others studies, based on FRET effect between two fluorophores, here FliM-CFP and CheY-YFP[113], or the amount of CheY-YFP in the cytoplasm have also evaluated the number of binding events of CheY-P to FliM. Some results are shown in figure 16. They evaluated the occupancy of FliM related to the concentration of CheY-P and its role to the CW or CWW behavior.

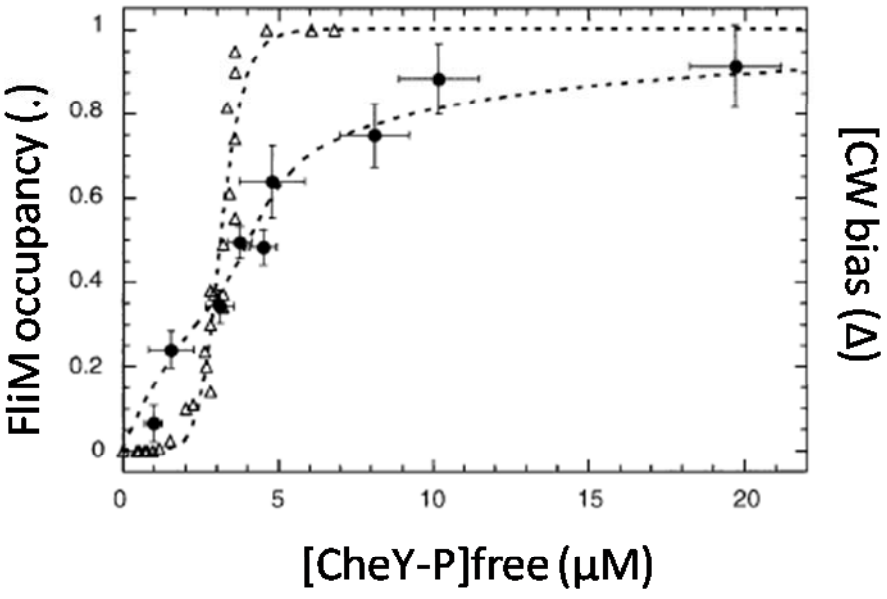


***Figure 16: Plot of FliM occupancy versus the concentration of free cytoplasmic CheY-P***. *Dashed lines are fits using an allosteric model [4] (Bias data is from Cluzel et al, Science 2000)*

A more general stochastic model[114] has been developed in which a ring of proteins, 34 FliM, displays cooperative interactions. Each protein can adopt two configurations, CW and CCW, and the direction of rotation depends upon how many proteins are in either state. Given a large enough coupling energy between adjacent FliM, the ring switches from a state in which nearly all the proteins are in a CW configuration to one in which nearly all proteins are in the CCW configuration. This model also accommodates pauses, which could be frequent when the coupling energy is small and the proteins tend to behave independently. However, all these models did not give an intrinsic view of the possible change within the C-ring structure neither the interaction with the stator. The structure of 3 switch proteins; FliG, FliM and FliN recently obtained have not been taken into account for the elaboration of a new model describing the switching mechanism. In summary, it is clear that a threshold number of CheY-P proteins bound to the C-ring is required for inducing the switching but the structural change occasioned on the C-ring resulting in the direction reversal is not elucidated and rarely discussed.

## E) Open Questions

Blair's model describes how the motor works, but several hypotheses proposed have not been confirmed by experimental results or observations. As described above, the different hypotheses were mainly based on indirect observation, mutagenesis on living bacteria and also on frozen extracted elements. Several questions arise when we take a deeper look into the current view of the nano-motor function.

### a. Stator function and assembly

-Each stator is composed of 4 MotA and 2 MotB, and composed of 2 proton channels.

This observation has been deduced from extraction of stator elements from bacteria [38]. The same spatial organization has been proposed to other members of the same protein family, for example TolA/TolB but no direct observation in vivo of the arrangement which confirm this assembly has been obtained. The role of the two proton channels remains ambiguous. Blair *et al* proposed that both protons channels worked as a unit, and the rotation is created thanks to an asymmetry structure of the rotor. How does the stator manage to direct the power stroke from one to the other sub-unit? Why does each stator need two subunits? Is there any synchronism between

these two subunits? Could the FliG be involved? The estimated numbers of proteins per flagellum found an average numbers of 16 MotB and 32 MotA, but the recent results have not confirmed these numbers. Why is there a difference between the "in vivo" number evaluation, 32 MotA, and the in vitro measurement 64 MotA [34; 38]? Figure 17 shows a bottom view of the stator complex, exhibiting 2 MotB embedded in 4 MotA. This assembly has been deduced from multiple mutagenesis experiment coupled to the recent evaluation of the molecular weight of one stator.

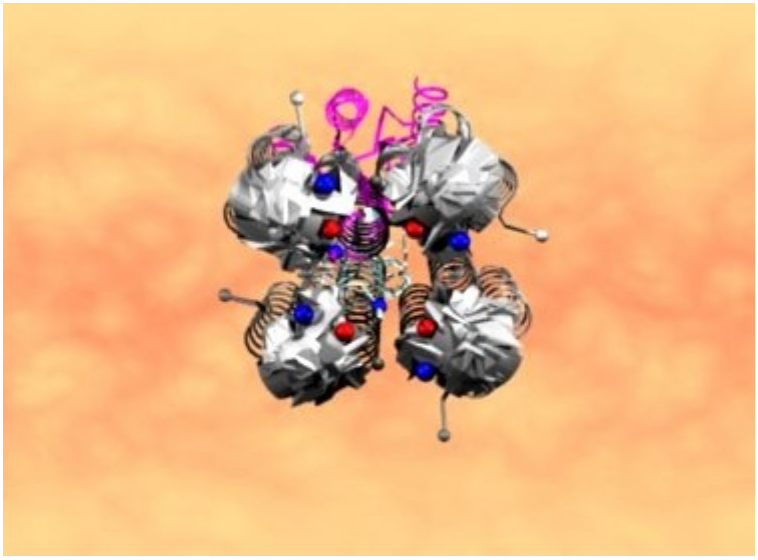

***Figure 17: Bottom view of the stator complex, exhibiting 4 MotA-cytoplasmic structures (unknown) and 2 Mot****B.*

-The bias-rotational behavior is generated by the presence of two sub-units within each stator complex, both of them creates a torque.

Both MotA and MotB structures are still unknown which prevents any proposal of deformation. However, the number of proteins and how they interact are crucial points. If the stator is composed of 4MotA and 2 MotB, the stator is divided into two sub-units, 2MotA 1MotB. Does each sub-unit generate a specific direction torque? Or does each sub-unit generate both direction and the FliG-C domain manages to interact with a specific part of the sub-unit? How does the proton channel work and choose which sub-unit has to be activated? The torque is expected to originate from a spatial deformation of MotA-C which moves the charged amino R90, E98 and E150, which then interact with the FliG-C charged amino acids. This movement, is vertical or horizontal? If vertical, how could we explain the creation of the rotation if the FliG-C is flexible? If the movement is horizontal, how can we explain the role of each stator sub unit and

how the FliG-C have access to the interaction site? How can it be that the FliG-C firmly is attached in order to resist the force coming from the MotA-C meanwhile flexible for allowing the CW/CCW switching process? And more important, how the FliG, supposedly at the top of the C-ring can interact with one subunit, and then after with the second one from the stator? FliG-C should extend itself several nanometers, probably more than 3 nanometers, to change its interactions site, but how is it possible in such dense place without altercating the motor function? We can expect that the cytoplasmic part of both MotA can deform, but the switching is related to FliG, not the stator. How could the protein, which has been partially crystallized, deform and increase its length by more than twice, especially in that case where there are two sites on interaction with the FliM, the gly-gly site and the EHSPQR site? And if the FliG-C must be flexible, how does it manage to stay aligned with MotA-C? Figure 18 shows the problem behind revealed by this hypothesis.

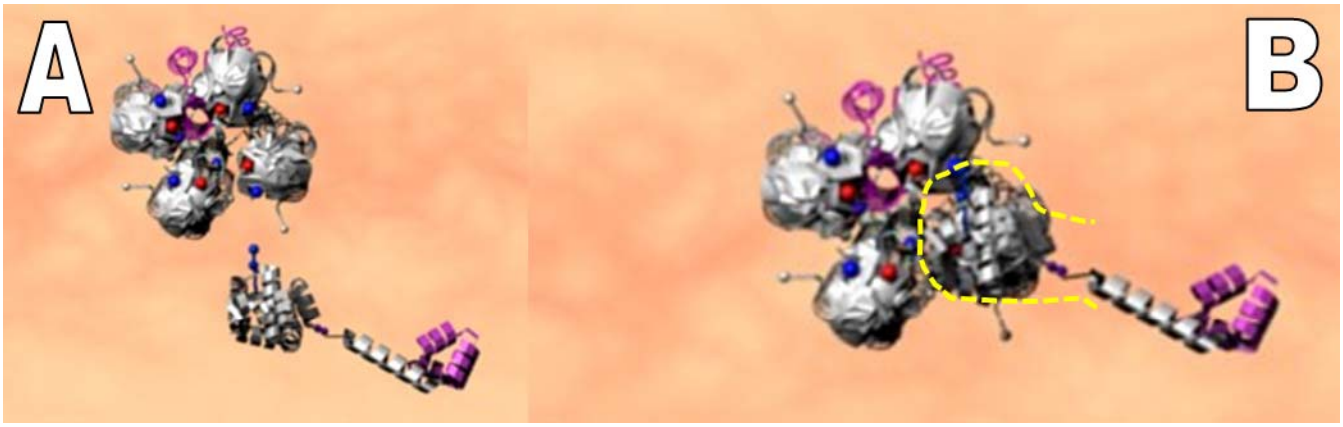


***Figure 18: Structural bottom view of the MotA-C/ FliG interactions****. A/ Proteins separated. B:/FliG interacts with MotA respecting cryo-TEM assembly. None of all sites are accessible for the C-terminal of FliG, delimited by the yellow trace.*

-Protons are bonding to Asp32, at the cytoplasmic side of the MotB protein. The bonding-releasing step creates the mechanical energy.

Asp32 is fundamental in the motor function, and its negative charge tends to favor a bonding/releasing process. However, the role of Asp32 could be very different. How are the protons released after they bind to Asp32? How does the Asp32, or in general the proton channel, handle the flow of protons? How are the protons released by the Asp32 despite the electrostatic interaction? None of these questions have been clearly answered by the previous models, which just proposed that the structural change of MotA and MotB proteins is responsible of that.

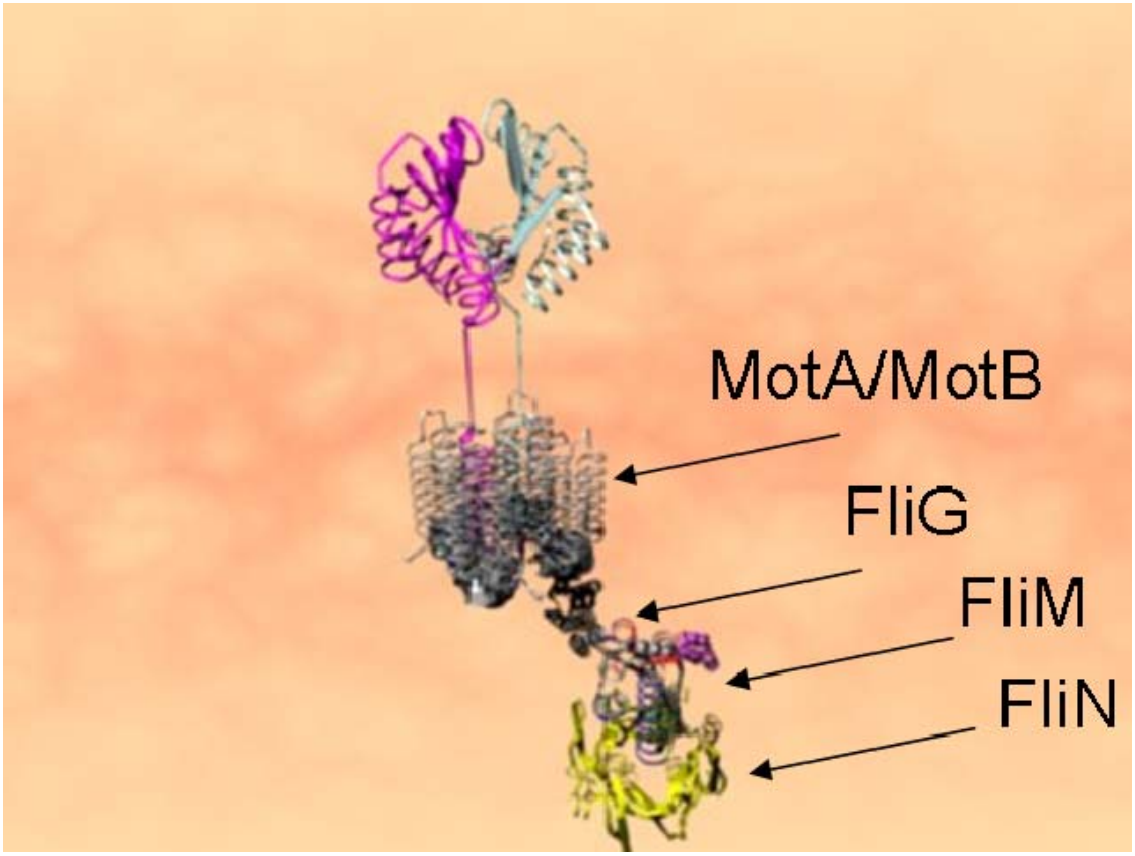


***Figure 19: Possible architecture of the different proteins, using an hypothesis of 4MotA, 2 MotB, 1 FliG 1 FliM 4 FliN***

-The MotA cytoplasmic part (MotA-C) is interacting with FliG proteins and this creates the rotation.

60 % of the MotA proteins are found into the cytoplasm, and amino acids of this part have been identified to interact with the FliG-C domain. The position of FliG-C domain in the nano-motor structure is then crucial to account for the interaction with MotA-C. The current view of the nano-motor locates FliG at the top side of the C-ring, and the FliG ring links the C-ring to the rotor. Figure 19 shows the current hypothesis of spatial arrangement of the motor proteins. The pictures obtained by TEM do show a C-ring sticked to the rotor, but the protocol of extraction does not remove the stator from the cell. Despite this point, the position of the stator proteins has been proposed just on the top of the C-ring. How does fit the cytoplasmic part of the MotA here? Figure 19 describes this structural problem. The MotA-C (MotA-Cytoplasmic part) is responsible of the rotation, but what could be the deformation responsible for that? Blair's and Berry's models proposed that when the protons bind to the MotB ASP32, they create a vertical

deformation of MotA-C. The deformation is a vertical one and due to an asymmetry of the FliG ring, it engenders the rotation. This idea is attractive, but one major default can be noticed: the force generated is vertical, not lateral, which means that it must exist a strong link between the C-ring and the rotor for transferring the torque to the rotor. However, this strong bonds has not been observed into the frozen capture reconstitution[54], which present a weak atomic density at this position. How does the C-ring remain linked to the rotor while each stator unit vertically pressures it? We can easily say that the force generated by the MotA-C is released by the lateral movement of the FliG-C, again, the FliG ring should be firmly attached and this bond should be visible using cryo-TEM.

-10 to 16 studs have been observed around the rotor in native membrane.

The main question here is how do all the stators work? How do they assemble? It has been proposed that each stator freely move within the inner membrane since it "meets" one rotor, then the peptidyloglycan site of the MotB firmly attaches the full complex to the cell wall meanwhile opening the proton channels. How the stator "feels" the rotor is ready to start? How does the stator complex avoids a non controlled assembly around the rotor? We can easily estimate the horizontal length of one complex, and compare it to the space available around the rotor. (See chapter 4). More than 12 complexes can fit in, how the motor could say "No thanks, I already have 8 complexes" if there is enough rooms for more? How does the number of complex influence the rotation speed? Numerous papers do not show that the rotor accelerates by 11 steps at maximum, but we do not know yet if there is just only 11 complexes, or maybe 22 synchronized? The resurrection studies tend to show that each stator act independently from the others but the questions of the existence of a relationship between each stator complex is still open. Figure 20 shows a top view which respects the dimension of each element. 8 stators are shown, but more stators can fit in the space left.

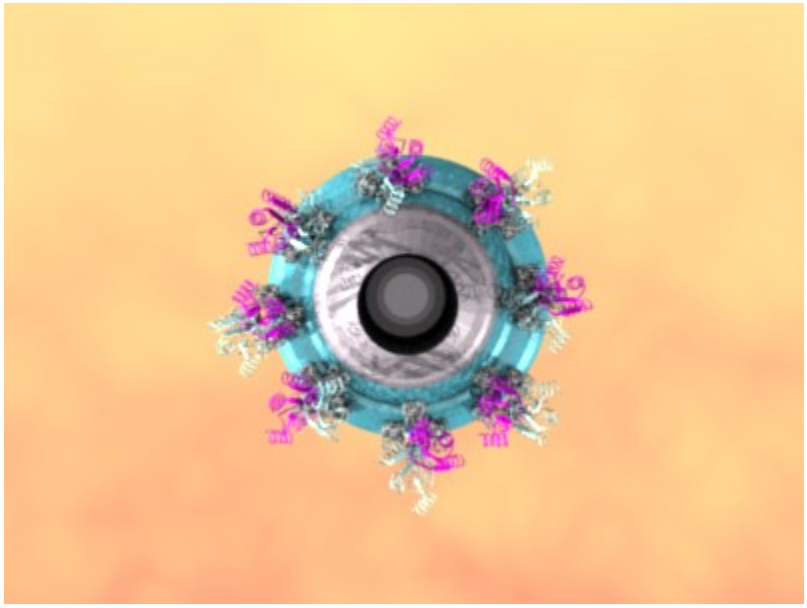

***Figure 20: Top view of the rotor surrounded by 8 stators sub units.***

## b. Interaction between the C-ring and the rotor

-The CheY-P binding FliM

While we assume that the C-ring is rotating as a unit with the rotor, the binding site FliM rotates at a high speed. The C-ring diameter is around 45 nm, each FliM is rotating at a speed of 30 µm/s, how can the CheY-P manage to bind? Specific interactions mechanisms are there compatible with such a rotation speed? The time to diffuse a distance of 45 nm is less than $10^{-4}$ second so it could be feasible. However, the precise and inner mechanism is unclear.

-The C-ring is firmly bonded to the rotor with the FliG proteins.

The rotor is fastly rotating, more than 300 rotations per second for some species, how the C-ring can rotate as fast into the cytoplasm? As far as you go from the cytoplasm to the external part of the cell, each compartment exhibits a lower density which could explain why the rotor is able to rotate without damaging the cell structure. But the cytoplasm is a dense viscous media, which could be comparable to honey by some ways[115; 116] , how does the C-ring rotate and why it is not damaged by all the proteins encountered inside the cytoplasm? We can imagine the formation of water molecules thanks to the incoming protons, which could reduce the friction of the C-ring in the cytoplasm, but this point remains not clear.

## c. Protons destiny and role

-The source of energy is a proton trans-membrane gradient and between 550 and 1200 protons are needed for each turn, which gives a number of 65 protons/stator/rotation.

Where are going all the protons? An easy calculation estimates that for a speed rate of 100 Hz, 100 rotations per second, there would be 120 000 protons going through the stator and inside the cytoplasm, and more than 7 millions of protons in one single minute! How the bacteria manage all these protons? How the motor proteins keep their shape with this amount of protons around? The different motor protein present a specific shape while they assemble, is their shape pH dependent?

## d. Protein positions

-$FliM_1FliN_4$ are likely to be the sub-units organization within the C-ring.

How do they self-organize? Where do we locate FliG? The structures of FliM FliN and FliG are available but no architecture of one C-ring element has been yet proposed, why? The assembly is mainly hypothetical, and no direct observation has confirmed or declined it. What is the role played by the FliN4 structure? Numerous questions arise about the C-ring organization and assembly. FliM is likely to interact with other FliMs, and it represents the backbone of the C-ring, FliM also interacts with FliN because no other proteins have been identified to interact with FliN, but also with FliG through two sites of the FliG, but also with CheY-P. It makes 4 interactions for one single element of the motor, while the FliN just interact with itself in order to form a tetramer. If we consider this hypothesis as a fact, the FliM would be the only link between the 34 sub-units which composed the C-ring, and makes its role fundamental for the structure and the rotation of the rotor. However, the precise emplacement of the FliM remains ambiguous, despite the recent proposal from Blair [13; 14].

-FliG is the key protein of the motor and interacts with FliM for the switching process, with MotA for the rotation generation and also with FliF as the basis of the rotor. There are 26 FliG, or a symmetry of 26 elements at the basis of the rotor, and 34 to 36 FliM on the C-ring.

As described above, FliG plays a fundamental role within the motor structure but despite its role, its precise localization remains not clear, and its interactions with the FliM still under discussion. The asymmetry numbers between FliG and FliM, but not between FliG and FliF let us think that the interaction between FliG and FliM could be different than between FliF and FliG. The structure of FliG has only resolved the C and M domains of the FliG protein, and the N terminal is still unresolved, which means that the global structure proposed earlier could change dramatically due this unknown domain. The size of the FliG ring, called M-ring is important, because as it is normally found at the cytoplasmic side of the MS-ring, its size can reveal the role played by the FliG within the motor, and also its interaction with the FliM, FliF and MotA. The different hypothesis about its position will be extensively discussed in this research work.

## F) Conclusions

As described during these pages, the Bacterial Flagellum Nano-motor is an amazing machinery at the nano-scale, composed of thousands of pieces, which all work together for propelling the bacterium and allowing its survival. Despite its complexity, only six proteins are directly involved into the rotation and switching process, but the role, interactions and precise positions remain ambiguous (see the list of open questions reported before). *In vivo* and *In vitro* approaches highlighted some aspects of the BFNM: *In vivo* by physical and mechanical data about the motor by observing the filament rotation, and *in vitro*, by extensive mutagenesis studies and crystallography, or structural advances by observing part of the motor using cryo-TEM. But each approach has also shown limitations, for example the extraction protocol of the rotor reduces the number of extracted elements and could also change the interaction between the motor pieces. Crystallography coupled to mutagenesis has given numerous structures of single elements, but these elements taken separately do not solve the supra-molecular architecture. As noticed recently by Takuji Mashimo *et al* [117] on their most recent FliG mutagenesis: "However, if the components form a supra-molecular structure like the C-ring, it is not straightforward enough to identify the functional sites on each proteins by the same genetic method" and they concluded by "We stress again that the data from genetic analyses and molecular biological experiments do not necessarily indicate direct interactions between components of interest in a supra-molecular structure…We need a new model that satisfy all data". The new approach, as for example the reconstitution into liposome of part of the motor

opened an interesting new way for studying the motor, by mimicking the native environment, by recreating the *In vivo* in *vitro,* by developing a controlled way to recreate the motor in vitro.

Let us now compare our study of the BFNM to the work of Swiss watch maker. He has received a swiss watch and he does not know how the watch works. He has identified all the components, thank to the seller, and he has an approximate map of the location of the pieces. This could be comparable to the definition of the BFNM genes, and the microscopy results. Then, one of the current approach consists in changing the shape of a single element, and ordering a new watch exhibiting this change. By comparing the old and the new watch, the watch maker deduces the role played by the modified piece. This summarizes the mutagenesis approach. He can also ask for the shape of the most important elements, extracted form the watch, this can be compared to the crystallography approach, but some pieces resist to this process, as for example the trans-membrane proteins MotA MotB and FliF, which limits the knowledge about the full watch. He can put some constraint on the watch, in order to define the rotation force, this is the biophysical approach, and finally he can also extract some parts outside the watch, more or less important for the watch, and observe their shape, size and symmetry. This is the cryo-TEM protocols. Despite all his effort, he is not sure he really knows how the watch works and he is not able to build it. Then he has a new idea, instead of starting by the full watch, he tried to build the core of the watch piece by piece, and observe the assembly step by step, with a final objective in mind, building in a controlled way the watch. In order to do that, he will use the known data, which pieces of the motor are crucial for its function, and order them. Then, he will try to study the interaction between theses pieces, but not as previously, in an environment close to the native one, the one found in the full watch while working, with the different constraints and conditions. These data will give him a better understanding of the watch mechanism. Then, he will use the pieces and let them interact together, trying to assemble, to self-assemble these pieces, assembles the full watch motor on a surface. He will reach two objectives at the same time, he will discover how the watch works, and also he will know how to build it, and maybe one day use it for other purposes. This example is a metaphor of my doctoral research work. Instead of assembling a watch, I tried to assemble the flagellar nano-motor of bacteria from purified proteins composing it. I developed a way to study the interaction between those proteins, using new tools which allow working in a controlled media, and I developed a technology which couples the natural self-assembly of proteins or motor elements, and the capability given by the nanobiotechnology to

create complex engineered surfaces. Working on the full motor was a big challenge, a challenge that can not be addressed within a thesis, but I tried to address 3 questions about the BFNM. Who is working with whom? Where is FliG? Is a new model possible to explain the BFNM mechanism? The assumption of this work is not to answer the long list of questions still open concerning the nano-motor, but rather to propose to the community a new methodological approach for investigating this fascinating machine. It is likely that, as always in science, the new data I will generate will raise more new questions than they will solve. It is up to the reader of this document to make his own feeling.

[1]H.C. Berg, R.A. Anderson, Nature 245 (1973) 380.
[2]G.H. Wadhams, J.P. Armitage, Nat Rev Mol Cell Biol 5 (2004) 1024.
[3]Q. Wen, G. Li, J. Tang, G. Huber, Journal of Statistical Physics 128 (2007) 257.
[4]H.C. Berg, Annual Review of Biochemistry 72 (2003) 19.
[5]R. Schmitt, Biophys. J. 85 (2003) 843.
[6]M.D. Manson, J. Bacteriol. 189 (2007) 291.
[7]D.R. Thomas, D.G. Morgan, D.J. DeRosier, Proceedings of the National Academy of Sciences 96 (1999) 10134.
[8]D.F. Blair, FEBS Letters
Protonmotive Mechanisms of Energy Transducing Enzymes 545 (2003) 86.
[9]J. Xing, F. Bai, R. Berry, G. Oster, Proceedings of the National Academy of Sciences 103 (2006) 1260.
[10]M.D. Manson, P. Tedesco, H.C. Berg, F.M. Harold, C.V.D. Drift, Proceedings of the National Academy of Sciences 74 (1977) 3060.
[11]R.E. Silversmith, R.B. Bourret, Trends in Microbiology 7 (1999) 16.
[12]M.M. McEvoy, A. Bren, M. Eisenbach, F.W. Dahlquist, Journal of Molecular Biology 289 (1999) 1423.
[13]S.-Y. Park, B. Lowder, A.M. Bilwes, D.F. Blair, B.R. Crane, Proceedings of the National Academy of Sciences 103 (2006) 11886.
[14]P.N. Brown, M. Terrazas, K. Paul, D.F. Blair, J. Bacteriol. 189 (2007) 305.
[15]M.A. Swan, J. Bacteriol. 161 (1985) 1137.
[16]N.R. Francis, V.M. Irikura, S. Yamaguchi, D.J. DeRosier, R.M. Macnab, Proceedings of the National Academy of Sciences of the United States of America 89 (1992) 6304.
[17]N.R. Francis, G.E. Sosinsky, D. Thomas, D.J. DeRosier, Journal of Molecular Biology 235 (1994) 1261.
[18]M.L. DePamphilis, J. Adler, J. Bacteriol. 105 (1971) 376.
[19]M.L. DePamphilis, J. Adler, J. Bacteriol. 105 (1971) 384.
[20]M.L. DePamphilis, J. Adler, J. Bacteriol. 105 (1971) 396.
[21]T. Suzuki, Y. Komeda, J. Bacteriol. 145 (1981) 1036.
[22]T. Kubori, S. Yamaguchi, S. Aizawa, J. Bacteriol. 179 (1997) 813.
[23]T. Ueno, K. Oosawa, S.-I. Aizawa, Journal of Molecular Biology 227 (1992) 672.
[24]K. Oosawa, T. Ueno, S. Aizawa, J. Bacteriol. 176 (1994) 3683.
[25]P.N. Brown, C.P. Hill, d.F. Blair, The EMBO journal 21 (2002) 3225.
[26]D. Thomas, D.G. Morgan, D.J. DeRosier, J. Bacteriol. 183 (2001) 6404.
[27]T. Yorimitsu, A. Mimaki, T. Yakushi, M. Homma, Journal of Molecular Biology 334 (2003) 567.
[28]J. Zhou, D.F. Blair, Journal of Molecular Biology 273 (1997) 428.
[29]S.A. Lloyd, D.F. Blair, Journal of Molecular Biology 266 (1997) 733.
[30]B.J. Lowder, M.D. Duyvesteyn, D.F. Blair, J. Bacteriol. 187 (2005) 5640.
[31]A. Garza, P. Bronstein, P. Valdez, L. Harris-Haller, M. Manson, J. Bacteriol. 178 (1996) 6116.
[32]J. Zhou, R.T. Fazzio, D.F. Blair, Journal of Molecular Biology 251 (1995) 237.
[33]A.G. Garza, R. Biran, J.A. Wohlschlegel, M.D. Manson, Journal of Molecular Biology 258 (1996) 270.
[34]S.M. Van Way, E.R. Hosking, T.F. Braun, M.D. Manson, Journal of Molecular Biology 297 (2000) 7.
[35]A. Roujeinikova, Proceedings of the National Academy of Sciences 105 (2008) 10348.

[36]S. Kojima, D.F. Blair, Biochemistry 43 (2004) 26.
[37]T.F. Braun, L.Q. Al-Mawsawi, S. Kojima, D.F. Blair, Biochemistry 43 (2004) 35.
[38]T.F. Braun, D.F. Blair, Biochemistry 40 (2001) 13051.
[39]H.G. Ridgway, M. Silverman, M.I. Simon, J. Bacteriol. 132 (1977) 657.
[40]R.L.J.N.S. Eric Cascales, Molecular Microbiology 42 (2001) 795.
[41]Yu Feng Zhai, W. Heijne, M.H.S. Jr, Biochemica and Biophysica acta 1614 (2003) 201.
[42]J.W. Coulton, R.G. Murray, J. Bacteriol. 136 (1978) 1037.
[43]S. Khan, M. Dapice, T.S. Reese, Journal of Molecular Biology 202 (1988) 575.
[44]S. Khan, D.M. Ivey, T.A. Krulwich, J. Bacteriol. 174 (1992) 5123.
[45]D.F. Blair, D.Y. Kim, H.C. Berg, J. Bacteriol. 173 (1991) 4049.
[46]J.V. René Mot, Molecular Microbiology 12 (1994) 333.
[47]J. Zhou, L.L. Sharp, H.L. Tang, S.A. Lloyd, S. Billings, T.F. Braun, D.F. Blair, J. Bacteriol. 180 (1998) 2729.
[48]E.R. Hosking, M.D. Manson, J. Bacteriol. 190 (2008) 5517.
[49]T.F. Braun, S. Poulson, J.B. Gully, J.C. Empey, S. Van Way, A. Putnam, D.F. Blair, J. Bacteriol. 181 (1999) 3542.
[50]P.N. Brown, M.A.A. Mathews, L.A. Joss, C.P. Hill, D.F. Blair, J. Bacteriol. 187 (2005) 2890.
[51]K. Paul, D.F. Blair, J. Bacteriol. 188 (2006) 2502.
[52]K. Paul, J.G. Harmon, D.F. Blair, J. Bacteriol. 188 (2006) 5240.
[53]T. Minamino, K. Imada, K. Namba, Current Opinion in Structural Biology (2008).
[54]D.R. Thomas, N.R. Francis, C. Xu, D.J. DeRosier, J. Bacteriol. 188 (2006) 7039.
[55]A. Shin-Ichi, Molecular Microbiology 19 (1996) 1.
[56]R.M. Macnab, J. Bacteriol. 181 (1999) 7149.
[57]T. Suzuki, T. Iino, T. Horiguchi, S. Yamaguchi, J. Bacteriol. 133 (1978) 904.
[58]K. Kutsukake, Y. Ohya, T. Iino, J. Bacteriol. 172 (1990) 741.
[59]Y. Komeda, J. Bacteriol. 150 (1982) 16.
[60]R. Liu, H. Ochman, Proceedings of the National Academy of Sciences 104 (2007) 7116.
[61]X. Liu, P. Matsumura, J. Bacteriol. 176 (1994) 7345.
[62]T.B. Adler J, J. gen microbiology 46 (1967) 175.
[63]W. Shi, Y. Zhou, J. Wild, J. Adler, C.A. Gross, J. Bacteriol. 174 (1992) 6256.
[64]B.M. Pruss, P. Matsumura, J. Bacteriol. 179 (1997) 5602.
[65]S.I. Aizawa, T. Kubori, Genes to Cells 3 (1998) 625.
[66]T. Kubori, N. Shimamoto, S. Yamaguchi, K. Namba, S.-I. Aizawa, Journal of Molecular Biology 226 (1992) 433.
[67]J. Malakooti, B. Ely, P. Matsumura, J. Bacteriol. 176 (1994) 189.
[68]K. Ohnishi, F. Fan, G.J. Schoenhals, M. Kihara, R.M. Macnab, J. Bacteriol. 179 (1997) 6092.
[69]T. Minamino, R.M. Macnab, J. Bacteriol. 182 (2000) 4906.
[70]M. Kihara, T. Minamino, S. Yamaguchi, R.M. Macnab, J. Bacteriol. 183 (2001) 1655.
[71]K.O.N.R.F.R.M.M. Fan Fan, Molecular Microbiology 26 (1997) 1035.
[72]A.P. Vogler, M. Homma, V.M. Irikura, R.M. Macnab, J. Bacteriol. 173 (1991) 3564.
[73]G. Dreyfus, A.W. Williams, I. Kawagishi, R.M. Macnab, J. Bacteriol. 175 (1993) 3131.
[74]K. Yonekura, S. Maki-Yonekura, K. Namba, Research in Microbiology 153 (2002) 191.
[75]S. Makishima, K. Komoriya, S. Yamaguchi, S.-I. Aizawa, Science 291 (2001) 2411.
[76]B. Stolz, H.C. Berg, J. Bacteriol. 173 (1991) 7033.
[77]K. Yonekura, T. Yakushi, T. Atsumi, S. Maki-Yonekura, M. Homma, K. Namba, Journal of Molecular Biology 357 (2006) 73.

[78]E. Katayama, T. Shiraishi, K. Oosawa, N. Baba, S.-I. Aizawa, Journal of Molecular Biology 255 (1996) 458.
[79]S. Khan, I.H. Khan, T.S. Reese, J. Bacteriol. 173 (1991) 2888.
[80]S. Khan, J. Bacteriol. 175 (1993) 2169.
[81]H. Suzuki, K. Yonekura, K. Namba, Journal of Molecular Biology 337 (2004) 105.
[82]G.E. Sosinsky, N.R. Francis, M.J.B. Stallmeyer, D.J. DeRosier, Journal of Molecular Biology 223 (1992) 171.
[83]S.H. Larsen, J. Adler, J.J. Gargus, R.W. Hogg, Proceedings of the National Academy of Sciences of the United States of America 71 (1974) 1239.
[84]S. Khan, R.M. Macnab, Journal of Molecular Biology 138 (1980) 563.
[85]S. Khan, R.M. Macnab, Journal of Molecular Biology 138 (1980) 599.
[86]C. van der Drift, J. Duiverman, H. Bexkens, A. Krijnen, J. Bacteriol. 124 (1975) 1142.
[87]M.D. Manson, P.M. Tedesco, H.C. Berg, Journal of Molecular Biology 138 (1980) 541.
[88]G. Lowe, M. Meister, H.C. Berg, Nature 325 (1987) 637.
[89]S.W. Reid, M.C. Leake, J.H. Chandler, C.-J. Lo, J.P. Armitage, R.M. Berry, Proceedings of the National Academy of Sciences 103 (2006) 8066.
[90]B.H. Blair DF, Science 242 (1988) 1678.
[91]M. Silverman, M. Simon, Nature 249 (1974) 73.
[92]Y. Sowa, A.D. Rowe, M.C. Leake, T. Yakushi, M. Homma, A. Ishijima, R.M. Berry, Nature 437 (2005) 916.
[93]S.M. Block, H.C. Berg, 309 (1984) 470.
[94]B. HC., ed. R Goldman, T Pollard, J Rosenbaum (1976) 47.
[95]A. Samuel, H. Berg, Proceedings of the National Academy of Sciences 92 (1995) 3502.
[96]A.D. Samuel, H.C. Berg, Biophys. J. 71 (1996) 918.
[97]H.C. Berg, L. Turner, Biophys. J. 65 (1993) 2201.
[98]R.M. Berry, H.C. Berg, Proceedings of the National Academy of Sciences 94 (1997) 14433.
[99]R.M. Berry, L. Turner, H.C. Berg, Biophys. J. 69 (1995) 280.
[100]D.C. Fung, H.C. Berg, 375 (1995) 809.
[101]X. Chen, H.C. Berg, Biophys. J. 78 (2000) 1036.
[102]J. Yuan, H.C. Berg, Proceedings of the National Academy of Sciences 105 (2008) 1182.
[103]G. Li, J.X. Tang, Biophys. J. 91 (2006) 2726.
[104]M. Eisenbach, A. Wolf, M. Welch, S.R. Caplan, I.R. Lapidus, R.M. Macnab, H. Aloni, O. Asher, Journal of Molecular Biology 211 (1990) 551.
[105]S. Kudo, Y. Magariyama, S.-I. Aizawa, Nature 346 (1990) 677.
[106]M. Meister, S.R. Caplan, H.C. Berg, Biophys. J. 55 (1989) 905.
[107]R.M. Macnab, Am. Soc. Microbiol (1995) 181.
[108]L. Turner, S.R. Caplan, H.C. Berg, Biophys. J. 71 (1996) 2227.
[109]K. Prasad, S.R. Caplan, M. Eisenbach, Journal of Molecular Biology 280 (1998) 821.
[110]B.E. Scharf, K.A. Fahrner, L. Turner, H.C. Berg, Proceedings of the National Academy of Sciences of the United States of America 95 (1998) 201.
[111]U. Alon, L. Camarena, M.G. Surette, B.A.y. Arcas, Y. Liu, S. Leibler, J.B. Stock, The EMBO journal 17 (1998) 4238.
[112]Monod.J, Wyman.J, C. J-P, J. Mol. Biol 12 (1965) 88.
[113]V. Sourjik, H.C. Berg, Proceedings of the National Academy of Sciences of the United States of America 99 (2002) 12669.
[114]T.A.J. Duke, N. Le Novere, D. Bray, Journal of Molecular Biology 308 (2001) 541.
[115]V.A. Fushimi K, J . Cell Bio 112 (1991) 19.

[116]P.N. Bicknese S, Shohet SB, Verkman AS., Biophys J. 65 (1993) 1272.
[117]T. Mashimo, Hashimoto, Manami, Yamaguchi, Shigeru, Aizawa, Shin-Ichi, J. Bacteriol. 189 (2007 ) 5153.

# Chapter II

# Who is working with who?

# Interactions

Summary

# A) Chemistry and Biochemistry techniques

## a. Introduction

The study of protein-protein interactions can be conceptually divided into major domains: identification of the biological problem, characterization of the diverse elements and manipulation of them. In general, assemblies of proteins have been analyzed using two complementary approaches: the biochemical and the genetical. Traditionally, the tools available to analyze protein-protein interactions in multicellular organisms have been restricted to biochemical approaches. However, despite obvious advantages, biochemical approaches can be time-consuming. Biochemical methods that detect proteins that bind to another protein generally result in the appearance of a band on a polyacrylamide gel. These methods are sometimes referred to as physical methods and include protein affinity chromatography, affinity blotting, immunoprecipitation and cross-linking. I will describe here few of these techniques which have been used for studying the proteins of the BFNM by other authors.

## b. Yeast Two hybrid technique

This technique, entitled "two-hybrid" or "interaction trap", enables not only the identification of interacting partners but also the characterization of known interaction couples. The yeast two-hybrid technique uses two protein domains that have specific functions: a DNA-binding domain (BD), that is capable of binding to DNA, and an activation domain (AD), that is capable of activating transcription of a reported gene. In normal transcription, both of these domains are required, whereby DNA is copied in the form of mRNA, which is later translated into protein inside a micro-organism (yeast, bacterium...). In order for DNA to be transcribed, it requires a protein called a transcriptional activator (TA). This protein binds to the “promoter”, a region situated upstream from the gene (coding region of the DNA) that serves as a docking site for the transcriptional protein. Once the TA is bound to the promoter, it is then able to activate transcription via its activation domain. Hence, the activity of a TA requires both a DNA binding domain and an activation domain. If either of these domains is absent, then transcription of the gene will fail. Furthermore, the binding domain and the activation domain do not necessarily have to be on the same protein. In fact, a protein with a DNA binding domain can activate transcription when simply bound to another protein containing an activation domain; this principle forms the basis for the yeast two-hybrid technique. In the two-hybrid assay, two fusion proteins are created: the protein of

interest (X), which is constructed to have a DNA binding domain attached to its N-terminus, and its potential binding partner (Y), which is fused to an activation domain. If protein X interacts with protein Y, the binding of these two will form an intact and functional transcriptional activator. This newly formed transcriptional activator will then go on to transcript a reporter gene, which is simply a gene whose protein product can be easily detected and measured. In this way, the amount of the reporter produced can be used as an indirect measure of the interaction between our protein of interest (Y) and its potential partner (Y) (Figure 1). Using this methodology, a large study has been performed about interactions between FliF, FliG, FliM, FliN with others proteins and themselves. [1; 2].

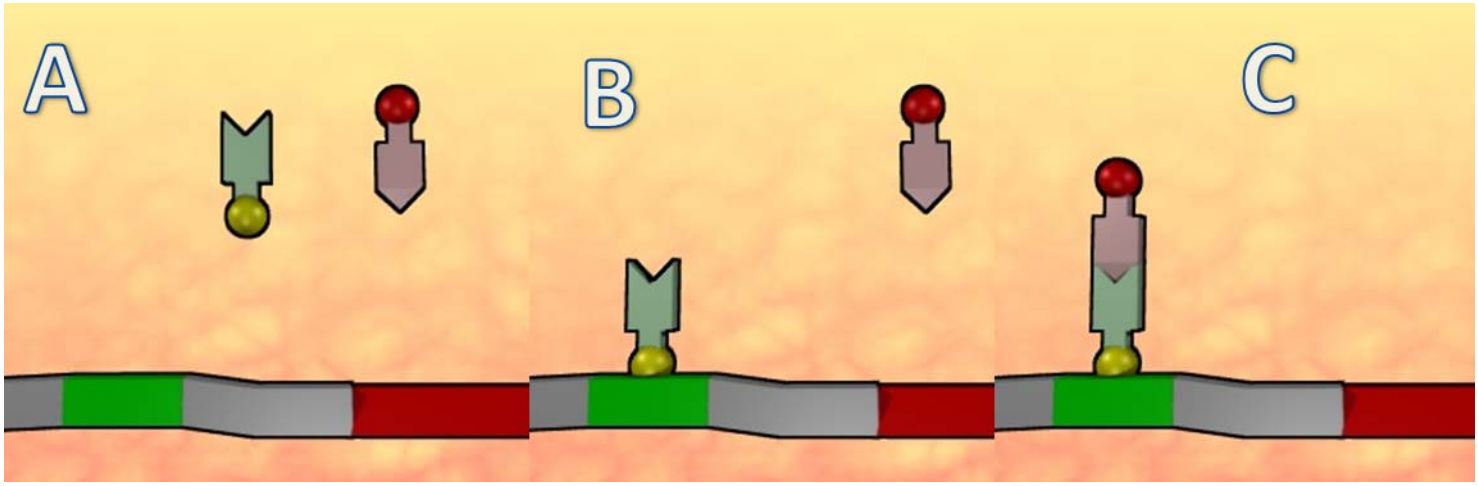


***Figure1:*** *Principle of the yeast two-hybrid technique that measures protein-protein interactions by measuring transcription of a reporter gene.*

## c. Western Blotting

The immunoblotting technique provides information about the presence, molecular weight, and/or quantity of a protein based on its ability to bind to specific antibodies. In a first step, the technique uses gel electrophoresis to separate proteins. They are then transferred to a membrane (typically nitrocellulose or PVDF (polyvinylidene fluoride), where they are probed using monoclonal or polyclonal antibodies specific to the target protein. By this way, interactions between FliG, FliM , FliN and CheY have been highlighted. [3; 4]. The principle is summarized below:

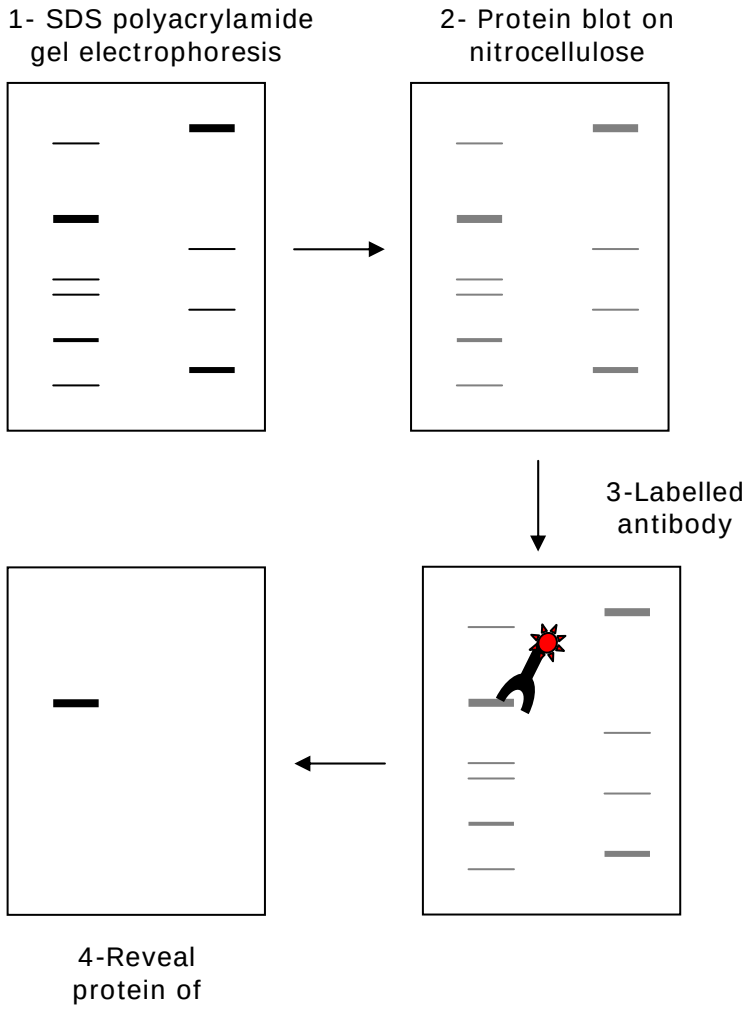


***Figure 2: Gel interactions analysis****.1) Proteins are separated by gel electrophoresis, usually SDS-PAGE. 2) The proteins are transfered to a sheet of special blotting paper, or membrane. The proteins retain the same pattern of separation they have on the gel. 3) The blot is incubated with a generic protein (such as milk proteins) to bind to any remaining sticky places on the nitrocellulose. An antibody is then added to the solution which is able to bind specifically to a protein. The antibody has an enzyme (e.g. alkaline phosphatase or horseradish peroxidase) or dye attached to it for labelling. 4) The location of the antibody is revealed by fluorescence imaging or through an enzymatic reaction involving the label entity grafted to the Ab.*

## d. Site-directed Mutagenesis

With site-directed mutagenesis it is possible to study in detail how proteins function and how they interact with other biological molecules. Using site-directed mutagenesis the information in the genetic material can be changed. A synthetic DNA fragment is used as a tool for changing one particular code word in the DNA molecule. This reprogrammed DNA molecule can direct the synthesis of a protein with an exchanged sequence of amino acids. Two possible ways have been developed, summarized in figure 3.

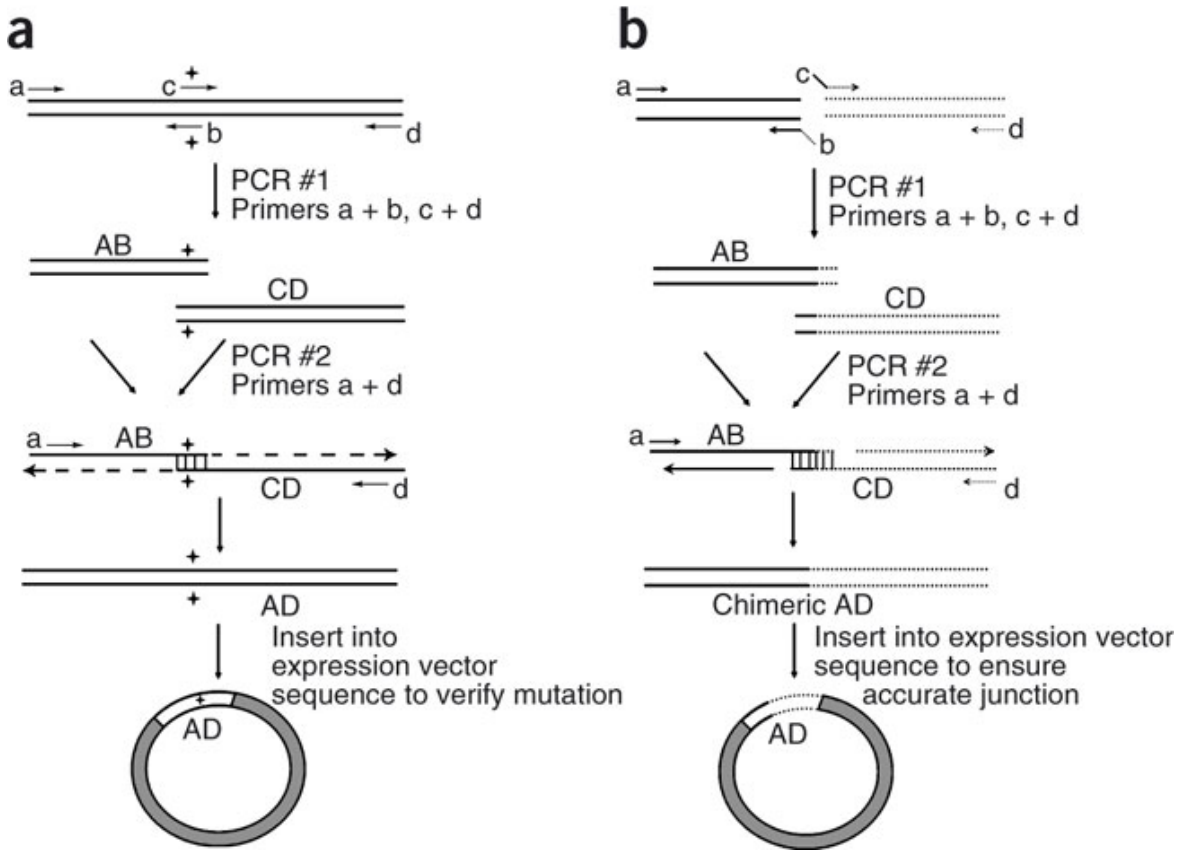


***Figure 3: Mutagenesis approach.*** *A/ Site-directed mutagenesis is accomplished by using mutagenic primers (b and c) and flanking primers (a and d) to generate intermediate PCR products AB and CD that are overlapping fragments of the entire product AD. Products AB and CD are denatured when used as template DNA for the second PCR; strands of each product hybridize at their overlapping, complementary regions that also contain the desired mutation (indicated by the cross). Amplification of product AD in PCR #2 is driven by primers a and d. Final product AD can be inserted into an expression vector (gray circle) to generate larger quantities of DNA, which should also be sequenced to ensure the presence of the desired mutation. B/ Chimeric gene products can be generated by two PCRs, as in* ***a****, except that internal primers b and c are not mutagenic. Instead, because the goal here is to splice together two different gene segments, primers b and c generate overlapping sequences by including nucleotides that span the junction of segments AB (solid line) and CD (dashed line). The second PCR generates the hybrid gene product AD that is then ready to insert into a vector (gray circle) for larger-scale production and verification of the accurate joining of gene segments AB and CD.*

Site-directed mutagenesis can be used, for example, to systematically change amino acids in enzymes, in order to better understand the function of these important biocatalysts. It is also possible to analyse how a protein is folded into its biologically active three-dimensional structure or for studying the complex cellular regulation of the genes and to increase our understanding of the mechanism behind genetic and infectious diseases,

including cancer. For investigating the BFNM, this technique has been largely used for studying the interactions and role played by numerous proteins, FliM and FliN [5],the presence of FliM and its role in the switching process [3], the role of MotA [6], the distinct role of protein domain parts [7; 8; 9; 10].

Despite this multiple approach and tools used during the last 30 years, several aspects of the BFNM remains ambiguous and each technique used, presented advantages and faults. The presence of chemical product during the different steps, the role played by others genes could influence the final results and leave some questions open about the interaction. The interaction between proteins in a complex architecture such as the BFNM could be problematic to study using these approaches for several reasons, the change of a single amino acid or a protein domain could “interfere” with others parts of the motor, and the results become difficult to interpret. We think that other tools can bring new data about the motor and complete our vision of the BFNM. These methods were the first developed in the early stage of the molecular biology for investigating the role and the interactions of proteins. More recently, new methods have emerged that enable this kind of investigation to be performed directly at the molecular scale. In this approach, it is therefore necessary to produce and purify the proteins of interest.

## B) Protein production, the first step

The primary task for studying protein interactions remains their production in large amounts. In order to achieve that, we need to copy and use the machinery of bacteria which already generates thousands of proteins. The structure of proteins mainly depends on the genes which encode a specific series of amino acids. A synthetic gene, called plasmid, can be created, duplicated and inserted into a bacterium for over-producing a selected protein, in our case one protein of the motor. We cannot use the “natural” proteins already present in the bacterium, due to their relatively low quantity. After gene modification, the level of expression is maintained under a critical level, beyond which the over expression turns out to be toxic for the bacterium. A complex system regulates the level of expression and this is the reason why we need to bypass the natural gene regulation by inserting this artificial gene. For our example, if we consider how many flagella are present in a single cell, 6 to 10 for E.coli, and how many proteins are present in each flagellum, the number of proteins is negligible, and this is the reason why we need to over-produce them. A second point has to be addressed, how can we extract them? The structure of the plasmid and its sequence is the key for

addressing this point. A plasmid is an extra-chromosomal DNA molecule separate from the chromosomal DNA which is capable of replicating independently of the chromosomal DNA. The term *plasmid* was first introduced by the American molecular biologist Joshua Lederberg in 1952. The plasmid-host relationship tends to be more symbiotic than parasitic (although this can also occur for some viruses, such as endoviruses) since plasmids can be exchanged between two bacteria with useful packages of DNA. Since their discovery, synthetic plasmids were created and used in genetic engineering, and in that case they are called vectors. Plasmids serve as important tools in genetics and biotechnologies, where they are used to multiply (make many copies of) or *express* particular genes. The process of protein production can be divided in several steps, which I will call first plasmid multiplication and selection, secondly production and then purification. These steps are schematically presented in figure 4.

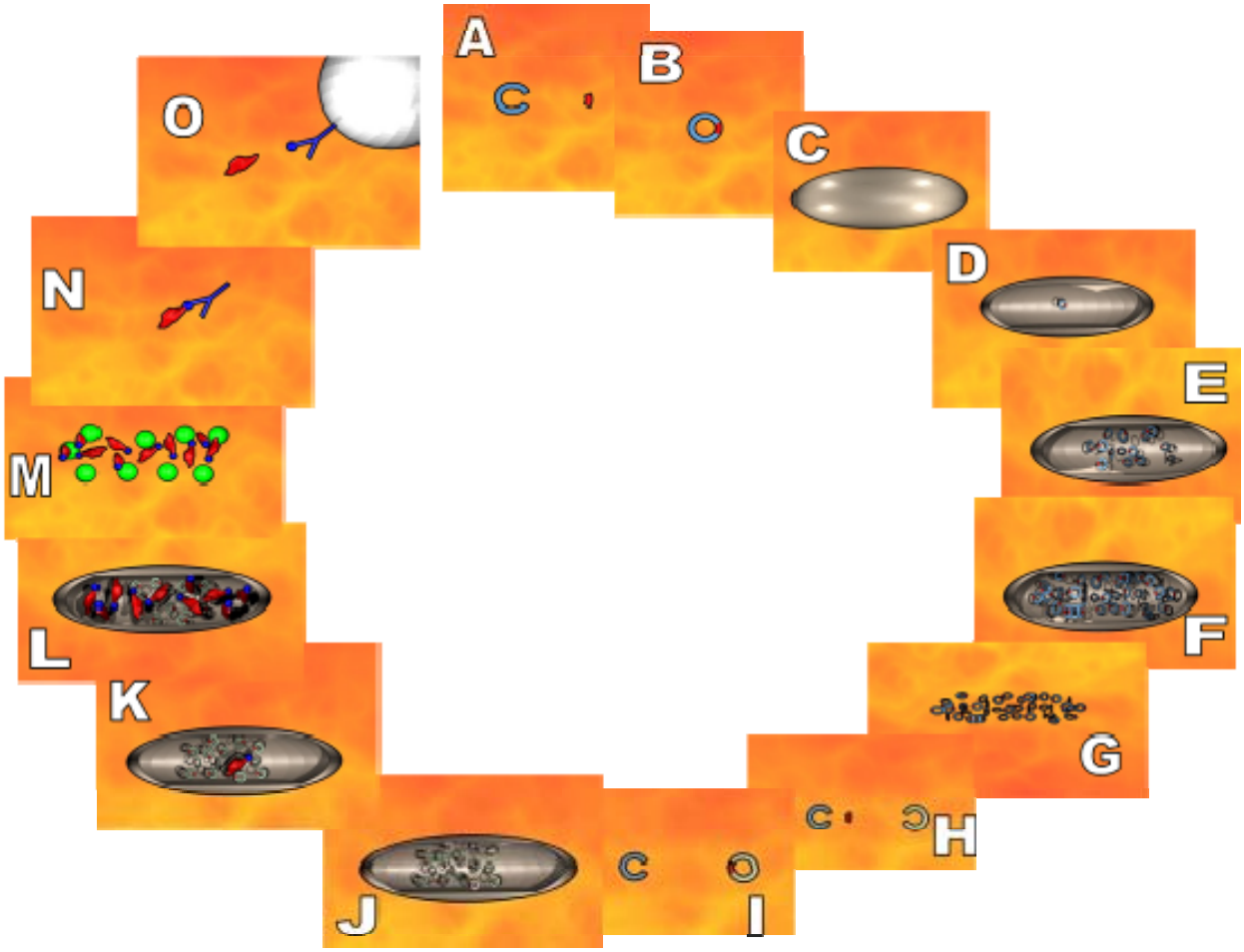


***Figure 4: Principle of protein production.*** *A: a gene is engineered and amplified using PCR technology. B: This gene is inserted in a plasmid. C,D: This plasmid is inserted in a first bacterium. This is the transformation step. E: the purpose is to multiply the plasmid for generating a large amount of the desired genes. G: The cell is lysed and plasmids are recovered. H: the gene is then removed. I: and inserted in a second plasmid, dedicated to the, the production of a specific protein, here the plasmid called pGS-21a. J: this new plasmid exhibiting the gene is then implemented in a second host. K: the plasmids start the production of a specific protein. L: Massive amount of proteins can be produced. M: cell is lysed but the targeted protein is mixed with the cytoplasm and cell residues. N: to facilitate the purification, the presence of the Glutathione-S-Transferase (Gst) allows to bind the selected protein to a specific anti-body (anti-Gst). O: This anti-body can be fixed to an agarose bead. An enzyme is used to cut the link between the protein and the Gst tag and releases a pure protein, this is the purification step.*

The gene to be replicated, for example *FliG*, is created, see figure 4, inserted, duplicated, extracted and purified. Several protocols used specific other functions encoded in the plasmid to make the bacteria resistant to antibiotics. Only bacteria which take up copies of

the plasmid survive the antibiotic, since the plasmid makes them resistant. In this way the antibiotics act as a filter to select only the modified bacteria. Now these bacteria can be grown in large amounts, harvested and lysed to isolate the plasmid of interest.

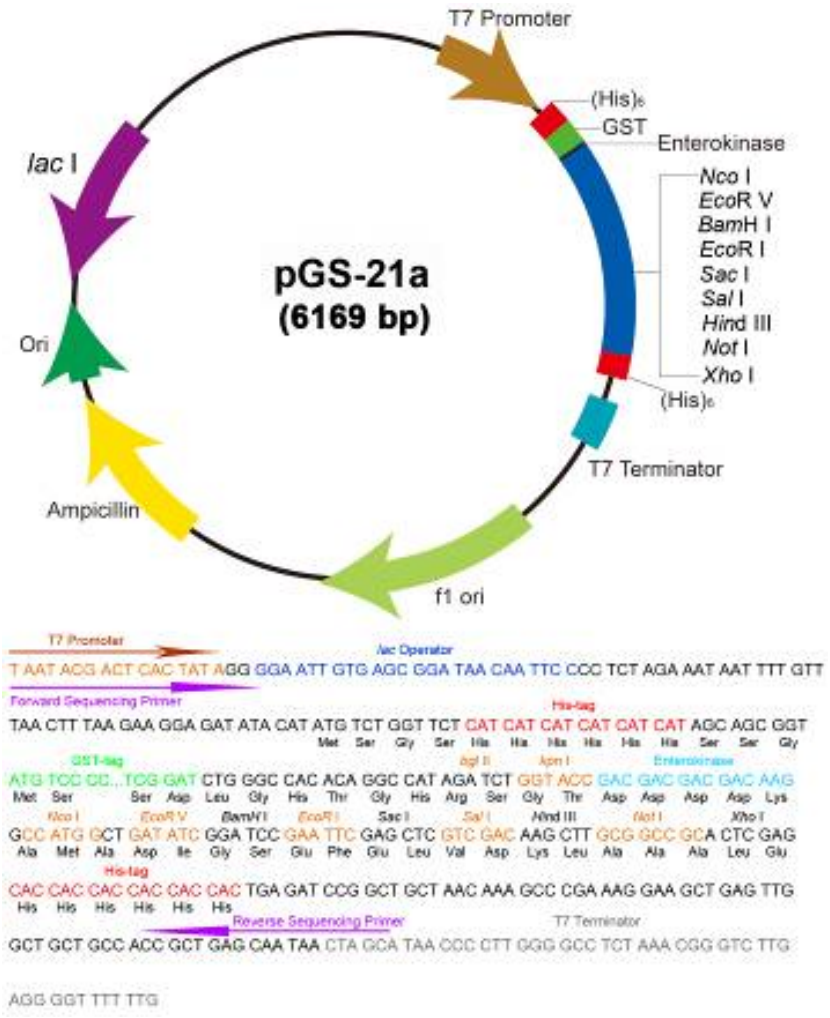


***Figure 5: the pGS-21A plasmid, dedicated to the protein production.***

The gene is then cut from this first plasmid and inserted in a second one, dedicated to the production of the selected protein. The plasmid used for this task is shown in figure 5. This plasmid harboring *FliG* is then inserted in a second bacterium, where the plasmid will use the cell machinery to over produce the FliG protein.

When the protein has been over-produced in a reasonable amount, bacteria are lysed and the last step of the process consists in purifying cellular extract. In order to separate the FliG proteins from the other proteins, a tag has been added when the protein was produced. This tag is generally added in the N-terminus of the protein, but can also be located at the C-

terminus. The role played by this tag is fundamental, because it allows the separation of the tagged proteins from the others, using an anti-gene/anti-body recognition. The tagged protein binds to a specific antibody, which has been previously fixed on beads or within purification columns. When all the tagged proteins are bound, enzymatic solution of enterokinase is introduced inside the column and cleaves precisely the link between the protein and the tag, which releases a pure protein. Several approaches have been developed along this route, but the main principle remained the same. The tag used was the Glutathione-s-transferase (Gst) which was added to the N-terminus of the six motor proteins, FliF, FliG, FliM, FliN, MotA and MotB. The production of the Gst-proteins was a success but the purification was more challenging and only 4 of them succeeded: FliG, FliM, FliN, and MotB. FliF and MotA construction failed at the purification step due to unknown reasons. The production of proteins remained a very challenging field, especially for membrane proteins, due to the specific *in vivo* environment needed for their structure, and this may be the reason why MotA and FliF which are trans-membrane proteins, failed to be purified. However, the production of tagged proteins was efficient enough to allow the elaboration of a bio-chip interaction protocol. Figure 6 shows a typical SDS-gel of the different produced proteins, with or without the Gst tag. The different molecular weights correspond to established data, including the tagged proteins (molecular mass of the Gst+ the protein of interest). When proteins are purified or at least extracted from cells, aliquots of different concentrations are prepared and stored at -80°c for reducing protein degradation. Proteins were stored no more than one month.

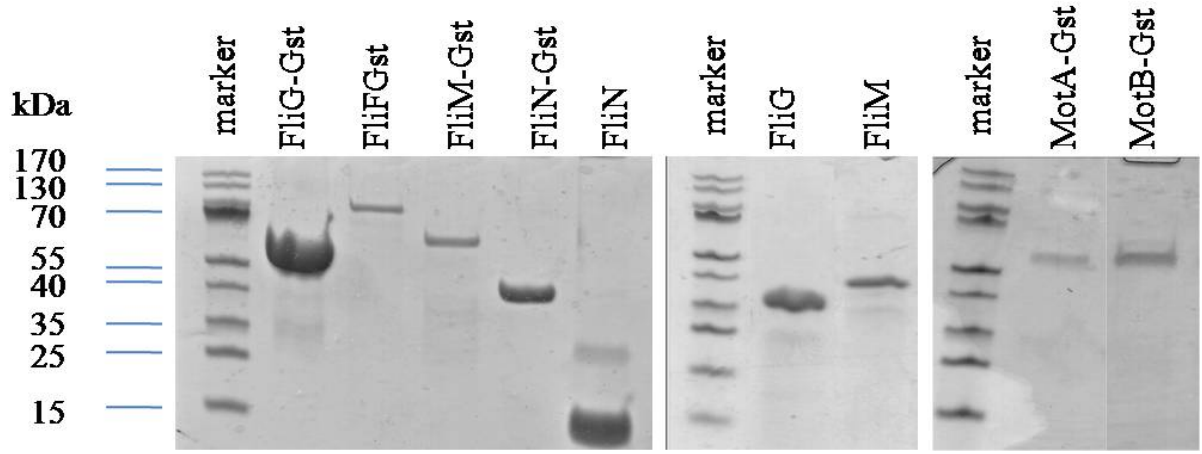


***Figure 6. SDS gel of the produced proteins.***

## C) Physical and Biophysical tools

As described in chapter I, genetics has already highlighted fundamental aspects of the motor function, starting from the role of each protein to the function of precise domains of these proteins. However, specific techniques have been developed to determine the interaction between two proteins, based on physical sensing. I will describe briefly two techniques, one based on an optical phenomenon: the Surface Plasmon Resonance (SPR) technique, and the second based on mechanical mass detection: the Quartz Crystal Micro balance-Dissipation (QCM-D). Both of them were tested during this work but I will concentrate only on the results obtained with the QCM-D technology.

### a. Surface Plasmon Resonance (SPR)

The Surface Plasmon Resonance (SPR) technique is one of the most famous optical techniques for characterizing specific interactions between bio-molecules. It is a label free and real time measurement method. Its discovery has been the consequence of progress on the theory describing the electromagnetic fields at the vicinity of surfaces (near-field) at the beginning of the last century. The physical principle of SPR can be summarized as follows: An oscillation of a charge density, called surface Plasmon is generated at the interface between two environments of dielectric constant with opposite sign, such as a metal and a dielectric for example. This oscillation is generated by an incident ray of light, a laser beam, in a specific spatial configuration. The generated wave, associated to this surface Plasmon, is coupled to a surface electromagnetic wave, parallel to the metal layer. Under appropriate experimental conditions (wavelength of incident light and angle of incidence) a sharp plasmonic resonance is observed corresponding to a massive transfer of energy from the incident light to the plasma oscillation. This sharp resonance is the basis of the detection, because when proteins will interact at the surface of the metal layer where the plasmons are excited, this resonance is shifted due to a minute modification of the refractive index close to the surface. The sensitivity of the method is very high due to the narrowness of the resonance peak. In practice, the shift of the resonance due to molecular adsorption at the metal surface of the sensor is monitored as follows. Under resonance conditions, a large amount of energy goes from the incident light to the plasmonic excitation and this transfer can be simply measured through the intensity of the reflected light at the surface of the sensor which exhibits a minimum. Under molecular adsorption, the system is shifted from the exact conditions of resonance, less energy is transferred to the plasmonic excitation and the reflected intensity grows. The measurement of the reflected intensity of light is therefore a very simple and

sensitive method for detecting molecular adsorption at the sensor surface. This experimental method has been implemented by many research groups and commercial companies. The most famous is Biacore®.

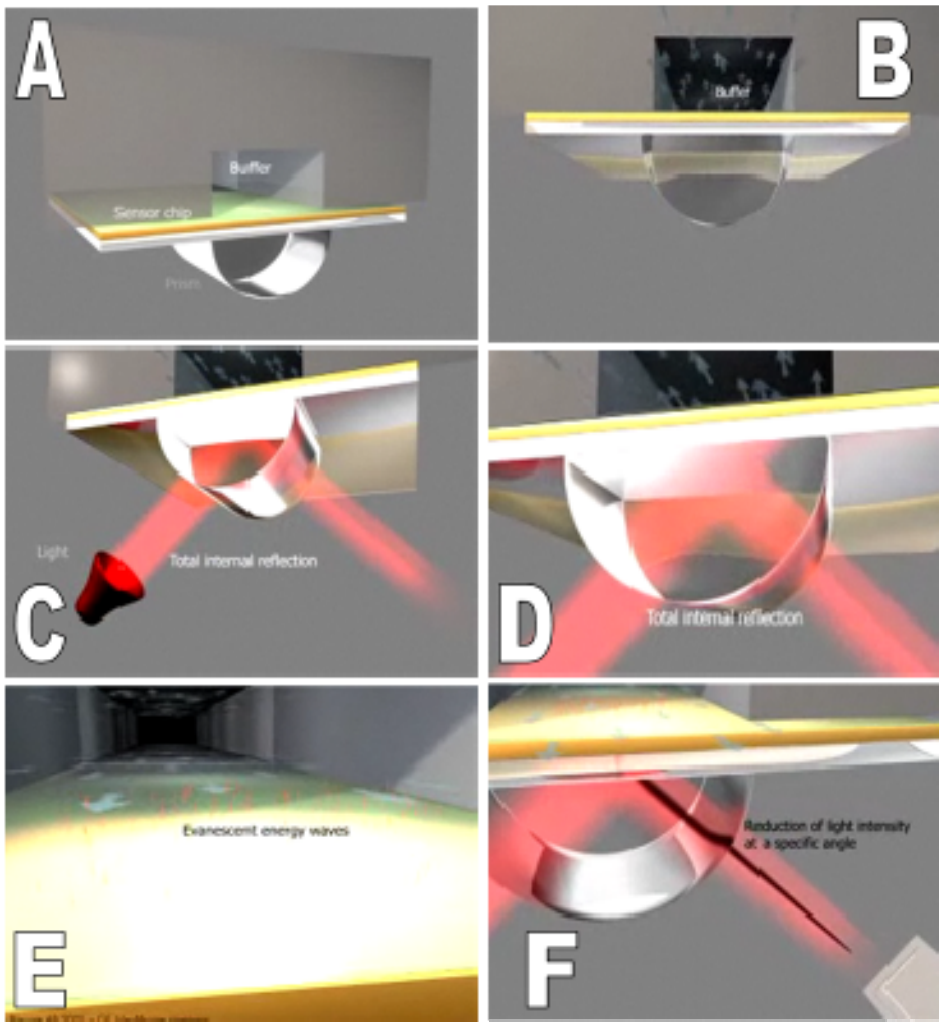


***Figure 7: SPR cartoon principle, from the Biacore® website.*** *A: large view of the set-up, starting from the bottom to the top by the prism, the sensor layer and a micro-fluidic channel for the circulation of buffer and molecules. B: bottom view of the system. C: illumination of the prism at an angle generating a total internal reflection. D: zoom in on the prism. E: An evanescent energy wave is generated at the top side of the sensor layer. F: Measurements are made through the reduction of light intensity at a specific angle. Images taken from Biacore website.*

Figure 7 represents the geometrical system. [11]

The first measurement using a SPR system dated from the early 80's by Nylander and Liedberg [12] for gaz detection, and was then followed by numerous applications for food analysis [13], proteomics [14] and drug testing[15]. All these discoveries have been rendered

possible by the development of a dedicated system, commercially available, and sold by the Biacore® Company, a division of the American company General Electric. The number of publications related to the use of SPR method has sensibly increased especially about the affinity testing between molecules, due to three advantages of the method: real time measurement, label free, sensivity. The monitoring of the reflected intensity of light enables a real time recording of the molecular adsorption at the surface of the sensor. From this kinetic information association, dissociation equilibrium constants can be obtained. Because, in-fine, the sensing relies on slight change of the refractive index at the vicinity of the sensor surface, it is not necessary to label or tag the molecule of interest. This key point is the major advantage of this technology. Finally, like almost the sensing methods relying on a sharp resonance phenomenon, the sensitivity of the detection (0.2nM) is the best currently commercially available. However the technique suffers from two inconvenient:

- the size of the molecule impacts directly on the sensitivity (small molecules induces so small optical changes that the detection limit is degraded for protein below 10KDa).

- the evanescent field senses a region very close to the surface (a few hundred of nm) [16] [17] and decreases exponentially. This constraint impacts drastically on the surface chemistry of the sensor. As a consequence, very few results involving more than 2 layers of molecules, one attached to the metal surface and the second in solution are reported. The high sensitivity established for the SPR method presented also a “dark side”; any change in the media will render the results difficult to interpret. The need for a relative complex experimental setup limits also the portability of the system. We have tested diverse interactions between motor proteins without success. The direct fixation of motor proteins on the surface has probably limited their active site for interacting with others.

## b. Quartz Micro-balance (QCM)

A quartz crystal microbalance (QCM) measures a mass per unit area by measuring the change of the resonance frequency of a quartz crystal mechanical resonator. Indeed this resonance is disturbed by the addition or removal of a small mass due to oxide growth/decay or film deposition at the surface of the acoustic resonator. The main principle is then a mass detector. Quartz is one member of a family of crystals that experience the piezoelectric effect. Since its early discovery by Curie in 1880, the piezoelectric effect attracted much attention, in high power sources, sensors, actuators, frequency standards, motors, etc. The relationship between applied voltage and mechanical deformation is now well known; this allows probing an acoustic resonance by electrical means and the reversibility of the process opened the way for bio-sensor conception. I will summarize here briefly the basic principle of acoustic wave generation which is the core of the QCM-D system. Applying alternating bias ac voltage to the quartz crystal induces mechanical oscillations. With an alternating bias between the electrodes of a properly orientated crystal, a standing shear wave is generated. Among other parameters, the resonance frequency of oscillation of the quartz crystal is dependent on the mass of the crystal. Figure 8 summarizes QCM-D principle.

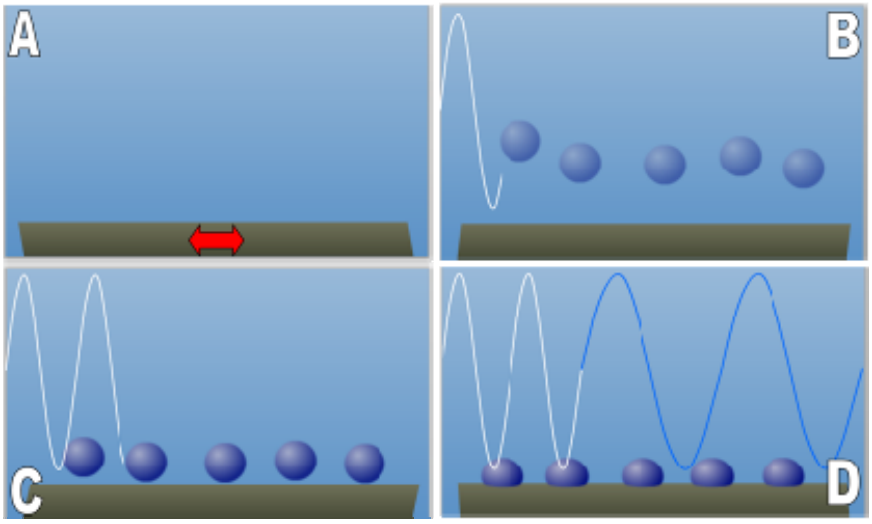


***Figure 8: QCM-D technology principle**. A: An oscillation is generated into a piezoelectric material through an electric controlled polarisation. The frequency is measured in real time while liquid is passed over the sensor. B: molecules are added through the fluidic chamber C: and start to adsorb at the sensor surface D: there resonance frequency shift is proportional to the additional mass. Images taken from Qsense website.*

During experiments, all the other influencing variables remain constant; thus a change in mass correlates directly to a change in resonance frequency. As mass is deposited on the surface of the crystal, consequently the resonance frequency decreases from its initial value.

The recent popularity of the QCM-D technology is coming from several points: Commercial avaibility ( Qsense company ®), temperature stability, sensitivity and capability to measure in a liquid medium. The origin of the QCM-D technology dates from Sauerbrey in 1959, who demonstrated a direct relationship between the mass variation and the resonance frequency shift [18]. This equation, presented below, has been established and verified using quartz as a piezoelectric material and this is the main reason why this technology is still today called Quartz Micro Balance.

$$\Delta m = (C_f/n)\Delta f$$

This equation shows the direct link between addition of mass, $\Delta m$ and the frequency shift $\Delta f$, through the mass sensitivity $C_f$ and the defined frequency harmonic n. For our experimental system, it has been estimated that the first harmonic n=1 has a mass sensitivity of -17,7pg/($mm^2$.Hz), and all the odd harmonic ( 3, 5, 7..) can also be used for measurement. The extreme sensibility of the first harmonic is sometimes problematic for its stability, and our results will be based on the monitoring of the $7^{th}$ harmonic. The first QCM-D systems were dedicated to air or vacuum measurements, as for example the growth of metal layer on surface [19] and models describing wave propagation have only proved the possible use in liquid media, quite recently [20]. The physical description of QCM-D has also exposed another physical parameter of interest which can be used for the detection: the energy dissipation. Data issues from the dissipation signal depict the viscous-elastic properties of the surface, which can for example reveal the conformation of some molecules at the surface. By coupling frequency and dissipation shift, the first measurement of bio-molecules interactions has been made on antigen/antibody on gold surface[21]. The interpretation of the mass added revealed, for example on the measurement of albumin adsorption, that the QCM-D measured the wet mass on the sensor surface, which opened the study of the influence of the buffer on proteins, such as for example the Mefp-1 from the mussel [22]. The fact that the QCM-D technology is a mass detector system implies that the system can follow in real time the addition of several layers of molecules and no limits on the total mass or total thickness of the deposit is encountered. This quality is a strong advantage when compared to SPR technique. Sandwich of molecules can be created on the sensor surface, which allows more complexity and more flexibility. It was one of the main reasons why we have investigated the interactions

between the motor proteins using QCM-D technology. The presence on the market of the QSense-E4, from the Q-sense Swedish Company, which exhibits 4 interactions chambers, allowed us to study in parallel, at the same time different interactions, or a same interaction in different buffers. This large flexibility of QCM-D technology was the motivation for preferring this method to SPR technique even if the detection limit is better with the latter.

# D) Interactions between proteins

## a. The biochip protocol

### i. Principle of surface preparation

As described in the introduction of this chapter, one of the ways to characterize an interaction between two molecules consists in fixing one of them on a surface and let a second one free to interact in solution. The sensor can then be optically, as for the Biacore technology, or mechanically sensitive as for the Quartz Micro Balance technology. The main principle is the same: the biomolecule of interest is fixed on a surface (the probe) and a specific binding partner is added in solution (the target). Different approaches for fixing the probe bio-molecule of interest can be used and I will divide them into two families, the non-covalent and the covalent.

#### 1. Non covalent, direct adsorption

This approach is the easiest and cheapest way to immobilize a molecule on a surface. It is mainly based on physisorption that can create weak interactions between molecules and a surface; “physical” adsorption is possible thanks to the electrostatic interactions between charged molecules, Van der Walls or hydrophobic-hydrophobic interactions. Compared to covalent bonding these interactions are one to two orders of magnitude weaker. Due to this weakness, the bond reversibility between molecule and surface must be taken in consideration. Extensive washing procedure or change in the buffer could change dramatically the molecule adsorption on the surface. But despite that, the direct adsorption has been proved to be easy and could be applied to a wide range of surfaces[23]. However, some drawbacks need to be discussed. The first point concerns the non controlled adsorption on the surface, especially about the non-homogeneity of the surface. As proved by Caruso and al [24], the distribution of molecules remains very irregular on the surface as depicted in figure 9 and the orientation of those molecules remains chaotic, which reduces the possible quantification of the detection [25]. Moreover, the second molecule could either interact with the first molecule or the surface, which limits the final interpretations.

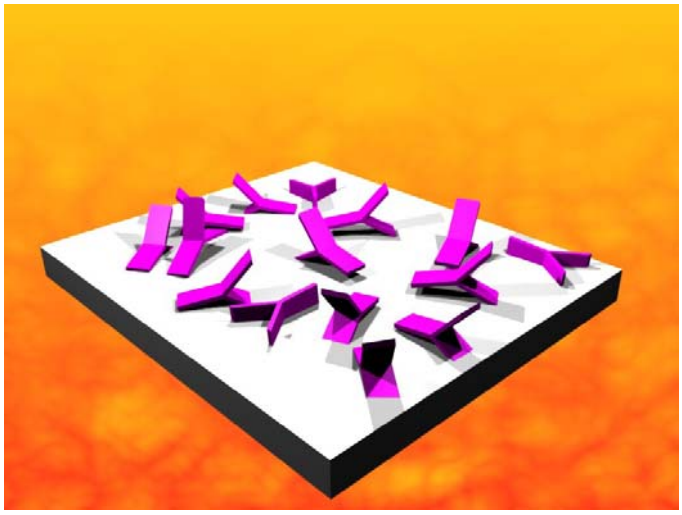

***Figure 9: Non specific adsorption of anti-bodies on a surface (schematic view showing the disorder)***

The control of the density and homogeneity of the probe molecule on the surface remains the major limitation of this approach. However, as described above, some techniques gave good results using specific protocol in order to address those problems. The choice of the surface coupled to an extensive use of fluorescence techniques for characterization permitted to obtain nice results using a such simple and relative low cost approach [26]. It was also due to these advantages (about price and simplest approach) that the direct adsorption has been widely used in several examples, including three different proteins and their respective anti-bodies [27]. These experiments have shown a large diversity on the results, which can be very selective, as for example the antigen fibrinogen/ antibodies anti-fibrinogen, or non selective for the couple anti-HSA/HSA. These results highlighted the limits of the non covalent adsorption, coming from the defaults already noticed, which mainly depends on the nature of the molecule of interest. In order to alleviate these drawbacks, the development of covalent binding approaches raised during the last few years.

## 2. Covalent immobilization

Despite the low cost and easy approach of the direct adsorption, covalent immobilization of molecules on a surface presents numerous advantages despite more complex protocol. The chemical bond is two orders of magnitude stronger than physisorption and this approach is more favorable to a specific binding of molecule on surface [28]. The needs for surface functionalization, wherein a chemical treatment creates a layer of binding molecules is the basic principle of the covalent approach. This chemistry treatment will

anchor selectively the primary molecule to the surface in a controlled way. The reproducibility and the robustness[29] present also major advantages for large studies of interactions. These protocols are particularly applicable for biomolecules as for example antibodies and proteins, due to the presence of specific binding sites already identified. These sites can be used without blocking the interaction site which would be involved into the further study. Sites such as amino groups or carboxylic functions can be used for grafting the molecules on the surface. However, the chemical modifications resulting from the surface-molecule interaction must preferentially take place on the sensor surface rather than on the molecules, in order to reduce the irreversible change within the molecular structure. Two surfaces are widely used for chemical surface modifications, Silicon oxide and gold surface, and different chemistry have been developed through the years [30; 31]. I will first describe the chemistry on gold which has been used by us for studying protein-protein interactions, and in chapter 3, I will describe the chemistry performed on silicon oxide surfaces.

### ii. Selected surface protocol

Our main idea for studying the motor protein interactions is based on the presence of a tag on the proteins, the Gst tag. By using the flexibility of the QCM-D technology to create successive layer of molecules at the surface, our idea consisted in covalently immobilizing an anti-Gst antibody, and add the first probe protein, exhibiting the Gst tag. This first assembly will play the role of a sensor surface, when a second protein, without the GST tag, interacts with the first tied on the surface as shown in figure 10.

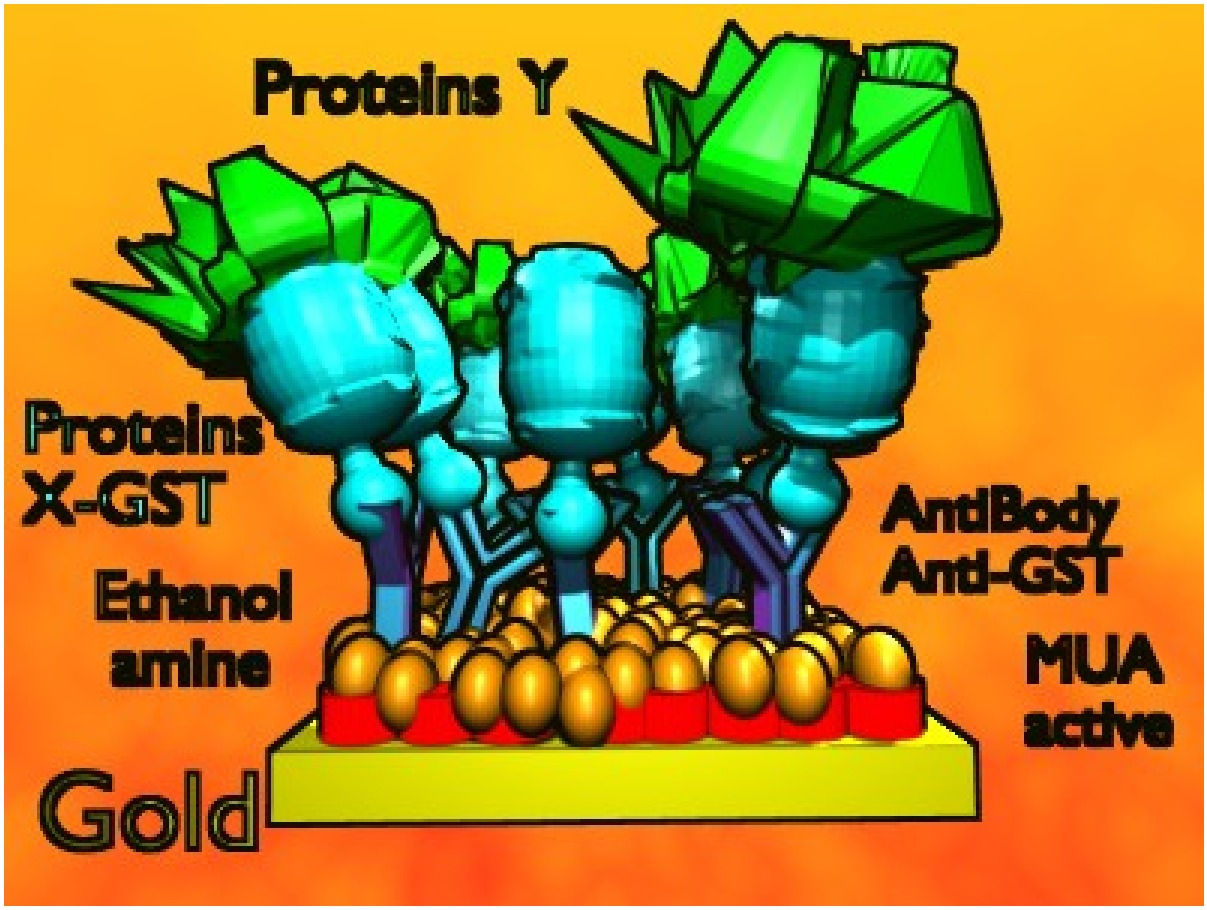


***Figure 10: Schematic view of the surface preparation of the QCM sensor for the investigation of proteins (X and Y) interactions.*** *Several layers of different molecules are clearly shown, starting from a covalent link between a gold surface and a thiol-COOH layer, to the interaction between the proteins X and Y.*

This figure summarizes the final sandwich assembly. The presence of 4 chambers on the QSense-E4 system gave the possibility to study the same interaction but in 4 different conditions (4 different buffers). We expected that this protocol could give new insight into the motor architecture and results will be shown later in this chapter. However, the primary task was to create a reliable and robust surface functionalization, starting from a gold sensor to the second protein to be detected. All the different steps of surface preparation are described in figure 12 and will be explained in the following paragraph.

The immobilization on gold surface is commonly used within the bio-sensors community, partially due to the quality of the chemical layer formed at its surface and also thanks to an easy chemical process. One of the most common molecule used for surface gold modifications are sulfide or di-sulfide. These molecules present a sulfide function, a spacer and an active terminal function, in our case a carboxylic acid. Layer of these kinds of molecules self-assemble on gold surface and give molecular coating of very high homogeneity and perfection as observed for example by STM ( Scanning Tunneling

Microscope). This self assembled monolayer (SAM) formation has been largely demonstrated for high throughput interactions [32]. The adsorption of thiols on a gold surface is described by this reaction:

$$R\text{-}SH + Au \longrightarrow R\text{-}S\text{-}Au + H^{+} + e^{-}$$

It is worth noticing that the fixation and formation of the SAM on the surface has not been totally and fully described. [33]. Our attention was attracted by a specific thiol, the MUA for (11-mercaptoundecanoic acid), which forms a SAM on the gold surface of the sensor. No prior treatment is needed for the formation of the SAM, however the use of ethanol as a solvent involves an important washing procedure with ethanol followed by pure water for different reasons. The washing procedure removes additional loosely attached thiol molecules. By washing, first by ethanol then pure milliQ water, amount of non-organized thiols which are not stable on the gold surface are removed. The specific structure of the MUA allows a monolayer to be formed, which gives a good and homogeneous surface activation[34]. The kinetics of SAM formation was considered relatively fast, less than a day depending on the selected thiol. The MUA SAM was formed within 12 hours. However SAM can also be formed by direct transfer of a pre-formed SAM layer on a PDMS stamp [35]. I will describe in more details in chapter 3, the use of this soft-lithography technique in order to generate patterns on surface. For surface functionnalization, the principle is more accessible and does not involve any technological step. A polymer, the polydimethylsiloxane (PDMS), cured at room temperature, forms a flat elastomer “stamp” where a drop of MUA diluted in ethanol solution is incubated during 5 minutes. A SAM layer spontaneously forms at the stamp surface, then the liquid is removed, the stamp dried and brought into contact with the gold sensor for 5 minutes. The SAM layer is transferred from the PDMS stamp surface to the gold sensor, which is then washed by free ethanol and pure water. Compared to adsorption, stamping presents many advantages. It reduced the gold sensor preparation by a factor of 100 (less than 15 minutes compared to 25 hours) with similar results. The choice of the thiol molecule is crucial depending on the couple between the active site on the bio-molecule and the active terminal function on the thiolated molecule. One popular chemical couple is the carboxylic -COOH/ amino function –NH2. The presence of amino function on the antibody let us choose a thiol molecule exhibiting a carboxylic function, and this carboxylic function can be transformed to $–COO^{-}$ capable to interact with function on the antibody. This activation was achieved by the use of a mixture in Hepes 1 of two molecules, EDC for N-

ethyl-N'-(3-dimethylaminopropyl)carbodiimide) and NHS for N-hydroxysuccinimide. This process forms an active ester on the carboxylic group figure 11.

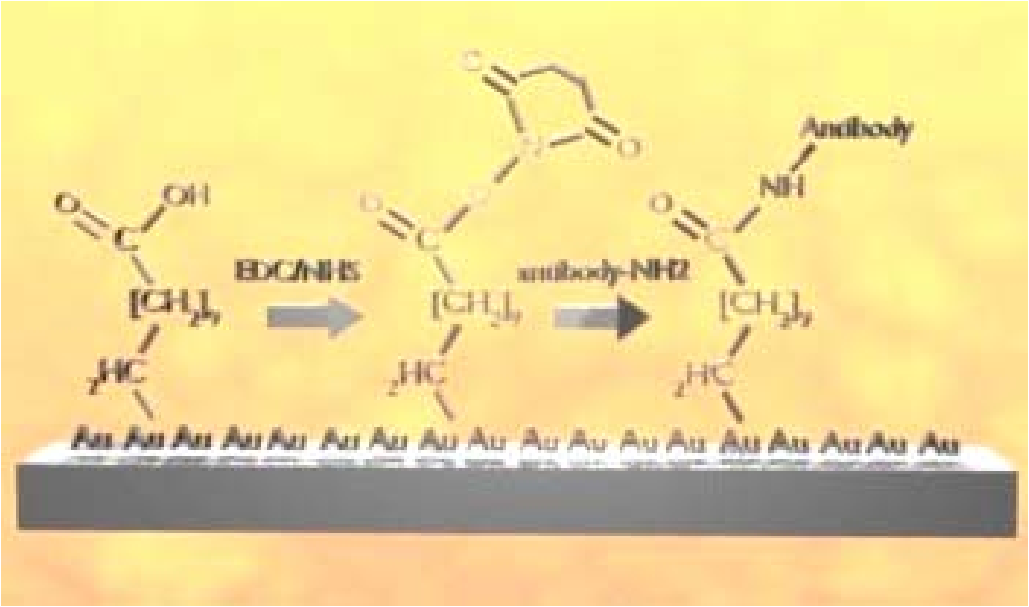


***Figure 11: Schematic view of the 11-mercaptoundecanoic acid activation.*** *A homogeneous layer of MUA, formed on a gold surface is activated using an EDC/NHS mixture. The carboxylic acid ending group is activated and forms an active ester which then fixes an antibody through an $NH_2$ group.*

This active ester reacts with an amino group of the antibody, which is now covalently attached to the gold surface. We then wash briefly the surface for removing the residues of the EDC/NHS complex first with hepes 1 and then with PBS (the antibody buffer). The washing procedure turned out be essential for the quality and interpretability of the recorded frequency shifts. As noticed before, the QCM-D technology is sensitive to adsorption events at the sensor surface, but can also be sensitive to modification of the buffer solution, as for example Hepes 1 and PBS. The reason is still under discussion but is probably coming from the different ions present into each buffer solution. This is the reason why, methodologically, prior each new molecule, its buffer need to be injected on each chamber for rendering visible this "buffer effect". This method allows us to distinguish this effect from molecular adsorption on the surface. This is the primary reason why Hepes 1 and then PBS were injected sequentially into each chamber. We choose an antibody concentration of 100 µg/ ml to cover the full gold sensor surface. Saturation was achieved after 45 minutes of incubation, as can be seen on annex 1. The next step: passivation and surface saturation of remaining active thiol functions is crucial for reaching a high specific interaction between proteins 1 and 2 (probe and target). In order to decrease non specific protein adsorption, a molar solution of ethanolamine is incubated for 40 minutes and bound to the remaining thiol functions still not

occupied. The presence of an alcohol function on the other side of the molecule also plays the role of an antifouling coating. We then wash again the surface using PBS and then inject the first Gst tagged protein (probe protein). The mass added on the sensor is much lower compared to the antibody adsorption, due to the relative small molecular weight of the protein-Gst complex (from 85 KDa (FliF-Gst) to 35 KDa (FliN-Gst)). I will discuss this point in the next section. We incubate several times the protein solution for insuring a complete interaction with all the antibodies attached to the surface. At this step, the non-specific interaction which occurs between the probe protein and the surface is not a problem for the rest of the experiment, because the final interaction of interest is not between the antibody/probe proteins, but rather between the probe and target proteins. We tried to add proteins without Gst-tag at this stage to the surface and the frequency shift observed was at least 5 times smaller than with the Gst-tag, which confirmed that most of the proteins bound to the surface thanks to the specific Gst-tag Anti Gst antibody interactions. The main purpose of these multiple functionalization was to produce a chip which exhibits a stable and robust occupied by the surface of a first protein, mostly well oriented and strongly attached to the surface. The last step of the process consisted in buffer injection in each chamber. Because the BFNM in motor is actuated by a flow of protons, and the movement of these protons is mainly based on a trans-membrane gradient of protons, we expect that the interaction between the different proteins of the BFNM can be pH dependent. This is the reason why, we worked at 4 different pH in PBS 5, 6, 7,4 and 9. Injection of these different pH buffers is the last step of the gold surface preparation. We have noticed that the change of pH is reversible, meaning that by re-injecting a pH 7,4 after a pH 5 buffer for example, no molecules are removed from the surface. It has been clearly observed in figure 13, step V.

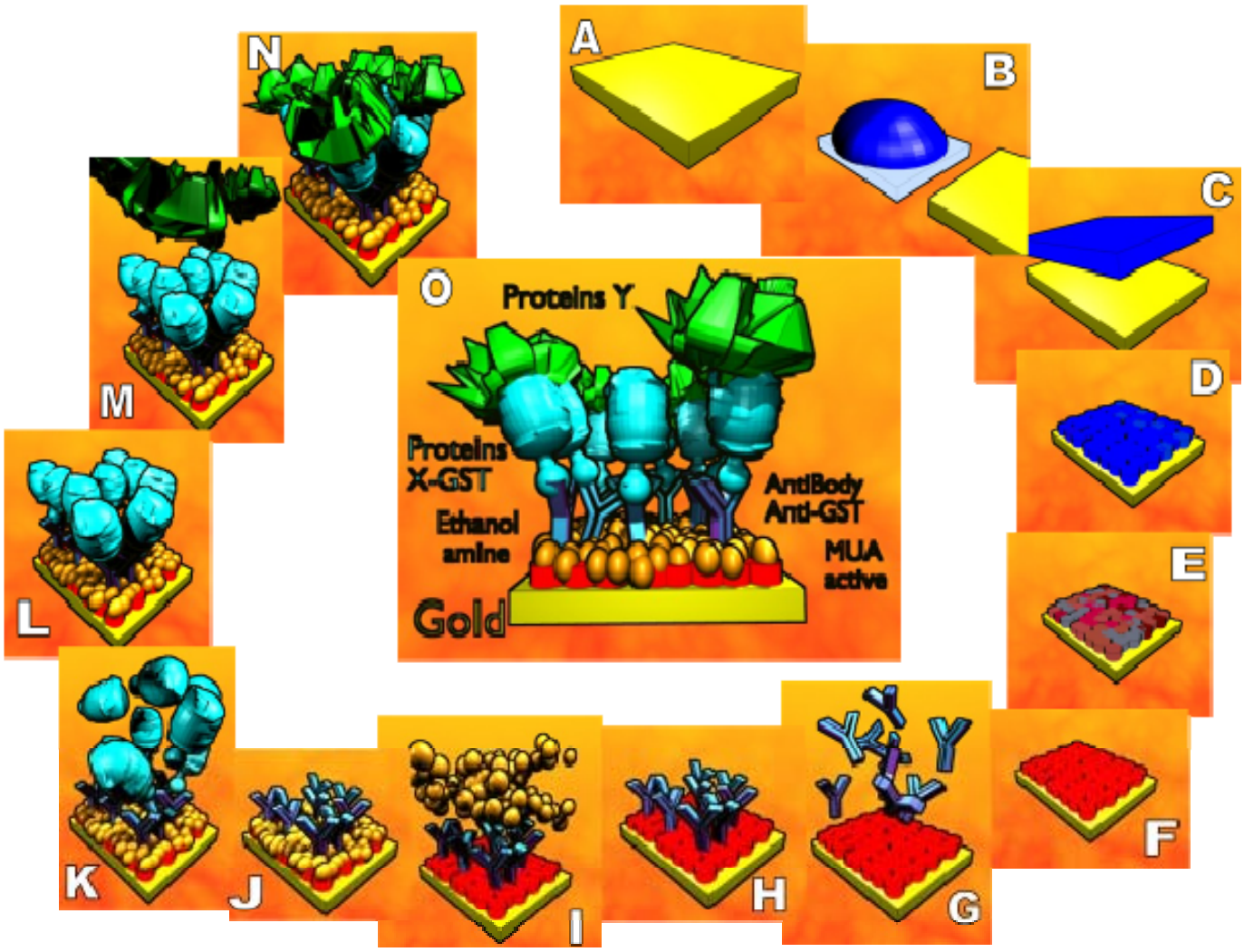


***Figure 12: The different steps of the biochip sensor protocol****. A: A thin layer of gold serves as a basis for the fixation of all the molecular architecture. B: A PDMS stamp is inked for 5 minutes with a 11-mercaptoundecanoic acid solution in ethanol. C: The stamp is dried and brought into contact with the gold sensor for 5 minutes. D: The surface is rinsed several times by ethanol and milliQ water. E: A mixture of NHS/EDC solution is incubated on the surface. F: The COOH group of the thiol molecules is changed into an active ester. G: An Anti-Gst antibody is covalently bounded on the surface. H: Saturation of the sensor surface with antibody is achieved in 45 minutes. I: An ethanolamine solution then passivates the surface. J: Since all the surface is saturated, we wash several times the sensor in order to remove loosely bounded molecules from the sensor. K: the first Gst-tagged proteins now interact with the antibody. L: We wash for removing all non bounded molecules. M: The second protein is injected. N: …and can interact with the probe protein fixed on the surface.*

In order to quantify the biochip specificity, several series of negative control have been pursued and results can be consulted in annex 1. We tested the formation and adsorption of antibodies directly on gold and after each step of the process. We also tried to switch the

layer formation, for example adding ethanolamine before antibodies. We also worked on the reactivity of the surface, by changing the timing between the incubation of the Gst-proteins on the prepared surface. Two crucial negative controls have been also elaborated; by a direct incubation of antibody after incubation of the Gst-tagged proteins, to quantify the number of tagged proteins bounded to the surface and not on the antibody. Pure Gst proteins were also injected on the anti-Gst antibody, followed by the purified proteins, in order to test the possible interaction between the pure proteins and the GST. All these results (visible in annex) confirmed the good quality of the process and the specificity of the biochip. As seen previously, we decided to study the interactions at 4 different pH, 5, 6, 7,4 and 9 in a PBS buffer. The temperature was maintained constant during the experiments, at 25 °C, and the buffer pH was adjusted and measured prior each experiment. Proteins were produced as described above and kept at -80°C prior each experiment, and slowly warmed, and diluted 1 hour before the experiment. Concentrations were adjusted for respecting the motor stoechiometry (For example 1 FliF for 1 FliG) and annex 1 presents the various concentrations used for the experiments. For each interaction, the monitoring of biochips surface preparation was recorded. The subsequent interaction between the probe and target is then recorded separately for better clarity. At least 2 concentrations for each experiment were tested, one at the plausible motor stoechiometry , and one 5 to 10 times smaller or larger depending on the studied interaction. However, the concentration of proteins was not a key factor for determining the affinity between the different proteins, as I will illustrate later.

## b. Results

### i. The Surface

Figure 13 exhibits a typical signal of the QCM-D sensor, recorded during a full surface preparation protocol where all the different steps of the protocol can be monitored. Both frequency and dissipation shift can be used, but I will only focus my analysis on the frequency signal. Figure 8 illustrates 4 different signals which correspond to the 4 chambers. Similar signals are observed from each chamber, but we notice that there is always variation between different sensors, probably coming from the sensor layer fabrication; this point will be discussed later. The first step, MUA layer formation, is not visible on the figure, because it is manually made before sensor installation within the Q-sense system. The traces are divided into 6 sections, corresponding to the major steps. (I) The MUA activation by the EDC/NHS mixture causes the first shift, mainly coming from a buffer effect rather than adding molecule

on the surface, because when the buffer is eluted, the signal increases up to its original level. This buffer injection is the frontier between the first and the second step, the anti-Gst antibody adsorption, which is revealed by a large shift in frequency (around 45 Hz) (II). When the signal is stabilized, which is interpreted by a full surface saturation with antibodies, ethanolamine incubation is responsible of the third step (III), the passivation for 40 minutes. Ethanolamine is a too small molecule for causing this large frequency shift, which again is mostly due to a buffer effect. We then inject a large amount of buffer (IV) for removing unbounded ethanolamine from the surface and inject the first protein, the Gst-protein, which causes the 5$^{th}$ step (V). When the traces are stabilized, meaning no more mass is added to the sensor, each chamber received a different buffer with pH ranging from 5 to 9. The chambers filled with a buffer of pH 7,4 and 9 were stable while chambers 5 and 6 exhibit a large jump in signal. To be sure that no molecules have been removed, we sequentially injected buffer at pH 7,4 and then again pH 5 or pH 6 and traces just fluctuate between two frequency values. The sensor is now ready for use to investigate a given protein/protein interaction. As a primary step, we characterized each single step by adding anti-Gst antibody as a negative control and results can be seen in annexe 1. It turned out that our protocol was robust and allowed the formation of two successive bio-molecule layers, a covalently bound anti-Gst antibody, and then a tagged protein.

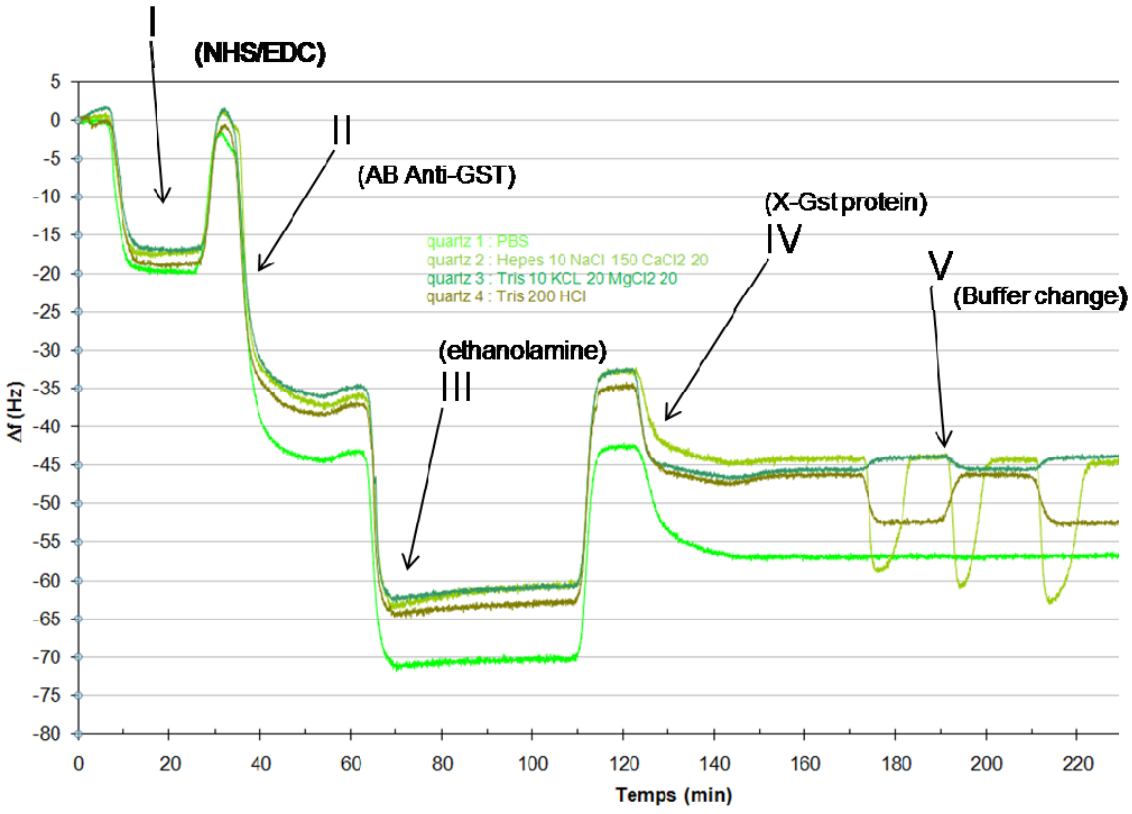

***Figure 13: QCM-D signals acquired during a surface preparation protocol****. 4 different chambers are recorded in parallel with 4 different buffer conditions. Same protocol is applied on each sensor. All the steps are described, only the last steps are not explained. The large drop visible on sensor 2, step 5, mainly comes from the presence of $CaCl_2$ in the buffer. Buffers are injected alternately with PBS for corroborating that the different buffers have not removed the molecules from the surface. Events on trace greenat step V are coming from a successive injection of buffer with different ions mixture.*

## 1. Anti-body anti-Gst adsorption.

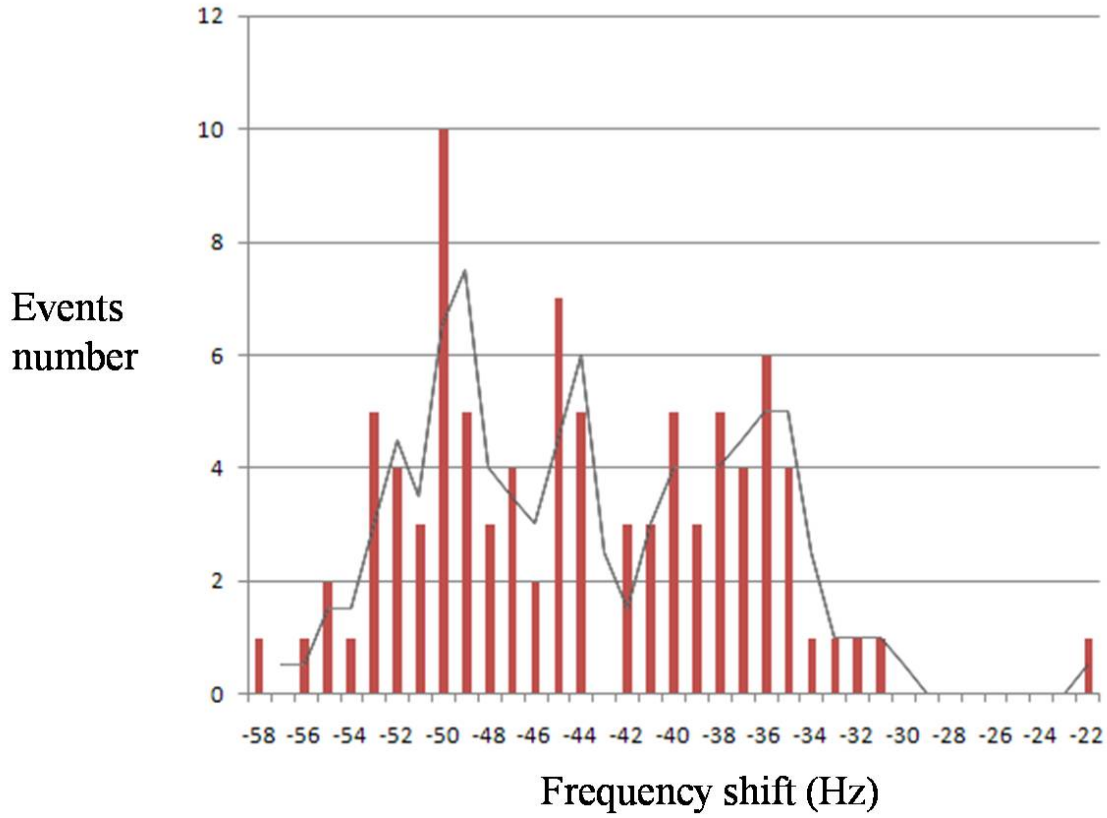


***Figure 14: Frequency shift of the anti-body adsorption on the Gold surface***

Figure 14 reviews at least 200 different experiments and shows the histogram of all the recorded frequency shifts observed after Antibody incubation during my whole thesis work. The adsorption of the anti-body anti-Gst is the first layer attached to the surface. We observed a relative large spectrum of shifts, from a -31Hz to -58Hz, with an average value of -44Hz. This dispersion was quite surprising at the beginning. In order to extract quantitative information from our data, it is absolutely necessary to know at the beginning the density of probe molecules on the sensor surface. As this density is related to the density of Antibodies Anti-Gst, it is crucial to record carefully the frequency shift measured during the incubation of the antibody. This procedure enables to compensate the dispersion of the frequency shifts that we have observed. For example, if we measured an anti-body anti-Gst adsorption shift of -

35Hz, and later a X-Gst frequency shift lower than expected, we compensate the second shift by taking care of the first shift, and so on. We noticed during the experiment that the cleaning procedure of the gold sensor was quite detrimental for its surface quality; despite the Qsense protocol proposed on their website. We tested several protocols but finally established our own by cleaning the gold sensor using a chemical mixture called “piranha”. It is a mixture composed of sulfuric acid and hydrogen peroxide (1:1 in our case). This solution is known to remove any organic compounds from a metal or silicon surface. This solution should normally be well suited for removing any proteins from the sensor surface without attacking the gold layer. However AFM characterization of the surface indicated that numerous holes formed during the cleaning procedure. Annex 1 shows a typical AFM imaging before and after sensor regeneration. Whatever the cleaning procedure we chose, the gold layer presented the same holes after treatment. We suspected that this surface modification was the main origin of this dispersion in the frequency shifts adsorption of the anti-body anti-Gst. In order to diminish any possible artifact, we only reproduced the same experiments on the same sensor series (for example FliN-Gst with FliM or FliN) and also limited our experiments only 4 times for each sensor.

## 2. The frequency-molecular mass relationship.

***Figure 15: Frequency shift function of the molecular mass.*** *Each point corresponds to a given protein.*

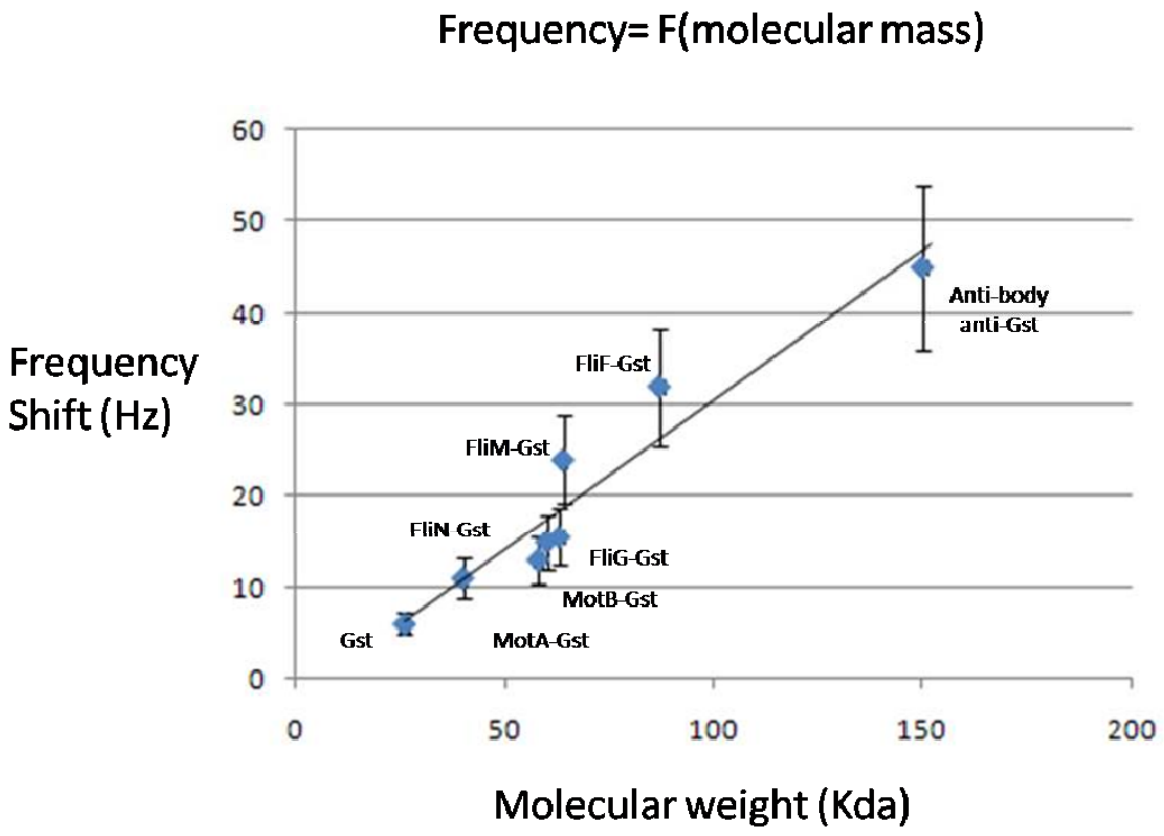

The QCM-D technology is a mass sensor, which means that in principle, if we assume that the number of proteins adsorbed on the surface is constant and independent of the molecular weight of these molecules, we can establish a direct relationship between the mass of the molecules injected and the frequency shift measured during the adsorption of molecule. By this way, we can confirm that the adsorption of our different molecules on the gold surface is in good agreement with their mass. We base these measurements only on the two first layers of our molecular multilayer, the adsorption of the ani-body anti-Gst and the X-Gst proteins. The pure proteins could not be considered in this figure, because their adsorption mainly depends of their affinity with the proteins already attached on the surface. This picture was elaborated using the adsorption signal of the Gst pure proteins (26 KDa), and other motor proteins (FliN-Gst, FliG-Gst, FliM-Gst, MotA-Gst, MotB-Gst, FliF-Gst) and finally pure anti-body anti-Gst. Figure 15 shows the obtained results. Each point on the curve represents the average from several measurements. We observe a clear correlation between the frequency shift measured during protein adsorption and the molecular weight of this protein. This result confirms our hypothesis that the density of sites where the different molecules can attach is constant and only depends on surface preparation, and do not depend on the size or mass of the proteins. The correlation coefficient between the molecular weight in (Kda) and the QCM-D frequency shift in Hz we have obtained is 0,31.

### ii. Methodology for quantifying the interaction between two proteins.

This paragraph explains the method we use for analyzing QCM-D data. Let us consider two proteins called A-Gst, and B, and the analysis of interaction between B in solution and A fixed on surface through its Gst tag.

Let $\Delta f_A$ and $\Delta f_B$, the frequency shifts recorded by the QCMD sensor after adsorption of proteins A and B respectively. According to Sauerbey equation (1), the additional mass per unit during adsorption of protein A is $\Delta m_A = C\Delta f_A$ (C being the mass sensibility coefficient). The surface density (number of proteins A/ unit surface) is therefore

$$d_A = (\Delta m_A * N) / Mw_A$$

(N: Avogrado number, $Mw_A$ : molecular weight of proteins A)

The same relation also runs for protein B adsorption. For quantitative analysis of the interactions between B and A, we define a simple ratio $I_{AB}$ given by:

$$I_{AB} = d_B/d_A$$

The higher the ratio, the higher the interaction between the proteins. According to the previous relations:

$$I_{AB} = d_B/d_A = (\Delta m_B . Mw_A) / (Mw_B \Delta m_A)$$

It is worth noticing that this ratio is independent of C (the mass sensitivity of the QCM sensor) and only depends on reliable quantities $\Delta f_A$ and $\Delta f_B$ (experimental measurements) and $Mw_A$ and $Mw_B$ molecular weights of the proteins.

This interaction ratio $I_{AB}$, will be used extensively in the following for the different proteins of interest and can be used for qualitative comparisons between different couples. Of course, we have not the pretention to derive affinity constants by this method but we simply introduce a robust and non questionable well defined experimental parameter.

### 1. Example of interactions between two proteins of the BFNM, the MotA-FliM interactions.

Due to the large number of studied interactions, I will only show here one couple, the MotA-FliM, other data can be seen in annexe 1 and will be summarized later. I will describe for this specific couple the procedure I pursued in order to address the question of their affinity or interaction within the BFNM. I base my analysis on the successive QCM-D traces, first the complex of the MotA-gst pictured in Figure 16 and then the FliM signal measurement on each chamber. Figure 16 displays the interaction factors $I_{MotA\text{-}FliM}$ as defined previously for 4 conditions of pH in PBS. In this experiment the MotA was tagged with Gst and fixed at the surface. A strong influence of pH on the affinity between MotA and FliM is clearly observed. For pH 5 and pH 6, the two molecules do not exhibit interaction while at pH 7,4 and pH 9 a strong interaction ( I= 0,4 and I=0,29) is evidenced. In a second step, we have also investigated the influence of the buffer composition.

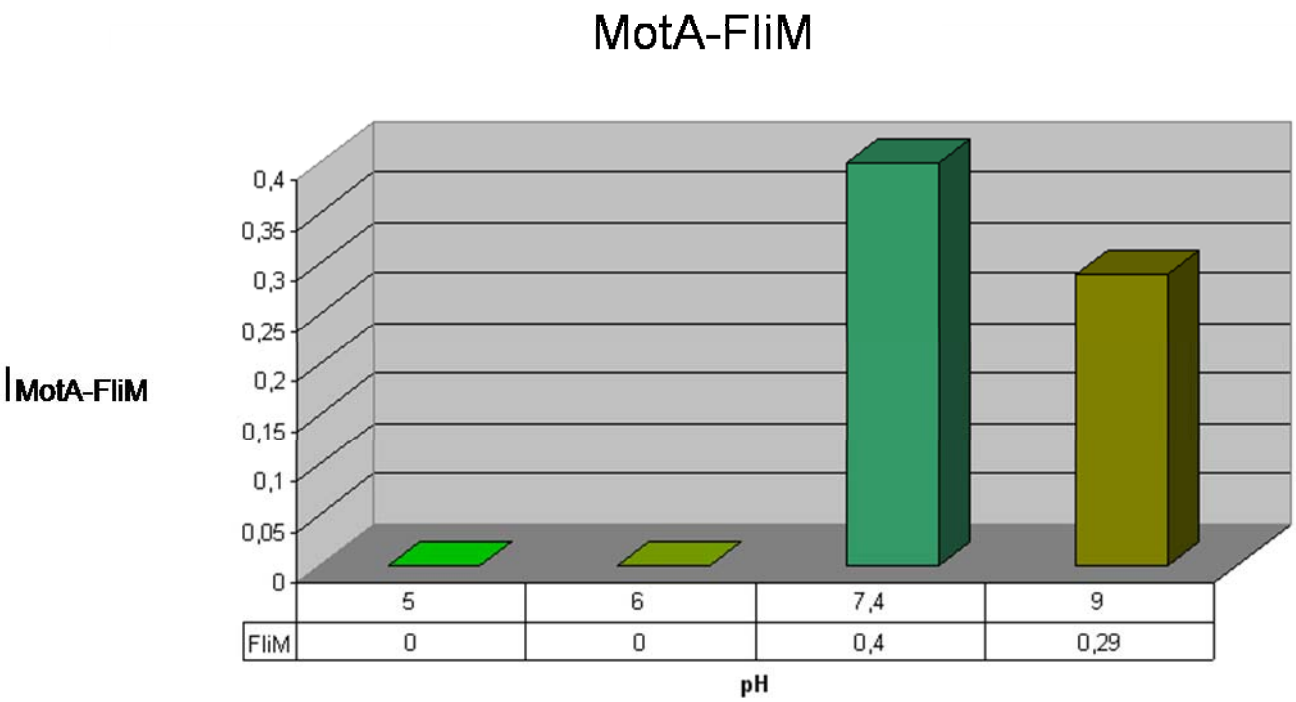


***Figure 16: Interaction ratio $I_{MotA}$/FliM in PBS buffer at four different pH.***

We put side by side the same MotA-Gst/ FliM interaction in 4 buffers , PBS , Hepes 10 mM NaCl 150 $CaCl_2$ 20 mM, Tris 10 mM KCl 20 mM $MgCl_2$ 20 mM and Tris 200mM HCl, all presenting the same pH value of 7,4. Results are displayed in figure 17A and synthesized in figure 17B. In each case, the strong interaction between MotA and FliM is observed at pH 7,4. The experimental value of the interaction factor I varies from 0,16 to 0,29 but it seems that the buffer composition has not a drastic influence on the result. Having verified that the choice of a specific buffer was not a limitation to the generality of our conclusions, we decided to select PBS buffer for the rest of the investigation.

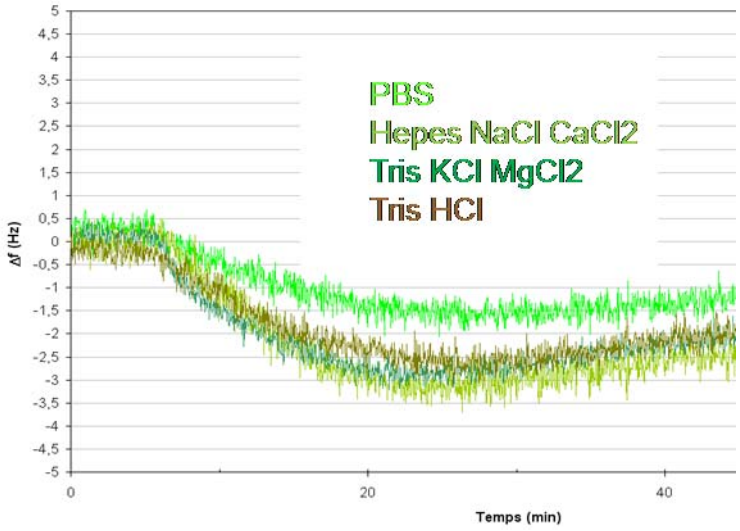


***Figure 17A: QCM-D traces of the interactions between FliM in solution and MotA fixed on the surface in 4 different buffers.***

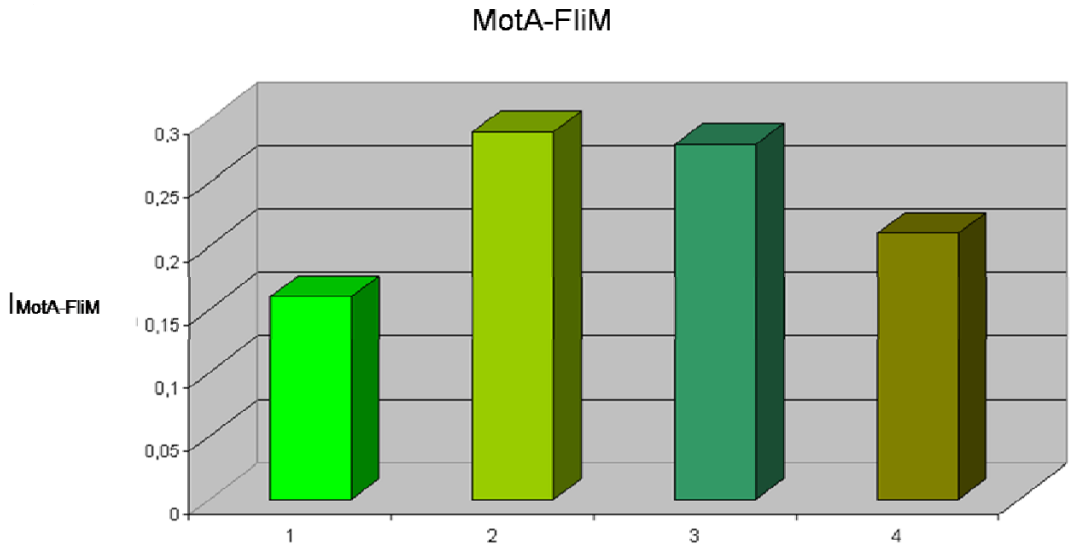


***Figure 17B: histogram of the interaction factor $I_{MotA\text{-}FliM}$ measured in different buffers at pH 7,4.*** *1: PBS , 2: Hepes 10 mM NaCl 150 $CaCl_2$ 20 mM, 3: Tris 10 mM KCl 20 mM $MgCl_2$ 20 mM, 4: Tris 200mM HCl.*

## iii. Synthesis

As noticed in the protein production section, we succeeded in the production of the 6 motor proteins directly involved into the actuation of the motor, however only four, FliM, FliN, FliG, and MotB were obtained without their Gst tag. This result allowed us to study the interactions between all the proteins bound to the surface thanks to the Gst tag, but only 4 in liquid. I calculated for each Gst-protein in 4 different pH PBS buffer their interaction with the

FliM, FliN, FliG, and MotB proteins. Example of results for the MotA-Gst is shown in figure 18.

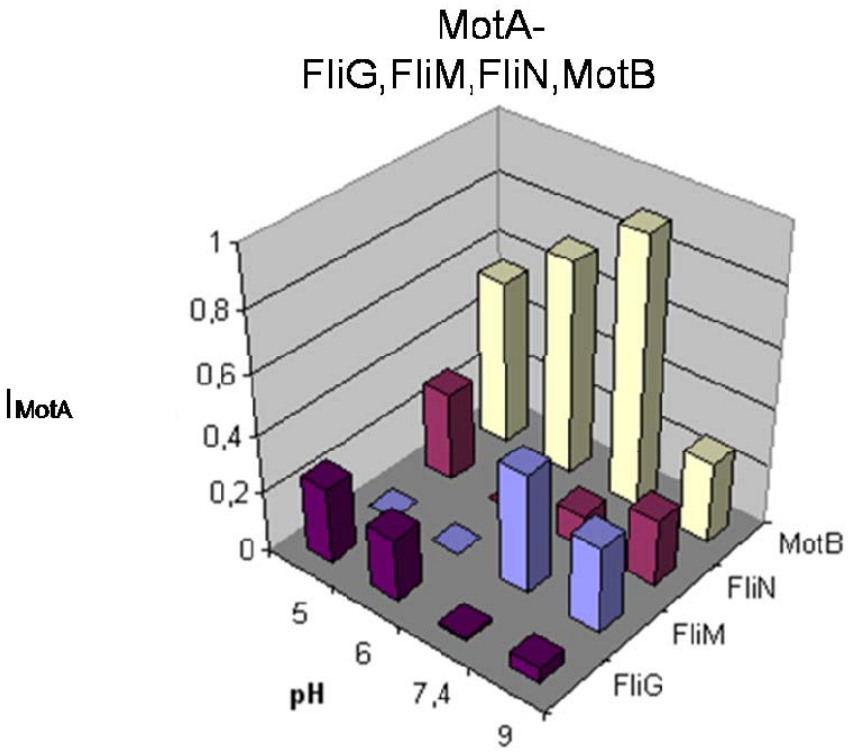


***Figure 18: Synthesis of the diverse interactions recorded with MotA.*** *The graphics shows I MotA/ (FliG;FliM;FliN;MotB) at 4 pH in PBS buffer. Interactions between MotA and the others motor proteins are clearly noticeable and pH dependent.*

Based on our observation, it turns out clearly that the MotA protein interacts differently with other proteins, and these interactions are pH dependent. Some interactions are stronger than others, but the amplitude of I should be taken carefully, due to the variability of the quality of sensor surface. The second point is related to the nature of the MotA protein. We are talking of trans-membrane proteins, so its native configuration could be largely altered by this fixation outside of a phospholipids membrane. So the interaction between MotA, MotB and others proteins should be handle with precautious. Based on numerous experiences, we can say that the adsorption on each sensor is not totally comparable, as seen in annex 1. As mentioned before I considered for each interaction the value of "I", for the antibody adsorption, followed by the Gst-proteins and finally the free one. A same experiment repeated several times always exhibited the same tendency with the respect to the Interaction factor I. However, due to the sensibility of the sensor system (between 2 and 5 nM), each study

repeated several times could give a slight different value. For our study, each couple was tested at least two times with two different proteins concentrations and same tendency was found in both cases. The value "I" has been averaged from these measurements. Same approach has been followed for all the studied interactions, and results are displayed in figure 19. Our protocol fixed the first protein by its N terminus, and this terminus could be involved into interaction with other proteins which indicates that some interactions, could not occur due to spatial conformation. This point will be discussed later.

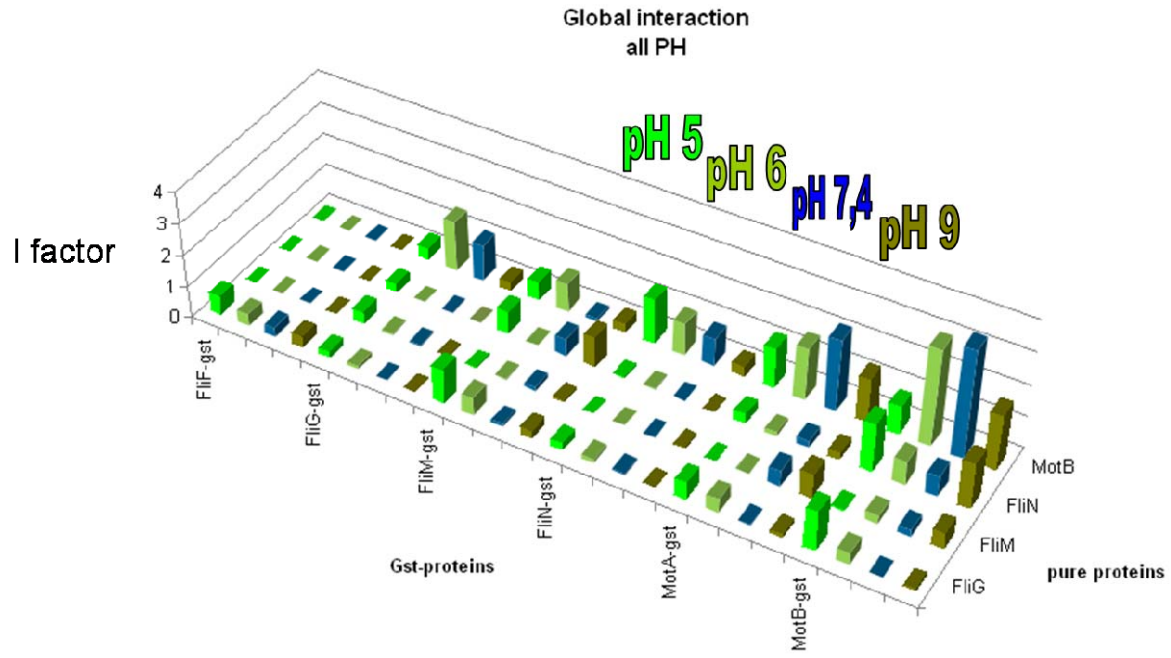


***Figure 19: Interactions factors for all the couple of proteins investigated at 4 different pH in PBS buffer.***

However, due to the structure of the motor, the interaction observed in acid buffer (pH 5) and also basic buffer (pH 9) will not be taken into account and remain to be analyzed. Experiences have demonstrated that bacteria can no longer swim in these buffers. I will discuss only the results on a relevant cytoplasmic pH of 7,4.

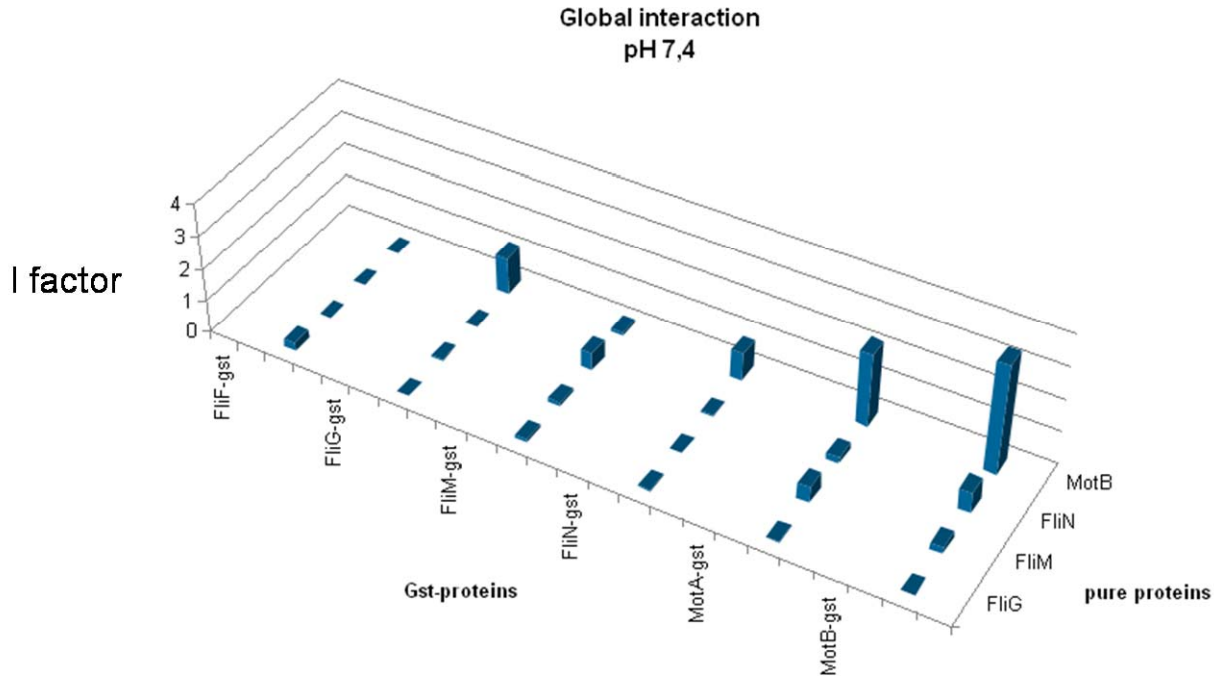


***Figure 20: Interactions factors for all the couples of proteins investigated in PBS at pH 7,4 close to the pH of the bacterium cytoplasm.***

## c. Discussion

As noticed before, only six proteins are directly involved into the motor function, 2 found on the rotor FliF and FliG, 2 found on the stator MotA-MotB and the last 2 FliM FliN in the C-ring. This organization will be discussed in chapter 4. The interactions between these different proteins have been already studied, as discussed above. However, these previous studies were performed in a defined medium, which was often related to the conditions of observation. The flexibility of those methods did not allow the study of the motor proteins interactions in liquid media. The QCM-D technology allows us to work in various buffers, which display different ionic concentration or pH conditions. This flexibility was used to reproduce some media change which could occur in the motor. By studying the protein interactions in 4 different pH buffers, we emphasized to picture the role played by the pH and addressed numerous questions about the motor. The motor is working well for an internal pH maintained by the bacteria between pH 7,4 and pH 9. This favorable environement is represented in our experiments by PBS buffer at pH 7,4 and 9. We altered the pH of the medium keeping in mind that some essential interactions between motor parts could be distorted while protons arriving into the cytoplasm. Based on our experiments, I decided to

synthesize and concentrate our results analysis on the interactions observed at pH 7,4. This pH could be considered at the cytoplasmic one and I will discuss the interactions in other pH with more precautions. This choice is mainly coming from the fact that the local pH in vivo around a motor has never been measured and any conclusion about interactions in other pH would depend on this measurement.

We would like to briefly discuss here the advantage of our surface preparation protocol which grafts proteins in an adequate spatial configuration thanks to the Gst tag. Numerous others options exist: the first other option could be based on a direct fixation of proteins on the MUA layer after activation, using the presence of amine function on proteins. But by this way, same limitations as the Biacore surface creation would be encountered: a non-oriented fixation of the protein. This approach would severely limit results interpretations. The second idea was to use an antibody/antigen link instead of an anti-Gst antibody. But again, by this way, the proteins would be linked in a specific way which is unknown and could complicate result interpretations. By using the tag Gst, we address all these remarks. However, the N-terminus of each Tagged proteins would remain difficult to access due to the Gst tag and this point could limit the identified interaction using the N-terminus C-terminus.

Figure 20 summarized the interactions observed at pH 7,4 and figure 21 presented them in a cartoon view of an hypothetical spatial arrangement of the motor.

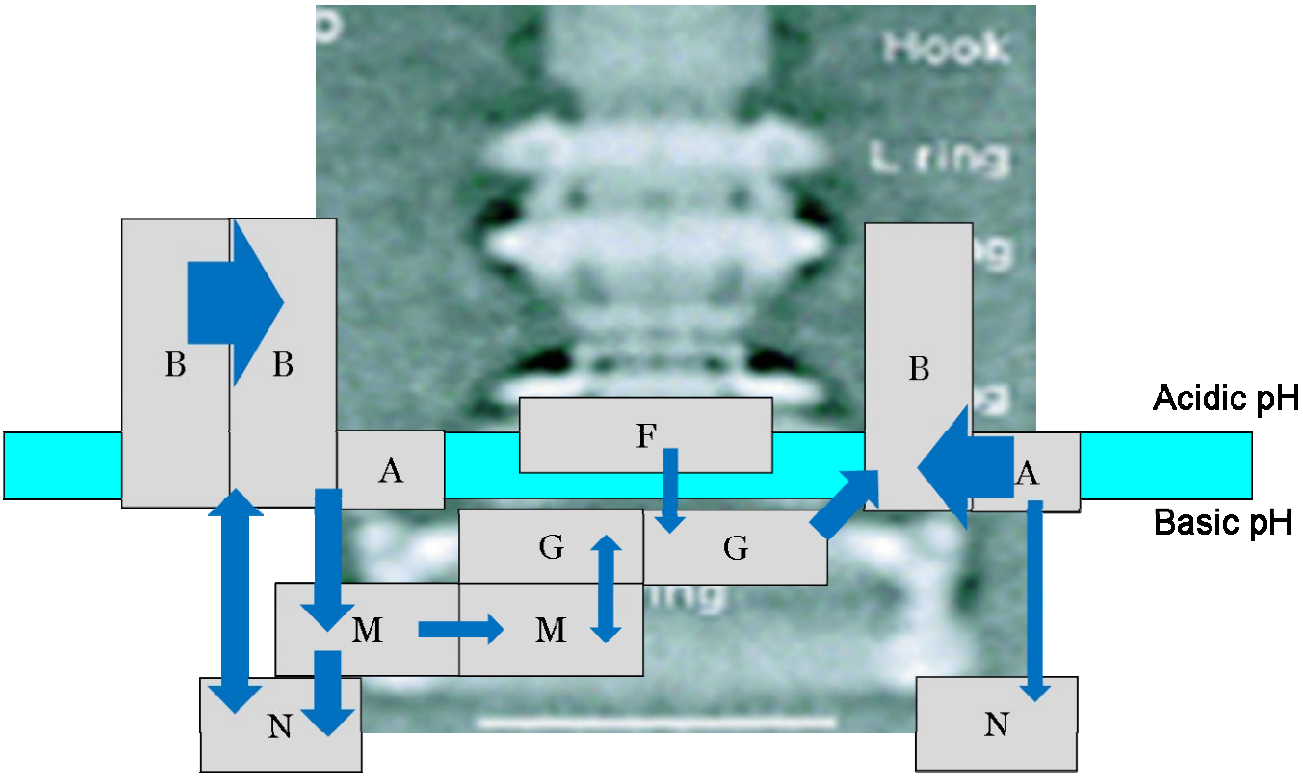


***Figure 21: Cartoon view of the interactions at pH 7,4.*** *Width of the arrows schematically represents the intensity of the interaction as given by the interaction factor I .*

The electrical charge of a protein has a major influence on its possible interaction with other partners. It is thus crucial to know this parameter for the proteins we have investigated. Based on the protein sequence, we have evaluated the iso-electric point for each protein. The isoelectric point (pI) is the pH at which a molecule carries no net electrical charge. Proteins contain naturally positive and negative charges, due to presence of specific amino acids. These charges are affected by the surrounding environment; especially the pH and can become positive or negative due to the loss or gain of protons. Due to these properties, proteins can thus be separated according to their pI on a polyacrylamide gel using technique called isoelectric focusing which utilizes a pH gradient to separate proteins. It is also the first step in 2D gel polyacrylamide gel electrophoresis. However, numerous software are now available to determine the net charge of a proteins based on the amino acids sequence. Several models have been proposed in the literature with slight different values. I will use the online program found on the web site http://isoelectric.ovh.org/. Several model of calculations are accessible but the following table is based on the EMBOSS algorithm. I noticed that the

values calculated for each protein can be slightly different from an algorithm to another, but the general tendency are identical. The figure 22 was obtained using the website http://www.embl-heidelberg.de/cgi/pi-wrapper.pl.

| FliF | | FliG | | FliM | | FliN | | MotA | | MotB | |
|---|---|---|---|---|---|---|---|---|---|---|---|
| pH | Charge | pH | Charge | pH | Charge | pH | Charge | pH | Charge | pH | Charge |
| 1 | 67.9023306473417 | 1 | 39.9073757191847 | 1 | 42.9181622538306 | 1 | 13.9338726858115 | 1 | 29.9328466819212 | 1 | 47.9201759684109 |
| 1.5 | 67.7034693771563 | 1.5 | 39.719388754494 | 1.5 | 42.7534189016735 | 1.5 | 13.8030089962055 | 1.5 | 29.7997299190972 | 1.5 | 47.7597868360824 |
| 2 | 67.1518160004646 | 2 | 39.2018156945742 | 2 | 42.3086384625483 | 2 | 13.4645578792912 | 2 | 29.4538492651988 | 2 | 47.3287748009734 |
| 2.5 | 65.7561078043001 | 2.5 | 37.9109125832728 | 2.5 | 41.2410802365119 | 2.5 | 12.7254118333894 | 2.5 | 28.6883491889479 | 2.5 | 46.3047206302194 |
| 3 | 62.2905420304005 | 3 | 34.7500898209081 | 3 | 38.7252455840096 | 3 | 11.176746871379 | 3 | 27.0328583284398 | 3 | 43.9253942844017 |
| 3.5 | 54.1603297751473 | 3.5 | 27.3846023186341 | 3.5 | 32.9481903719387 | 3.5 | 7.90654227066764 | 3.5 | 23.2964048284361 | 3.5 | 38.5565151948679 |
| 4 | 39.7069958472817 | 4 | 14.3461476104478 | 4 | 22.7255376226194 | 4 | 2.6032266923024 | 4 | 16.4140728522483 | 4 | 29.325094401375 |
| 4.5 | 23.5524940322684 | 4.5 | -0.137381639765785 | 4.5 | 11.2883631280389 | 4.5 | -2.69062584118472 | 4.5 | 8.2630756516306 | 4.5 | 19.3765886653855 |
| 5 | 12.4821924795588 | 5 | -9.89310663158753 | 5 | 3.3481518504281 | 5 | -5.91188672616909 | 5 | 2.40895478703415 | 5 | 12.6920880985687 |
| 5.5 | 6.58553709803373 | 5.5 | -14.7109408441478 | 5.5 | -1.15818641930524 | 5.5 | -7.28242264521683 | 5.5 | -0.852125260144611 | 5.5 | 9.02668098320157 |
| 6 | 2.81767947489098 | 6 | -17.2657653434461 | 6 | -4.42899273199612 | 6 | -7.76707061356266 | 6 | -3.06416982103689 | 6 | 6.47780119855768 |
| 6.5 | 0.178727286332531 | 6.5 | -18.8066060409598 | 6.5 | -6.91170823210578 | 6.5 | -7.92726938738441 | 6.5 | -4.67717151746144 | 6.5 | 4.59039501539394 |
| 7 | -1.20584723334011 | 7 | -19.5697573324978 | 7 | -8.26990547783137 | 7 | -7.9820143581509 | 7 | -5.56182793325462 | 7 | 3.58082013019651 |
| 7.5 | -1.77959206223774 | 7.5 | -19.87879107534 | 7.5 | -8.89974631714471 | 7.5 | -8.01033489258718 | 7.5 | -6.01362449577616 | 7.5 | 3.15766290003993 |
| 8 | -2.07317591881284 | 8 | -20.0314870810762 | 8 | -9.34239470263298 | 8 | -8.05352459343708 | 8 | -6.42879266263508 | 8 | 2.93342097812499 |
| 8.5 | -2.47118137157035 | 8.5 | -20.2286939338031 | 8.5 | -9.9063845311457 | 8.5 | -8.17172003705546 | 8.5 | -7.08783116596842 | 8.5 | 2.61431861542972 |
| 9 | -3.48633689447377 | 9 | -20.7236248326658 | 9 | -10.8161230270859 | 9 | -8.50758735598626 | 9 | -8.33033328843577 | 9 | 1.79106703863948 |
| 9.5 | -6.08913781303432 | 9.5 | -21.9911725003073 | 9.5 | -12.6174316374928 | 9.5 | -9.33737443976618 | 9.5 | -10.986418570616 | 9.5 | -0.317785854190035 |

***Figure 22: Pi Vs surface charge of the proteins at different pH****. The 4 tested pH have been marked on the table. bright green rectangle pH 5, dark green rectangle pH 6, blue pH 7,4 and brown pH 9.*

I will discuss the interactions in three cases: the expected and detected, those expected that were not detected in our experiments, and unexpected.

**The expected and detected interactions:**

-MotA/MotB and MotB/MotB.

The two stators proteins strongly interact in any buffer at any pH. This result confirms the stability of the stator within the motor architecture. The opposite value of the net charge at pH 7,4 ( 3,58 for MotB and -5,56 for MotA) also confirms the strong interaction observed. We have not tested the injection of pure MotA on a MotB-Gst sensor but this result will probably go in the same direction. Those interactions were the higher response from the all experiments, at least 2 to 3 times stronger than for any other couples of proteins (respectively MotB/MotA-Gst 2,23 and MotB/MotB-Gst 3,37).

-FliM/FliN

The spin backbone of the C-ring structure was also detected, despite same negative pI, but only by fixing the FliM and injecting the FliN. The role played by the spatial conformation and the presence of the Gst tag on the grafted protein can explain this final result, due to the role played by the N-terminus into the interaction between FliN and FliM REF. The intensity of the interaction was lower than expected (0,53) and this value could have different origin. It can either come from a natural tetramer organization of the FliN, which diminish the possible interaction with the grafted FliM-Gst. But it can also highlight the need for a third partner for assembling the C-ring, as for example the FliG.

-FliF/FliG

This interaction was really weak compared to what we expected. As noticed before and showed in chapter 4, we suspected that the FliG naturally self-assembled into rings, directly in solution or in contact with the FliF proteins, for forming the MS-ring. We think that the lower value obtained here is due to the presence of already formed rings of FliG which cannot interact easily with FliF, grafted on the surface. However, this explanation is purely hypothetical. The value obtained, 0,27, remained still far from negligible.

-MotA/FliG

This interaction was known to be the source of the rotor movement. This interaction was established using our approach for an acid pH, which corroborates the role played by the protons into the interaction. This interaction is not the higher (0,02) and it is also a good thing, because this interaction is a very dynamic one, not a structural one. It could have been detrimental for the rotation that the MotA too strongly binds to the FliG.

-FliM/FliM

The FliM/FliM interaction was weaker than expected (0,11). The role of the N-terminus of the FliM protein could be responsible for that, but it has not been identified to be involved into this interaction. The need for another protein could be the reason for that relative weak interaction.

**Expected interactions, not observed in this work.**

-FliG/FliG

The FliG/FliG interaction was not observed during our study at pH 7,4, and at an extremely weak interactions was seen at acid pH. The presence of proteins aggregates of 25 nm of diameter in solution, as observed in chapter 3, could prove that the FliG was already assembled into a ring, which reduces the possible interaction with proteins grafted on a surface. However, this explanation remains purely hypothetical. We have tested several times with several protein batches and none of them have interacted with the FliG-Gst. This result highlighted also the good specificity of the sensor elaboration.

-FliN/FliN

This interaction was not observed. Based on the FliN tetramer assembly, we suspect that the FliN was either already assembled on the surface and in liquid. However, this result reveals a more interesting result: the FliN tetramer cannot interact with other tetramers, which implies that another partner is probably needed to relate all FliN assembly. It could be FliM or FliG, or stator proteins.

-FliG/FliM

This interaction is the key support for all the current model of the BFNM. Numerous studies based on mutagenesis and also structural data supported an interaction between these two proteins. However, the last result obtained using Cryo-TEM revealed an asymmetry between the FliG and FliM numbers and also a weak atomic density between the C-ring and the rotor, symbolized by the FliM and the FliG. We tested it several times and the interactions always occurred in an acid buffer, lower than 6 which could be explained by their electrostatic charges. They are both negative at pH 7,4, but in opposite sign for acid pH, which could explain their interactions at pH 5. However, the interaction was higher by fixing FliM and passing FliG than the opposite case. We think that the FliM fixed on the surface bounded FliG proteins already formed into the M-ring, which resulted a higher mass added on the surface. In the opposite case, the FliG were fixed on the surface and only FliM relatively independent interacted, which gave a lower additional mass. This difference of response reveals that the FliM self-organization is not similar to the FliG ring organization, and the link between the C-ring sub-units is related to the FliM self-assembly but others proteins could be involved. The interaction between FliM and FliG was always observed in acid pH, which is very far from

the bacteria cytoplasm medium. The observation of the FliG-FliM interactions using others approaches based on mutagenesis and affinity blots could have been made in conditions which amplified artificially the affinity between the proteins, conditions which could be very different than the native ones. Same questions arise about the extraction protocol for the cryo-TEM observation.

**Unexpected interactions detected in our work.**

-FliG/MotB

This interaction remains one of the most intriguous one. The high value (1,14) when we injected MotB on a FliG-Gst was not confirmed by the opposite case (0,02 for FliG/MotB-Gst). The role played by the electrostatic charges (respectively positive +3,58 for MotB and -19,56 for FliG) could explain partially this interaction but does not explain why it remains stronger in one direction than in the other one. Only a spatial localization of the interaction could explain this behavior, by proposing that the C terminus of the FliG could interact with the N-terminus of the MotB. This hypothesis could explain the lowest value when the N terminus of the MotB is not accessible when grafted with the Gst on the surface. This interaction has neither been observed nor proposed by any model. The presence of such interactions at pH 7,4 could be problematic for a rotation of FliG. The role played by this interaction will be largely discussed in chapter 4.

-FliN/MotB

The interactions measured between FliN and MotB were the second larger in value after the stator interactions. FliN/MotB-Gst (0,64) and MotB/FliN-Gst ( 0,84) confirm the importance of this interaction and its reality. The opposite values of their electrostatic charge could be responsible for this interaction. FliN strongly interacts with MotB whatever which protein is grafted or injected. This interaction could be the proof of the direct role played by the stator with the C-ring assembly. It shows again that if this interaction really occurs in the motor, the rotation of the C-ring is not possible.

-FliM/MotA

The FliM/MotA-Gst interaction has been observed years ago [36] but for unknown reason neglected. Both proteins present negative electrostatic charge. We have not tested the MotA/FliM-Gst due to the difficulty of MotA purification using our protocol. This interaction

could involve the cytoplasm part of the MotA which represent 2/3 of its mass. The presence of such interaction reduces also the possibility of a C-ring rotation.

-MotB/FliM

Both interactions are clearly seen (0,2 for FliM/MotB-Gst and 0,11 for MotB/FliM-Gst). However, their opposite electrostatic charge could be responsible for this interaction which is weaker compared to others. If electrostatic interactions are not responsible for this interaction, other domains as the N terminus of both proteins could be involved. As for FliM/MotA or MotB/FliN, the presence of this interaction totally contradicts the hypothesis of a C-ring rotation.

Some interactions were observed between proteins which could take place in the current view of the BFNM structure, but numerous one were observed for the first time using the QCM-D technology: between the MotB and the FliN, between the MotB and FliM, between MotB and FliG, between FliM and MotA (already observed previously), between FliG and FliN and between MotA and FliN. The role and influence played by their electrostatic charges have been taken into consideration. However, the presence of numerous interactions between stator and C-ring elements was a huge surprise, but should be handle with precautious. Working with trans-membrane proteins outside of a phospholipids environment opened the question about the protein configuration of these proteins, here FliF and MotA, which present hydrophobic parts. I will consider them as reliable for the moment, but the study of their interactions with others motors proteins will need to address using others protocol of fixation, probably by mixing formation of phospholipids bilayer to pure proteins. How could the motor self-assemble in a specific order if some of its elements naturally interact with others non-respecting the final assembly? How could the C-ring rotate as a unit with the rotor is some of its elements interact with the fixed stator? I think that most of these new interactions gave us an access not only to the final structure of the BFNM, but also to the assembly stage. The hypothesis of an interaction between the stator and the C-ring, through FliM and FliN directly instead of FliG will be discussed in chapter 4 in our model hypothesis but emphasizes the need for a new vision of the BFNM structure.

## E) Conclusion

As shown and discussed, numerous interactions have been studied using the QCM-D technology. Based on the established protein assembly, we could visualize the protein interactions into a cartoon view, presented in figure 13. New interactions were observed and discussed. This approach of protein-protein interaction based on a new sensing technique (QCM) brought new data. Our protocol is based on three essential points: the need for good quality purified proteins. This task remains the major and critical bottleneck for this kind of experiment, as we have seen for example when we tried to purify FliF or MotA. The second point is the specificity of the interaction. We tried to minimize the non-specific adsorption on the surface which is also the key for viable interpretation. Other protocol can be elaborated and could improve again this specificity. The last point is the role played by the medium either here by adjusting the pH, or the concentration of cations and anions. Working in PBS or others in vitro buffers will never replace the native bacterial cytoplasm medium, but this point is common for all in vitro experiments. This point will be addressed soon by pursuing series of experiment in a new buffer. We started by a single protein fixed and a second passed in solution, but multiplexed experiment could also be designed in our approach by mixing directly proteins to be fixed or protein in solution. This original protocol could evidence the role played by other elements into the assembly, for example by mixing FliG and FliM and add FliN. New series are currently under investigation. Another new parameter of interest is the temperature. Numerous studies showed that the BFNM is sensible to the temperature. All my experiments were achieved at 25°C. The same experiments could be achieved at 37°C or lower than 25°C in order to analyze the role played by the temperature in the stability of the interactions. All these points confirm the feeling we do have that the QCM-D technology could play a fundamental and essential role in a near future, with more flexibility than other approaches. All of the results obtained will be injected in chapter 4 in a new model describing the BFNM.

[1]D.L. Marykwas, S.A. Schmidt, H.C. Berg*, Journal of Molecular Biology 256 (1996) 564.
[2]D. Marykwas, H. Berg, J. Bacteriol. 178 (1996) 1289.
[3]H. Tang, D. Blair, J. Bacteriol. 177 (1995) 3485.
[4]A.S. Toker, R.M. Macnab, Journal of Molecular Biology 273 (1997) 623.
[5]H. Tang, S. Billings, X. Wang, L. Sharp, D. Blair, J. Bacteriol. 177 (1995) 3496.
[6]J. Zhou, D.F. Blair, Journal of Molecular Biology 273 (1997) 428.
[7]A. Bren, M. Eisenbach, Journal of Molecular Biology 278 (1998) 507.
[8]M.A.A. Mathews, H.L. Tang, D.F. Blair, J. Bacteriol. 180 (1998) 5580.
[9]J. Zhou, L.L. Sharp, H.L. Tang, S.A. Lloyd, S. Billings, T.F. Braun, D.F. Blair, J. Bacteriol. 180 (1998) 2729.
[10]T.F. Braun, S. Poulson, J.B. Gully, J.C. Empey, S. Van Way, A. Putnam, D.F. Blair, J. Bacteriol. 181 (1999) 3542.
[11]L.F. U. Jönsson, B. Ivarsson, B. Johnsson, R. Karlsson, K. Lundh, S. Läfas, B. Persson, H. Roos, I. Rönnberg, S. Sjölander, E. Stenberg, R. Stahlberg, C. Urbaniczky, H. Ostlin, and M. Malmqvist, Biotechniques 11 (1991) 620.
[12]B.l. C. Nylander, Sensors and Actuators 3 (1982) 78.
[13]G.C.A.M. Bokken, R.J. Corbee, F. van Knapen, A.A. Bergwerff, FEMS Microbiology Letters 222 (2003) 75.
[14]J-P.Esteve. Frédéric Lopez, PROTEOMICS 3 (2003) 402.
[15]Robin L. Thurmond, European Journal of Biochemistry 268 (2001) 5747.
[16]H.R. E. Krestschmann, Z. Natureforsh 23A (1968) 2135.
[17]A. Otto, Z. Physics 216 (1968) 398.
[18]G. Sauerberg, Z. Physics 155 (1959) 206.
[19]A. Ruocco, M.P. Donzello, F. Evangelista, G. Stefani, Physical Review B 67 (2003) 155408.
[20]M.R. M.V. Voinova, M. Jonson, B. Kasemo, Physics Scripta 59 (1999) 391.
[21]F. Hook, M. Rodahl, B. Kasemo, P. Brzezinski, Proceedings of the National Academy of Sciences of the United States of America 95 (1998) 12271.
[22]F. Hook, B. Kasemo, T. Nylander, C. Fant, K. Sott, H. Elwing, Analytical Chemistry 73 (2001) 5796.
[23]K.J. Catt, G.W. Tregear, H.G. Burger, C. Skermer, Clinica Chimica Acta 27 (1970) 267.
[24]F. Caruso, E. Rodda, D.N. Furlong, Journal of Colloid and Interface Science 178 (1996) 104.
[25]A. Sadana, Chemical Reviews 92 (1992) 1799.
[26]D.S. Tawfik, B.S. Green, R. Chap, M. Sela, Z. Eshhar, Proceedings of the National Academy of Sciences of the United States of America 90 (1993) 373.
[27]F. Höök, et al., Colloids and Surfaces B: Biointerfaces 24 (2002) 155.
[28]G.J. Leggett, C.J. Roberts, P.M. Williams, M.C. Davies, D.E. Jackson, S.J.B. Tendler, Langmuir 9 (1993) 2356.
[29]J. Wang, L.M. Frostman, M.D. Ward, The Journal of Physical Chemistry 96 (1992) 5224.
[30]K. Robert, Journal of Molecular Recognition 17 (2004) 151.
[31]W. Alain, Electroanalysis 10 (1998) 1217.
[32]S.J.V.Z. T.wink, A. Bult, W.P. Van Bennekom, The Analyst 122 (1997).
[33]M.M. Biener, J. Biener, C.M. Friend, Langmuir 21 (2005) 1668.
[34]Y.T. Kim, R.L. McCarley, A.J. Bard, Langmuir 9 (1993) 1941.
[35]M. Mrksich, G.M. Whitesides, Trends in Biotechnology 13 (1995) 228.
[36]H. Tang, T.F. Braun, D.F. Blair, Journal of Molecular Biology 261 (1996) 209.

# Chapter III
# A journey at the nano-scale
# Assembly of a part of the motor on an engineered surface

Summary

# A) Introduction

As described in chapter I, the BFNM is a fabulous machine which propels its host at high speed. Despite the fact that scientists have observed the rotation of the flagellum in vivo during the last thirty years, have established the names and numbers of the different motor pieces and defined approximately the role played by each of them, the details of its mechanism remain unknown, partially due to the difficulties encountered for observing the motor at the nano-scale. Nano-scale imaging can be divided into two categories, *in vivo* and *in vitro*, both of them have brought data about the BFNM.

*In vivo* approach based on mutagenesis and "resurrection" experiments were described in chapter I. By coupling mutagenesis to biophysical approach, Berg *et al* have developed the "resurrection" methodology[1; 2]. Cells have been fixed to a surface and rotation generated by the BFNM observed through the movement of a nano-bead sticked to a genetically modified flagellum which displayed only the hook as an external part. By applying a force to this bead using optical tweezers and magnetic tweezers, they opened a new route for acquiring mechanical data about the BFNM, as for example the torque speed-relationship or the dependency of the rotation rate to the protons motive force (pmf). This approach presented the advantages of mixing mechanical data to structural change. They developed biophysics tools for studying rotation at the nano-scale *in vivo*. New experiments have been proposed, by adding fluorescence dye to the motor proteins for example. These experiments revealed some dynamical aspect of the BFNM function, for example the chemotaxis process and interactions with the BFNM [3; 4], the movement of proteins[5] or some unexpected data about the addition of new proteins upon rotation[6]. However, the fluorescence observation of single BFNM is intrinsically limited by the optical resolution, which reduces the possibility to count each element in a single motor, and place them in a 3D environment. Most of the observations of the mutagenesis experiments were just obtained by monitoring the movement of individual cells and by measuring the radius of a colony after several hours of development in a Petri dish. Observation at the nano-scale of a single motor

under rotation has not been achieved and probably will not be until new techniques are proposed.

On the other side, *in vitro* experiments, using cryo-TEM produced images of the BFNM (see chapter I). Starting by the work of DePamphilis and julius Adler in 1971[7], to more recently Derosier *et al* [8; 9; 10; 11; 12; 13] through the years a reliable method for extracting, replicating and imaging part of the motor has been developed.

By coupling mutagenesis with structural data, they visualized the effect of mutations on the BFNM assembly and deduced the presence and role played by each of the element. Following this approach, other researchers tried to visualize part of the motor, directly formed and purified from cell [14] or rebuilt into artificial structure [15]. The major default of these experiments was inherent to the sample preparation, in freeze situation and sometimes using a replica instead of the real proteins units, conditions quite far from the native ones. The use of cryo-TEM also remains challenging for image interpretation due to the poor signal to noise ratio.

Both approaches, *in vivo* and *in vitro* have advanced our knowledge about the BFNM, but have also probably reached their limits due to sample preparation or resolution limit due to light diffraction. A new method mixing advantages from both approaches and reducing limits encountered needs to be developed. In this work we propose to engineer a surface mimetic of the membrane of bacteria and assemble parts of the BFNM. I choose to pattern the surface, using a soft-lithography method, for reducing the area of interest allowing a more reliable method for studying locally the arrangement of proteins on the membrane. This primary task will allow the different proteins from the motor to behave like in their native environment but in a defined area where I can study their arrangement. The second advantage will come from using a novel method to visualize the different assemblies generated on the engineered surface: Atomic Force Microscope (AFM). AFM has proven to routinely observe details at the nano-scale, in air and more importantly in liquid with a good signal to noise ratio.

We thus propose an ambitious way to study the motor, by coupling surface engineering and self-assembly, with topographical imaging at the nano-scale. Before

presenting my results, I will summarize the different tools I have used for studying the BFNM, then the surface I generated and finally the data about the assembly of motor proteins on these surfaces.

## B) Experimental tools

### a. Fluorescence microscopy

Fluorescence microscopy has been developed through the early age of optical microscopy and represents today the most common tool used for studying *in vivo* or *in vitro* biological structures. The main principle consists of a controlled emission of a light at a specific wavelength. This emission is provoked through optical excitation which induces a cycle of electronic transition between several energy states. This cycle is the base of fluorescence emission, through radiative transitions. The emitted light has a longer wavelength compared to the excitation. Figure 1 reviews this principle.

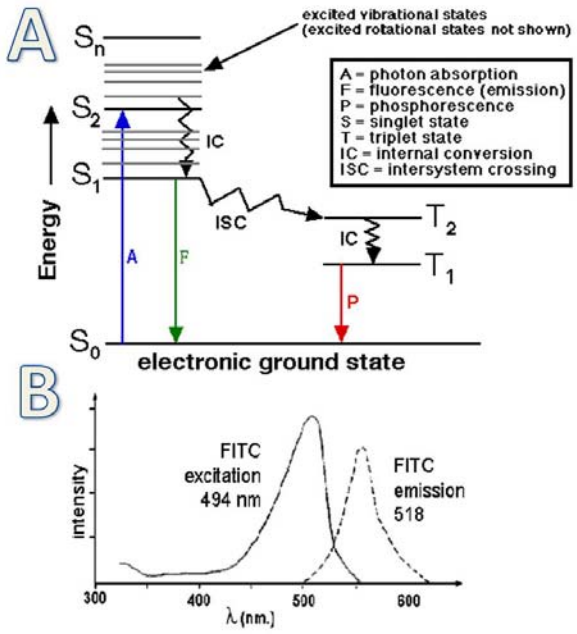


***Figure 1: Principle of fluorescence microscopy.*** *A/ the Jablonski diagram indicating the transitions between energy states. B/ Excitation and emission of a fluorophore molecule, Fluorescein Iso Thio Cyanate (FITC) commonly used for biological applications.*

One of the first applications in history was noticed in China, around the year 1000, where the emperor was observing every night a painted cow, drawn with a supposed magic paint. Since that period, numerous applications have been found especially for biological purposes, numerous molecules have been identified to fulfill usable fluorescent properties and most of these molecules have been used as a tag to other molecules of interest[16]. A list of available fluorophores with numerous applications can be found in http://www.analytchem.tugraz.at/fluorophores/. The use of tagged molecules opened large spectrum of applications, either *in vitro* or *in vivo*, partially due to the early development of genetic engineering. For example, DNA can be tagged and its movement within the nucleus of a cell can be monitored. Proteins which self-assemble into supra-molecular assemblies as for example the micro-tubules skeleton, can be tagged and the dynamics of the assembly process can be observed[17]. The use of fluorescence microscopy is a practical and non invasive tool to characterize samples and numerous biological applications are only based on fluorescence imaging. In our work, fluorescence has been used as a control method for validating the initial steps of our process. In the literature, only two experiments have been done so far, for following the dynamics of FliG and MotB proteins[18; 19] and a few proteins involved in chemotaxis[5; 6]. Fluorescent tags have been added to the filament proteins and rotation was monitored[20]. A more advanced fluorescence method was used for studying the proximity of two motor components: FliM and CheY-P. This technique, called FRET for Fluorescence Resonance Energy Transfer, when using chromophore, or more generally Forster Resonant Energy Transfer, named from a german scientist[21], is based on an energy transfer between two coupled quantum states. Two different dyes are grafted to two different neighboring molecules. A “donor” dye in its excited state can transfer energy by a non radiative long range dipole-dipole coupling mechanism to a second dye, which will play the “acceptor” role and emits light. This energy transfer is dependent to the distance between the two tagged molecules, and occurs typically for separation less than 10 nm. The recording of light intensity is therefore the signature of this coupling and by the way reveals the separation between the two molecules giving interesting structural information. Interactions between proteins, DNA proteins or conformational change have been studied using FRET[22] and one of the most common acceptor-donor couple, the

CFP-YFP (cyan fluorescent protein and yellow fluorescent protein) is largely used today. Figure 2 shows the basic principle of a FRET experiment.

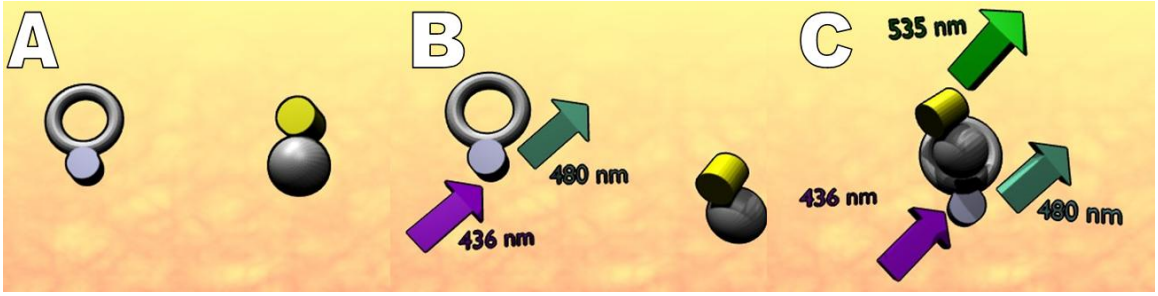


***Figure 2: FRET experiment principle****. A/ Two molecules, here represented by a torus and a bowl are tagged by two adequate fluorophores, CFT and YFT.B/ The torus protein is illuminated (wavelength of 436 nm) which provokes a primary emission at 480 nm. The second protein remains non-fluorescent because it does not adsorb at 436 nm. . C/ when the two tagged proteins interact and get spatially closer (less than 10 nm) and energy is transferred from CFT to the YFT, which starts to emit a new detectable wavelength at 535nm.*

These two dyes are derivative from the GFP, Green Fluorescent Protein. This experiment has been made on the CheY-P and FliM proteins, and allowed to monitor the interaction dynamic between these two molecules. This technique unlocked possibilities for studying the motor assembly, but the need for adding fluorophores at the N or the C terminus of the proteins has reduced immediately the possible couples to be studied. Fluorescence imaging remained a formidable and accessible tool for studying *in vivo* and *in vitro* the motor and I will present in this chapter the different fluorescence technique I used. Nevertheless, the lifetime of a fluorophore is relatively limited under exposure, due to the chemical changes (oxidation) in the fluorescent molecules, which reduces the possible long-term observation. This so called “bleaching” property has been used to develop a fluorescence technique called FRAP for Fluorescence Recovery After Photobleaching, which can monitor the diffusion of fluorophore on a surface. I will emphasize later on this technique. It is worth noticing that nanotechnologies have permitted to design new fluorescent tags not subject to bleaching which rely on quantum confinement in semiconductor nanocrystals. These so called quantum dots are protected from chemical changes and their lifetime is therefore very large. Another advantage in that through their size their emission wavelength can be controlled allowing multiplexed

fluorescence imaging to be performed. These new capabilities (long lifetime, multiplexing) are going to enhance considerably the potential of fluorescence characterization.

## b. Atomic Force Microscopy (AFM)

The atomic force microscope (AFM) or scanning force microscope (SFM) is a high-resolution type of scanning microscope, with demonstrated resolution of fractions of nanometer, 3 orders of magnitude better than the optical diffraction limit. The invention of the scanning tunneling microscope by Gerd Binnig and Heinrich Rohrer in the early 1980s, a development that earned them the Nobel Prize for Physics in 1986, is generally considered as the precursor of the AFM invention which was made by Binnig, Quate and Gerber in 1986[23]. The AFM is one of the foremost tool for imaging, measuring and manipulating matter at the nanoscale and its spectrum of applications has largely passed over the classical science barriers. The main principle of AFM is quite simple, a probe, interacts with a surface and the vertical and lateral deflections of this probe due to interacting forces are monitored and generate images of the surface. The most elegant invention of the AFM relies on the method used for measuring the minute force between the tip and the surface. This tip is integrated at the end of a long flexible cantilever fabricated using microfabrication silicon technology. The design of the cantilever (length, width, thickness) enables the adjustment of its flexibility (expressed as a stiffness constant in N/m). The small interacting forces between a small tip and the sample ( below 1nN) are amplified by this cantilever and generate lateral and vertical deflections that can be measured optically using a simple laser beam reflected at the top of this cantilever and collected by a position sensitive photodiode , see figure 3.

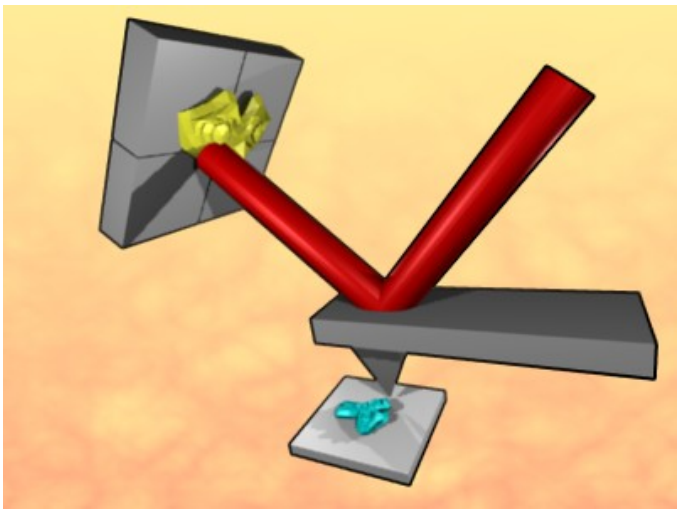

***Figure 3: AFM principle****. A Cantilever is moved on a surface through a controlled piezo based system. The cantilever holds a sharp triangular tip which interacts with the surface sample, here a monkey face for example (in blue). The vertical and lateral deflections of the cantilever are recorded through a laser beam which reflects on the cantilever top side and is collected on a photo-detector panels. The photo-detectors reconstitute an image of the scanned surface, here a part of the monkey face in yellow.*

Positioning of the cantilever is achieved by piezoelectric elements and permits tiny, accurate and precise scanning. The last part of the system relies on an electronic interface command which enable a very precise scanning. In most cases a feedback mechanism is employed to adjust the tip-to-sample distance to maintain a constant interacting force which reduces the risk of damaging both cantilever and sample. The tip is typically silicon or silicon nitride with a radius of curvature on the order of nanometers. The role played by the tip radius on the image formation will be discussed later. Several kinds of AFM set-up are available today: the sample is mounted on a piezoelectric tube which moves the sample in the *z* direction for maintaining a constant force, and the *x* and *y* directions for scanning the sample. In this configuration, the sample is moving while the cantilever is fixed. In more recent designs, the tip is mounted on a vertical piezo scanner while the sample is being scanned in X and Y using another piezo block. In that case, both sample and cantilever are moving. In the last configuration, the cantilever only moves, the sample remaining immobile while scanning. However, the essential point of all these set-ups is the system stability. Whatever the configuration, AFM can be operated in a number of modes, depending on the application but I will describe here only two imagery mode, static (contact) mode and dynamic mode. In contact mode, the force

between the tip and the surface is kept constant during scanning by maintaining a constant deflection. The tip just drags across the surface at a constant force, which can be adapted in real time in order to avoid sample damage. The image is then formed by the variations of the Z piezo necessary to maintain the force constant. The quality of this imaging mode mainly depends on two parameters: the cantilever stiffness and the tip radius. Close to the surface of the sample, attractive forces can be quite strong, causing the tip to 'snap-in' to the surface causing a brutal contact or indentation of the surface. The stiffness of the cantilever should be small enough for allowing scanning without damaging the sample, but large enough for limiting irreversible damage on the tip or the surface. The tip radius is also critical for allowing high resolution imaging. The exact role played by the tip dimension for soft nano-object in liquid environment is still under discussion[24; 25]. Static mode AFM is almost always done in contact where the interacting force is repulsive. The tip-surface interaction could sometimes generate different images between the repulsive or attractive force, and create some artifact of the sample. During contact mode imaging, only one parameter can be adjusted, a parameter called “set-point.  By adjusting the set-point, we define the force at which the tip interacts with the surface. Contact mode has been largely used through the years, starting from the material science, polymer and biological sample [26; 27; 28]. The other major imaging mode is called the dynamic mode, or tapping mode, wherein the cantilever is externally forced to oscillate at a given resonance frequency. This up and down oscillation is driven by a small piezoelectric element mounted in the AFM tip holder. The amplitude of this oscillation is greater than 10 nm, typically 100 to 200 nm. The tip-sample interactions forces (Van der Waals force or dipole-dipole interaction, electrostatic forces) modify the oscillation amplitude, phase. These changes with respect to the external reference actuation oscillator provide information about the sample surface and generate the image. An electronic device uses the piezoelectric actuator to control the height of the cantilever above the sample. This device adjusts the height to maintain constant the cantilever oscillation amplitude. This oscillation mode, also called tapping mode is generally considered as an improvement compared to the contact mode, especially about the damage done by the tip dragging on the surface. However, the cantilever stiffness must be higher compared to those used in contact mode, for allowing stable imaging

conditions. Unlike the contact mode, several parameters can be changed while scanning, including the oscillation amplitude and the average distance tip-surface.

AFM presents numerous advantages for imaging at the nano-scale, and its resolution can be competitive with those obtained using Scanning Electron Microscope (SEM) or Transmission Electron Microscope (TEM). Samples viewed by AFM do not require any special treatments (such as metal/carbon coatings) that would irreversibly change or damage the sample; however the sample must be strongly fixed on the surface. One of the major advantages is the flexibility of the environmental conditions in which AFM can image, from the vacuum[29], to air  REF and liquid[30] , with similar resolution. This makes possible to study biological macromolecules and even living organisms [31; 32; 33] SEM can only properly work in vacuum for high resolution. However, several disadvantages of AFM compared with the scanning electron microscope (SEM) exist:

- The image size ; SEM can image an area on the order of millimeters by millimeters with a depth of field on the order of millimeters ,compared to 150 $\mu m^2$ at the largest for object with a maximum height on the order of micrometers.

- The need for signal processing of images: it is crucial to remember that the final information is not a real topography but a force. Several processing modes are possible, including for example flattening, which apply mathematical algorithm in order to compensate the sample flatness. As described before, several signals can extracted, height deflection, lateral deflection also called sometimes friction, and also a signal called vertical deflection. A feedback control is implemented into the AFM system which permits to the piezo elements to compensate the vertical movement of tip in order to maintain the force constant. The vertical deflection monitors this adjustment.

- The slow rate imaging in the order of 5 Hz (5 lines per second) at the best conditions means that several minutes are requiried for a typical scan, while SEM is capable of generating video frames. The relatively slow rate of scanning during AFM imaging often leads to thermal drift in the image[34; 35] making the AFM microscope less suited for measuring accurate distances between details of an image, and also for fast biological process. However, several fast-acting set-ups have been suggested to increase microscope scanning productivity [36; 37], and results have been obtained by Toshio

Ando [38; 39; 40] at high speed on small sample size. These results opened the way for future AFM imaging at higher rates. AFM images can also be affected by hysteresis of the piezoelectric material [41] and cross-talk between the (x,y,z) axis that may require software treatments and filtering. Such filtering could "flatten" out real topographical features. However, newer AFMs use real-time correction software (for example, feature-oriented scanning) or closed-loop scanners which practically eliminate these problems.

- A second inconvenience can come from an incorrect choice of tip and cantilever for the required resolution which can lead to image artifacts[42; 43]. The choice of the "good" cantilever reveals another limitation of the AFM, the probe pollution, in liquid for example. AFM is an invasive technique due to the tip-surface interactions and contact as noticed for example by Yves Dufrenes about cell imaging[44]. Such tip pollution could create some artifact on the final image and could lead to wrong conclusions. Images issued from AFM should always be taken carefully.

Another major application of AFM (besides imaging) is force-spectroscopy, the measurement of force-distance curves. In this spectroscopy mode, the AFM tip is approached and retracted from the surface and its deflection recorded. The force spectroscopy was first routinely used to evaluate the force applied on the sample while scanning, and by extension was later applied on all sample surfaces for investigating local mechanical properties (elasticity). These measurements have been used to measure nanoscale contacts, atomic bonding, Van der Waals forces, and Casimir forces, dissolution forces in liquids and single molecule stretching and rupture forces[45; 46; 47]. Forces of the order of a few pico-Newton can now be routinely measured with a vertical distance resolution of better than 0.1 nanometer.

Despite its relative young age, AFM microscope has spread all over science fields, starting from material science to recently life science. A new generation of AFM systems coupled AFM imaging to classical optical imagery, as for example fluorescence microscopy. New set-ups, coupling an inverted optical microscope to an AFM, permit now to overlap structural information from the AFM to biological structures identified optically. The second new improvement of this system is the fact that the sample can be easily aligned with the tip compared to the "blind" approach [48; 49; 50; 51]. This improvement earns time because the area of interest can be identified directly. However,

the resolution achieved by those systems remains lower compared to those obtained by AFM stand-alone systems. Recent review of the numerous applications into life science showed that the application field of AFM increases every day [28] Despite its advantages, AFM was only used for one experiment [52] on the BFNM.

### c. Discussions

AFM can be used to study the BFNM. By observing in liquid medium on suitable surfaces it is possible to be close to "native" conditions. However, the slow scan rate and probe pollution are present and results obtained by AFM must be treated carefully. By coupling fluorescence microscopy with AFM, we will be able to find areas of interest using fluorescence microscopy, and access to nanometric resolution in liquid media with the AFM. We hope that this new approach for visualizing part of the BFNM in liquid will bring new data about the BFNM architecture and help us to better understand how could work the BFNM. The primary task in order to study the motor was to generate a surface which could mimic the native environment of the BFNM, and this environment is a phospholipidic bilayer.

## C) Engineered surface

### a. The native environment, the Phospholipids bilayer

The first step for building part of the BFNM in vitro, consisted in creating a native environment, as close as possible of the one encountered by the motor proteins inside the bacterium. As described in chapter 1, the BFNM is a complex structure with several distinct parts inside and outside of the bacterium and is deeply embedded into different layers. These layers separate the inner part from the outer part of the cell, and these layers are called "membrane". They are mainly composed of phospholipids and also numerous complexes of proteins. For studying the BFNM in vitro, elaborating in a controlled way a membrane was the necessary primary block.

### i. Structure and role.

Phospholipids are a class of lipids which are a major component of all biological membranes. Phospholipids are composed of two main parts: a diglyceride coupled to a phosphate group, which is often called fatty acid tails, and a simple organic molecule such as choline for example called the head. The 'head' of a phospholipid is hydrophilic and the lipophilic 'tails' are hydrophobic.

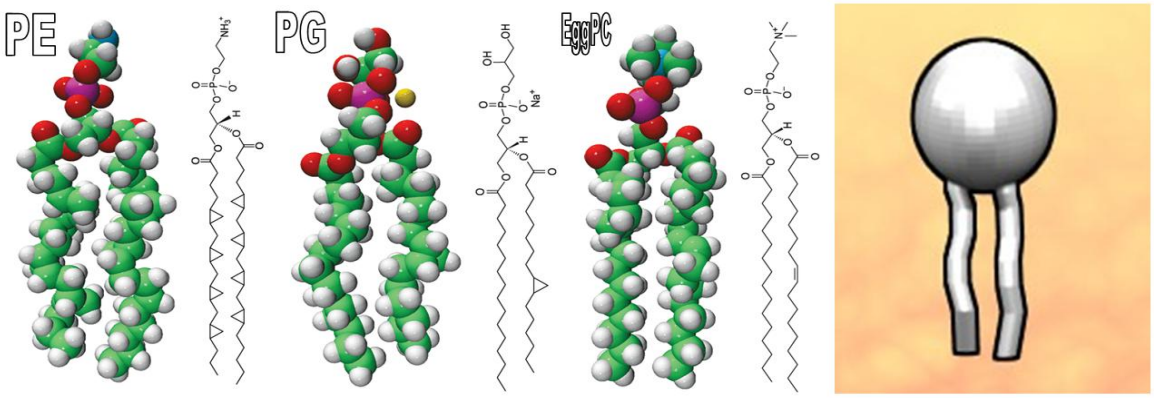


***Figure 4: Structure of phospholipids used in this work.*** *Left to right, Phosphatidyl-ethanolamine (PE), Phosphatidyl-glycerol (PG), Egg Phosphatidylcholine (EggPC), and a schema used for later illustration.*

The structure of these molecules permit the formation of a bilayer, composed of two layers of lipids arranged so that their hydrocarbon tails face one another to form an oily core held together by hydrophobic interactions, while their charged heads face the aqueous solutions on either side of the membrane. The hydrophile interfacial regions are saturated with water, while the lipophilic core region contains essentially no water. These molecules can be found on a 2 dimensional structure called a phospholipids bilayer, or in 3 dimension structures called liposomes. However, three major structures are naturally found in nature, micelle, liposome and lipid bilayer. Micelle structure is not widely used in biological system and not revelant for our subject and I will concentrate only on the two others, the liposome and the bilayer presented in figure 5.

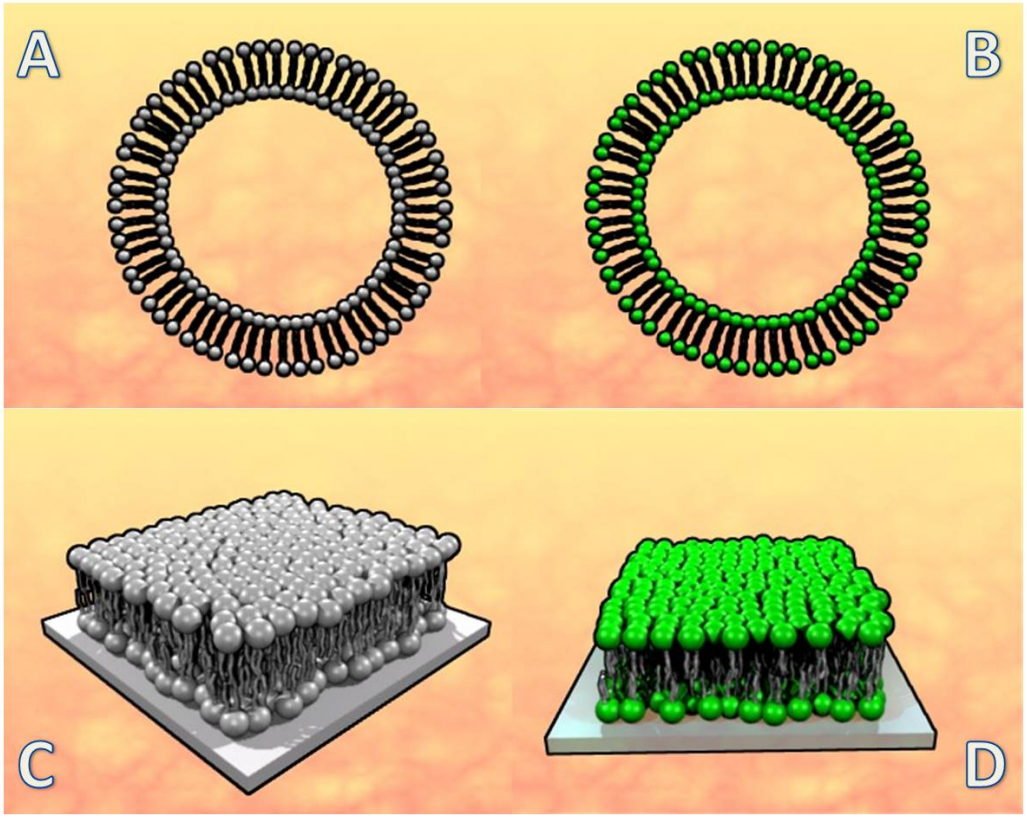


***Figure 5: Phospholipids assembly****. A/ liposome structure, a 3 dimension assembly of a bilayer, without fluorescent dye. B/ liposome with a green flurophore grafted to the hydrophilic head, as for example FITC dye. C/ a SPBM view after "fusion" of liposome from A. D/ A fluorescence SPBM formed by fusion of B liposome.*

As described above, phospholipids bilayers occur when hydrophobic tails line up against one another, forming a membrane with hydrophilic heads on both sides facing the water. This particular assembly generates a membrane and its essential structure was discovered in 1925 by two Dutch physicians, E.Gorter and F.Grendel. [53]. Then in 1965, Alec Bangham [54] showed that phospholipids, when introduced into an aqueous environment, spontaneously form a structure called "liposomes". This structure can be compared to small balloons of lipid bilayer which can entrap molecules inside them. This observation confirmed definitely that the membrane which protects the inner part of cell from the outside was also composed of a phospholipids bilayer. The structure of a bilayer explains its function as a barrier. Because of the oily core of the bilayer, it is only permeable to small hydrophobic solutes (such as chloroform or ethanol), but has a very low permeability to polar inorganic compounds and ionic molecules. For a cell, this

means that even small molecules, such as sugars and salts, are contained inside it. The membrane is capable of elastic movement, and has fluid properties, in which embedded proteins (integral or peripheral proteins) and phospholipids molecules are able to move laterally. Such movement can be pictured by the “Fluid Mosaic Model” that describes the membrane as a mosaic of lipid molecules that act as a solvent for all the substances and proteins within it,[55; 56; 57]. Proteins and lipid molecules are then free to diffuse laterally through the lipid matrix and migrate inside the membrane. This model is still under debate but has been largely accepted in its principle [58; 59]. The properties of the bilayer are influenced by a variety of factors, including the lipid composition, temperature and membrane pressure. Their thickness depends from their composition and especially the length of the fatty acid chains; however a thickness of 3 to 5 nm is largely accepted as an average. However, phospholipids in bilayer have an intrinsic property to exhibit two possible phases, liquid or gel, depending on temperature and lipid mixture. For example, mixing cholesterol and Phosphocholine (POPC) at defined temperature allow the formation of clear separated phases, called “rafts” [60; 61]. These rafts are crucial for cell function[62; 63], for example for G-proteins activity[64]. The membranes in cells are more complicated because they contain a variety of different classes of lipids, although the vast majority of the lipids are phospholipids and cholesterol. The main phospholipids encountered in eukaryote cells are phosphatidylcholine, phosphatidyl-ethanolamine, phosphatidylserine, phosphatidyl-inositol and sphingomyelin. Glycolipids usually account for a few percent of the lipid molecules. Bacteria appear to have other bilayer mixture, the main lipids are phosphatidyl-ethanolamine (PE), phosphatidyl-glycerol (PG) and cardiolipin and this is the reason why we decided to work with those lipids. Large numbers of phospholipids exist in nature, and their features are the nature of the lipid head groups and the length and degree of saturation of the hydrocarbon. The three main structures I experimented are shown in figure 4. EggPC, PE and PG. EggPC is largely considered as a model for studying phospholipids, however PE and PG are the main components of the native inner bacteria membrane. By mixing PE and PG at an appropriate ratio, we could recreate in vitro a membrane close enough to the bacterial one for assembling the BFNM.

### ii. Formation of the Supported Phospholipids Bilayer Membrane (SPBM)

#### 1. Principle

As described above, phospholipids have a tendency to self-assemble when placed in water, and form two kind of structures, a 3 dimensional structure called liposome or phospholipids bilayers. These phospholipids bilayers when formed on a surface are called Supported Phospholipids Bilayer(SPB), due to the presence of a thin water layer between the bilayer and the substrate which "supports" the bilayer. There are several names proposed in the literature, Supported Phospholipids Bilayer (SPB) [65], Supported Bilayer Membrane (SBM) [66] and others, but because I worked with a bacterial lipids mixture, I decided to call it Supported Phospholipidic Bilayer Membrane (SPBM), each term gives an insight into the structure: Supported for working on a surface, Phospholipidic because of their composition, Bilayer for their structure and Membrane because its composition was close to the inner bacterial membrane. In order to study the BFNM on a surface, we needed to generate this kind of SPBM. There are two ways for achieving this goal, one by using liposomes, a second one by successive formation of the two phospholipidics layers using a Langmuir Blodget process. I will only describe the liposome route which is the one I have selected because the presence of charged phospholipids, as for example phosphatidylglycerol (PG), reduced the possible application of the LB technique. Liposomes are relatively stable in liquid, but tend to fuse and spread on a hydrophilic surface and form a structure similar to the membrane of cells, a SPBM [67; 68; 69; 70; 71]. The disturbance caused by the contact with an hydrophilic surface can indeed destabilize the 3D architecture for a 2D bilayer supported at the sample surface. This process is driven by subtile minimization of surface and elastic energies. Figure 6 summarizes the "fusion" process.

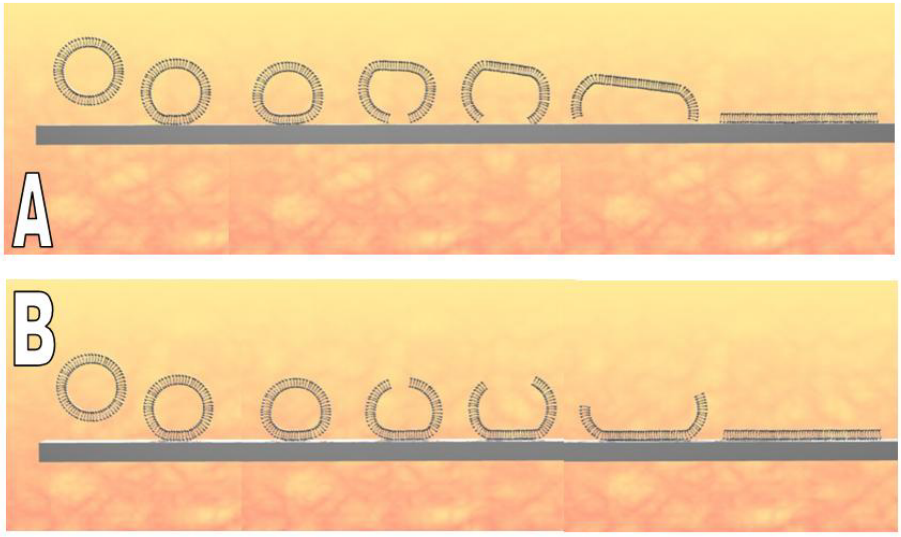


***Figure 6: Fusion process of liposomes****. A/ The "bottom" hypothesis where liposome rupture occurs at the surface side. B/ The "top" hypothesis, where liposome break at the top. The precise phenomenon remains unclear and is apparently related to the phospholipids mixture. Experiments are currently pursued by several team for addressing this question.*

## 2. From phospholipids to Supported Phospholipids Bilayer Membranes (SPBM)

The process of a SPBM formation was divided into 7 steps, starting from the phospholipids storage to the final observation of the formed SPBM.

Generally, phospholipids were sold into two forms, powder or diluted in chloroform, and bought from Avanti ®, see annex 2 material details. Powder form needed to be diluted into cleaned and pure chloroform up to a defined concentration. Solutions were stored for 6 months at -20 °C.

If the final phospholipidic mixture is composed of several kinds of phospholipids, for example EggPC and fluorophore phospholipids, for example FITC-DHPE, I mixed them under argon environment for evaporating chloroform at least 10°C above the transition temperature. This temperature was defined to be the temperature between liquid and gel phase of the SPBM. For reducing oxidation of the fatty acid tails, chloroform was first evaporated under argon or at least $N_2$ stream. This step played an essential role for the quality of the final SPBM. After the first evaporation the lipid

mixture was put in a primary vacuum chamber overnight for removing any residue of solvent.

The next step consisted to hydrate the lipid mixture with a defined buffer. Details of the buffers will be given later. There are two ways to generate an homogeneous liposome size distribution, the sonication and the extraction. The hydrated mixture can be sonicated using a sonic probe for 10 minutes into an ice batch for avoiding damage on the lipid structure due to the heat generated by the sonication process. The other way to generate liposomes is the extrusion method, based on a multiple passage of the lipid mixture into a porous membrane. The lipids formed liposomes through the passage in the pores. I did not use this approach, partially due to the change into the lipid concentration during this experiment. Indeed, numerous of them sticked to the porous membrane while extrusion and the membrane are colored after extraction which confirmed that a large number of phospholipids were lost in the process. Controlling the liposome concentration was essential for the next step of the process, and it was the main reason which pushed me to choose the sonication instead the extraction method.

Solution was then centrifuged for 10 minutes at 10000g. During sonication, some titanium nano-particules can be detached from the sonic probe. These nano-particules could be problematic latter for the formation of a homogeneous SPBM. By centrifuging the solution, nano-particules were concentrated at the bottom of an eppendorf and only the liquid was pumped.

Measurements of the diameter of the formed liposomes were achieved using a Dynamic Light Scattering (DLS) system. This system measured the average diameter of the liposome. Solution was then stored at 4°C for a week. Solution can be re-sonicated just prior experiments, but will need also to be centrifuged again. Oxidation of the fatty tails could be also problematic and working with a fresh liposome solution remains preferable.

Surfaces, generally regular cover glass slide where liposome can form the SPBM were cleaned successively in iso-propanol in an ultrasonic bath for 5 minutes; follow by a second ultrasonic batch in deionized water. Surface is then dried using $N_2$ stream and finally put in a plasma oxygen chamber for 5 minutes. The plasma oxygen treatment

"activates" the surface and increased its hydrophilicity by creating Si-O-H bonds at the surface.

Liposomes, at a defined concentration are then incubated on the activated surface for a specific time. Sample are then washed several times using the buffer for removing non-adsorbed liposomes. The SPBM is formed and ready to be analyzed or used. The full process does not exceed an hour, plus the overnight in a vacuum chamber.

### iii. Characterizations

Several experiments permit to characterize the formation of a SPBM on a surface, from fluorescence microscopy to AFM in liquid medium. I will separate the results between the two lipids mixture I used, which displayed different behaviors. I worked with 5 different phospholipids mixtures, EggPC, *E.coli* full extract, *E.Coli* polar extract, phosphatidylethanolamine natural extract (PE) mixed with phosphatidylglycerol (PG) natural extract and POPE (synthetic extract) mixed with POPG (synthetic extract). I have not shown the chemical structure of POPE and POPG in figure 4 because I finally concentrated on only two of them, EggPC and PE-PG. Differences between the *E.Coli* extracted solutions and PE-PG were not significant, but the control of the composition by mixing different ratio of PE and PG opened more flexibility than the extracted solution. For each solution, a small percentage, from 1 to 3%, of FITC-DHPE was added for fluorescence microscopy. This point will be discussed later in this chapter.

For the two solutions, characterizations were divided into 4 different experiments, starting from the DLS measurement of the diameter of the formed liposomes just after sonication, followed by a study of the fusion process on a $SiO_2$ surface using Quartz Micro Balance technology, then fluorescence microscopy after the SPBM final formation on the surface and finally AFM imaging.

Prior to experiments, the choice of the buffer composition and the ratio between different lipids was crucial. EggPC was mixed with FITC-DHPE with a respective percentage of 98/2 in a buffer I will name MOPS (4-Morpholinepropanesulfonic acid 10mM, NaCl 100mM, $NaN_3$ 0,02 %W/V, pH 7,4), and PE/PG/FITC-DHPE at 73/25/2 in a final buffer named hepes 3 ( hepes 10mM NaCl 150 mM $CaCl_2$ 20mM), based on the

work of Domenech *et al*[72]. For the PE-PG solution, a specific protocol was elaborated based on DLS measurements.

## 1. Dynamic Light Scattering measurements and sonication protocols.

DLS measurements were made directly after sonication of the lipids mixture in their respective buffer, and each 10 minutes after during 2 hours, and then 4, 6 and 12 hours later. Results for PE-PG are displayed in figure 7.

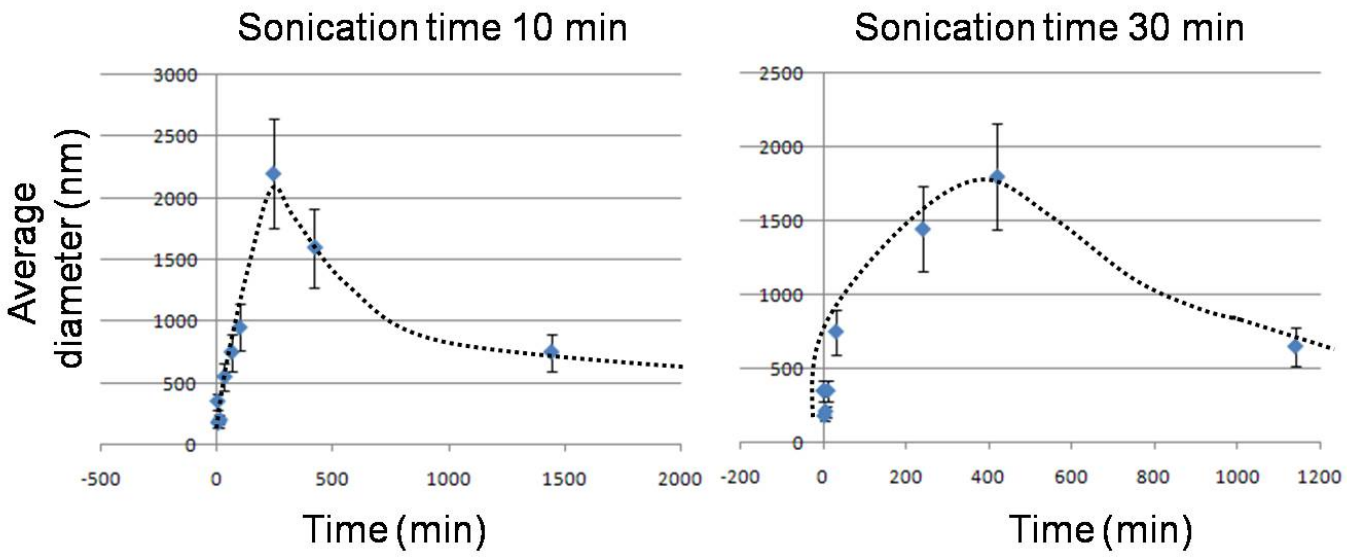


***Figure 7: PE-PG average diameter over time.*** *The average diameter of PE-PG lipsome increased up to several microns in a short period of time, less than 5 minutes, whatever the sonication time. However, a shaking procedure using vortex after 4 hours disassemble the PE-PG liposome aggregates. The liposomes diameter slowly decreased to a average value of 800 nm. The need for a shaking procedure every 1 to 2 hours for avoiding the reformation of large aggregate is illustrated.*

I do not display the average diameter of EggPC liposome due to their stability over time. This diameter remains to a value of 100 nm with some times two clear distinct diameters at 80 and 120 nm. The average diameter remains stable over a week. The behavior of both liposome solutions was therefore clearly different. While the average diameter of EggPC liposome remains relatively constant the PE-PG liposome displayed a more coalescence characteristic. While the average diameter of EggPC after sonication

turned out to be 100 nm, PE-PG liposome are larger, 350 nm and this average diameter increased up to 1 µm in less than 10 minutes, and then after 4 hours to an average value of 2 µm. Measurement with DLS turned out at this time impossible due to the formation of large clusters of liposomes. A gentle agitation using a vortex, 5 hours after sonication disassemble the observed aggregates and the average diameter tends to decrease slowly to a final average value of 800 nm. I tried different concentration of phospholipids, different buffer compositions and also different sonication times, but nothing changed this tendency. This behavior was detrimental for the fusion process on the surface, and especially for further imaging using AFM. The coalescence characteristic of the PE-PG liposome was not a real surprise, due to the presence of charged phospholipids and also cations in the buffer. I changed several parameters, by decreasing the cations concentration or changing the ratio of PG into the phospholipids mixture, but none of these attempts fixed the coalescence problem. To tackle this point, I elaborated a slightly different protocol for the PE-PG liposome formation. Maintaining the PE-PG liposome in their final buffer was the key problem, and for circumvent this problem, I sonicated the phospholipids mixture in a Hepes 1 buffer, composed only of Hepes 10 mM and NaCl 150 mM. I preserved the phospholipids mixture sonicated in these buffer prior experiments. DLS or incubation of this solution did not exhibit results comparable to those acquired with the previous protocol. Then the solution was just mixed prior experiments with a solution I named Hepes 4 (hepes 10mM NaCl 150 $CaCl_2$ 40) in order to create the final Hepes 3 buffer. Solution was then sonicated for 1 minute in an ice bath just before incubation on the surface. Incubation was limited to 5-10 minutes for circumventing the coalescence of liposome on the sample. By this way, I prevented the formation of large aggregates of liposome and allowed the formation of a SPBM without major defaults.

## 2. QCM-D analysis of SPBM formation

The formation of the SPBM can be monitored using the QCM-D technology taking profit from the real time analysis provided by the sensor (Kasemo *et al* [73; 74] [75; 76] demonstrated that the formation of a SPBM can be easily detected on different kind of sensors and established the different signals which correspond to vesicle

adsorption, single layer formation or fusion follow by SPBM formation. Based on these studies, we put side by side the formation of the SPBM for the EggPC solution and the PE-PG solution. Results are displayed on figure 8. Formation of the SPBM for both solutions apparently did not exhibit the same characteristics. The sensor used here presented a $SiO_2$ layer and is similar to the surface we will work on.

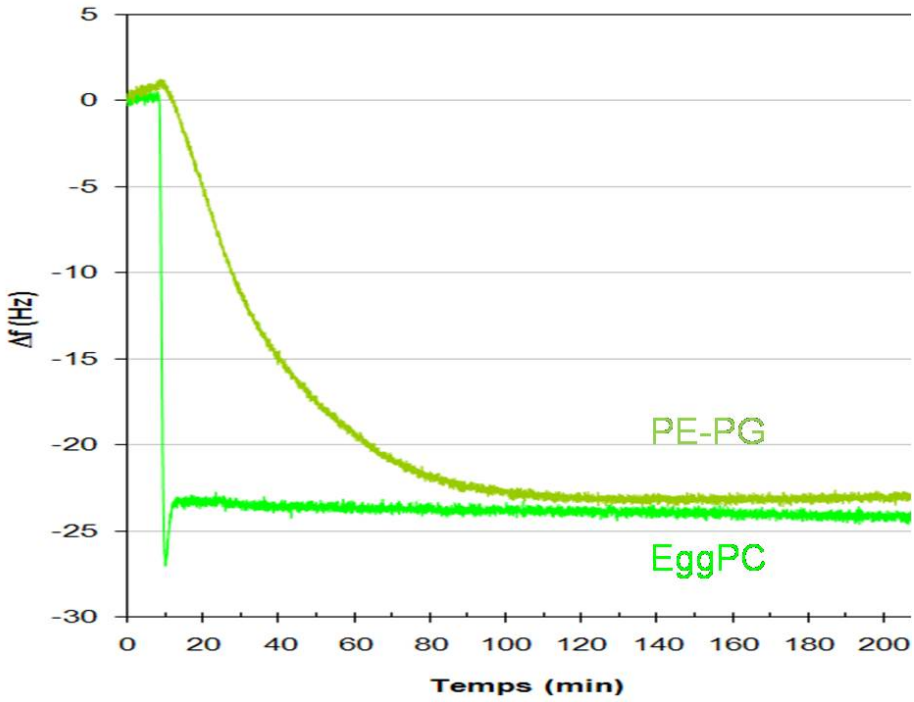


***Figure 8: Real time measurement formation of SPBM with the QCM sensors****. Light green, E.Coli Phospholipids, intense green EggPC mixture.*

As expected, the EggPC SPBM formation was comparable to established data. Liposome spontaneously adsorbed on the sensor surface. When the density of liposomes adsorbed on the surface reached a critical value, the stress between adjacent liposome causes their rupture. This rupture releases water encapsulated inside the liposomes. These three steps can be seen, on the QCM trace: Fast adsorption of liposome (Δf=-27 Hz in figure 8), rupture and releases of water (frequency shift of +4 Hz) and finally stabilization of the formed SPBM at a Δf=-23 Hz. For the PE-PG solution, the data obtained were drastically different. The fast adsorption of liposomes on the surface is not detected. The frequency smoothly decreased and stabilizes once again to the same value of Δf=-23 Hz. Formation of PE-PG SPBM is more comparable to the slow addition of isolated SPBM

patches, which revealed an independent behavior of each liposome, compared to the collective spreading characteristic of the EggPC vesicles. The formation of the PE-PG SPBM can be compared to a puzzle formation, piece by piece with different shapes and sizes, as seen by the diameter measurement. However, full surface can be covered, but the timeline was at least 4 times longer compared to the case of EggPC liposome. This observation was crucial for the next experiment; a full surface can be successfully covered with a homogeneous SPBM for EggPC liposomes but for PE-PG liposomes as well.

## 3. Fluorescence microscopy

By adding a fluorophore into the phospholipids mixture, the use of fluorescence microscopy permits the direct observation of the fluid properties of the SPBM formed on the surface. Based on the numerous studies about the characteristic of SPBM, two kinds of measurements can be performed to corroborate the presence and quality of the SPBM: direct observation and Fluorescence Recovery After Photobleaching (FRAP) measurements[77; 78]. Both methods have been used. As seen in figure 09, the EggPC SPBM covers the whole surface of the sample with no detectable defects. The only way to observe the fluid properties of the membrane that can attest its quality was the achievement of FRAP measurements. FRAP is divided into three parts: photo-bleaching a specific selected area, turning off light exposure for a defined time, and finally measurement of the recovery of the fluorescence from this area. Due to the diffusion of the tag phospholipids on the surface, unbleached fluorophores enter the illumination zone and light emission from this area grows up upon time. By measuring the emitted intensity of the defined area at precise interval of time, we have access to the diffusion rate of the elements on the surface. By this way, we demonstrate the fluid behavior of the SPBM. The success of this technique relies on the lifetime of the fluorophore. The fluorophore must photo-bleach but not too fast in order to permit the measurement. Results on the EggPC SPBM structure are shown in figure 09 and gave an average diffusion rate of 1,5 to 2 μm/s, comparable to previously published value[79; 80; 81].

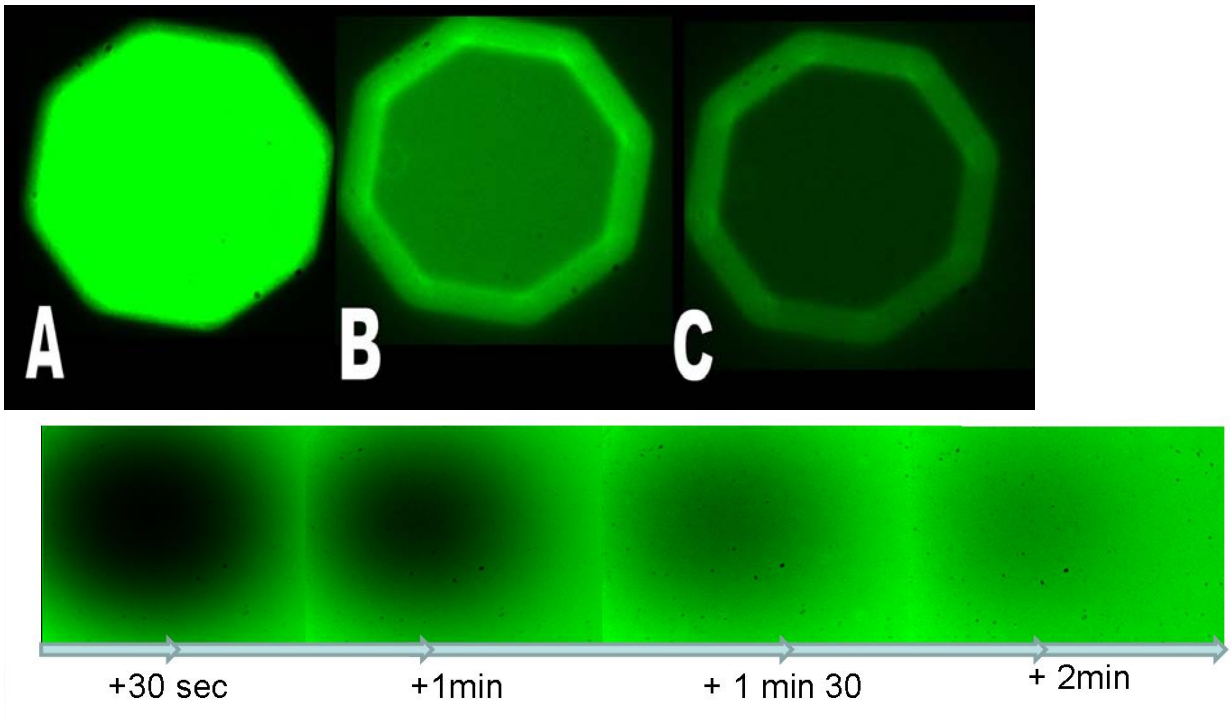


***Figure 09: FRAP experiments on the EggPC SPBM****. A/ A microscope aperture served as a mask for illumination a selected area of the membrane. B/ and C/ Upon illumination the fluorophores tagged on the phospholipids "bleached" under the exposure and turn dark. Due to lateral diffusion of phospholipids, the fluorescence is recovered in the illumination area after exposure. (see bottom images after 30 secondes, 1 minute, 1'30 and 2 minutes).*

For the PE-PG SPBM, direct observation of the surface after the fusion process revealed a series of SPBM islands. (See Figure 10).

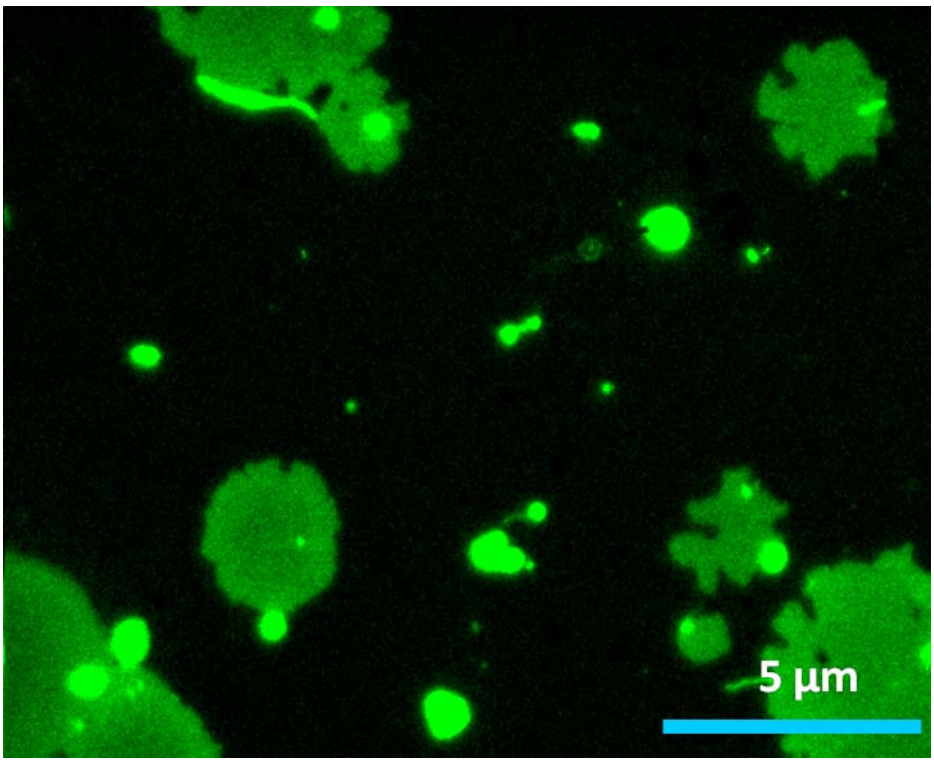


***Figure 10: PE-PG SPBM "islands".*** *Numerous patches of SPBM are formed on the surface with different sizes and shapes. By increasing incubation time, we can cover 80% of the surface but I deliberately show here only small isolated island of SPBM for supporting the "puzzle" formation of the SPBM.*

The size and shapes of those SPBM patches were not regular, and their distribution on the surface can be compared to a paint spreading. By adjusting concentration and incubation time, 80% of the surface can be covered. However, by changing the concentration and the incubation time, liposome coalescence effects previously described needed to be taken into account. FRAP was also pursued but gave more complex results. Due to the large distribution of PE-PG patch size, it turned out that the diffusion was problematic to measure, due to the size of the photobleached area which was larger than the patches on the surface. Despite the fact we covered 80% of the surface; the influence of the frontiers between the isolated patches was large enough to pertubate FRAP measurements. We observed diffusion within each SPBM patch, but the precise measurement of the coefficient requires additional investigations.

## 4. AFM imaging of SPBMs

AFM has been largely used for studying SPBM [68; 73; 82; 83; 84], starting by single SPBM patch and raft formation due to the presence of two phases. Several characteristic are well-known about SPBM, thickness and roughness. Thickness mainly depends of the phospholipids mixture and can vary from 3 nm to 5 nm. The SPBM roughness is known to be very flat, less than 200pm which makes it easily recognizable compared to glass slide roughness (±1 nm). Figure 11 and 12 displayed results obtained on EggPC SPBM and a single PEPG SPBM patch in contact mode.

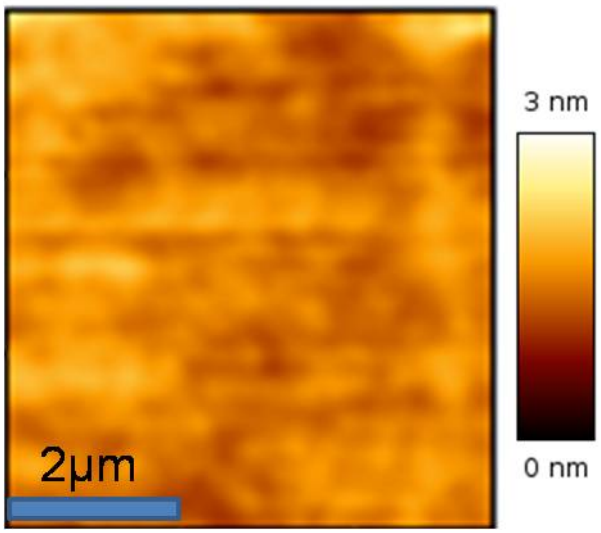


***Figure 11: AFM image of EggPC SPBM****. Contact mode in PBS buffer, cantilever MLCT Veeco stiffness 10mN/m. height signal. The surface is fully covered by EggPC SPBM. The roughness of this membrane does not exceed 150 pm compared to the roughness of regular glass slide evaluated between 700pm to 1nm*

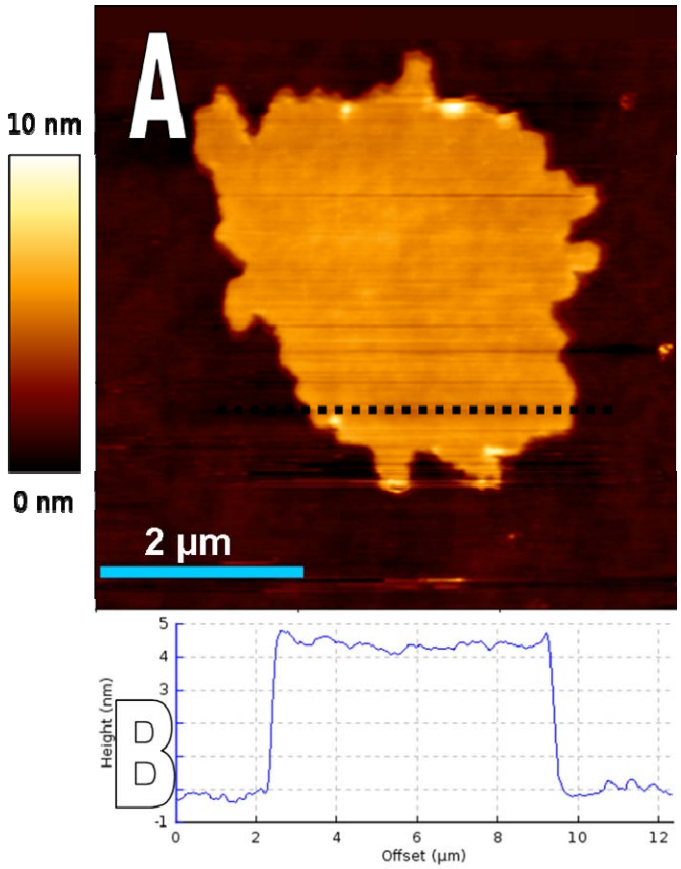


***Figure 12: A single PEPG SPBM patch*** *.Contact mode in hepes 3 buffer. Cantilever MLCT from veeco presenting a stiffness of 10mN/m. A/ Height signal. B/ cross section of A.*

Since AFM records topographical information it is straightforward to measure the thickness of the SPBM such as in the profile shown in figure 12. Thickness was evaluated to 3 nm for the EggPC SPBM and 4 nm for the PE-PG SPBM, in good accordance with previous data[72]. By adjusting the PE-PG concentration and time, 80% of the surface can be covered by the SPBM. However, the puzzles PE-PG SPBM helped us for measuring the thickness of the SPBM. The perfect covering of the EggPC was in that case more problematic and roughness was more easily measurable than thickness.

Force spectroscopy was also used to confirm the SPBM presence on a surface. The AFM tip is approached and retracted from the surface and the static deflection of the cantilever is recorded as a function of piezoelectric displacement. The principle is described in figure 13. During the contact, the cantilever tip can pass through the SPBM. This scratching of the SPBM is detectable through a small kink that appears on the

approach trace. This kink, highlighted by an arrow in figure 13B,C gives the thickness of the indented layer. Figure 13 shows typical force curves for EggPC and PE-PG SPBM.

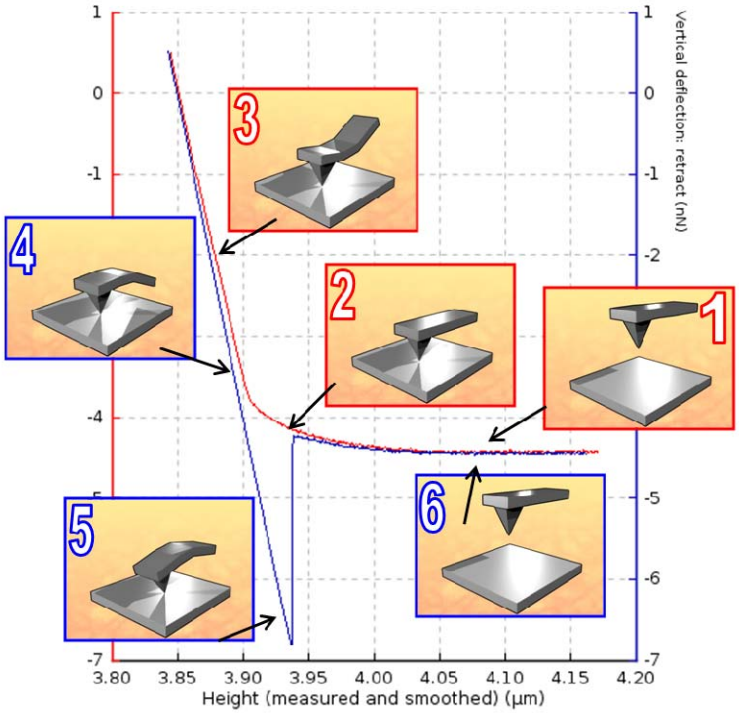


***Figure 13A: Force spectroscopy principle****. The AFM system records the vertical deflection of the AFM probe during a cycle of approach and retraction of the tip. These measurements can be divided into 6 steps. 1/ the AFM probe approach the surface but 'feels' no attractive or repulsive force. 2/ the probe 'contacts' the surface…3/..and starts to bend due to the resistivity of the material, generally glass slide, mica or silica. The vertical deflection increased proportionally to the force applied on the probe. 4/ the probe start to retract from the surface and the cantilever bends due to the adhesion force between the surface and the probe. 5/ the cantilever bends until it pulls out from the surface…6/..And comes back to a position where no interactions are felt by the AFM probe.*

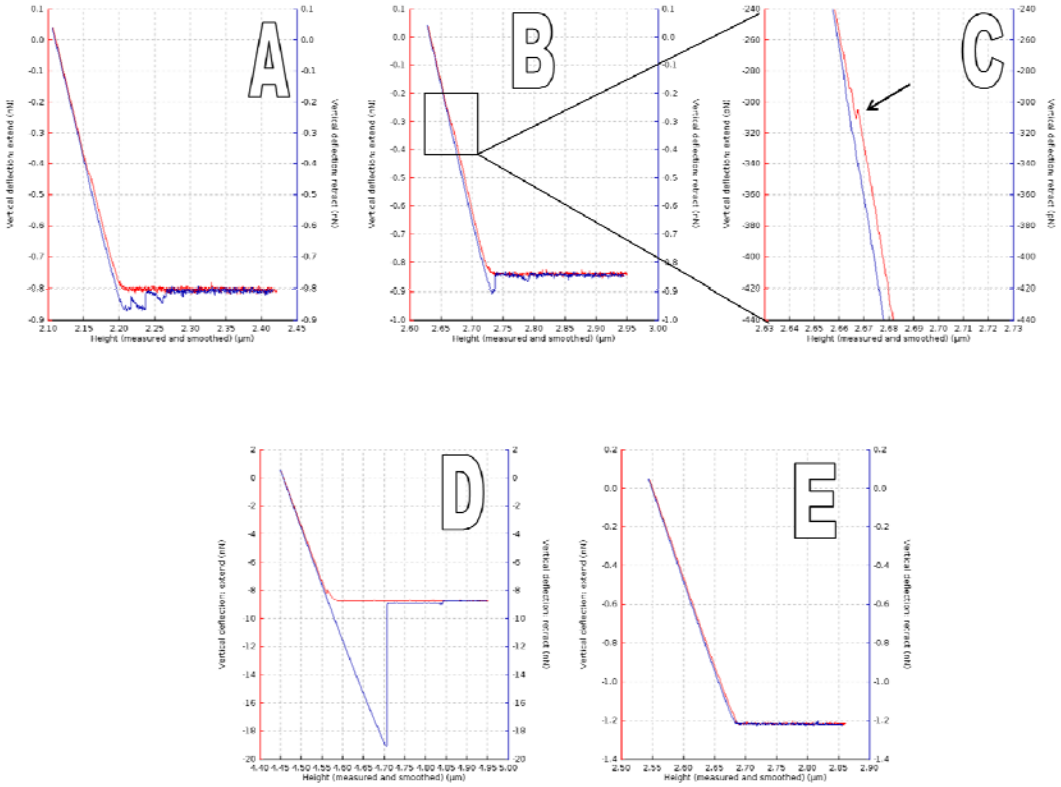


***Figure 13B: typical Force spectroscopy curves.*** *During the contact on the approaching trace, we can detect a small kink which corresponds to the passage of the AFM probe through the SPBM. A and B/ force curves on PE-PG SPBM, C/Enlarged view of B displaying a visible kink marked by an arrow. The thickness of the layer can be deduced from the amplitude of this kink. D/ force curve on activated $SiO_2$ surface, a large adhesion can be observed. E/ A perfect curve where no adhesion can be found, obtained between a coated AFM probe and an homogeneous surface of $SiO_2$ non activated.*

Force spectroscopy enabled us to verify the presence of SPBM on the surface. Indeed when a membrane is below the tip large adhesion peaks can be observed on the retractation trace (compared figure 13B D and figure 13B E). Secondly, the observation of the indentation of the SPBM on the approach trace enabled us to have a measurement of the membrane thickness. Same values have been obtained with this methodology compared with the direct thickness measurement obtained at an edge of SPBM by imaging (see figure 12).

### iv. Discussion

Formation of the primary block for the full assembly of the motor was attained. By working in parallel on a well-know system such as EggPC and a more experimental lipid mixture PE-PG, we compared the results and adjusted numerous parameters for the PE-PG mixture. The formation of a homogeneous SPBM was achieved, but only the formation on small surfaces will be interesting for next step. By adding proteins on a large surface, and due to the slow rate of AFM imaging, large SPBM would be detrimental for AFM imaging, by increasing the experimental time and also the probe pollution while searching an area of interest. By studying first the formation of the SPBM, we have optimized conditions for SPBM formation, but numerous questions rose about the future location of the BFNM assembly. How could we manage to spatially localize the future proteins assembly? How could we limit the proteins diffusion on the SPBM? These questions will be addressed by coupling self-assembly with surface patterning.

## D) Coupling patterning and self-assembly

The principle of the patterning is shown in figure 14. The capacity of designing domains of SPBM at the micrometric and nanometric scale was the primary objective for allowing the nanoscale imaging of the motor by AFM. However, it is worth noticing that this technology is generic to any kind of device or biochip involving membranes proteins. Even if I will not describe all other possible applications of these patterned SPBM, the reader must keep in mind that the process we have elaborated will be re used for many others purposes than the BFNM.

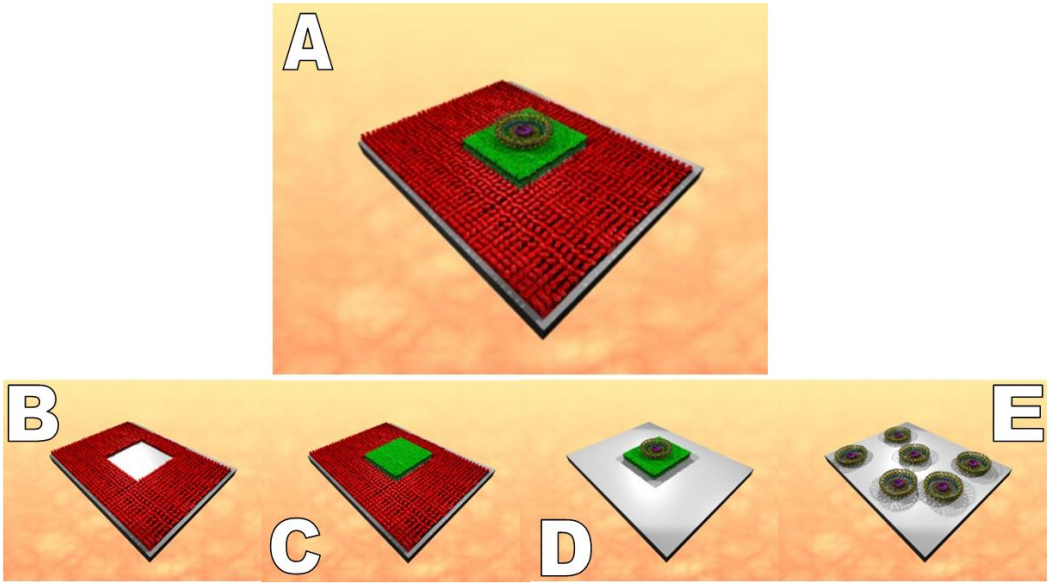


***Figure 14: Principle of Patterned SPBM (P-SPBM).*** *A/ the final assembly, starting by a layer of patterned antifouling molecules (red), a SPBM (green), and membrane proteins displayed on the SPBM. B/ The anti-fouling pattern. C/ The P-SPBM after formation of the SPBM within the pattern. D/ A single SPBM patch with proteins. E/ Proteins incubated on unpatterned surface. All these steps will be characterized before the final assembly.*

## a. Introduction

Patterning surfaces has been the purpose of intense research for decades, starting by the creation of the first written language several decades ago to the patterning methods currently used in the micro-electronics field. But the same target was in mind; transmit information through a design elaborated on a surface. Our purpose is not so different, by creating a pattern on the surface; we would like to generate specific areas with specific functions for multiple applications. Pattern generation on surfaces can be classified in two families: Top down and Bottom up techniques. Top-down has been mostly developed by the micro-electronic engineering, based on photolithography or electron beam lithography [85], or more recently by spotting bio-molecules for DNA biochip using micro [86] or nano-plumes [87; 88]. Bottom up approach has been recently developed through the self-assembly of nano-objects[89; 90]. Unlike the Top-down approach, which is based on reducing object size until a desired dimension is attainted ,

the Bottom up approach uses chemical or physical forces to self-assemble together large numbers of object in a deterministic way[91; 92; 93; 94]. By reconstructing the BFNM, our approach is a mix of the two, the Top-down for generating a pattern of SPBM, and the bottom up approach by letting the BFNM proteins self-assemble together. Most of proteins and phospholipids naturally self-assembled at the nano-scale, which means that the primary task was to create the patterns at the surface wherein first the SPBM and then the BFNM proteins will self-assemble.

The primary choice for generating a pattern at the micro and nano-scale was the choice of the molecules, which will avoid formation of SPBM and be a good protein anti-fouling molecule. Several molecules have been identified to eliminate proteins adsorption and liposome fusion, [95; 96; 97; 98; 99; 100] including proteins, silane and Polyethylene Glycol (PEG) molecules. The molecule will have to fulfill several essentials points: it must bind to the surface, here a $Si0_2$ surface or mica surface, covalently or by electrostatic bonds, it has to be anti-fouling for both proteins and phospholipids, this molecule needs to be compatible with the patterning technique, and finally this molecule should be stable upon AFM imaging for reducing "pollution" effect.

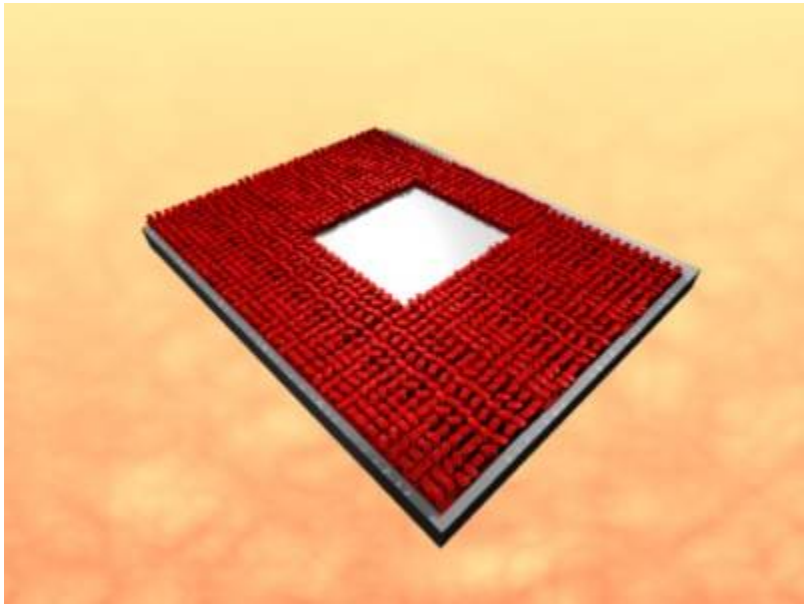

***Figure 15: the first patterned layer, the anti-fouling layer.***

## b. Choice of the molecules

Bovine Serum Albumin (BSA)(see annex 2 for references) proteins have been used for this type of purpose, but their organization on a surface remains poorly understood and its role as a repellent in numerous protocol has not been elucidated[101]. On the other hand, I have selected a molecule called Pll-g-PEG for Poly-L-lysine-grafted-Poly(ethyleneglycol) (see annex 2 for reference). Pll-g-PEG is a member of a family of polycationic PEG copolymer which spontaneously binds on a negatively charged surface. The formation and adsorption of Pll-g-PEG has been largely studied by Spencer *et al* [102; 103; 104; 105; 106; 107] and structure of the Pll-g-PEG molecule is shown in figure 16. The molecule adsorption on a negatively charged surface mainly come from the lysine amino acids which are positively charged, which creates an electrostatic interaction with the surface. Spencer's studies evaluated the density of a Pll-g-PEG layer after incubation and also its anti-fouling properties and illustrated that Pll-g-PEG presented numerous advantages compared to others repellent molecules: water based buffer, stability *in vitro* over time and the flexibility to change the PEG/ Lysine ratio, or adding other "head", such as a fluorophore group RhodaminB, FITC, or also biotin[108]. This flexibility opened the possibility to elaborate relative complex surface with different kind of Pll-g-PEG molecules.

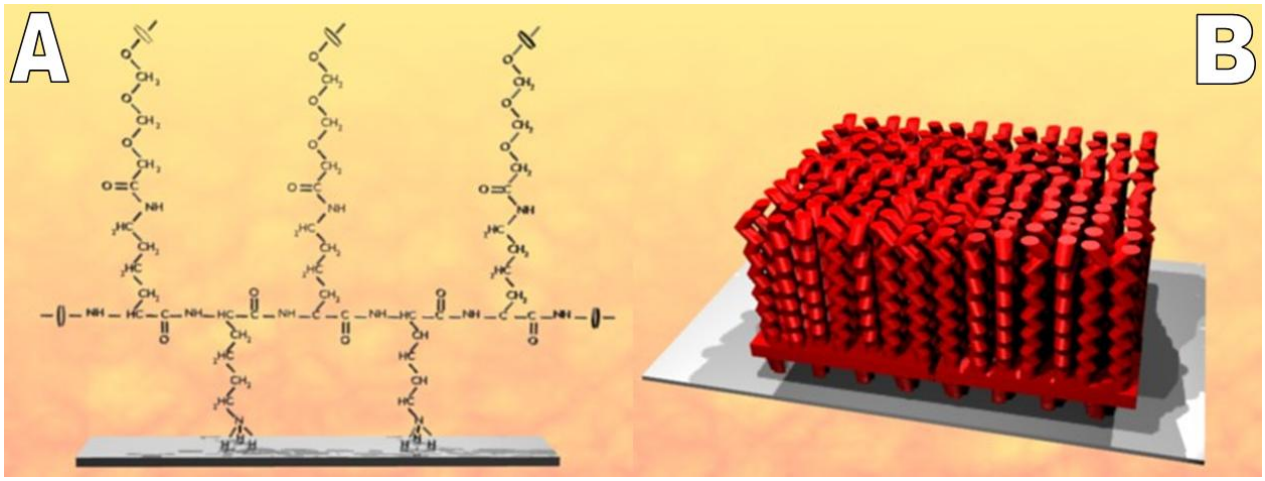


***Figure 16: Pll-g-PEG molecules.*** *A/ Chemical structure, with a lysine backbone and chains of PEG. B/Schematic view of a dense layer of Pll-g-PEG molecules on a surface.*

I tested both molecules for playing the role of barriers patterns on the surface: the BSA which has been identified to work quite well and Pll-g-PEG. Both of them were tagged by a fluorophore RhodamineB which permitted an imagery using classical optical tools. In order to determine which molecule is the best, three points needed to be addressed: anti-fouling for phospholipids and proteins, stable on a $SiO_2$ surface under liquid environment, and compatibility with AFM imaging. All these points were tested using successively: QCM-D technology for testing the interaction between the repellent molecules and the molecules of interest, then the fluorescence microscopy for the stability of the patterns in liquid media, and finally the AFM for imaging the patterned-SPBM plus the motor proteins.

### i. Interactions

As described in chapter 2, one of the most flexible tools for studying the interaction between molecules is the QCM-D. Unlike the interactions between motor proteins, I elaborated a simple approach consisting of only two steps: the sensor presented a $SiO_2$ layer (model QX303 from QSense )which would mimic our sample surface, the candidate antifouling molecules are both deposited on the surface, using an incubation or a direct transfer from a PDMS stamp, then liposome and motor proteins are injected over the sensor and interactions are recorded. We compared results between BSA and Pll-g-PEG, and also between incubated and stamped molecules.

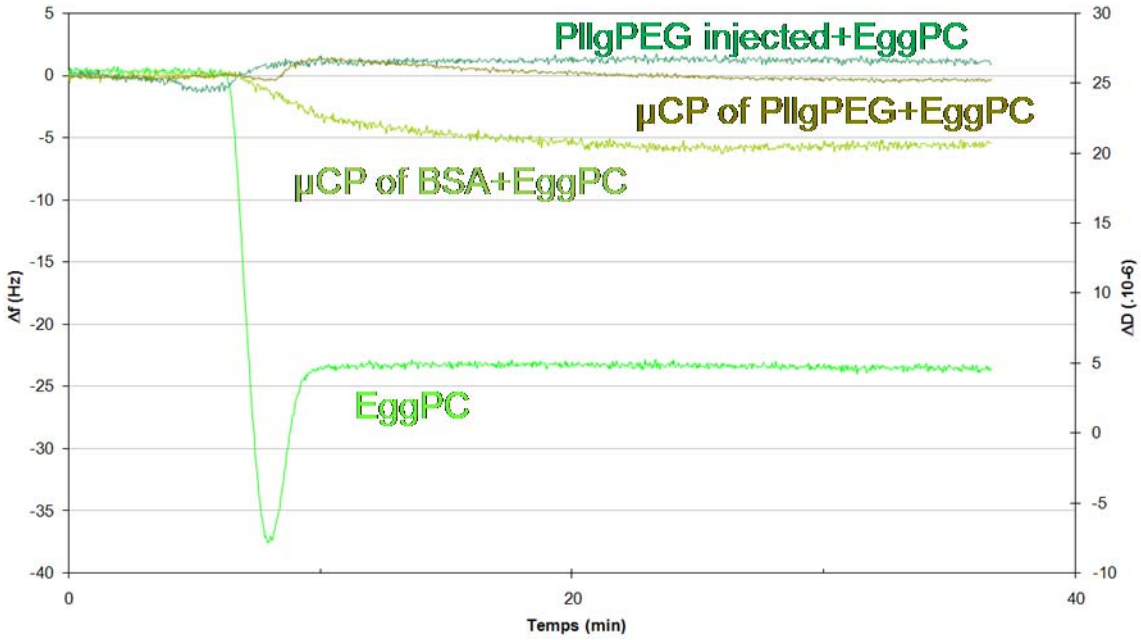


***Figure 17: Anti-fouling experiments using QCM.*** *4 QCM traces are visible and correspond to EggPC Liposomes injection simultaneously in the 4 QCM chambers. Bright green/ SPBM formation with the three steps previously described. Green/ BSA layer deposited by µCP prior to injection. A frequency shift of 5 Hz is recorded. BlueGreen/ PllgPEG injected on the sensor prior to experiments. A small frequency variation is detected but the signal stabilized after 20 minutes to its original value. Brown/ PllgPEG printed on the sensor.*

First, both anti-fouling molecules did not exhibit the same response when incubated or printed. For this analysis, we tested surfaces of different energies: with and without plasma oxygen activation. By measuring the surface angles, hydrophilic or hydrophobic behavior could be deduced and in our case were very different on both situations. Regular glass slide shows a contact angle of 80° before activation, and more than 140° after. BSA proteins adsorb quite homogenously on both kinds of surface. However, it turned out that this layer of BSA was not stable at the surface when washing with a buffer solution. Conversely, for BSA proteins not incubated on the surface but printed with a flat stamp, the stability of the coating was greatly improved. In the case of Pll-g-PEG molecules, layers deposited by incubation or printing turned out to resist washing steps only in the case of plasma activated surface. Based on these observations, we have systematically worked with plasma activated surfaces for the following. Injection of liposome and proteins are shown in figure 17 for Pll-g-PEG and BSA layers,

incubated and stamped for the first one and only stamped for the second one. A sensor without any coating on its surface was used as a witness for SPBM formation, in order to compare response in the different chambers. As expected, QCM analysis indicates that SPBM cannot be formed on these surfaces either coated with BSA or pll-g-PEG molecules. For protein adsorption, Pll-g-PEG surfaces exhibit no trace of adsorption while BSA surfaces display a small frequency shift (5Hz) which can be considered as negligible. Based on these results, we observed that the deposited layer was robust enough and both molecules remained anti-fouling. We concluded that both molecules can be used as anti-fouling molecules for the SPBM formation and protein. I tested the injection of PE-PG liposomes but the slow rate formation of the SPBM on the surface recorded was detrimental for QCM recording analysis.

### ii. Generating the patterns by Micro-Contact Printing (μCP)

The second step was the observation of the stability of the patterns in liquid medium. As described briefly above, molecules can be either incubated on a surface for creating a homogenous anti-fouling layer, or deposited in a controlled way in order to generate a pattern on the surface. This pattern will later serve as a mask for generating the SPBM only in the uncoated areas of the patterns. Several methods have been proposed for creating patterns on a surface and mixing these patterns with a self-assembly of a SPBM. Metal[99] and also BSA proteins[109] have been tested. One of the employed methods was based on a soft-lithography method called Micro-Contact Printing (μCP). This technique has been first proposed by Kumar and G. M Whitesides [110; 111] for the deposition of thiols molecules on a gold surface using a deformable based polymer stamp. This technique enables routinely the patterning at the micro or nano-scale of a large panel of molecules, starting from thiols[110], proteins[112; 113], anti-bodies [114; 115; 116] and Pll-g-PEG[106; 117]. I will first depict the full process of μCP, and then the results obtained with our molecules.

#### 1. μCP method

μCP principle is derived from the Gutenberg invention, several hundred years ago: the transfer of an ink from a stamp to a surface in a defined series of patterns.

Gutenberg developed it with a paper ink, using a metal stamp where letters had been etched. The contact of the metal inked stamp with a paper was achieved using a press system. This contact transferred the ink from the metal stamp to the paper. This invention can be considered as one of the most important of mankind, because it allowed for the first time of history the large reproduction and diffusion of knowledge through the world. The same basic principle was reproduced by Kumar and Whiteside[110] when they used instead of a metal stamp, a polymer stamp, and instead of an ink a molecular solution. The principle of µCP is described in figure 18.

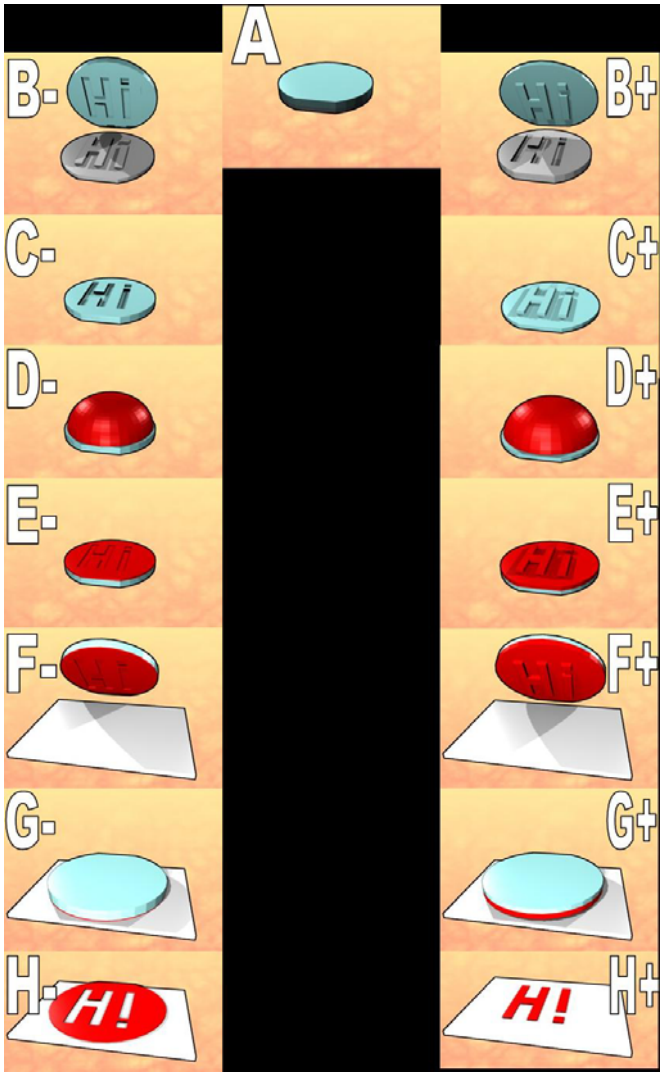


***Figure 18: Micro-Contact Printing (µCP) principle****. Two kinds of patterns are presented, positive on the right and negative on the left. A/ A PDMS stamp is generated by casting against a patterned silicon wafer. B/ The stamp is gently cut and removed from the silicon mold. C/ A perfect replica of the patterned can be seen on the PDMS stamp. D/ The PDMS stamp is inked with a solution containing the molecules to be*

*patterned, in our case BSA or Pll-g-PEG. E/ Liquid is removed and the stamp is dried several seconds. F/ A surface has been cleaned and serves as a sample. G/ The stamp is gently brought in contact during a defined time without applying any external pressure. H/ The stamp is removed from the surface. Ink has been transferred respecting the patterns in contact with the surface.*

The primary step of the μCP process consisted of designing patterns on the stamp, and for doing that they used the replica method from a silicon master. Silicon masters exhibiting patterns at the micro and nano-scale were generated by photo or electron-beam lithography, technologies issued from the micro-electronics area. These techniques are described in annex 3. Figure 19 shows the different masters used for the micro-scale experiments and also for the nano-scale.

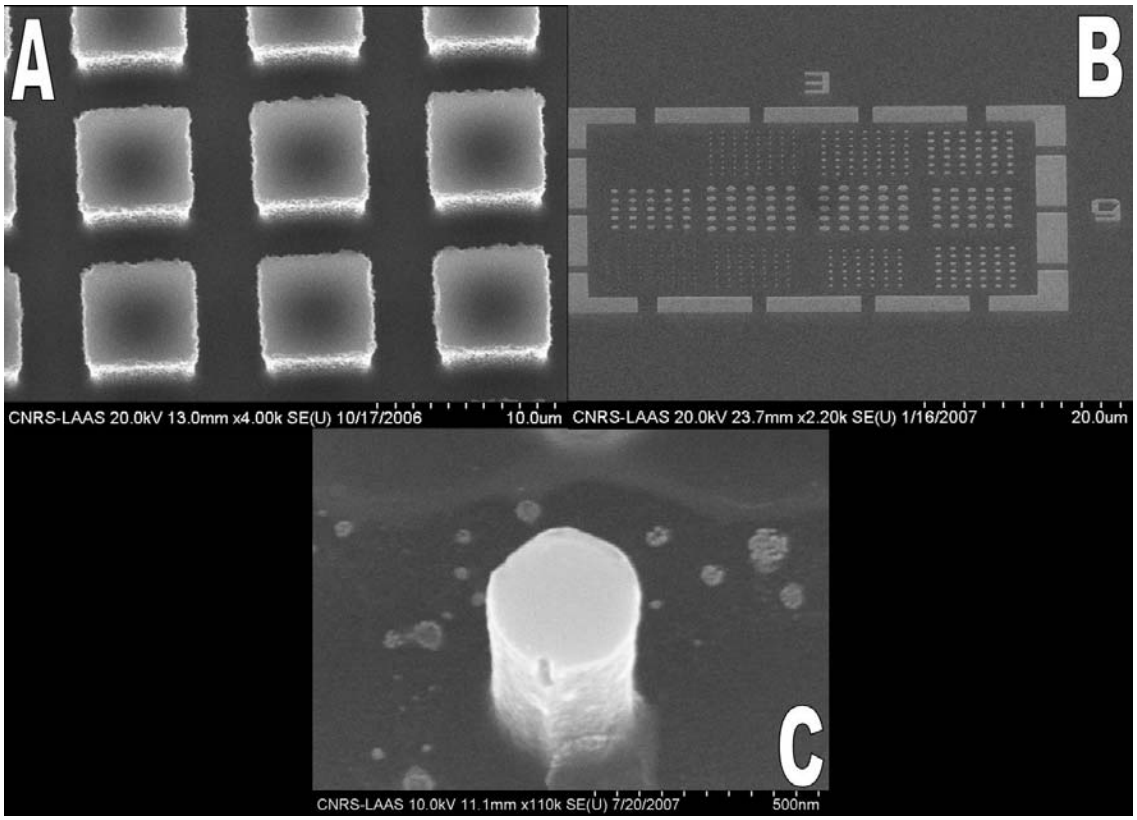


***Figure 19: SEM images of some patterns of silicon masters.*** *A/ Square of micro-pattern obtained by photolithography. B/ Series of nano-pillars obtained by e-beam lithography C/ Single nano-pillars of 400 nm diameter.*

The micro-patterns were not difficult to create, since photo-lithography has been largely studied and does not present major difficulties. However, the fabrication of nano-

patterns was more challenging. Because we wanted to print anti-fouling molecules covering most of the surfaces, it is thus necessary to generate a master where small areas have been etched. For this reason and for minimizing exposure time in e-beam lithography, we have employed a positive resist PMMA and a lift off process presented in annex 3.

Once the silicon master is generated, it is possible to produce a large number of polymer replica by casting. For all my work, I have used the same silicon master. A pre-polymer solution called Poly-DiMethyl-Siloxane (PDMS) composed of a base and an initiator was mixed at defined mass proportion (10 for 1), degassed in a vacuum chamber for removing air bubbles and spread on the silicon master surface. A polymerization reaction occurs into the pre-polymer solution, explained in figure 20.

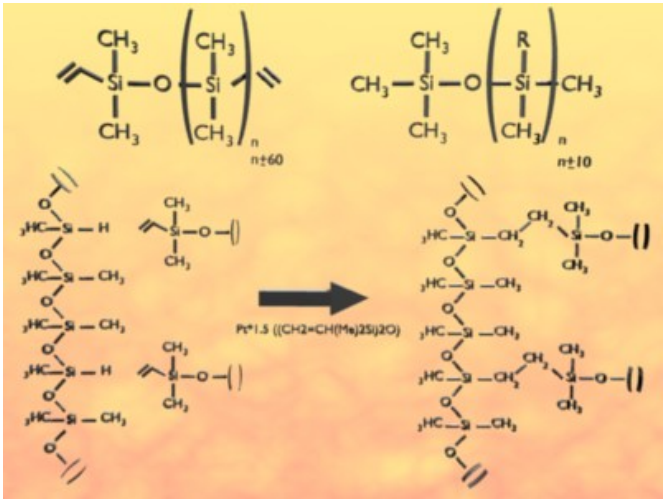

***Figure 20: Schematic view of the PDMS Sylgard 184 ®.*** *Two main components are shown on the top and the chemical formation of long polymer chain on the bottom.*

The pre-polymer solution in its liquid phase turned to a solid and elastic material exhibiting a perfect negative replica of the silicium master. This polymerization is achieved at 80°C overnight [110].

This stamp is then gently cast and removed from the master and inked with a desired solution, in our case a solution containing BSA proteins or Pll-g-PEG molecules. The solution is incubated for a short period of time, less than 2 minutes, dried under nitrogen gas and put manually into contact with a plasma activated glass slide. Molecules are transferred from the stamp surface to the glass slide during the contact. In my experiments, the contact time necessary to obtain high quality pattern was as short as 1

minute. Several points should be controlled for allowing a good pattern's transfer: the ink concentration and the incubation time, the drying step, the contact time and the stamp handling.

As expected, if the ink solution is incubated for a long period of time on the stamp, numerous layers of molecules can form and would be further transferred to the surface which could be detrimental for further analysis. By controlling both solution concentration and the time of incubation, we can control the density of molecules adsorbed on the stamp surface. The drying step is essential for removing liquid from the stamp surface and should be done carefully. An empiric approach let me observe that 30 seconds of drying under nitrogen flowing was optimum in general. Contact time parameter is quite similar to inking time, as long as the stamp remains in contact with the surface, a large number of molecules can be transferred at the surface. Moreover, molecules coming from the PDMS stamp can diffuse on the surface while the stamp contacts the surface, and this diffusion can be detrimental for pattern definition. In order to minimize this effect, the contact time was chosen to be below one minute. The last parameter is stamp handling. Due to its elasticity, and also due to its high adhesive behavior, the PDMS stamp must be handled with precautions during the drying step and also during the contact. By pressuring the stamp, it is possible to deform the patterns.

## 2. Results

Figure 21 shows typical patterns obtained by μCP for both BSA and Pll-g-PEG molecules. Patterns at the micro-scale and nano-scale were achieved for both molecules using same PDMS master design. Through optical imaging the good definition of the micrometric patterns can be clearly observed. No defects are visible and only small variations on the fluorescence intensity are seen within the patterns. However, fluorescence microscopy does just give qualitative information about the pattern and other characterization are needed for confirming the quality and stability of the patterns on the surface. Patterns were observed both in air and liquid. The quality of patterns has not been alterated by the liquid and lines remains identical. For the nanoscale patterns due to Rayleigh criterion it is not possible to distinguish clearly the patterns and nanoscale characterization is required.

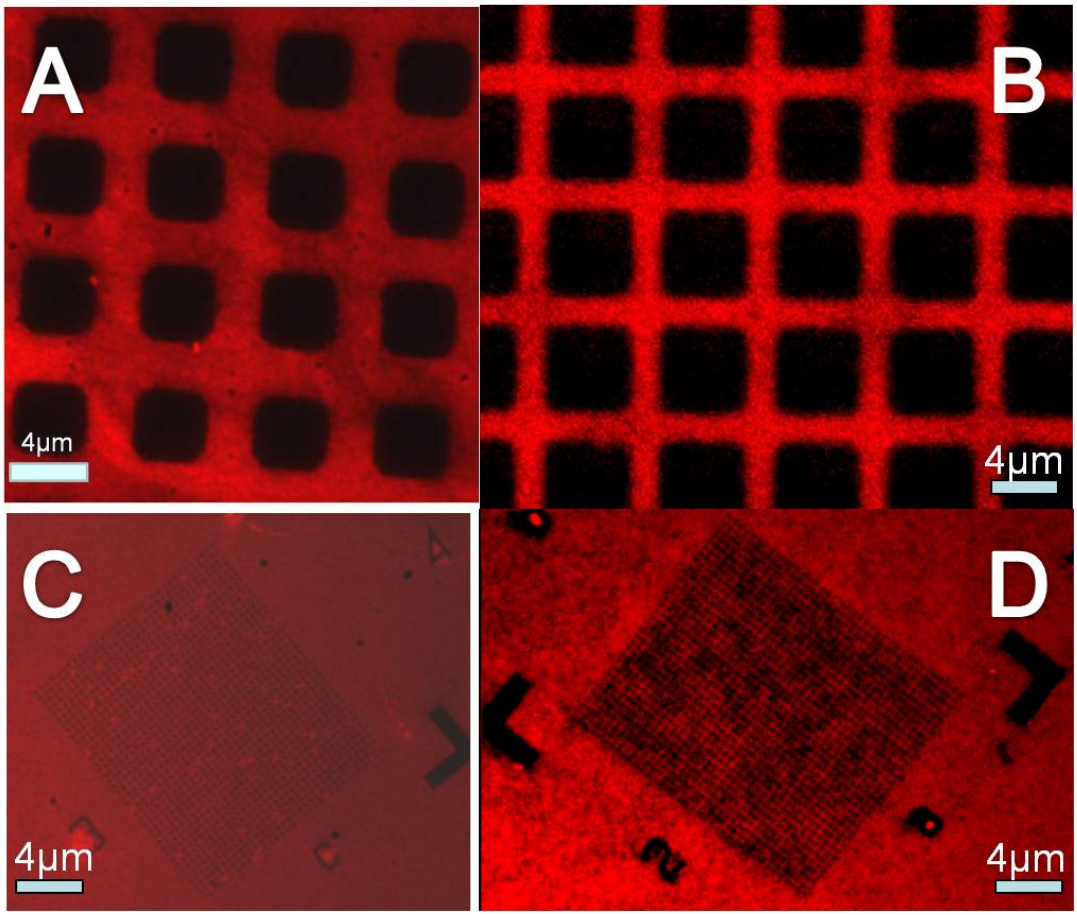


***Figure 21: Fluorescence imaging of the patterns produced by µCP.*** *A/ Grid Micro patterns of Pll-g-PEG-rhodamine molecules. B/ Grid Micro patterns of BSA-rhodamine proteins. C/ nano patterns of Pll-g-PEG-rhodamine.D nano-patterns of BSA-rhodamine.*

### iii. AFM characterization

The last criterion for selecting the appropriate anti-fouling molecule is the stability under AFM analysis. AFM will be used for imaging surface with at least 3 different molecules, the anti-fouling molecule BSA or Pll-g-PEG, the SPBM and the motor proteins. Major limits for achieving high resolution would be the architecture stability under AFM imaging, and AFM probe contamination. By adjusting the force applied by the probe on the surface, we could minimize the damage caused by the AFM imaging process, but the contamination of the probe by loosely fixed molecules is out of experimental control. I started logically by imaging the patterns obtained by µCP for both BSA and Pll-g-PEG at the microscale and nanoscale and compared the images obtained

and also the probe contamination. Figure 22 shows AFM imaging of both BSA and Pll-g-PEG patterns.

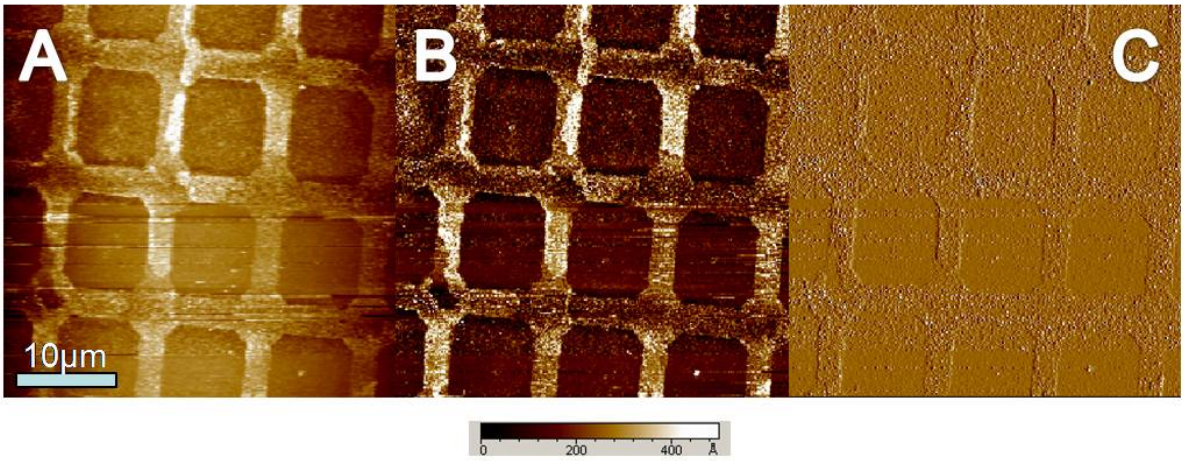


***Figure 22A: AFM images of the micro-patterns of BSA deposited by µCP on the activated surface****. Observed in contact mode in PBS buffer with a MLCT probe from VEECO, stiffness 10mN/m, force evaluated below 100 nN. A/Height signal before flattening. B/height flattened signal. C/Vertical deflection. The different signals tend to prove that the BSA proteins patterned remains stable under AFM imaging.*

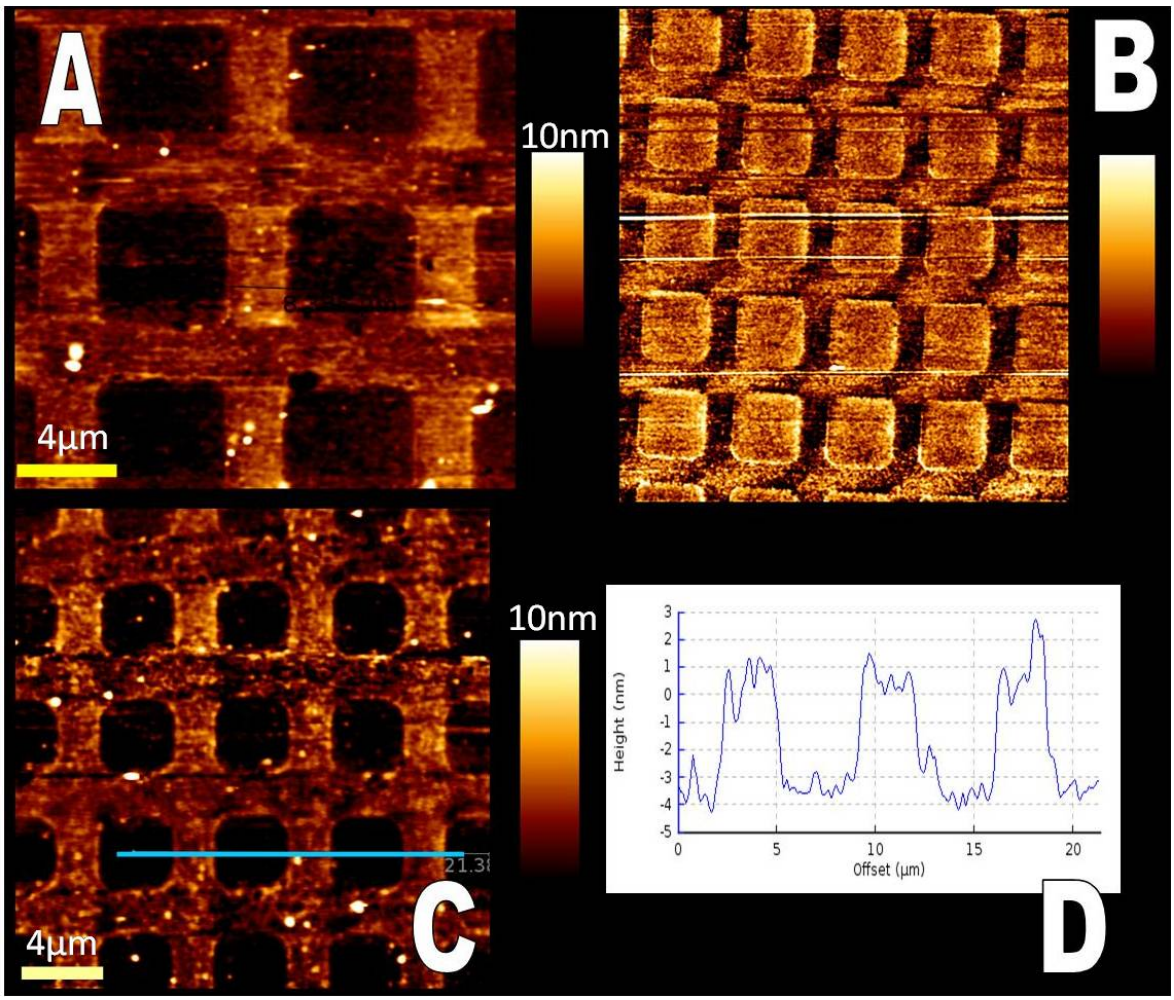


***Figure 22B: AFM images of Pll-g-PEG patterns deposited by µCP at the micro-scale****. Obtained in contact mode in Hepes1 buffer with a OBL probe from Olympus, stiffness 5mN/m, force evaluated below 50nN. A: height image of squares of 8 µm with lines of 2 µm. B: lateral deflection of same patterns as A/ but with an enlarged view. C: squares of 4 µm with 2 µm lines. D: Cross section of C which reveals a line thickness of 5 nm.*

BSA and Pll-g-PEG patterns deposited by µCP were clearly visible using AFM in their respective buffer (PBS and Hepes1). Both molecules were observable using AFM but in different conditions. It turned out that the BSA patterns were more easily observable using different stiffness cantilever compared to the Pll-g-PEG patterns. Both were stable under imaging, but due to the elastic structure of the PEG brush, it appeared that imaging Pll-g-PEG patterns was only possible with flexible cantilever presenting stiffness under 10mN/m which permits to image with force below 50pN. It is also visible that we are in a situation close to the monolayer of molecules, from 5 to 10 nm for BSA

and around 5 nm for the Pll-g-PEG which will be important for the next step. The major difference between BSA and Pll-g-PEG patterns turned out to be the tip pollution or contamination. The AFM tip was contaminated despite our effort to minimize the sample probe interaction but not in the same order of magnitude. Figure 23 highlighted an AFM tip after BSA sample analysis compared to a one after Pll-g-PEG sample. Differences are clearly visible.

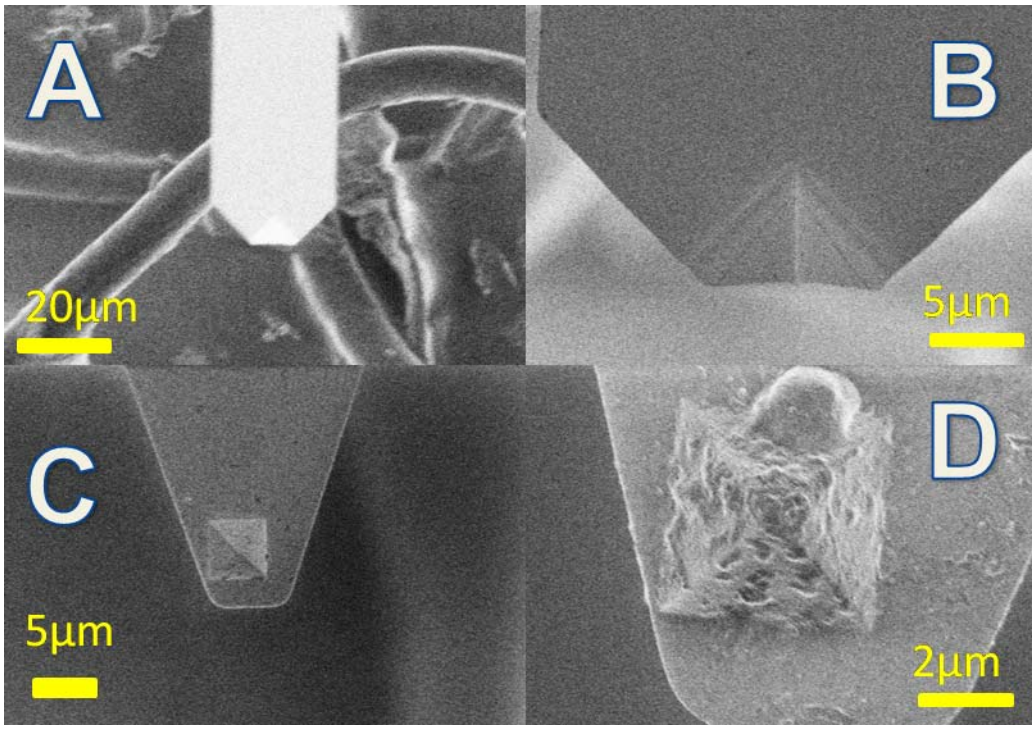


***Figure 23: SEM imaging of the AFM probe after imaging.*** *A/ Large view of OBL probe after imaging Pll-g-PEG patterns. B/ Enlarged view of A. C/ MLCT probe after BSA imaging. D/ Enlarged view of C. Pollution is clearly visible on the AFM probe after BSA imaging with large contamination cluster while only trace of molecules are visible on the OBL probe after Pll-g-PEG imaging.*

Both molecules tend to contaminate the AFM tip while scanning but not with same order of magnitude. It is difficult to evaluate in which magnitude this pollution will be problematic for AFM imaging of the next steps of the sample elaboration, but it is clear that BSA proteins contamination will be definitely more problematic for tip-sample interactions and later images analysis.

Through the interactions, stability and AFM analysis and especially tip pollution, it turned out that the Pll-g-PEG molecules presented more advantages compared to the

BSA molecules, especially about the AFM imaging which was crucial for our purpose. The low probe pollution of the probe by scanning Pll-g-PEG patterns will be indeed the key for imaging the final assembly on the surface despite the difficulty to image the Pll-g-PEG patterns alone.

I noticed that the thickness of the Pll-g-PEG layer changed depending on what kind of buffer we were working in, going from 5 nm for hepes 1 to 2,5 nm for hepes 3. The role played by the ions in the hepes 3 could be the source of this thickness difference and has been put in evidence recently [118].

## c. Patterned-Supported Phospholipids Bilayer Membrane

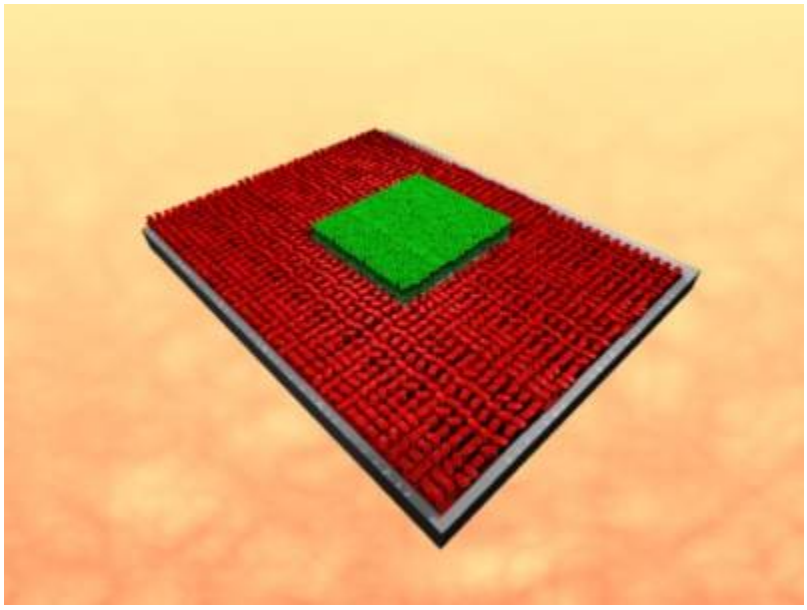

***Figure 24: Schematic view of the patterned Supported Phospholipidics Bilayer Membrane P-SPBM.***

By choosing the Pll-g-PEG molecules for patterning the surface, the next step of the final assembly consists in the SPBM formation within the defined areas on the surface. We worked with the two phospholipids solution already tested, EggPC and PEPG. EggPC played the role of a model. Figure 24 pictures the step of the final assembly described here.

### i. Protocol

After pattern generation, the SPBM formation can be implemented. The process of SPBM formation, as described above, was different between the EggPC and PEPG solution. EggPC liposomes tend to form quickly a homogenous SPBM in any available area of the surface, due to the collective behavior of the liposome [119; 120], compared to PE-PG liposome where a puzzle of SPBM patches forms on the surface. We incubated the freshly EggPC liposome solution at 100µg/ml for 5 minutes and wash extensively the surface with free buffer. For PE-PG solution, we followed the new established protocol and incubated the liposome solution at 100µg/ml for 10 minutes and washed the surface using hepes 1 buffer. Both surfaces must be kept in water due to the sensitivity of the SPBM to air.

### ii. Fluorescence characterization

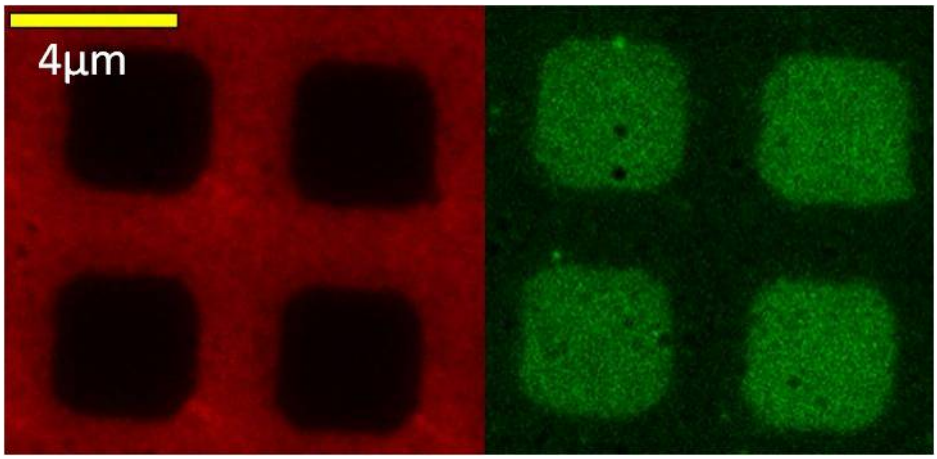


***Figure 25:P-SPBM at the microscale of EggPC and PE-PG SPBM.*** *Top view left/ Pll-g-PEG-rhodamine patterns top view right EggPC SPBM. Scale bar 5 µm.Bottom view left/ Pll-g-PEG patterns. Bottom view right/ PE-PG SPBM.*

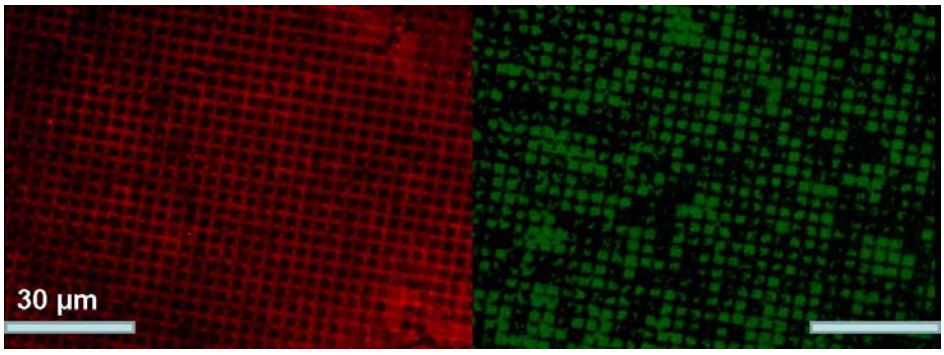

Figure 25 displays results obtained for EggPC and PE-PG P-SPBM. As expected, EggPC liposomes fused in every space free from Pll-g-PEG on the surface while only patches of PE-PG can be observed. I deliberately present a large view of the PE-PG P-SPBM to highlight this point compared to a homogenous covering with EggPC P-SPBM. By counting the numbers of patterns filled by PE-PG SPBM, almost 65 to 75% of the squares display SPBM patches, compared to 100% for the EggPC solution. I tried several and successive incubation of PE-PG liposome solution on the same sample, for fulfilling the remained free space, but could not exceed an occupation rate of 80%. For confirming the separated behavior of the P-SPBM, FRAP experiments were done on both samples. Figure 26 showed typical results for the EggPC solution.

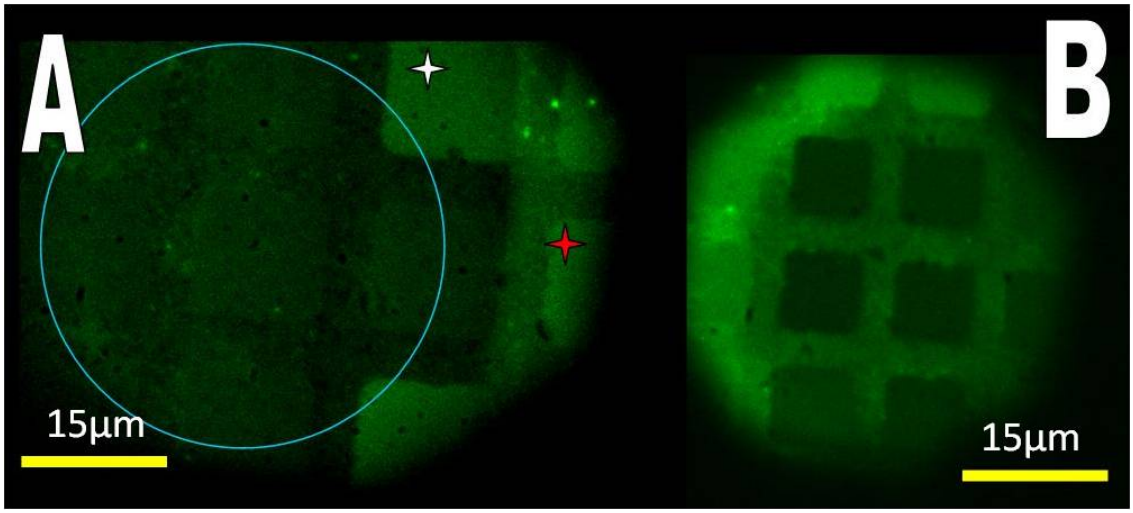


***Figure 26: FRAP experiments with Pll-g-PEG patterns and EggPC P-SPBM.*** *A/The circle displays the microscope aperture and white star and red star the different fluorescence light emission from domains outside of the aperture light emission. Scale bar 10 µm. B/ enlarged view of different squares. Scale bar 15µm*

It is clear from FRAP characterization that the phospholipids can only diffuse within one pattern, and can not overpass the Pll-g-PEG lines. FRAP experiments were done as follows: microscope aperture was reduced to illuminate only a limited numbers of squares until no fluorescence emission was visible. By observing the bleached area after exposure, several levels of fluorescence intensity could be observed, from totally black which correspond to 100% of photo-bleached lipids, through a second level where only a certain percentage had been photo-bleached, which gave a “grey” level

corresponding to a mix between photo-bleached and non photo-bleached lipids, to finally a bright level where a very limited number of lipids had been photo-bleached. The presence of multi-levels confirmed that phospholipids only diffuse inside a patterned domain and do not diffuse from one SPBM patch to another. If the lipids could cross the Pll-g-PEG patterns, we should observe after a long period of time the same emission intensity everywhere, whatever the area. This was never the case in our experiments. For the PE-PG experiments, the fact that the patterns were not 100% filled by the SPBM partially addressed that question. We monitored FRAP experiments on separated SPBM patches which never mixed together, which gave indeed the same result as for the EggPC sample. The fluorescence microscopy was also used for characterizing the nano-P-SPBM with a more complex result to interpret.

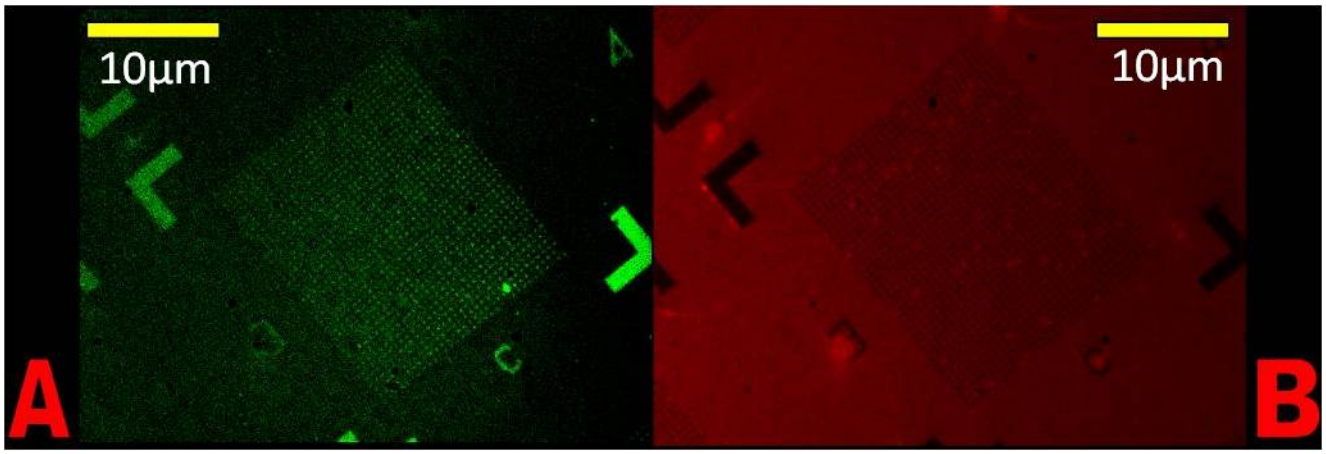


***Figure 27: Fluorescence imaging of 400 nm P-SPBM of EggPC*** *.A/ Image of EggPC P-SPBM. B/Image of Pll-g-PEG patterns.*

Figure 27 displays results obtained with EggPC solution on Pll-g-PEG patterns. P-SPBM of EggPC at the nano-scale were visible using fluorescence microscopy but it turned out to be difficult to conclude based on this analysis if the formation of P-SPBM really took place within the 400 nm patterns. However, we observed no fluorescence when we incubated PE-PG solution on these patterns. It was not a real big surprise due to the previous evaluation of the PE-PG liposome average diameter, which exceed the accessible surface on the sample. AFM characterization will be the only tool which can conclude to the formation of P-SPBM at the nanoscale.

### iii. AFM characterization

The next critical question is the possibility or not to image these P-SPBM with AFM in liquid? By choosing the contact mode and a low AFM probe stiffness 5mN/m, I could successfully image these samples. Figure 28 displays the results obtained.

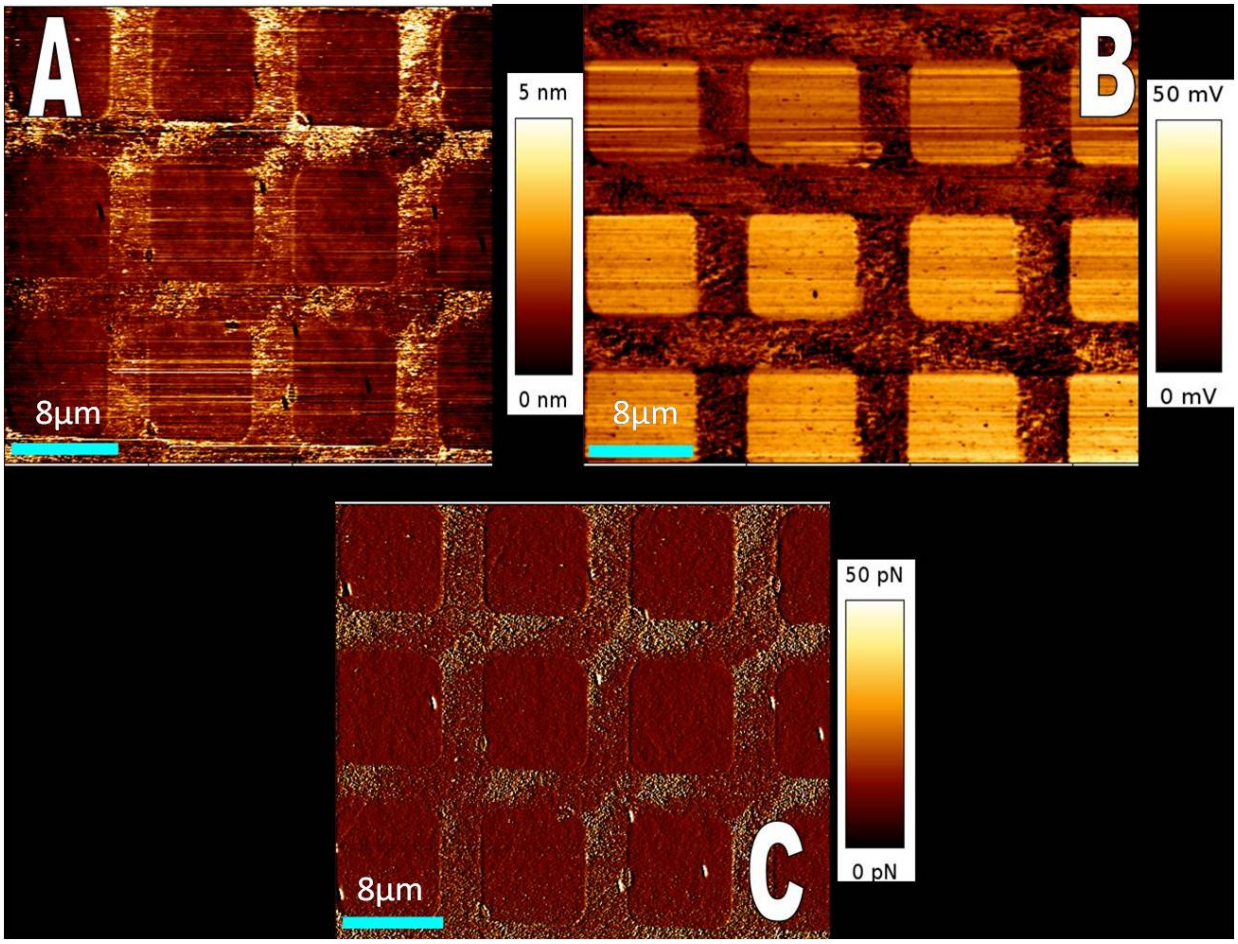


***Figure 28 top: P-SPBM of EggPC at the microscale within 8 µm patterns****. Contact mode in PBS buffer, stiffness probe 5mN/m, and force below 50pN. A/ Height signal, scale bar 8 µm. B/ Lateral signal. C/ Vertical deflection signal. Bottom P-SPBM with 4 µm patterns A/ Height signal. B/Vertical deflection and C/ Cross section of the height signal A.*

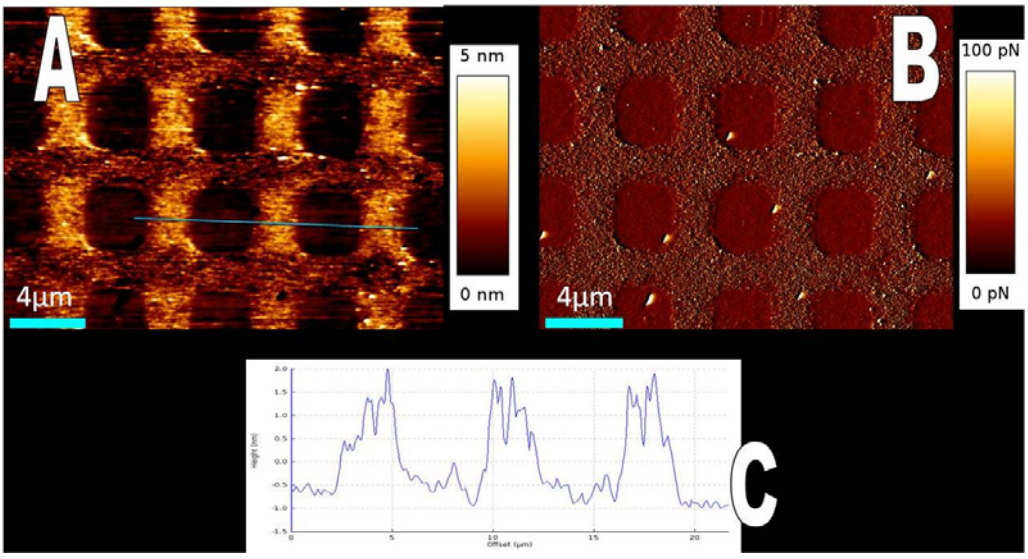


The different signals, height signals, vertical deflection and lateral deflection allow distinguishing the presence of different molecules at the sample surface. The first sample I imaged was the P-SPBM from the EggPC solution. Due to the thickness of the SPBM, between 3 to 4 nm, and the Pll-g-PEG layer around 5nm, we should see lines above square with a height difference around 1 to 2 nm, depending on the Pll-g-PEG brush extension. By imaging the sample surface, the expected results were achieved; lines were observed above square and confirmed the presence of SPBM at desired area. However, the apparent thickness of a Pll-g-PEG layer could change depending the presence of charges, or the mechanical dragging effect of the probe. The control of the force was crucial at this step for the imaging process. Indeed, by applying a large force on the probe, we changed dramatically the picture obtained, as seen in figure 29 where square were higher than Pll-g-PEG patterns.

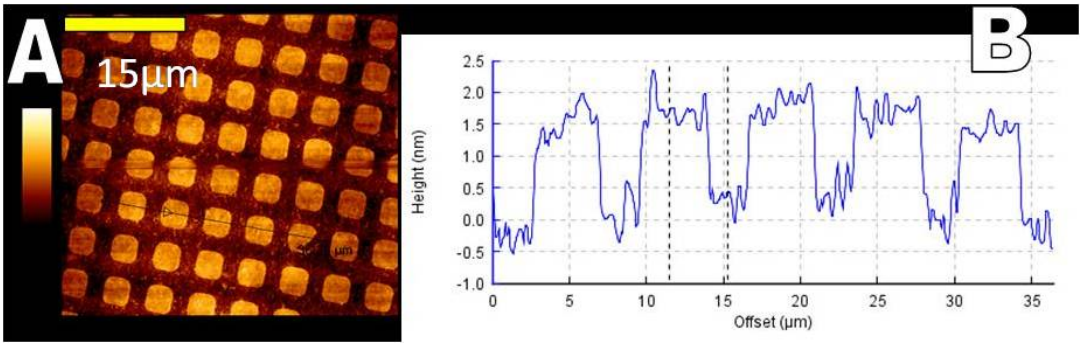


***Figure 29. AFM images of EggPC P-SPBM with higher force****.A/ Height signal. B/ Cross section.*

We think that the soft Pll-g-PEG brush is sensitive to a mechanical stress due to the force applied by the AFM probe, which reduced its thickness. In contrast, the P-SPBM due to its good lateral and vertical cohesion is less sensitive to the stress. This is why by changing the applied force, a negative image of the sample surface can be obtained. This result highlights the fact that the control of the force will play a major and essential role in the next step for imaging the full assembly. After the formation of the P-SPBM at the microscale, we tried to visualize the results obtained at the nano-scale, in nano-patches of 400 nm. The EggPC result is displayed in figure 30 while no results were obtained for the PE-PG solution.

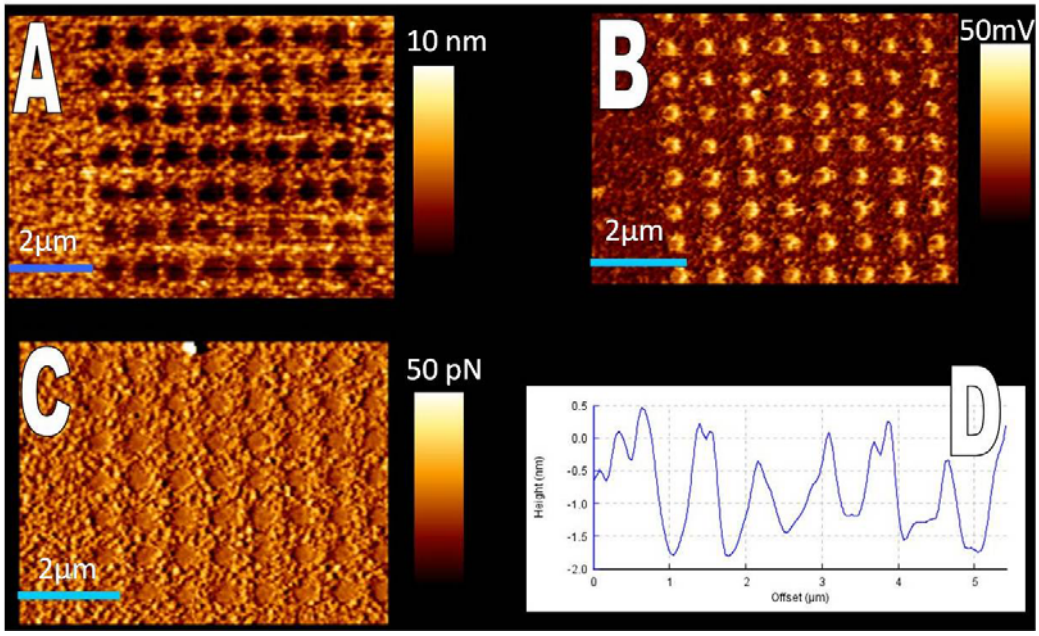


***Figure 30: P-SPBM of EggPC at the nanoscale.*** *Contact mode in PBS, stiffness 5mN/m, force below 50 nN. A/ Height signal. B/ Lateral deflection. C/ vertical deflection*

The AFM images obtained for P-SPBM at the nanoscale were encouraging but some severe limitations appear while scanning. Despite the low contamination of the tip by Pll-g-PEG molecules, the needs for scanning at different scales before reaching a single nano domain increases the contamination risk of the probe which was detrimental for the imaging conditions. This point could be overcome by a chemical hydrophobic treatment of the tip for reducing the tip contamination. However, the ratio of the surface anti-fouling molecule/SPBM shows that the tip will interact most of the time with

antifouling molecules instead of SPBM, which increase any way the risk of tip pollution. The second point was that I never observed the presence of PE-PG SPBM within the Pll-g-PEG patterns at the nanoscale. A calculation reveals that a single PE-PG liposome exhibiting a diameter of 400 nm cannot form a SPBM inside the patterns, which confirm both fluorescence and AFM analyse. However, numerous images of PE-PG P-SPBM were obtained at the microscale using AFM in liquid media.

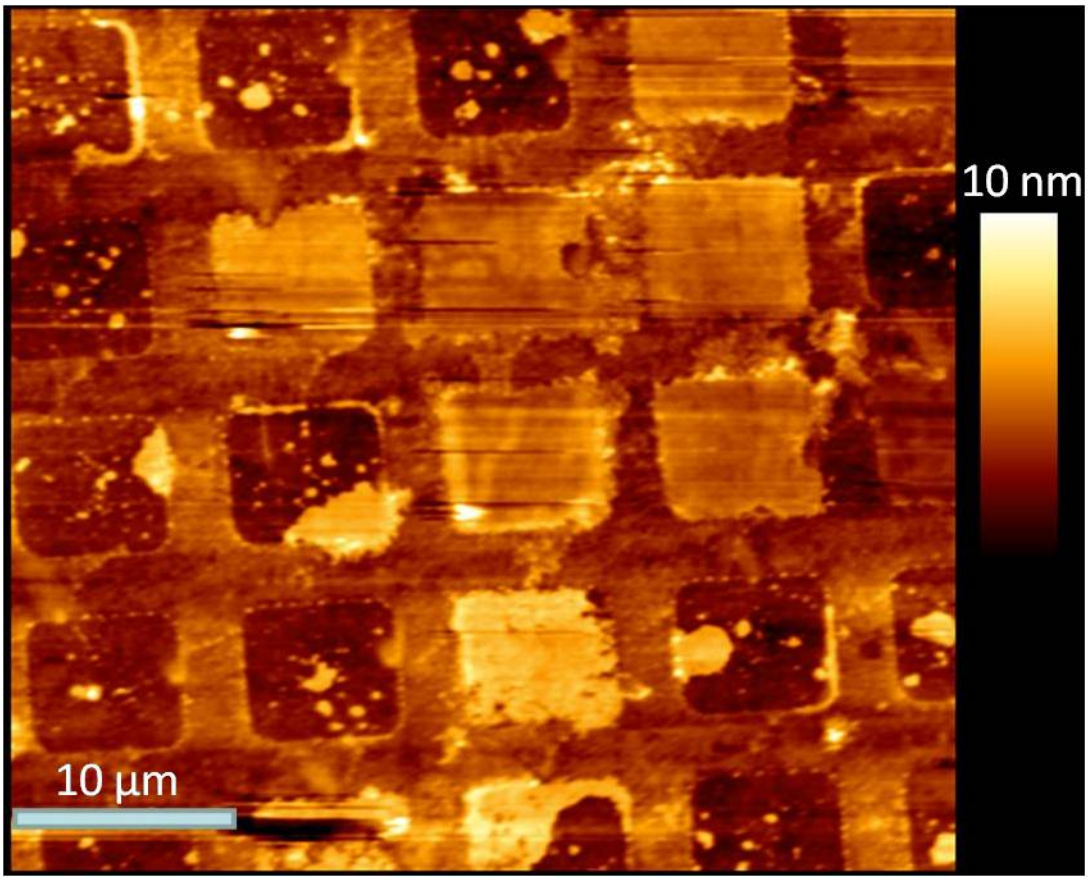


***Figure 31: PE-PG P-SPBM at the microscale.*** *Contact mode in hepes 3 buffer, cantilever stiffness 5mN/m, force below 50 nN. Lines of Pll-g-PEG are clearly visible while some square are partially filled with PE-PG SPBM.*

AFM analysis confirmed the fluorescence images obtained previously. SPBM are clearly visible on the surface within the Pll-g-PEG patterns. However, PE-PG SPBM does not fill all squares defined by the Pll-g-PEG patterns despite numerous incubation/washing procedures. The SPBM squares are clearly higher than the Pll-g-PEG lines despite a theorical value of 5 nm for both. However, images of the Pll-g-PEG patterns in hepes 3 buffer which contains bivalent ions, $Ca^{2+}$, reveals lines with an

average thickness of 2,5 to 3 nm( data not shown). This point supports the different thickness displayed in figure 31. As noticed before, several AFM systems are now commercially available and some proposed a set up which permits to couple AFM to fluorescence microscopy on the same system. The AFM set up used for most of this work has been mounted in an inverted microscope, which enabled the use of both fluorescence microscopy and also AFM imaging. I was thus able to integrate directly on the same image both fluorescence and AFM images, as presented in figure 32.

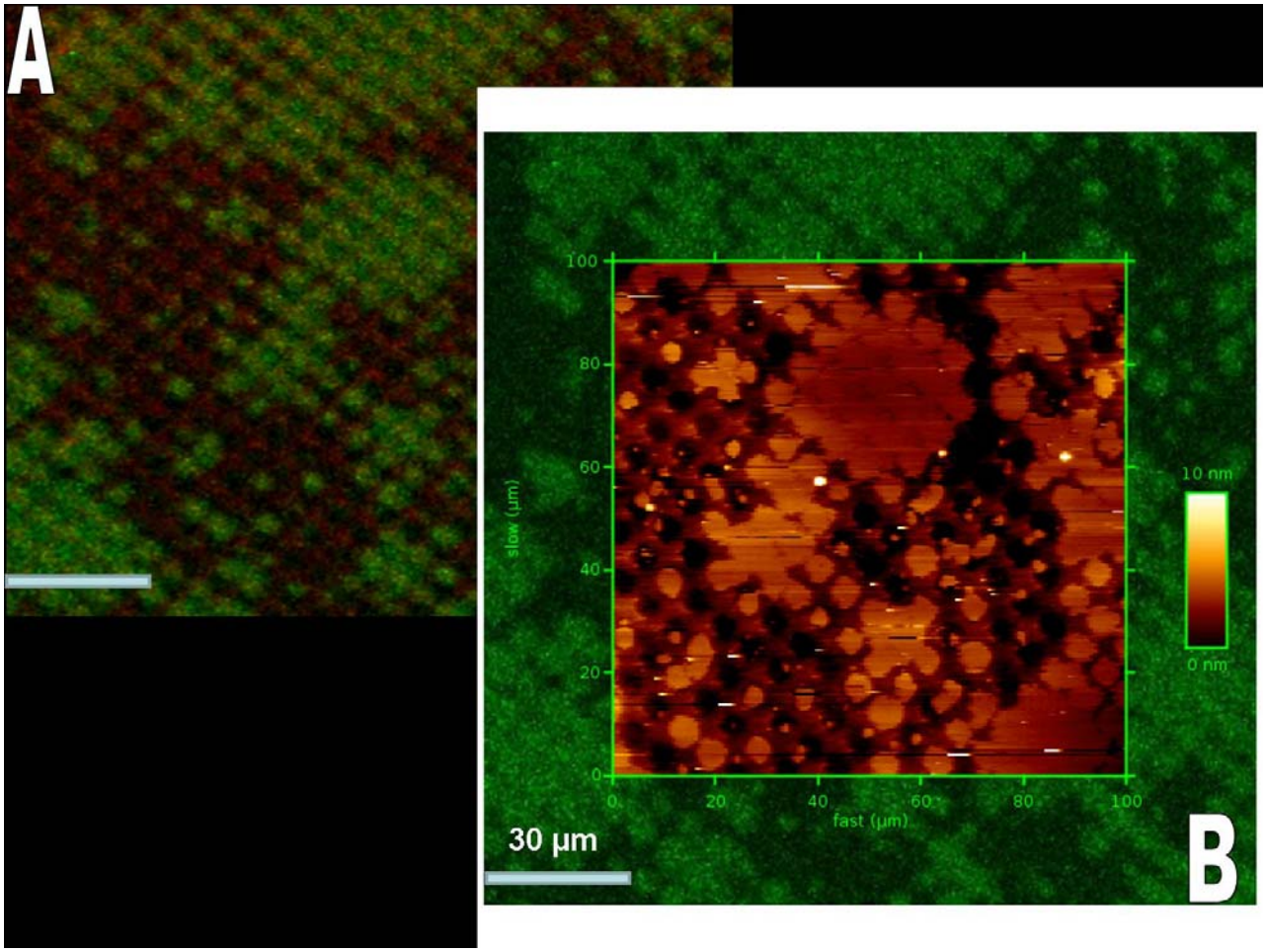


***Figure 32: fluorescence coupled to AFM imaging after PE-PG SPBM formation.*** *A/Fluorescence image with both tagged molecules visible, Pll-g-PEG in red and PEPG-SPBM in green. B/ AFM images coupled to the green fluorescence image.*

The image proposed in figure 32 synthesized both fluorescence and AFM analysis of the PE-PG P-SPBM. The relatively poor quality of the fluorescence images mainly comes from the fluorescence camera and could be improved in the near future. The

picture which mixes fluorescence image and AFM is quite impressive and constitutes the first ever result obtained on this kind of sample. By this way, the gain of time is considerable because we could access both qualitative (fluorescence) and quantitative (AFM) data about our surface. The picture proposed here shows also that some SPBM could cross ever the Pll-g-PEG patterns. We suspect that there is a possible interaction between PG and the poly lysine molecules present in the Pll-g-PEG. However, this point will need to be addressed in the future and was not detrimental for our work.

P-SPBM of both lipid solutions have been generated, proteins can be incubated on the sample. However, prior to experiment that, interactions between the formed SPBM and the motor proteins needed to be studied for addressing the question of which membrane could be better use for building the BFNM. In order to do that, we monitored the interactions of the motor proteins with the SPBM using again the QCM-D technology.

## d. Interactions between membrane and proteins

Once P-SPBM has been generated, we needed to study which lipids mixture will serve as a basis for protein assembly. For tackling this issue, I monitored the interaction between pre-formed SPBM on a QCM-D sensor and proteins [121]. Formation of homogenous SPBM on a QCM-D $SiO_2$ sensor has been already achieved previously, see section above, and production of purified motor proteins also in chapter 2. Interactions between EggPC SPBM and PE-PG SPBM with the motor proteins have been monitored in parallel using the same proteins batch production, for limiting the possible variations between different series of purified proteins. Figure 33 pictures the results of interactions between SPBM and motor proteins in PBS buffer.

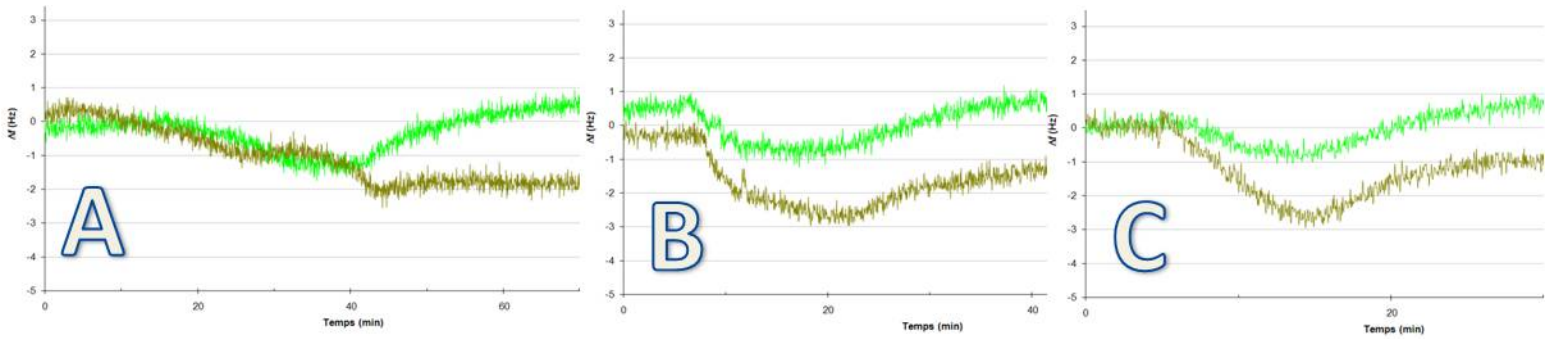


***Figure 33: Interactions between SPBM and motor protein monitored by QCM.*** *Bright green shows the interactions proteins / EggPC SPBM and brown proteins / PE-PG SPBM. A/ FliG 50µg/ml, B/ FliM 50µg/ml and C/ FliN 50µg/ml. FliG tend to adsorb on PE-PG compared to EggPC while results are more difficult to interpret for FliM and FliN.*

It is relatively clear that most of the motor proteins, FliG FliM and FliN, spontaneously adsorb on the PE-PG SPBM compared to EggPC SPBM. We sequentially injected the proteins in this order FliG, FliM and FliN. No specific interactions were observed in the EggPC chamber but the frequency shift detected in the PE-PG chamber tends to prove the interaction between proteins and membrane. The behavior was clearly different between the two SPBM. The question about the possible interaction between FliG and then FliM and FliN is open and further experiments by injecting directly FliM could address that point. In order to address the question of the selectivity of this interaction, we passed over both SPBM a BSA protein solution which displayed no specific interactions on both SPBM. We evaluated also the possible presence of default on the SPBM by adding successively solution of SPBM for fulfilling the possible "hole" within the SPBM surface and experiments were repeated several times. The result was clear and without any doubt, PE-PG SPBM would be the adequate membrane for assembling the BFNM.

## E) Motor protein

Massive amounts of purified proteins have been produced and were ready to incubate on the SPBM. By observing them on the SPBM, we would like to tackle one of the major questions of the BFNM: the size and shape of the different parts. We think that the observation in liquid using AFM would open the possibility to definitely address some structural questions about the global architecture of the BFNM. As noticed in chapter 1, one of the big questions about the BFNM is the position of FliG proteins [13; 122; 123; 124]. Based on cryo-TEM studies, on its crystal structure and also on numerous mutagenesis studies, it has been accepted that FliG could be placed at three positions into the BFNM architecture: at the bottom of the rotor, at an intermediate position between the rotor and the C-ring, or completely at the C-ring top position. These three hypotheses are shown in figure 34.

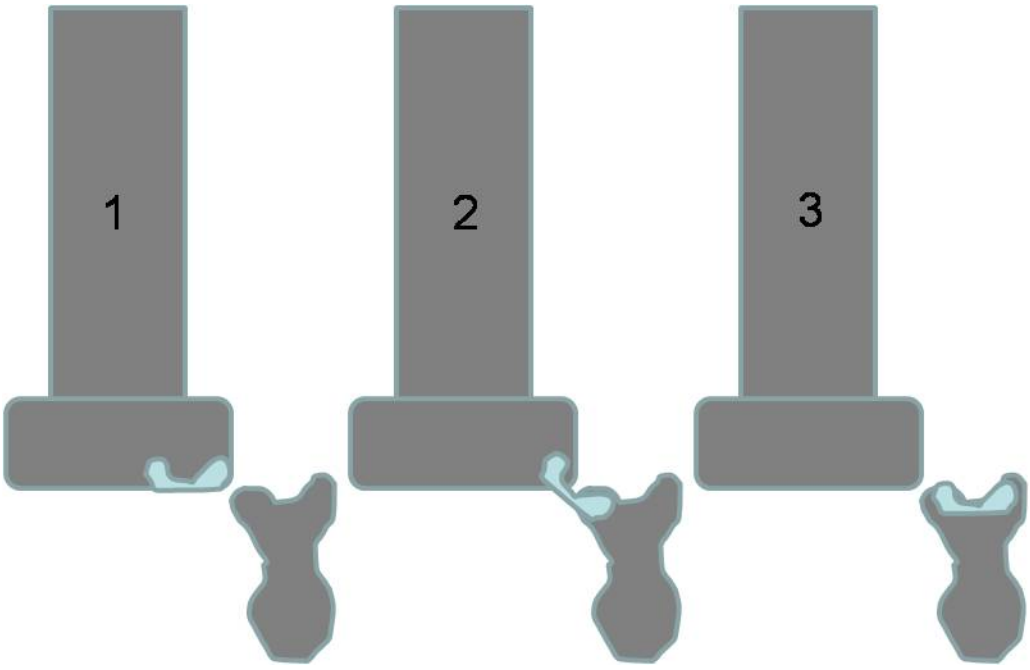


***Figure 34: The three hypothetical positions of the FliG proteins within the BFNM architecture.***

However, none of the previous studies has definitely answered that question, partially due to a symmetry problem between the number of FliG and the FliM proteins [125]. Numerous models have proposed explanations about this asymmetry, but to my

mind none of them can be confirmed, due to the lack of direct observation of the FliG assembly *in vivo*. Only a cryo-TEM approach gave interesting results about the MS-ring assembly and size [14], but for unknown reason this results has been neglected later by most of the contributions. AFM in liquid of the protein assembly FliF and FliG could address this question. By overproducing the motor proteins, we observe first on a mica surface the distribution of protein aggregates, and then directly on a SPBM and also on a P-SPBM. For example, if the FliG would not self-assemble directly into the so called M-ring, we should observe at the surface numerous aggregates with different sizes. FliF, despite the presence of the remaining Gst tag was also observed on both mica and SPBM surfaces and finally a mix of FliG FliM and FliN will be observed. Based on these results, we could be able to propose a shape and size for each of these elements and these results could serve as a basis of the new model describing the BFNM in chapter 4.

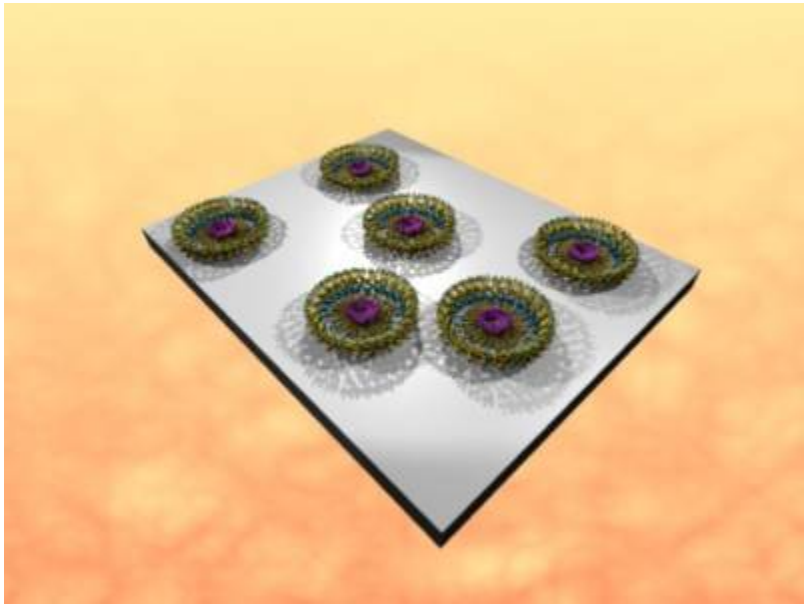

***Figure 35: Schematic view of proteins assembled on the surface***

## a. Motor proteins on untreated surfaces

### i. Pure proteins

We tested the direct observation of the purified proteins FliG, FliM, FliN, MotB on the surface and FliF-Gst and MotA-Gst. For the tagged proteins, only FliF has been previously imaged using AFM in air 10 years ago by K. Kurihara *et al* [52] and this is the only example to my knowledge of AFM imaging of pure motor proteins. Results for FliF-

Gst on untreated surface were difficult to interpret, and nothing was clearly obtained for MotA-Gst, MotB-Gst, FliM and FliN, only FliG proteins displayed interesting results, as shown in figure 36. FliG was incubated at a low concentration (10µg/ml) for 1 hour to 6 hours on a mica surface and rinsing several times. Mica has been identified to be a perfect surface designed for AFM imaging of single elements, as proteins assembly and also patches of membranes, as for example purple membrane with bacteriodhopsin [24] or other Integral Membrane Proteins [126; 127]. FliG represents the "key" protein for the motor structure. The interactions between FliG and FliF formed the cytoplasmic side of the rotor[12; 128], the multiple interaction with MotA the source of the rotation [129; 130; 131], and finally the role of FliG-FliM interactions for the switching [122; 132]. Figure 36 displayed results obtained in both tapping and contact mode of FliG proteins on an untreated mica surface.

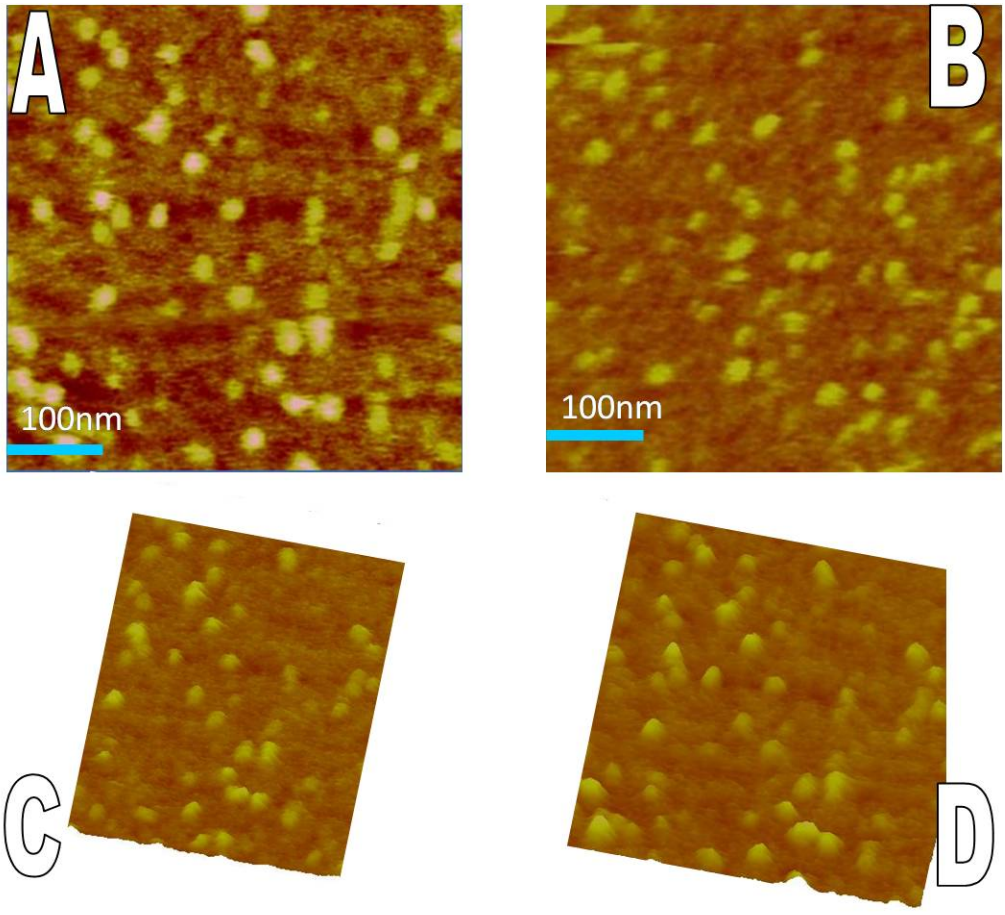

***Figure 36A: AFM images of FliG proteins on a mica surface.*** *Tapping mode in PBS buffer, force evaluated below 50nN for all images .A/ Tapping mode height image using OTR4 from Olympus, cantilever stiffness 20mN/m. B/ Height image using MSCT probe. C.D/ 3D reconstructions views of A and B.*

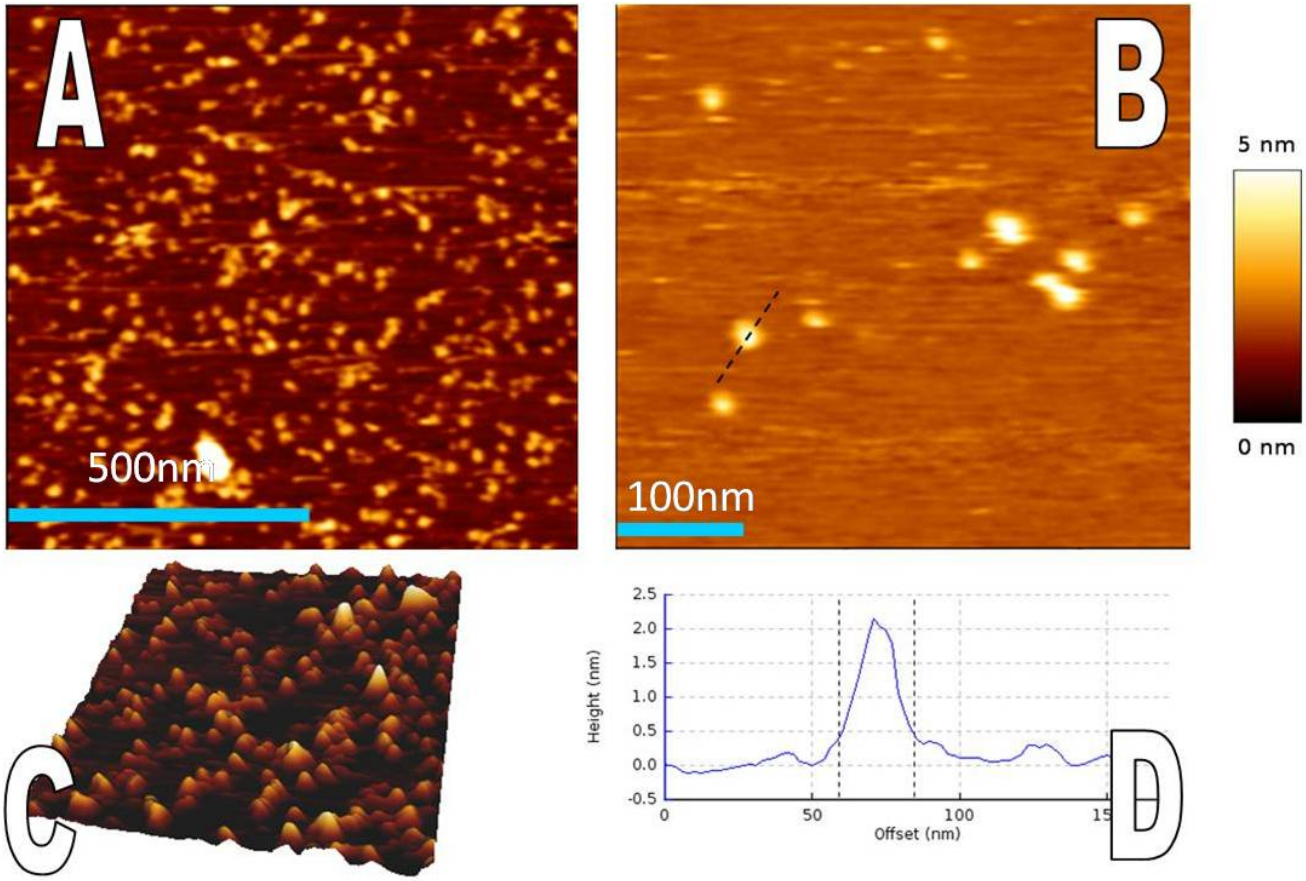


***Figure 36B: AFM images of FliG proteins on mica surface.*** *contact mode in PBS buffer, OBL probe cantilever stiffness 5mN/m. A/ Large view of FliG proteins aggregate. B/ Enlarged view of aggregates. C/ 3D view of part of A. D/ cross section of a single aggregate.*

We clearly observe the presence of a homogenous distribution of protein-aggregates on the surface, which address the question of the possible direct self-assembly of the FliG in the buffer. We measured the surface and diameter of these aggregates (method is presented in annex 4) and the obtained distribution is presented in figure 37.

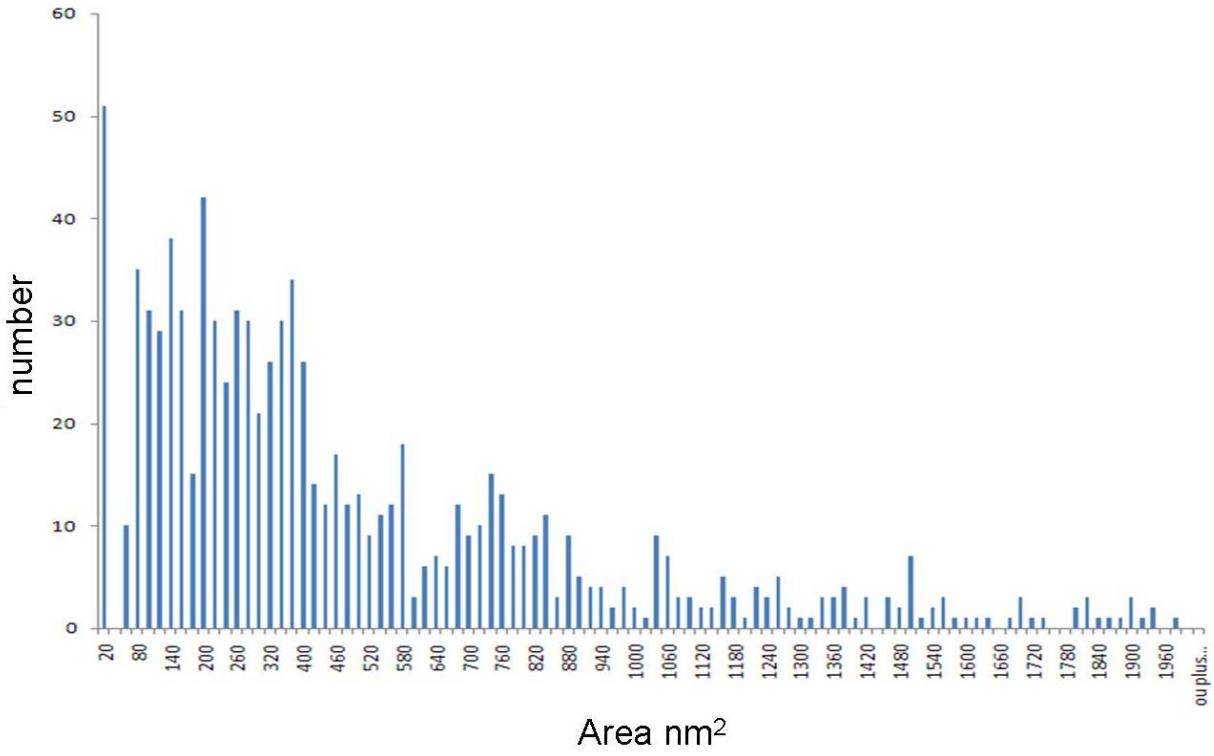


***Figure 37: Size distribution of the measured FliG aggregates on the mica surface***

It turned out quite clearly that we are in presence of only two families of protein aggregates, with an average of 22 to 24 nm for the first one, which represents 70 % of all imaged aggregates, and 30 nm for the second family. In order to visualize the inner aggregate organization, we tried to improve the resolution on a single aggregate without success. We suspected that the role played by the deformation of the aggregate could be detrimental for the protein observation and reduced our chance of observing nano-organization and symmetry within a single aggregate. This measure of FliG proteins aggregate was done for the first time by AFM imaging in liquid and present a unique result never demonstrated before. The height of the observed aggregates was more difficult to interpret due to the difference between tapping (average of 6 nm) and contact mode (2,5nm). Based on the possible spatial arrangement of FliG within the motor, the value obtained in tapping is not compatible with the motor structure. This point will be discussed later.

### ii. Other motor proteins

Despite my effort, imaging of the other motor proteins did not give significant results on mica, for different reasons. Probe contamination by the proteins was the primary reason, which reduced the time life of a tip in solution, and also the validity of the obtained images. AFM in liquid is also known for generating numerous artifacts and none of the results obtained with the other motor proteins could be validated. Further studies should be done on this point, by reducing the probe contamination through chemical treatment with anti-fouling molecules.

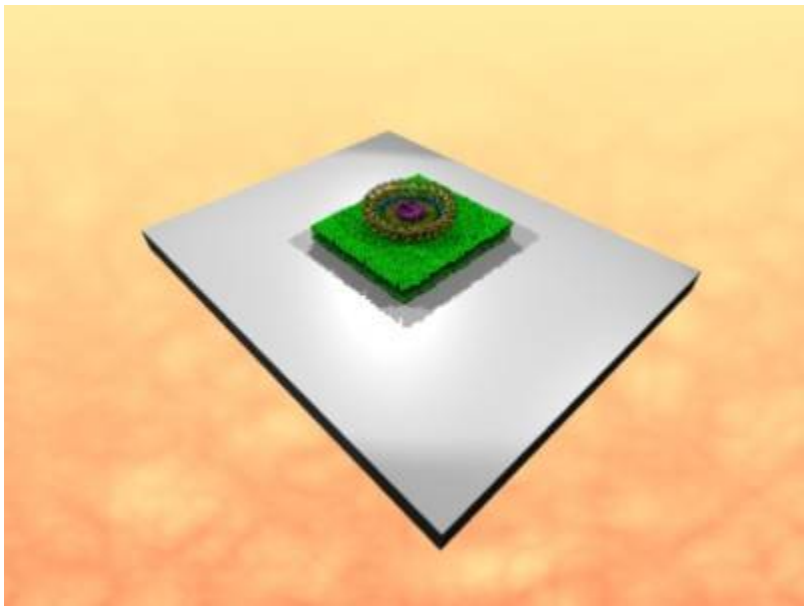

***Figure 38: Schematic view of proteins on the SPBM***

## b. Motor proteins on SPBM membrane

Based on the results obtained on the mica surface, we incubated the FliF-GST and the pure FliG proteins on SPBM (see figure 38) and also on P-SPBM. The interactions between the motor proteins and the SPBM have been demonstrated before by the QCM-D study, but the direct observation for addressing structural questions remained our primary objective. We incubated directly the FliF-GST on PE-PG patches, and FliG on both patches of PE-PG and also P-SPBM.

## i. FliF-GST on PE-PG patches

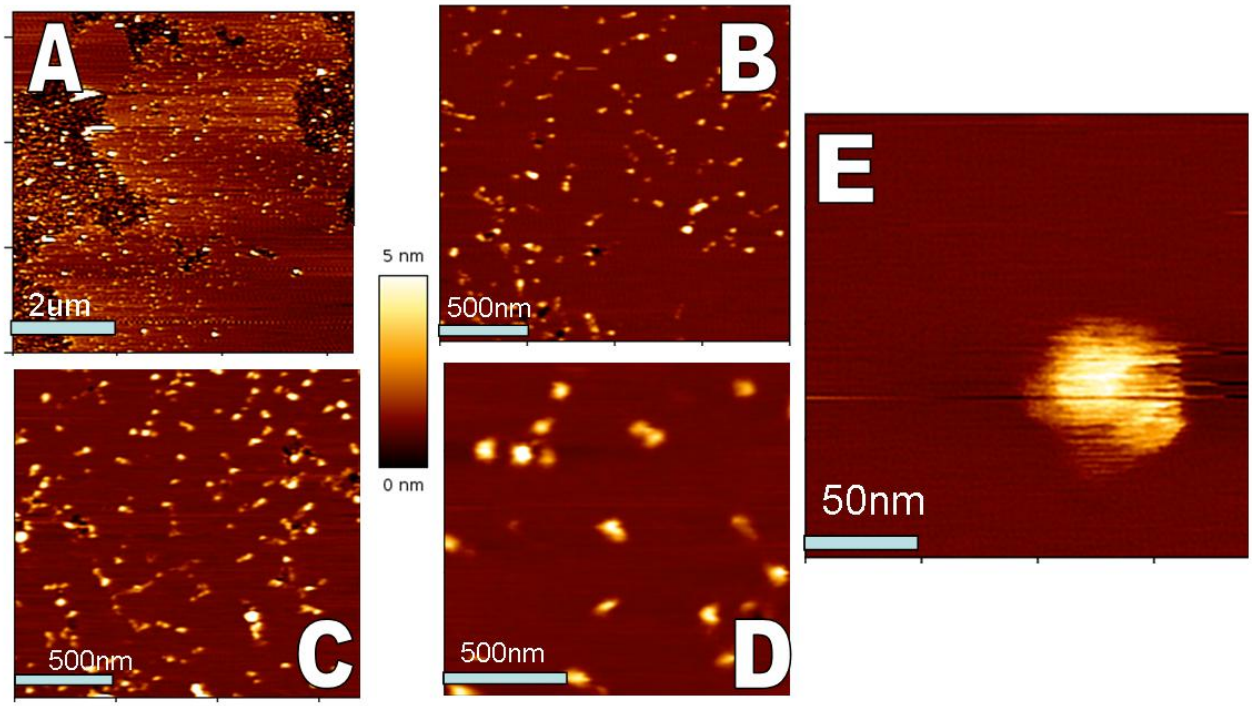


***Figure 39: AFM images of FliF-Gst proteins on PE-PG SPBM.*** *Contact mode in PBS buffer, cantilever stiffness 5mN/m. force below 50pN. A/ Large view of a SPBM exhibiting proteins aggregates on its surface. B-C-D/ Enlarged view of A. E/ Zoom in a single protein aggregate.*

Figure 39 displays AFM images obtained after 2 hours of incubation of FliF-GST on PE-PG SPBM. Numerous spots are clearly visible on the SPBM surface and the size distribution of these aggregates was similar as the one obtained on mica surface but images were more easily accessible. This observation confirmed the strong affinity of the FliF proteins with the PE-PG SPBM. However, the size of the aggregates as seen by AFM should be considered carefully due to the GST tag presence on the N-terminus of the proteins, which probably enlarge the aggregate size. Despite these images, we do not answer the question if the FliF, which is a trans-membrane protein, passed through the PEPG-SPBM. We increased the applied force on the surface for removing only the protein. If a hole then appears, this would indicate that the protein goes through the membrane, while if nothing is seen, this would indicate that the proteins remained on the

top side of the SPBM. Despite our effort, the probe contamination erased our chance to picture the same area after the pick up which let this question opened.

### ii. FliG on PE-PG patches

Same approach was applied for FliG proteins with a clear difference. Based on established data, in any hypothetical position, FliG is found at the interface between the Phospholipids inner membrane and the cytoplasm. By incubating the proteins on the surface, AFM imaging gave us a clear result presented in figure 40.

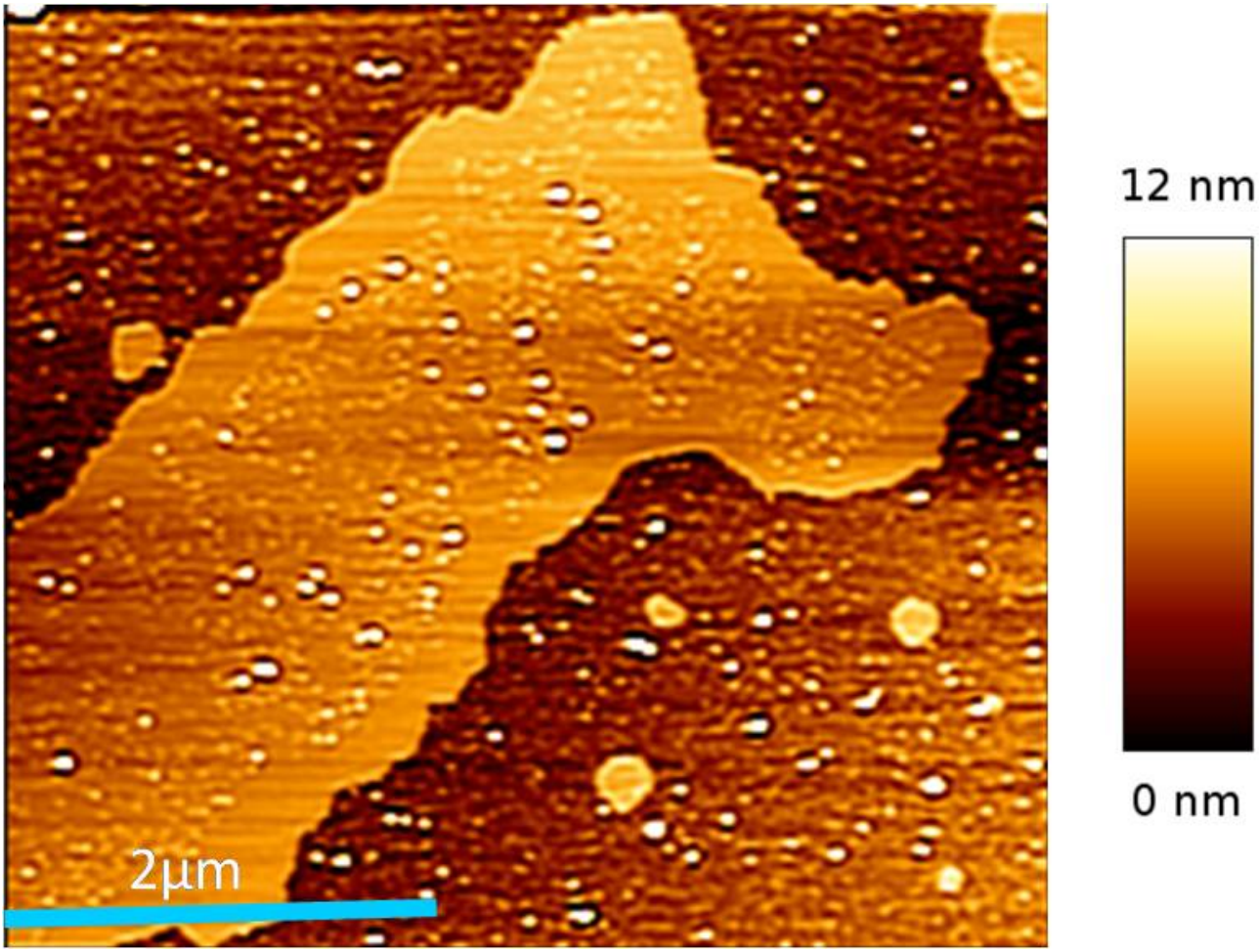


***Figure 40: AFM image of PE-PG SPBM with FliG proteins****. Contact mode in PBS buffer, OBL cantilever with a stiffness of 5mN/m. Force below 50pN. Height signal.*

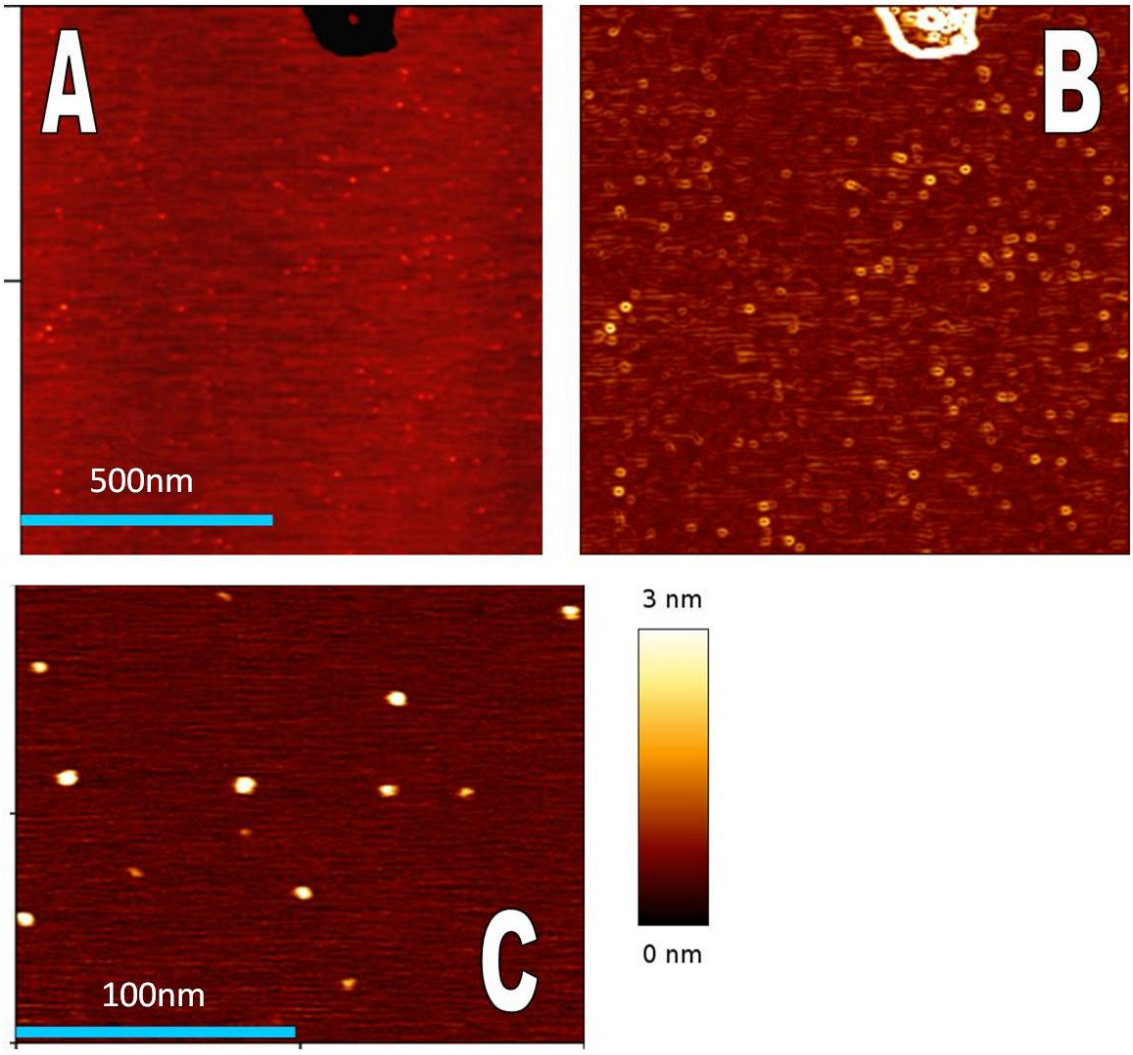


***Figure 41: AFM Zoom image on the PE-PG SPBM surface presenting proteins aggregates.*** *Contact mode in PBS buffer, cantilever stiffness 5mN/m, force below 50pN. A/ Height image of a large view. B/ Vertical deflection of A. C/Zoom in independent aggregates.*

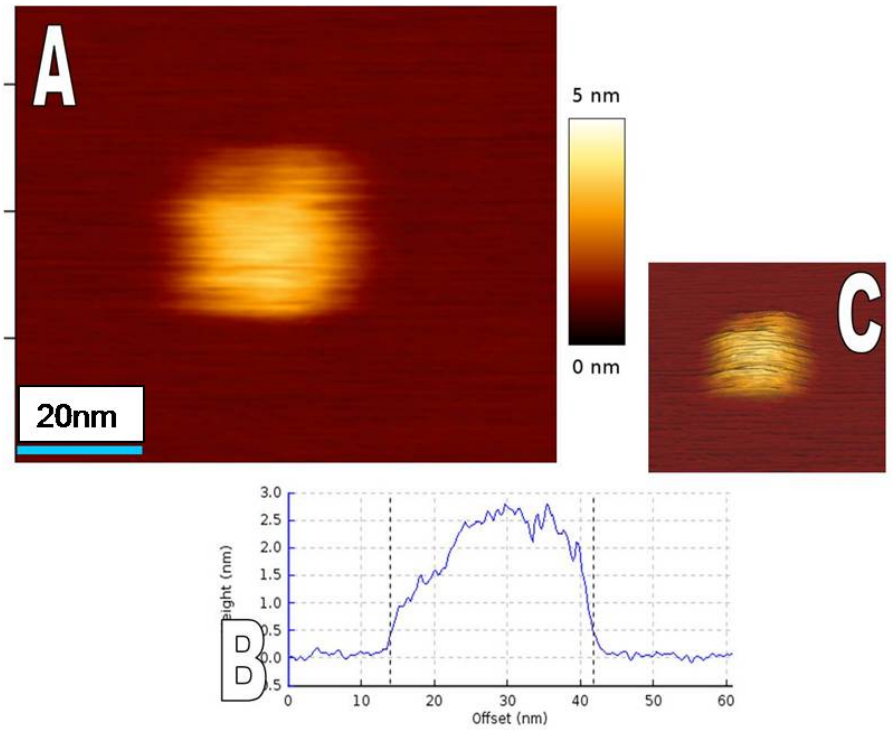


***Figure 42: AFM image of a single FliG aggregate.*** *Contact mode in PBS buffer, OBL cantilever 5mN/m, force below 50nN. A/ Height signal. B/ Cross section of A. C/ 3D view of A.*

Compared to the SPBM without proteins, the presence of aggregate confirmed us the interactions observed using QCM-D between FliG and PE-PG SPBM. Numerous aggregates were found, principally at the edge of SPBM patches. The presence of large amounts of protein aggregates at the edges of the membrane remains an open question, but this result was repeatedly obtained on different samples with different batches of proteins. By using the same method for measuring the aggregate size, we obtained a size distribution similar to the one obtained on the mica surface.

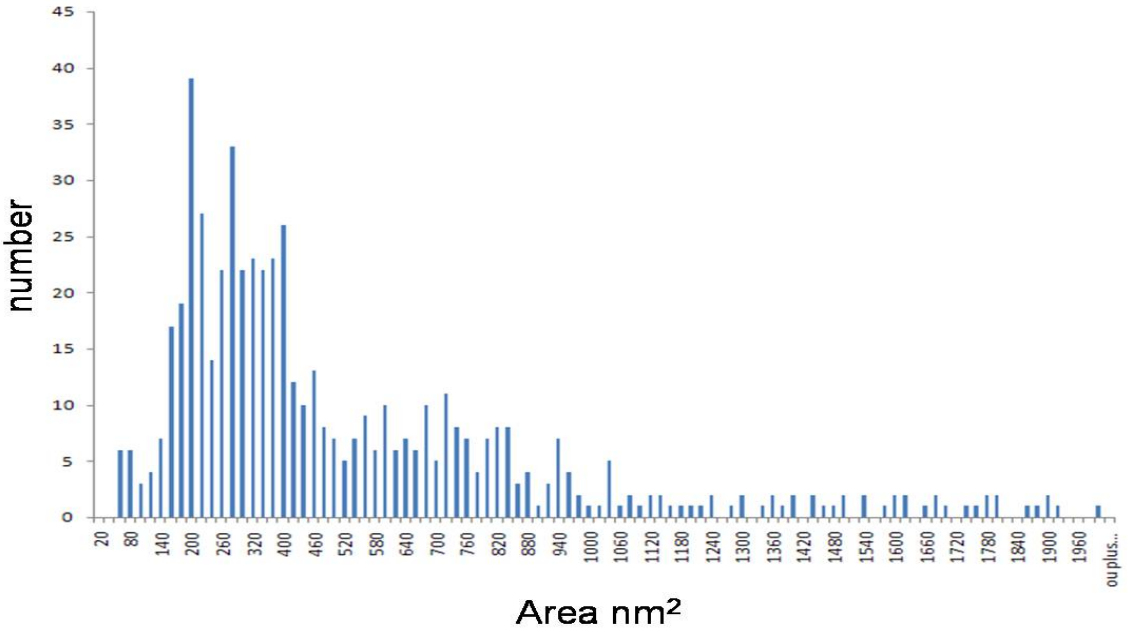


***Figure 43: Size distribution of the measured FliG aggregates on the PE-PG SPBM.***

This result constitutes for the first time a direct observation in liquid in vitro of a pure motor proteins assembly. The average diameter was in a good accordance with the one found after imaging on mica, with 80% of the observed aggregate found between 18 and 22 nm, and 15% between 28 and 33 nm. This distribution highlights the size and shape of FliG aggregate on a PE-PG SPBM and could be considered similar to the one observed in bacteria. Several buffers were tried: PBS, Hepes 1 and Hepes 2 compatible with the SPBM structure and same result were found. The thickness also was measured for the first time and gave an average of 2,5 nm, however thickness of single aggregate should be handled with precautious due to the role of sample-probe interaction.

### iii. FliG on PE-PG P-SPBM

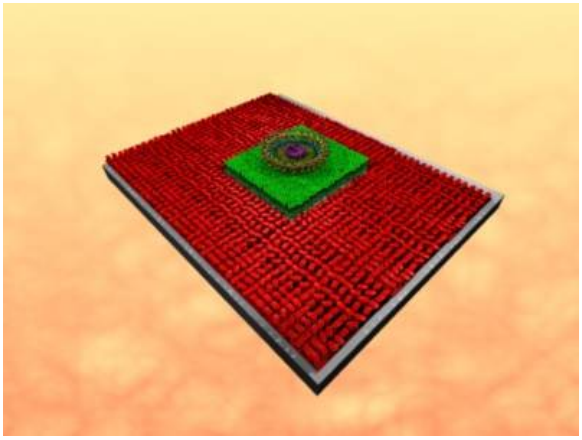

***Figure 44: Schematic view of the final assembly, proteins on a PE-PG P-SPBM.***

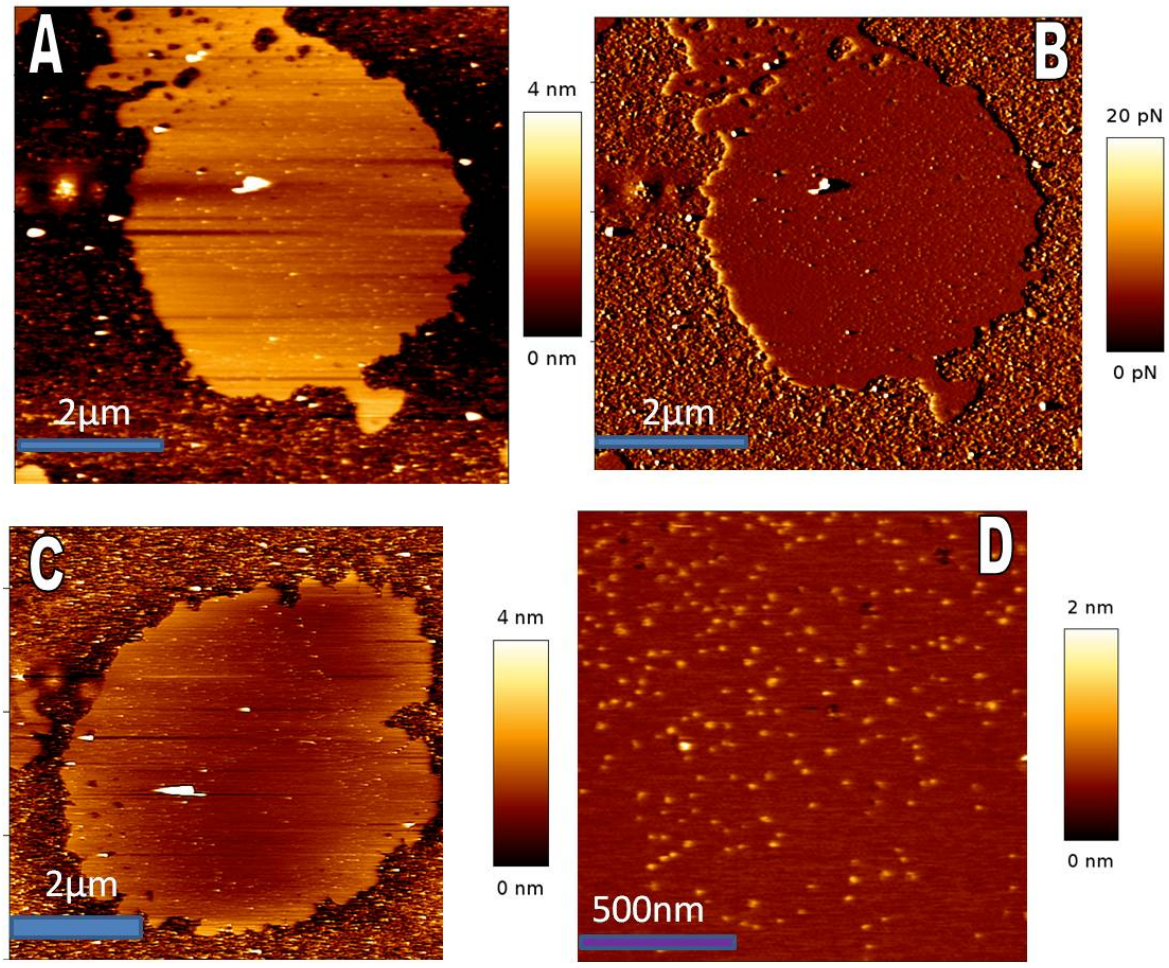


***Figure 45: PE-PG P-SPBM exhibiting FliG aggregates****. Contact mode, OBL cantilever stiffness 5mN/m, force below 50 pN. A/ Height signal of 4 µm patch of PE-PG P-SPMB with proteins aggregates. B/ Vertical signal of A. C/ Height signal Other pattern. D/ Height signal of an enlarged view of FliG aggregates on C.*

Despite the result obtained above, the major limitation was the number of patterns which exhibited aggregates. For an unknown reason, not all the SPBM patches presented large amount of proteins. By increasing the protein concentration, we increased the number of patches showing aggregates, but we increased at the same time the amount of proteins adsorbed directly on the mica surface, which could be detrimental for AFM imaging. In order to address this critical issue, the role played by the P-SPBM is essential. It resolved several points: it reduced the possible area of interest for the incubated proteins, due to the presence on a large part of the sample of anti-fouling molecules, the Pll-g-PEG, and "forced" them to interact only with the P-SPBM. It also allowed me to image directly a specific area of the sample instead of a random research of possible SPBM patches with proteins. Due to the slow rate of AFM imaging, these two points were essential. Figure 45 displayed P-SPBM with proteins.

### iv. Discussion

AFM in liquid can give high resolution images of protein assembly, or 2D crystal of proteins. However, the role played by the AFM probe must be considered. The tip convolution effect could drastically alter the size of the object imaged using AFM [24; 31], however its influence is far from being established, especially on a single object at the nano-scale. In order to address this essential question and confirm the size distribution of the measured aggregates, I imaged the same sample using numerous AFM probes, exhibiting different probe radii, from 10 to 15 nm for the MSCT and OTR4 model, to 20 nm for the biolever model. Same images were obtained with all these probes. It has been demonstrated that for sample of proteins, for example ATP synthase[127], or LH1-LH2[126], size and shape of the object measured were similar to those obtained with non invasive methods which suggested that for these samples, tip broadening effect does not apply. Most likely, we think that it was also the case for our sample. We thus consider that the histogram of FliG aggregates obtained by AFM imaging is representative of the real size of the M-ring. The most frequent diameter of FliG aggregate is peaked at a value of 20 nm.

## F) Conclusions

Based on the three FliG hypothetical positions inside the BFNM (see figure 34) , we summarize our results as follows: i/ The first position is mainly supported by a large amount (80%) of aggregates exhibiting a diameter between 18 and 22 nm, ii/ The second position could be represented by the second population of aggregates (15%), with a diameter ranging from 27 to 32 nm. It is however worth noticing that we have not been able to observe a hole or a depression at the center of the aggregate, iii/ The third position cannot be supported by our results since no significant amount of aggregates was observed having a diameter between 40 and 45 nm. Same area distributions were found on mica and SPBM and also on P-SPBM. This observation let us think that the protein aggregates were identical on these surfaces. Previous studies on purified FliG clusters show that FliG rings are stable under different analysis conditions and their size or shape are not disturbed by sample preparations. However, large clusters of proteins of hundred of nanometers were found on the mica, which could result of proteins aggregation during the production and purification. These clusters appear sometimes on SPBM, but in a very low number and are not stable under AFM imaging. We found that 80% of the FliG aggregates were circular and exhibited an average diameter of 20nm, on both mica surface and also on a SPBM mimetic of *E.Coli* inner membrane. This result let us think that the FliG protein assembly could fit in the first position, in the inner side of the rotor. The aggregates observed were relatively stable under AFM scanning. This was not a surprise since due to their crucial role in the motor function, the spatial arrangement of the FliG ring should remain firmly assembled while the motor is in function. The second observation was crucial because it was the first time, to our knowledge, that a motor protein has been observed in an environment reproducing quite well native conditions. As proposed by Blair *et al*, FliG is divided into 3 parts already crystallized[124; 133]. They proposed recently that the FliG middle part, FliGm and FliG C-termini FliGc could be separated by a distance close to 3 nm, which would create a ring larger supporting the two last position hypothesis. We indeed observed in our area distribution a second population of aggregates between 540 to 820 $nm^2$ which could correspond to the second hypothesis. This population was relatively low compared to the first dominant one 1:4 but more important, this assembly mainly depends of the FliG-FliM interaction. This type of

assembly also should present a hole in its center and despite our effort for imaging it, the aggregates turned out to exhibit no noticeable depression in their center. We searched for aggregates presenting a diameter of 40 nm or more, and the few observed (less than 2% of all aggregates) were not stable under AFM imaging and rapidly damaged.

Based on these observations, the possible emplacement of the FliG ring on the top side of the C-ring (figure 34) cannot be supported. We based this conclusion on the fact that the FliG protein aggregates presented here were in an environment close to the native one. Results obtained with Cryo-TEM have not supported a full emplacement of the FliG within the C ring, but more at the interface between the M and the C-ring (position 2). According to our AFM observations, positions 1 and 2 could be possible, but our data did not present the second position as preferential. Indeed, only 15 % of the aggregates measured were in the range corresponding to this spatial arrangement. However, the shape and size of the FliG assembly could change due to the presence of others proteins, especially FliF. Despite our effort for purifying FliF, we have not been able to design experiements with FliF and FliG together which could address this point. Futher experiments are needed to confirm that the FliG ring diameter remains identical when mixed with other proteins. However, I think that the presence of the depression in the middle of the FliG ring could come from the assembly with the FliF and would enlarged the FliG ring by a few nanometers. 26 FliG should be involved in the assembly and the observation or not of a small depression at the center of the assembly could help us in discriminating better hypothesis 1 and 2. This possible FliF-FliG assembly could correspond to the diameter of the second family observed here, with an average diameter of 25 to 30 nm instead of 20 to 25 nm. FliG could already and by themselves be assembled in a spatial configuration which could be ready for assembly with the FliF. The second point concerned the role of the phospholipids membrane. We think that the role of the membrane is crucial for a good assembly of the flagellum elements and the possible interaction between FliG and the inner bacteria membrane is under study. The third hypothesis for the FliG spatial arrangement is currently based on the interaction site between FliM and FliG proteins, but to our knowledge no spatial arrangement based only on the full crystal structures have been proposed yet.

We concluded that AFM in liquid medium can bring new results to the community for elucidating the structure and mechanisms of the flagellar nano-motor of bacteria. We observed the spontaneous formation of aggregates of FliG proteins incubated after purification on mica surfaces and supported E-Coli bilayer membranes. The careful analysis of the sizes of these aggregates indicates that the average diameter is around 20 nm. Previous investigation carried out on the FliF protein with AFM, has not given relevant results due to the relative low definition of the observed aggregates, but our results confirmed the larger size of the FliF aggregates; however the difficulty to purify the FliF using our approach has diminished the viability of results. On the other hand, our results on FliG on a SPBM let us think that we are in presence of the so called M-ring of the motor in its native environment reproduced in vitro. The recorded average dimension of the FliG aggregates permited us to exclude its location inside the C-ring. Two proposed positions remain compatible with our study (in the rotor or at the interface between the rotor and the C-ring). Our data were in better accordance with a position inside the rotor but new experiments at higher resolution are necessary for being completely affirmative. This new approach brought new information about the 3D assembly in liquid of two motor proteins, but the same methodology can be employed with others proteins involved in the motor until larger pieces of this nano-machine could be assembled on engineered surfaces.

## G) Perspectives

As described above, this result on FliG proteins opened the way for extensive study of the BFNM, but also other nano-bio-machine present in cells. By mixing the top-down for engineering a surface and the bottom up for self-assembly a SPBM and then the protein machinery, we could recreate artificially complex system in vitro, and avoid the problem for observing them at work in vivo. For the BFNM, primary results on the mix of FliG FliM and FliN gave interesting images (see chapter 4) but this result should be further confirmed on more samples. The observation of a ring at the dimension observed using cryo-TEM composed of 3 proteins: the FliG FliM and FliN would be a second major step for studying the BFNM in vitro. It would also tackle the possible role played

by the tip convolution in imaging the motor proteins in vitro. But again, this result should be confirmed by additional images.

Through this study, numerous points can be discussed, starting by the SPBM PE-PG formation to the role played by the buffer in imaging the protein structure. The first limiting point, despite my effort, is the coalescence of the PE-PG liposomes. As described above, the average diameter tended to increase relatively fast and after 20 minutes, liposome aggregates can be seen by eyes. It was detrimental for the fusion process and also for the AFM imaging. I tried to change the ratio between PE-PG, and also try to use E.Coli full extract (charged and non charged) but none of these attempts have resolved that problem. The buffer, based on $CaCl_2$ has been used by Domenech *et al* [72] and served as a basis for my work, but I think that new buffer should be tested. This coalescence effect was also quite surprising, due to the role played by this lipid mixture into the E.Coli structure, as the inner membrane. By trying to mimic the inner bacteria buffer, this effect could be diminished. Further work is needed on that point.

The second aspect of my work, the creation and use of P-SPBM has been largely based on the EggPC mixture for which the best results have been obtained. The patterning method used, the Micro Contact printing, promised a very interesting way to study lipid behavior and also protein assembly, as described here, however several questions needed to be addressed. The primary purpose for the creating P-SPBM was to reduce the proteins diffusion on the surface for allowing AFM imaging. Despite our evaluation of the SPBM diffusion rate (in order of 1.5µm/s), the proteins observed using AFM did not diffuse at that speed, but more in the order of nanometer/minute. This observation is very interesting but further studies using fluorescence tagged motor proteins could address this point quantitatively. The impact of the formation of P-SPBM was important on my work, due to the easy way to find an interesting area, by coupling fluorescence microscopy to AFM imaging. It decreased the time spent for searching where the SPBM are and where proteins are assembled. This point is a major advance for AFM imaging, and alleviates partially the slow scanning rate problem. However, in order to increase the benefit of this technique, the choice of the anti-fouling molecule is primordial. Pll-g-PEG molecules have proven their efficiency for both proteins and lipid mixture, and presented advantages compared to the BSA coating, however, the

electrostatic interactions limited the stability of the Pll-g-PEG layer. For example, changing the pH or the ion charges altered the layer thickness and stability for AFM imaging. Other molecules, probably PEG-silane could be further used in order to create a covalent layer of molecules instead of electrostatic bonding. Nevertheless, I deeply trusted that the P-SPBM technique will be widely used for studying the phospholipids diffusion and also proteins into defined area.

A major limit of this approach concerns the study of trans-membrane proteins. The insertion of trans-membrane proteins into a pre-formed SPBM has been a major issue in numerous studies [28]. Two ways emerged during the last few years: the use of native membrane [31; 126; 127] or the insertion of purified proteins into SPBM [134; 135]. Both of them presented advantaged and default, but none of them have been considered as perfect. The use of native membrane needs an extensive and sometimes complex extraction protocol from the cell, and the insertion way require to first purify membrane proteins, which could be challenging, and then inserting them using chemical detergent in SPBM. By working on purified motor proteins, our approach could be similar to the second one, but the use of detergent could damage the engineered surface. Another way would consist in building proteo-liposome, instead of inserting proteins directly on the SPBM. But same limitation as the use of chemical detergent is encountered and the fusion of those structures on a surface is far from being straightforward [136; 137].

For working on the stator part of the BFNM, we will meet those problems. A new approach is needed and one possible way would be the cell free expression system [138]. Through the last decade, numerous studies have shown that the expression system of E.Coli for example, can be extracted and encapsulated into a liposome. These systems can express a various range of proteins, from the GFP to more recently the α-hemolysin. These systems present the advantage to directly produce purified proteins, which eliminates the in vitro purification step which is problematic for membrane proteins. The major limit remains for the moment the direct insertion of the produced proteins into the liposome bilayer, but when this problem will be solved, it could represent a new way to study the motor assembly directly on a liposome, or on a SPBM generated from these liposomes.

[1]S.M. Block, H.C. Berg, MicroBiology 309 (1984) 470.
[2]B.H. Blair DF, Science 242 (1988) 1678.
[3]V. Sourjik, H.C. Berg, Proceedings of the National Academy of Sciences of the United States of America 99 (2002) 123.
[4]V. Sourjik, H.C. Berg, Proceedings of the National Academy of Sciences of the United States of America 99 (2002) 12669.
[5]H. Fukuoka, Y. Sowa, S. Kojima, A. Ishijima, M. Homma, Journal of Molecular Biology 367 (2007) 692.
[6]M.C. Leake, J.H. Chandler, G.H. Wadhams, F. Bai, R.M. Berry, J.P. Armitage, Nature 443 (2006) 355.
[7]M.L. DePamphilis, J. Adler, J. Bacteriol. 105 (1971) 376.
[8]G. Sosinsky, N. Francis, D. DeRosier, J. Wall, M. Simon, J. Hainfeld, Proceedings of the National Academy of Sciences 89 (1992) 4801.
[9]G.E. Sosinsky, N.R. Francis, M.J.B. Stallmeyer, D.J. DeRosier, Journal of Molecular Biology 223 (1992) 171.
[10]N.R. Francis, G.E. Sosinsky, D. Thomas, D.J. DeRosier, Journal of Molecular Biology 235 (1994) 1261.
[11]D.R. Thomas, D.G. Morgan, D.J. DeRosier, Proceedings of the National Academy of Sciences 96 (1999) 10134.
[12]D. Thomas, D.G. Morgan, D.J. DeRosier, J. Bacteriol. 183 (2001) 6404.
[13]D.R. Thomas, N.R. Francis, C. Xu, D.J. DeRosier, J. Bacteriol. 188 (2006) 7039.
[14]H. Suzuki, K. Yonekura, K. Namba, Journal of Molecular Biology 337 (2004) 105.
[15]K. Yonekura, T. Yakushi, T. Atsumi, S. Maki-Yonekura, M. Homma, K. Namba, Journal of Molecular Biology 357 (2006) 73.
[16]R.L. Joseph, R.M. Barry, Journal of Biomedical Optics 13 (2008) 029901.
[17]D. Zhang, P. Wadsworth, P.K. Hepler, Proceedings of the National Academy of Sciences of the United States of America 87 (1990) 8820.
[18]M.M. McEvoy, A. Bren, M. Eisenbach, F.W. Dahlquist, Journal of Molecular Biology 289 (1999) 1423.
[19]S. Khan, D. Pierce, R.D. Vale, Current Biology 10 (2000) 927.
[20]L. Turner, W.S. Ryu, H.C. Berg, J. Bacteriol. 182 (2000) 2793.
[21]F. T, Naturwissenschaften 6 (1946) 166.
[22]A. Hillisch, M. Lorenz, S. Diekmann, Current Opinion in Structural Biology 11 (2001) 201.
[23]G. Binnig, H. Rohrer, C. Gerber, E. Weibel, Phys. Rev. Lett. 56 (1986) 930.
[24]A. Engel, C.-A. Schoenenberger, D.J. Müller, Current Opinion in Structural Biology 7 (1997) 279.
[25]Z. Shao, J. Yang, Quarterly Reviews of Biophysics 28 (1995) 195 251.
[26]B. Bhushan.
[27]D.M.-H.W. Dr. Sergei N. Magonov, Frontmatter, Surface Analysis with STM and AFM, 2007, pp. I.
[28]G. Kada, F. Kienberger, P. Hinterdorfer, Nano Today 3 (2008) 12.
[29]F.J. Giessibl, Japanese journal of applied physics 33 (1994) 3726.
[30]Y. Lyubchenko, L. Shlyakhtenko, R. Harrington, P. Oden, S. Lindsay, Proceedings of the National Academy of Sciences of the United States of America 90 (1993) 2137.

[31]A. Engel, D.J. Müller, Nature Structural Biology 7 (2000 ) 715
[32]J.K.H. Horber, M.J. Miles, Science 302 (2003) 1002.
[33]B.Bhushan, H.Fuchs, S.Hosaka, Springer Verlag (2006) 143.
[34]R.V. Lapshin, Nanotechnology 15 (2004) 1135.
[35]R.V. Lapshin, Meas. Sci. Technol 18 (2007) 907.
[36]V.L. Rostislav, Review of Scientific Instruments 69 (1998) 3268.
[37]A.D.L. Humphris, M.J. Miles, J.K. Hobbs, Applied Physics Letters 86 (2005) 034106.
[38]T. Ando, N. Kodera, D. Maruyama, E. Takai, K. Saito, A. Toda, Jpn. J. Appl. Phys (2002) 4851.
[39]T. Ando, N. Kodera, E. Takai, D. Maruyama, K. Saito, A. Toda, Proceedings of the National Academy of Sciences of the United States of America 98 (2001) 12468.
[40]T. Ando, T. Uchihashi, N. Kodera, D. Yamamoto, A. Miyagi, M. Taniguchi, H. Yamashita, Pflügers Archiv European Journal of Physiology 456 (2008) 211.
[41]R.V. Lapshin, Review of Scientific Instruments (1995).
[42]M.H. VAN CLEEF, S. A.; WATSON, G. S.; MYHRA, S., Journal of Microscopy 81 (1996) 2.
[43]W.R. Bowen, T.A. Doneva, Journal of Membrane Science 171 (2000) 141.
[44]Y.F. Dufrene, J. Bacteriol. 184 (2002) 5205.
[45]A. Ebner, P. Hinterdorfer, H.J. Gruber, Ultramicroscopy 107 (2007) 922.
[46]J. Preiner, H. Janovjak, C. Rankl, H. Knaus, D.A. Cisneros, A. Kedrov, F. Kienberger, D.J. Muller, P. Hinterdorfer, Biophysical Journal 93 (2007) 930.
[47]B. Bonanni, A.S.M. Kamruzzahan, A.R. Bizzarri, C. Rankl, H.J. Gruber, P. Hinterdorfer, S. Cannistraro, Biophysical Journal 89 (2005) 2783.
[48]R. Kassies, K.O.V.d. Werf., A. Lenferink, C.N. Hunter, J.D. Olsen, V.Subrmaniam, C. Otto, Journal of Microscopy 217 (2005) 109.
[49]Enrico Defranchi, Microscopy Research and Technique 67 (2005) 27.
[50]J.A. Dvorak, Methods 29 (2003) 86.
[51] Alexander Gaiduk, ChemPhysChem 6 (2005) 976.
[52]K. Kurihara, M. Mizukami, K. Suzuki, K. Oosawa, Colloids and Surfaces A: Physicochemical and Engineering Aspects 109 (1996) 375.
[53]E. Gorter, F. Grendel, J. Exp. Med. 41 (1925) 439.
[54]D.B. Alec, A.D Bergham BioEssays 17 (1995) 1081.
[55]S.J. Singer, G.L. Nicolson, Science 175 (1972) 720.
[56]K. Jacobson, E.D. Sheets, R. Simson, Science 268 (1995) 1441.
[57]J.N. Israelachvili, Biochimica et Biophysica Acta (BBA) - Biomembranes 469 (1977) 221.
[58]A. Wieniewska, J.Draus, .K Subczynski, Cellular&Molecular Biology Letters 8 (2003) 147
[59]D.M. Engelman, Nature 438 (2005) 578.
[60]J.L. Thewalt, M. Bloom, Biophysical Journal 63 (1992) 1176.
[61]T.P.W. McMullen, R.N.A.H. Lewis, R.N. McElhaney, Current Opinion in Colloid & Interface Science 8 (2004) 459.
[62]K. Simons, D. Toomre, Nat Rev Mol Cell Biol 1 (2000) 31.
[63]D.A. Brown, E. London, Annual Review of Cell and Developmental Biology 14 (1998) 111.

[64]S. Moffett, D.A. Brown, M.E. Linder, J. Biol. Chem. 275 (2000) 2191.
[65]L.K. Tamm, H.M. McConnell, Biophysical Journal 47 (1985) 105.
[66]E. Sackmann, Science 271 (1996) 43.
[67]E. Kalb, S. Frey, L.K. Tamm, Biochimica et Biophysica Acta (BBA) - Biomembranes 1103 (1992) 307.
[68]H. Schonherr, J.M. Johnson, P. Lenz, C.W. Frank, S.G. Boxer, Langmuir 20 (2004) 11600.
[69]T.H. Watts, A.A. Brian, J.W. Kappler, P. Marrack, H.M. McConnell, Proceedings of the National Academy of Sciences of the United States of America 81 (1984) 7564.
[70]H.M. McConnell, T.H. Watts, R.M. Weis, A.A. Brian, Biochimica et Biophysica Acta (BBA) - Reviews on Biomembranes 864 (1986) 95.
[71]T.H. Watts, H.E. Gaub, H.M. McConnell, Nature 320 (1986) 179.
[72]Ò. Doménech, S. Merino-Montero, M.T. Montero, J. Hernández-Borrell, Colloids and Surfaces B: Biointerfaces 47 (2006) 102.
[73]R. Richter, A. Mukhopadhyay, A. Brisson, Biophys. J. 85 (2003) 3035.
[74]C.A. Keller, B. Kasemo, Biophysical Journal 75 (1998) 1397.
[75]C.A. Keller, K. Glasmästar, V.P. Zhdanov, B. Kasemo, Phys. Rev. Lett. 84 (2000) 5443
[76]E. Reimhult, M. Zach, F. Hook, B. Kasemo, Langmuir 22 (2006) 3313.
[77]P.G. Saffman, M. DelbrÃ¼ck, Proceedings of the National Academy of Sciences of the United States of America 72 (1975) 3111.
[78]E.A.J. Reits, J.J. Neefjes, Nat Cell Biol 3 (2001) E145.
[79]P. Eggl, D. Pink, B. Quinn, H. Ringsdorf, E. Sackmann, Macromolecules 23 (1990) 3472.
[80]L. Zhang, S. Granick, Proceedings of the National Academy of Sciences of the United States of America 102 (2005) 9118.
[81]Y. Gambin, R. Lopez-Esparza, M. Reffay, E. Sierecki, N.S. Gov, M. Genest, R.S. Hodges, W. Urbach, Proceedings of the National Academy of Sciences of the United States of America 103 (2006) 2098.
[82]S. Singh, D.J. Keller, Biophysical Journal 60 (1991) 1401.
[83]P.E. Milhiet, M.C. Giocondi, C. Le Grimellec, The scientific world 3 (2003) 59.
[84]M.C.G. P. E. Milhiet, and C. Le Grimellec, The Scientific world 3 (2003) 59.
[85]G.E. Moore, electronics 38 (1965) 114.
[86]http://cmgm.stanford.edu/pbrown/index.html.
[87]D.Saya, T. Leichle, J.B.Pourciel, C.Bergaud, L.Nicu, J. Micromech. Microeng. 17 (2007).
[88]T. Leichle, D.Saya, P.Belaubre, J.B.Pourciel, F.Mathieu, J.P. Laur, L. Nicu, C.Bergaud, Sensors and Actuators A 132 (2006) 590.
[89]G. Subramanian, V.N. Manoharan, J.D. Thorne, D.J. Pine, Advances Materials 11 (1999) 1261.
[90]T. Kraus, L. Malaquin, E. Delamarche, H.Schmit, N.D.Spencer, H. Wolf, Advances Materials 17 (2005) 2438.
[91]J.Guan, L.J. Lee, PNAS 102 (2005) 18321.
[92]I.Langmuir, K. Blodgett, U.S. patent 2,220,860
[93]P.W.K. Rothemund, Nature 440 (2006).

[94]A. Cerf, J.-C. Cau, C. Vieu, Colloids and Surfaces B: Biointerfaces 65 (2008) 285.
[95]J.S. Hovis, S.G. Boxer, Langmuir 16 (2000) 894.
[96]J.S. Hovis, S.G. Boxer, Langmuir 17 (2001) 3400.
[97]R.N. Orth, J. Kameoka, W.R. Zipfel, B. Ilic, W.W. Webb, T.G. Clark, H.G. Craighead, Biophys. J. 85 (2003) 3066.
[98]P. Lenz, C.M. Ajo-Franklin, S.G. Boxer, Langmuir 20 (2004) 11092.
[99]B.L. Jackson, J.T. Groves, Langmuir 23 (2007) 2052.
[100]K. Pilnam, b. Sang Eun Lee, b. Ho Sup Jung, b. Hea Yeon Lee, T. Kawaib, K.Y. Suh*a, Lab on a chip **6** (2005) 54
[101]B. Sweryda-Krawiec, H. Devaraj, G. Jacob, J.J. Hickman, Langmuir 20 (2004) 2054.
[102]G.L. Kenausis, J. Voros, D.L. Elbert, N. Huang, R. Hofer, L. Ruiz-Taylor, M. Textor, J.A. Hubbell, N.D. Spencer, J. Phys. Chem. B 104 (2000) 3298.
[103]N.-P. Huang, R. Michel, J. Voros, M. Textor, R. Hofer, A. Rossi, D.L. Elbert, J.A. Hubbell, N.D. Spencer, Langmuir 17 (2001) 489.
[104]F.F. Rossetti, I. Reviakine, G. Csucs, F. Assi, J. Voros, M. Textor, Biophys. J. 87 (2004) 1711.
[105]M. Heuberger, T. Drobek, N.D. Spencer, Biophys. J. 88 (2005) 495.
[106]V. Saravia, S. Kupcu, M. Nolte, C. Huber, D. Pum, A. Fery, U.B. Sleytr, J.L. Toca-Herrera, Journal of Biotechnology 130 (2007) 247.
[107]S. Lee, N.D. Spencer, Langmuir 24 (2008) 9479.
[108]N.-P. Huang, J. Voros, S.M. De Paul, M. Textor, N.D. Spencer, Langmuir 18 (2002) 220.
[109]J. Chalmeau, L. Salomé, C. Thibault, C. Severac, C. Vieu, Microelectronic Engineering 84 (2007) 1754.
[110]A. Kumar, G.M. Whitesides, Applied Physics Letters 63 (1993) 2002.
[111]B.D. Gates, Q. Xu, M. Stewart, D. Ryan, C.G. Willson, G.M. Whitesides, Chem. Rev. 105 (2005) 1171.
[112]J.P.R. A. Bernard, B. Michel, H. R. Bosshard, E. Delamarche,, Advanced Materials 12 (2000) 1067.
[113]A. Bernard, E. Delamarche, H. Schmid, B. Michel, H.R. Bosshard, H. Biebuyck, Langmuir 14 (1998) 2225.
[114]J.P. Renault, A. Bernard, A. Bietsch, B. Michel, H.R. Bosshard, E. Delamarche, M. Kreiter, B. Hecht, U.P. Wild, The Journal of Physical Chemistry B 107 (2003) 703.
[115]J.P. Renault, A. Bernard, A. Bietsch, B. Michel, H.R. Bosshard, E. Delamarche, M. Kreiter, B. Hecht, U.P. Wild, J. Phys. Chem. B 107 (2003) 703.
[116]B. Michel, et al., IBM J. Res. & Dev. 45 (2001).
[117]J.W. Lussi, D. Falconnet, J.A. Hubbell, M. Textor, G. Csucs, Biomaterials 27 (2006) 2534.
[118]L.D. Unsworth, H. Sheardown, J.L. Brash, Langmuir (2008).
[119]P. Nollert, H. Kiefer, F. Jahnig, Biophys. J. 69 (1995) 1447.
[120]B. Kasemo, Current Opinion in Solid State and Materials Science 3 (1998) 451.
[121]K.Glasmastar, C. Larsson, F. Hook, B. Kasemo, Journal of Colloid and Interface Science 246 (2002) 40.
[122]P.N. Brown, M. Terrazas, K. Paul, D.F. Blair, J. Bacteriol. 189 (2007) 305.

[123]K.A. Morehouse, I.G. Goodfellow, R.E. Sockett, J. Bacteriol. 187 (2005) 1695.
[124]B.J. Lowder, M.D. Duyvesteyn, D.F. Blair, J. Bacteriol. 187 (2005) 5640.
[125]M.D. Manson, J. Bacteriol. 189 (2007) 291.
[126]S. Scheuring, D. Levy, J.-L. Rigaud, Biochimica et Biophysica Acta (BBA) - Biomembranes 1712 (2005) 109.
[127]N. Buzhynskyy, P. Sens, V. Prima, J.N. Sturgis, S. Scheuring, Biophys. J. 93 (2007) 2870.
[128]T. Ueno, K. Oosawa, S.-I. Aizawa, Journal of Molecular Biology 227 (1992) 672.
[129]J. Zhou, D.F. Blair, Journal of Molecular Biology 273 (1997) 428.
[130]T.F. Braun, S. Poulson, J.B. Gully, J.C. Empey, S. Van Way, A. Putnam, D.F. Blair, J. Bacteriol. 181 (1999) 3542.
[131]T. Yorimitsu, A. Mimaki, T. Yakushi, M. Homma, Journal of Molecular Biology 334 (2003) 567.
[132]S.-Y. Park, B. Lowder, A.M. Bilwes, D.F. Blair, B.R. Crane, Proceedings of the National Academy of Sciences 103 (2006) 11886.
[133]P.N. Brown, C.P. Hill, d.F. Blair, The EMBO journal 21 (2002) 3225.
[134]P.-E. Milhiet, F. Gubellini, A. Berquand, P. Dosset, J.-L. Rigaud, C. Le Grimellec, D. Levy, Biophys. J. 91 (2006) 3268.
[135]A. Berquand, D. Lévy, F. Gubellini, C. Le Grimellec, P.-E. Milhiet, Ultramicroscopy 107 (2007) 928.
[136]J.-L. Rigaud, B. Pitard, D. Levy, Biochimica et Biophysica Acta (BBA) - Bioenergetics 1231 (1995) 223.
[137]J. Jass, T. Tjärnhage, G. Puu, Biophysical Journal 79 (2000) 3153.
[138]V. Noireaux, A. Libchaber, Proceedings of the National Academy of Sciences of the United States of America 101 (2004) 17669.

# Chapter IV
# The model strikes back
# Our vision of the Bacterial Flagellar Nano Motor

Summary

As noticed before, Nature has assembled through evolution numerous systems, starting from the nano-scale to the human scale. Through the micro-biology and the genetics, we know more about how things work at our scale and at the cellular scale, but the inner mechanism of cell remains a challenge. Lot of biological processes have been discovered and widely studied during the last 30 years, but the mechanical aspects of the thousands of nano-bio-machines found inside a single cell remains a new field, comparable to the Eldorado for the Spanish discovers in the 1600's. What we will learn will shape what could be nano-bio-technology for the decade ahead, due to the enormous advantages of Nature over human's factories or ways of doing things, everything self-assemble and do not require tons of energy. From the DNA to assembly of cells, everything is dancing like in a ballet, and the BFNM is a good example of such a complexity at the nanoscale. We are probably at a period of time, where the two big Micro-sciences are merging, where the top-down approach fuse to the bottom-up as described by Georges M. Whitesides[1] or by M. Stephen[2]. Micro-electronics and nanotechnologies bring top-down processes for generating surfaces with desired functions and the micro-biology is bringing bottom-up processes, based on the self-assembly. But before we can use these natural bio-systems, we need to know how they work, how they are built, and this it is the first axis I developed during my thesis: how the motor works through the study of the interactions between proteins. I will summarize the results obtained in chapter 2 and couple them with the result from the second axis, the structural approach, developed in chapter 3. Both axis brought data about the BFNM, and helped me to elaborate a new model of how could work the BFNM, a model which answers several points addressed in chapter 1. The model I will propose is not perfect, and further studies will be needed to confirm it or decline it, but I hope that through the data and the vision I have, my contribution will be considered by the community. I will finally propose perspectives to continue my work and increases its possible impact, with preliminary results which encourage us to continue the effort on this direction.

# A) A new model for the BFMN

## a. Synthesis of our results

### i. Structural approach

Two major results were obtained about the motor architecture, the size of some proteic elements and interactions between motor proteins, and their dependence with the pH of the medium. Our structural results indicate that FliG proteins tend to self-assemble directly into rings, which are apparently later added to the MS-ring composed by FliF. The size of this ring is primordial in all models because the FliG position is a key element for the motor structure. Based on our results, FliG rings make apparently an averaged diameter of 18 to 22 nm for 80 % of the observed rings, and 27 to 32 nm for 15% of the total population, see figure 1.

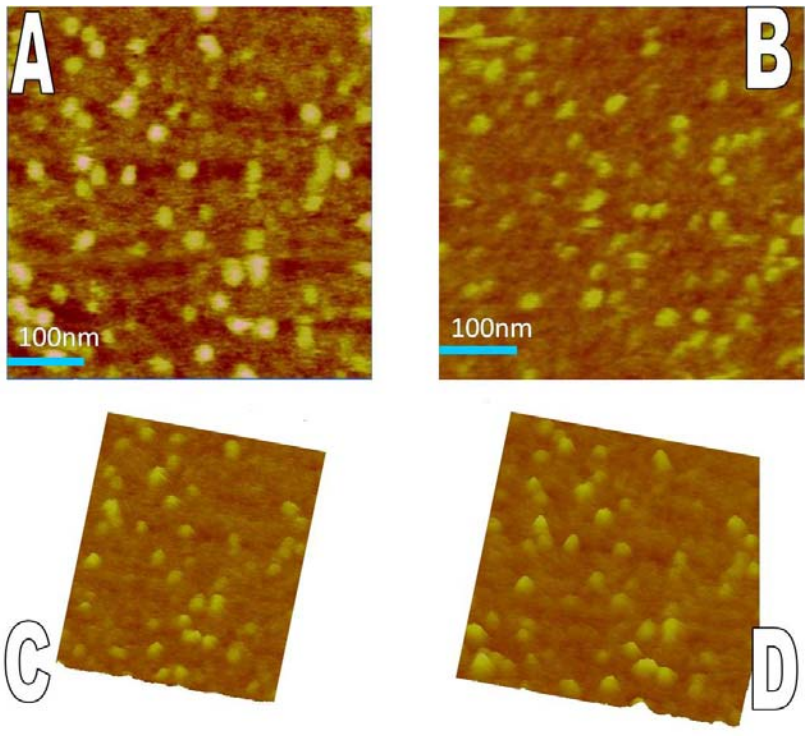


***Figure 1: AFM images of FliG proteins on a mica surface.*** *tapping mode in PBS buffer, force evaluated below 50pN for all images .A/ Tapping mode height image using OTR4 from Olympus, cantilever stiffness 20mN/m. B/ Height image using MSCT probe. C.D/ 3D reconstructions views of A and B.*

Sub-units organization of the observed structure was not accessible despite our efforts, but further studies could improve image resolution. These images coupled to the

clear and relevant results about FliG aggregates highlighted the possibility of using AFM in liquid to bring data about the BFNM partially re-assembled *in vitro.* FliG aggregates, presented in figure 1, have brought a new perspective about FliG assembly in liquid and on a surface. The distribution obtained confirmed that FliG tend to assemble in the so called M-ring. When FliG is mixed with FliM and FliN, the structure found displayed an average radius of 45 nm, in good accordance with the ring observed by cryo-TEM, with two different thicknesses which could correspond to an external ring composed of FliM and FliN and an inner ring composed of the FliG. Figure 2 shows the result obtained on FliG/FliM/FliN complexes. However, these results are recent for being considered as viable and numerous tests would be needed to confirm this type of architecture.

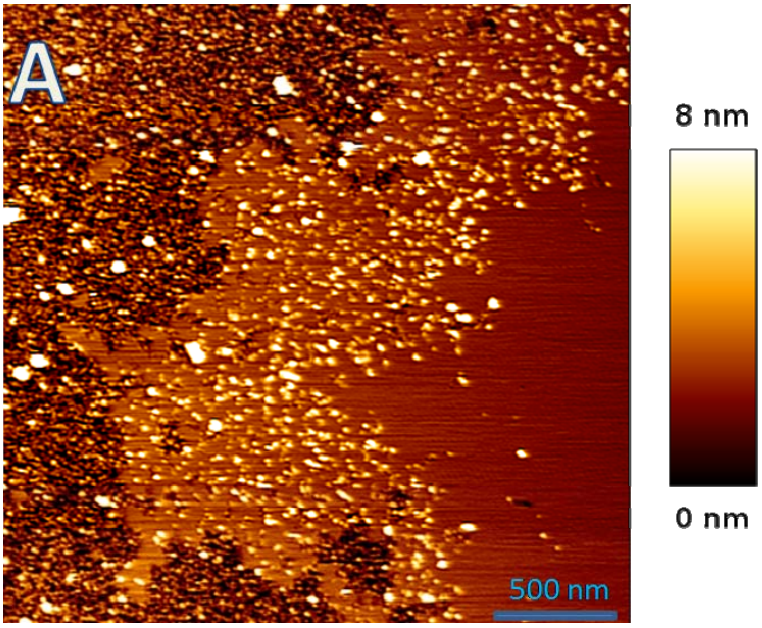

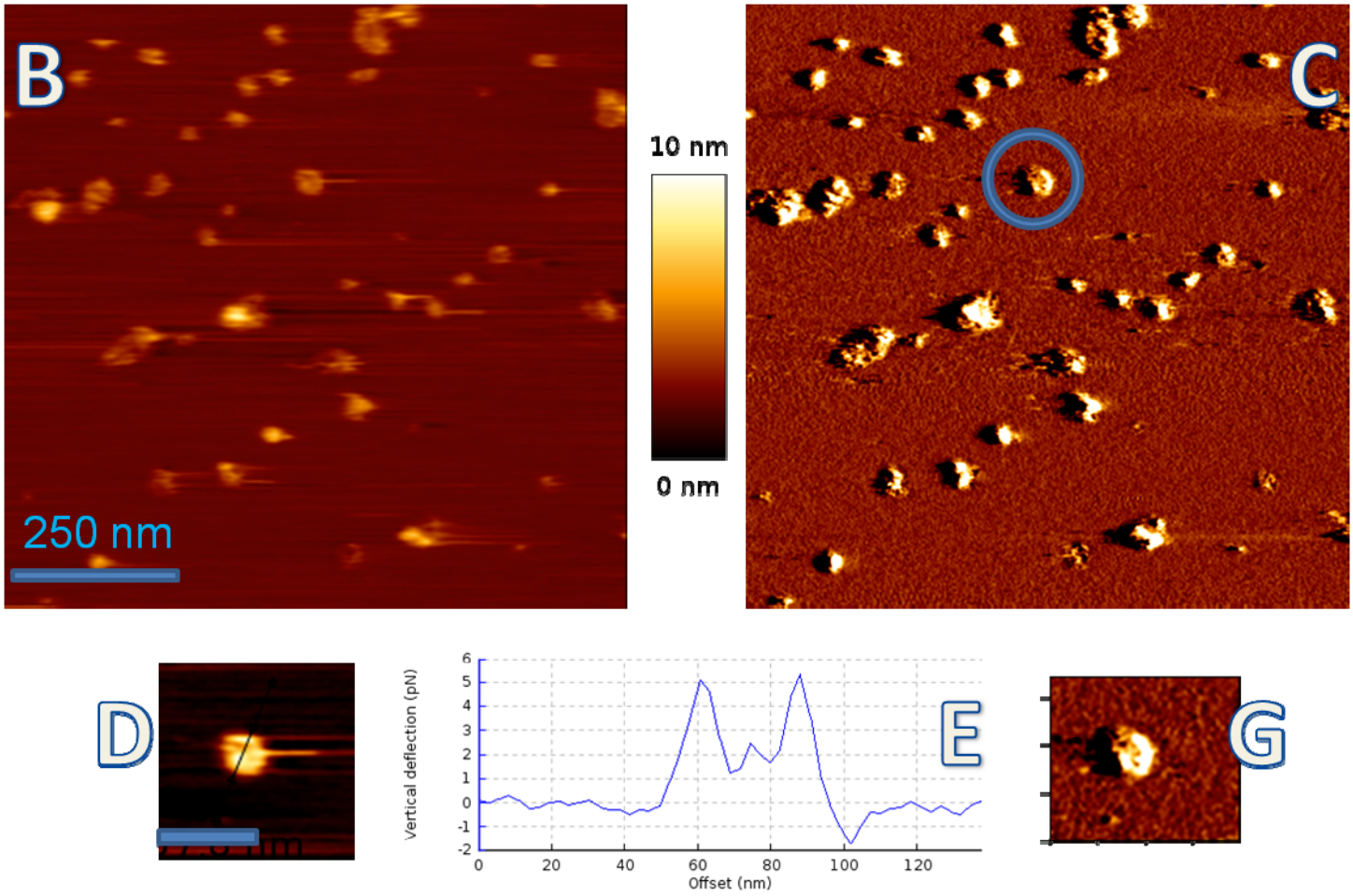


***Figure 2: AFM images of FliG/FliM/FLiN mixture on a E.Coli SPBM***. *A/Large view of the surface exhibiting SPBM partially covered by proteins. B: Enlarged view of the SPBM with proteins aggregates. Height signal. C: Vertical deflection signal of B. D/ zoom in a single aggregate. E/ cross section of D. E/ Vertical deflection of D. A thickness of 5 nm is visible with a clear depression in the middle. The center of the aggregates presents a thickness of 2nm which is in a good accordance with previous results presented in chapter 3 about the FliG ring.*

These images brought some clues to propose a possible assembly of the BFNM, in order to respect the different dimensions of the observed elements. These results should be handled carefully in our hypothesis describing the BFNM assembly and function. Due to possible AFM artifacts (see chapter 3) and also by the fact that a protein observed independently could be different when mixed with others motor elements. The first result obtained with protein mixtures confort us in our approach and do not conflict with our previous results about FliG alone. We could position the structure formed by the

FliG at the cytoplasmic side of the rotor, or at an intermediate position between the rotor and the C-ring. I will favor this second position, due to the possible enlargement of the FliG ring when added with FliF rings already formed within the membrane.

### ii. Interactions studies

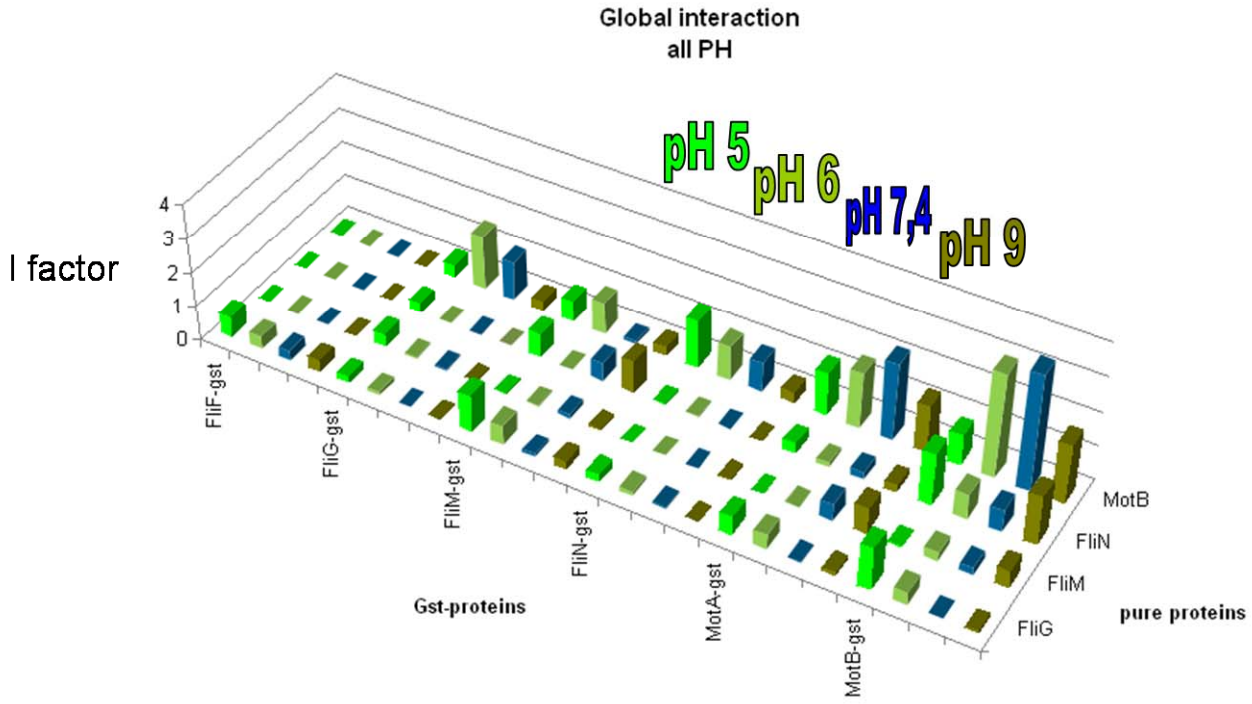

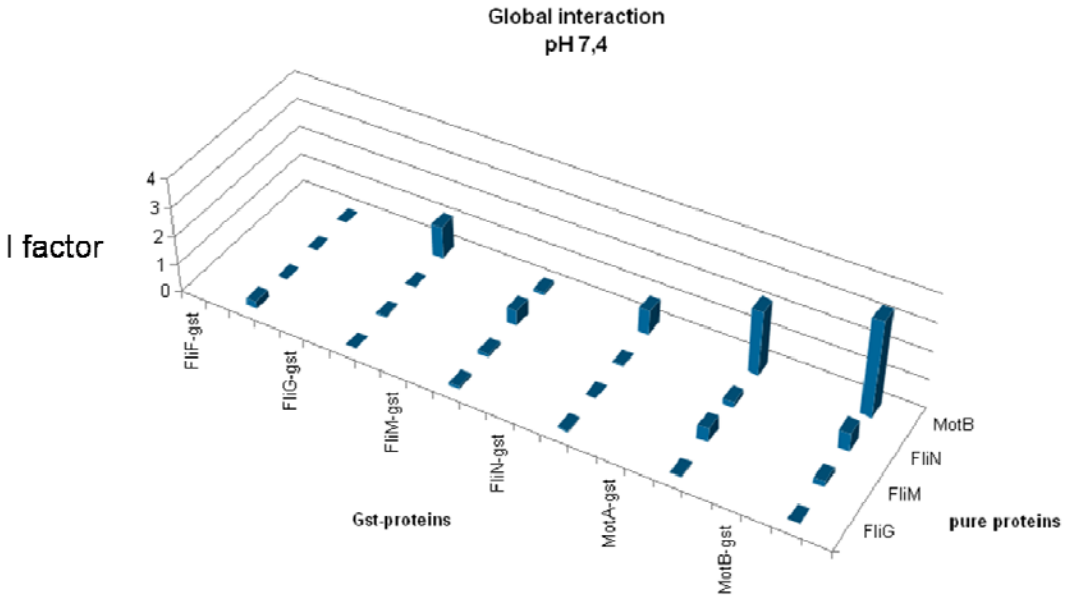


***Figure 3/ Summary of the interactions between proteins in 4 buffers exhibiting different pH and at pH7.4***

Interactions between purified proteins in a controlled medium highlighted some interactions never observed before using more classical microbiology tools. We have already discussed in chapter 2 the validity of those results and I will consider them as reliable, despite the question about their configuration, as for MotA and FliF for example.

The main point needed to be considered for proposing a reliable model is the native bacteria pH at the cytoplasmic side of the BFNM. Some studies evaluated the bacteria cytoplasmic pH around 7,6 to 8 and this value is crucial for a good motility [3]. We can consider that the proteins which interact in a range value of pH between 7 and 9 are relevant in the BFNM while working. The remaining question is what about the other interactions observed which happens in acid pH? I do not have yet the answer but I will propose a hypothesis about them which could account for all the observed interactions. The interactions which occur in a basic or neutral pH mainly involved the C-ring, FliM with itself, FliN FliM, and also MotA-FliM and MotB-FliM. The interactions in acid buffer mainly concern the FliG proteins, and their interactions with the rest of the BFNM: MotA-FliG, FliM-FliG, FliN-FliG, MotB-FliG, FliG with itself, and the remaining interactions occurred for all pH: MotB with itself, MotB-FliN, FliF-FliG, MotA-FliN. I consider that this pH classification reveals an important thing about the BFNM: on one

hand interactions for its assembly and on the other hand functionnal interactions. As far as we understand the motor function as a proton pump, a massive amount of protons is passing through the stator and pull in the cytoplasm. Numerous processes within the cytoplasm apparently maintain the pH at a good range for allowing the BFNM to work. This is the reason why some interactions appear in basic solution, the assembly ones, and others in acid media the functional ones. However, this hypothesis will need to be confirmed by numerous experiments in different buffers exhibiting different ions or salt concentration in order to be as close as possible to the native conditions of the bacterial cytoplasm. I will consider only the interactions at pH 7,4 for elaborating a reliable hypothesis about the motor function.

## b. A new model for describing the motor mechanism

### i. The current view about the BFNM mechanism.

Before describing our hypothesis, I will summarize the current accepted view of the BFNM assembly and function, based on the numerous publications of the diverse group which are working on the BFNM. Figure 4 summarizes the current vision of the BFNM architecture for a single unit and the simplified shape we chose to schematically represent the different sub-units.

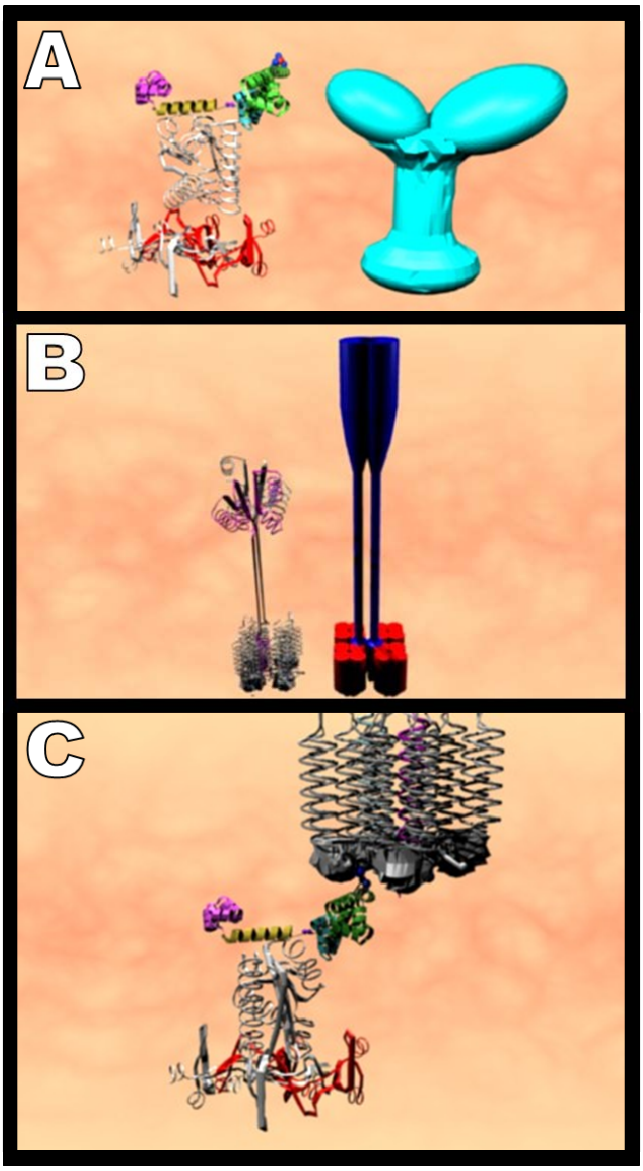


***Figure 4: Schematic view of the BFNM.*** *A/ the C-ring structure, left: FliG covering the top, FliM in the middle position and FliN tetramer at the bottom; right: the schematic representation. B/the stator assembly, left: 2 MotB embedded in 4 MotA; right: the schematic representation. C/ The architecture of the C-ring. FliG interacts vertically with the cytoplasmic part of MotA.*

Figure 5 shows the global assembly, starting by the C-ring structure to the final motor assembly.

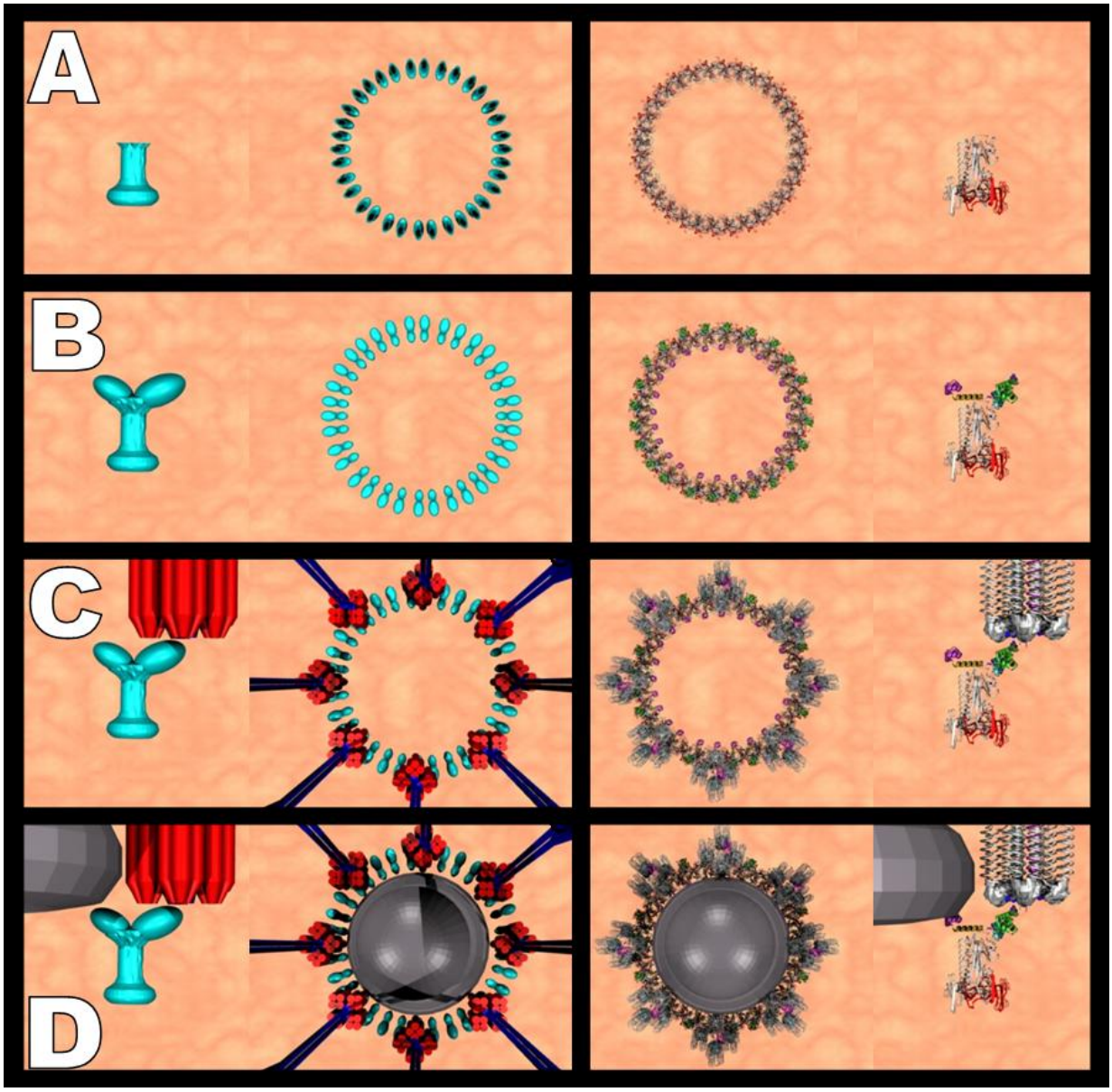


***Figure 5: the global architecture of the BFNM*** *A/ The FliM/FliN assembly, which compose the bottom and middle part of the C-ring. B/ The addition of FliG at the top of the C-ring. C/The stator is inserted into the structure. D/ The FliF, major component of the rotor is finally added.*

The structural position of the diverse elements is mainly supported by two points, the FliM/FliG interactions and the CryoTEM view of an extracted basal body of the BFNM. Figure 6 shows the rotation process as proposed by Blair *et al* and also the switching steps. The source of energy of the rotation is coming from the passage of protons through the stator complex. These protons are supposed to interact with the ASP32 of MotB and through an unelucidated phenomenon of release, generate the torque within the stator complex. The cytoplasmic part of MotA interacts with FliG, thanks to

the charged amino acids, and generates the rotation. The switching process only concerns the rotor and C-ring, which are considered as a unit due to the interaction FliM/FliG. When CheY-P binds to FliM, it changes the shape or form of the FliG ring (M-ring) and extends the FliG-C domain, which now interacts with another part of the stator complex. This new interaction generates a rotation in the opposite direction. Figure 6 shows the different steps of rotation and switching. The question about the synchronism between the different units during the switching has not been addressed yet, excepted by mathematical simulations.

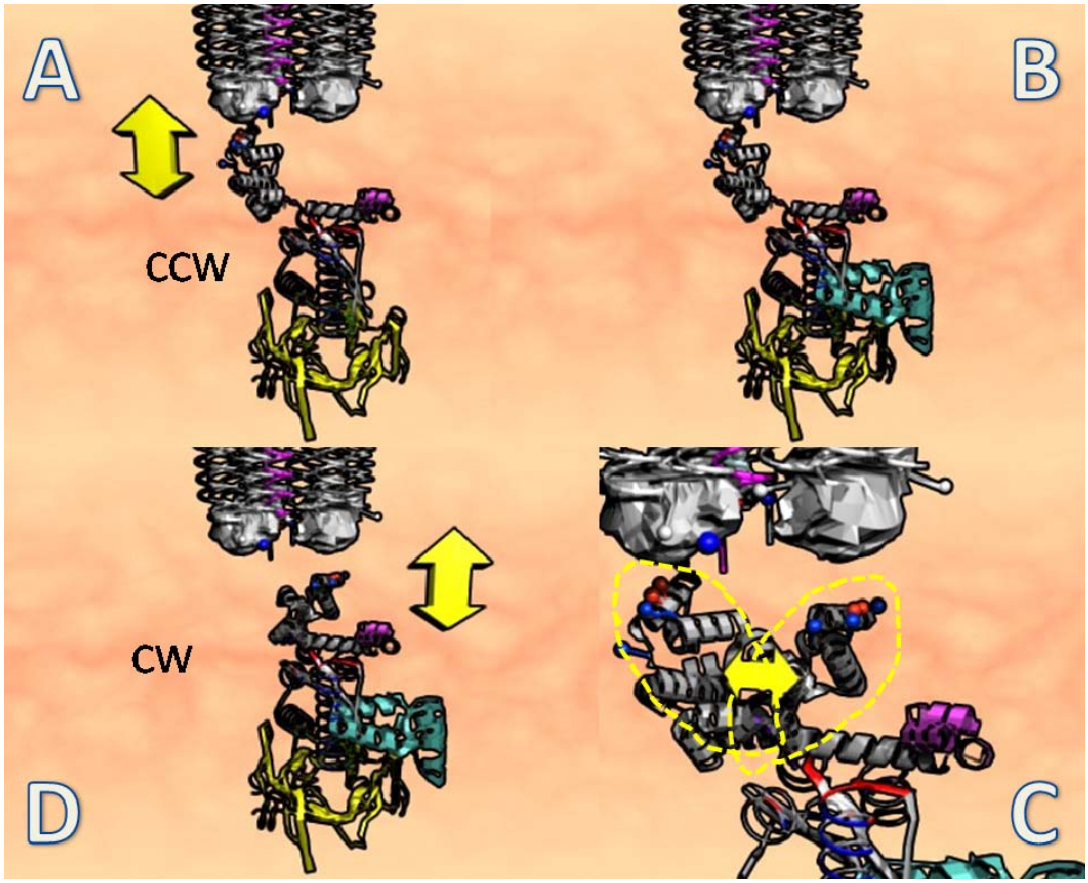


***Figure 6: Schematic view of the rotation and switching process.*** *A/ FliG interacts vertically with the cytoplamic part of MotA in order to generate the rotation. B/ CheY-P binds to FliM. C/ it provoke a lateral movement of FliG-C through two possible interactions sites not represented here. There are two stable positions for FliGc corresponding to CCW and CW states. D/ FliGc now interacts with another part of the MotA's cytoplasmic part and this interactions generates the rotation in the opposite direction.*

## ii. Our Vision of the BFNM

### 1. Structure

The data I obtained during my research work cannot address all the questions about the BFNM, so some aspects of our model will be based on these new results but some others will consist of proposals based on others publications or directly new ideas. The first difference between our model and the current view of the BFNM reside in the position of FliG within the BFNM architecture, based on the AFM images we have obtained. Figure 7 reviews our vision of the architecture of the BFNM.

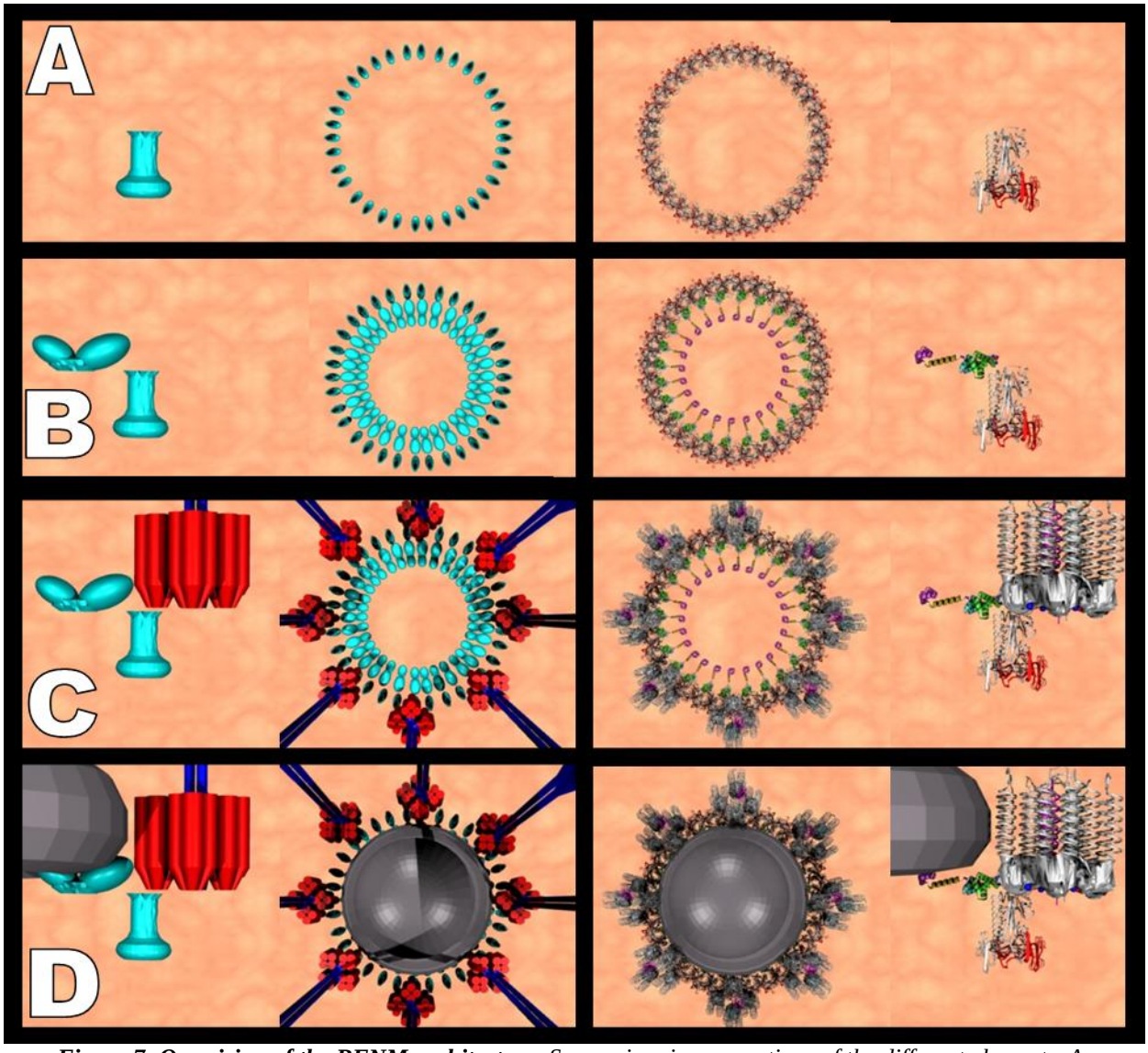


***Figure 7: Our vision of the BFNM architecture.*** *Successives incorporations of the different elements. A: FliM and FliN in the C-ring. B: FliG plus C-ring. FliG is shifted to the inner diameter of the rotor. C: stator assembly. D: And finally the FliF rotor.*

Our structural vision of the motor is also based on a remark about the images obtained by cryo-microscopy, especially the work published by Derosier *et al.[4; 5]*. The images they proposed in their paper [6] opened for us a major question about the identification of FliG FliM and FliN in the "Y" elements of the C-ring. **We suspect that during the extraction procedure, the cytoplasmic part of MotA sticks to the C-ring and is responsible for the external part of the "Y".** Numerous experiments have been done since the first images, and to our knowledge, no extraction experiment have been

tested using a "*MotA*- mutant". This idea is also supported by the interactions we have obtained in chapter 2. The FliM-MotA interaction, (I=0.93±0.18) is relatively high compared to others interactions into the motor, as for example FliM/FliG 0.56±0.11. However, we do not think that the full MotA is extracted, just the cytoplasmic part of the stator complex which is directly interacting with both FliG and FliM. We suspect that the protocol designed for the extraction enhances the affinity between the different proteins and is also partially responsible for the extraction of some stator elements. Another support to this architecture is the recent work of Jensen *et al* [7] which have imaged another bacteria species, *Treponema Primitia,* presenting a polar flagella. The BFNM found at the base look relatively is similar to the BFNM found in *E.Coli* for its mechanical properties, however the images they obtained by cryomicroscopy reveals a radical different architecture. The symmetry of stator was found to be 16 and more important the position of the C-ring was found too far from the rotor to be directly connected to it. The vertical alignment of the C-ring to the stator elements supports, to our mind, the direct interactions between the cytoplasmic side of the stator and C-ring.

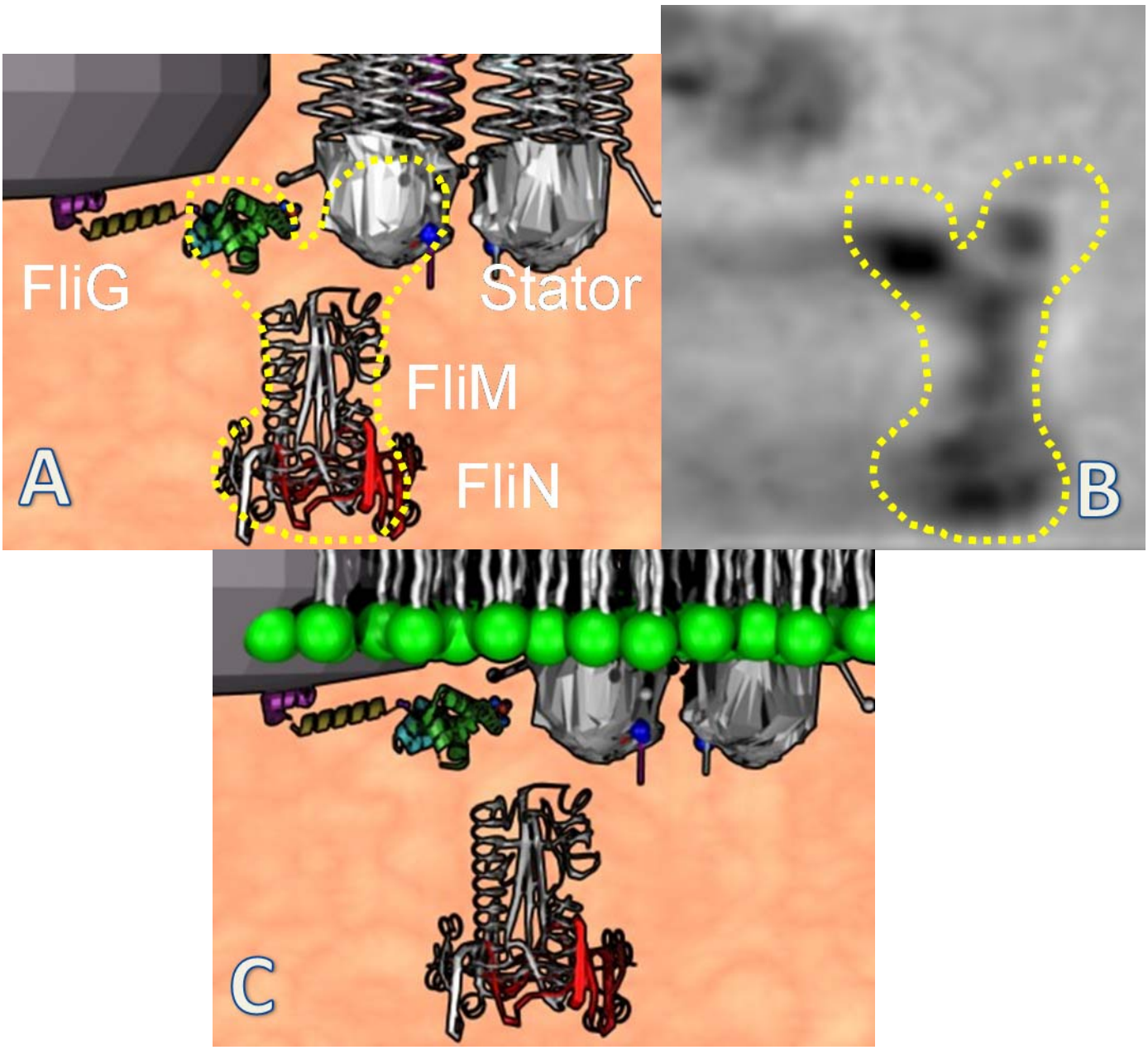


***Figure 8: Spatial configuration of single unit elements, composed of 1 FliG, 1 FliM, the FliN assembly and the cytoplasm part of the stator***. *A/ the proteins assembly with a yellow lines compared to cryoTEM images on B. extracted from ref [4].B/ the cryoTEM images of the C-ring. C/ proteins elements with the phospholipids surrounding them.*

One of the way to confirm our idea will be to extract the rotor following the same protocol but on a mutant lacking both MotA and MotB.

## 2. Rotation and stepping

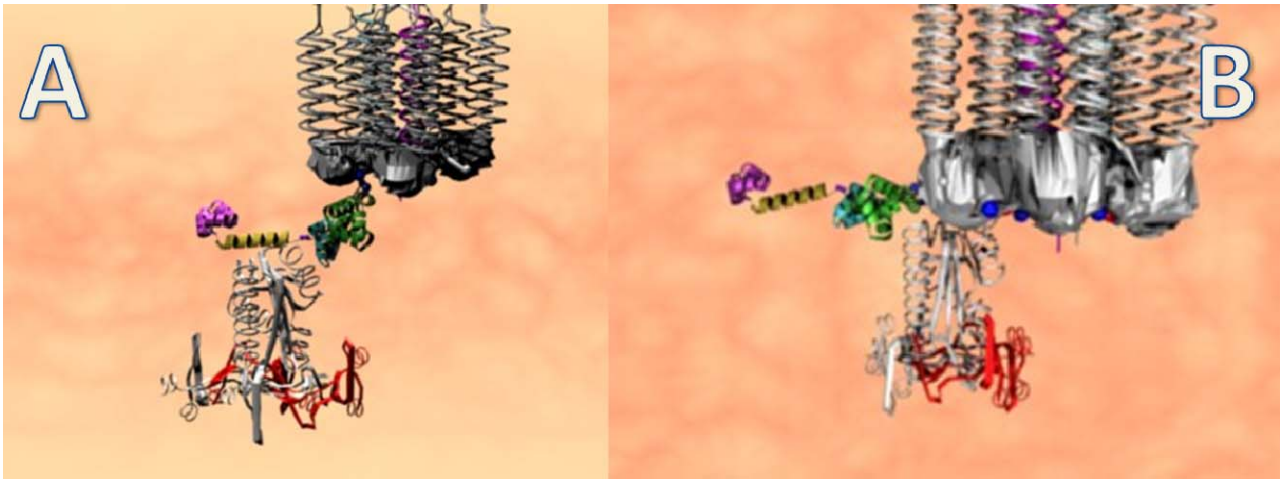


***Figure 9: schematic view of two possible assembly of the C-ring/stator*** *A/ current view of the FliG position. B/ Our position of the FliG, slightly inside the rotor which permits a direct interaction between the C-ring and the stator.*

The major difference can be seen on the figure 9, showing two different assembly of FliG, wherein FliG is slightly shifted inside the rotor. This change is support by the AFM imaging we have provided. FliG ring diameter is closer to 25-30nm instead of 45nm as supposedly admitted today. This position changes drastically the interactions sites with the stator. **We proposed a horizontal interaction between FliG and MotA. The identified charged amino acids are still responsible for the rotation.** This new position is the first change between our model and the current view. This new assembly is also supported by the presence of an interaction between the C-ring proteins FliM and both MotA and MotB, which have not been observed before. **These interactions exclude the rotation of the C-ring as a sub-unit of the rotor and anchor the C-ring to the stator.** How could we explain the rotation with this architecture? Figure 10 proposes a possible mechanism based on the lateral and vertical displacement of the charged amino acids of MotA, found in the cytoplasm part of MotA. **This mechanism is based on a horizontal interaction between FliG and MotA and the presence of two vertical "levels" of interactions between FliG and MotA charges.** This mechanism is based on two series of interactions already identified: the role of ASP32 of MotB [8] and the importance of the charged amino acids of both MotA and FliG. [9; 10; 11]. However, our lecture of their role is not so different. The proposed mechanism could also accommodate the dependence of the rotation to the PMF or SMF, and also the mechanical data obtained

by resurrection experiments. Numerical simulations could be envisioned to confront this new hypothesis to the numerous data already obtained about the generated torque, the torque/speed relationship etc. However, two direct questions have to be addressed in this vision of the rotation: why the stator needs 4 MotA and 2 MotB and two protons channel if just 2MotA and 1 MotB are enough? And how could we explain that 26 steps have been found? The first question addresses what I consider the major weakness of the BFNM, the consumption of some motor proteins while spinning. J.P *Armitage et al[12]* highlighted an interesting aspect of the BFNM, the turnover of a membrane protein, MotB. This observation reveals that the motor need to change few of its components while spinning, probably due to some damage generated by its high frequency rotation. The role played by the second couples MotA/MotB could be envisioned as a replacement wheel in a car. When one piece is damaged, through an unknown phenomenon, the motor ejects the defect proteins and replaces it right away by a second assembly.

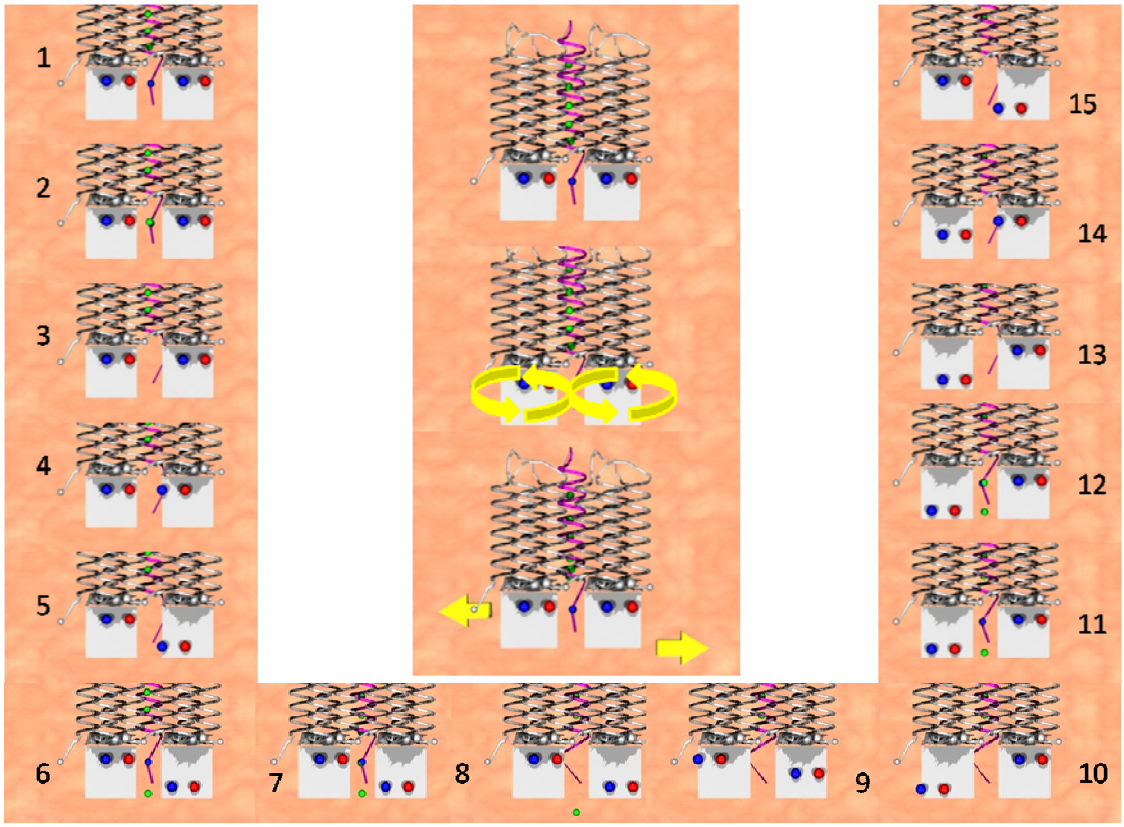


***Figure 10: A plausible mechanism for the rotation****. A horizontal interaction between FliG and MotA is responsible of the rotation. The figure only shows a sequence of event within the stator*

*assembly. The central image shows a vertical lateral view of the stator complex, exhibiting 2 MotA and 1 MotB, the other sub-units of the stator are not visible here. The charged amino acids of MotA have been schematically represented by the red and blue spheres on a grey square representative of the MotA cytoplasmic part. The blue sphere found in the middle represents the ASP32 from MotB. The two yellow arrows symbolize the direction of the rotation generated by the charges. Our sequence of events explains how the rotation is* ***generated in both direction****s. (1) A successive series of protons is present in the channel created by the stator.Their precise locations are still unknown. (2) A proton binds to the ASP32. (3) it provokes a structural change within the cytoplasmic part of MotB…(4)…which generates an horizontal deformation of the MotA charges to the top left. This movement is the key for generating the rotation of the rotor, meanwhile all the stator are doing the same movement. This movement makes FliG rotating to the left too, thanks to the electrostatic interactions between the charged amino acids. (5) The deformation is now vertical and the charges go down left. (6) The proton is released from the ASP32 and a new cycle can start with the second MotA. The first MotA cannot deform while their charges are not back at the beginning position. (7) A new proton binds ASP32 while the charges of the first MotA moves to the down right at the bottom position. (8) This movement is responsible for the rotation in the opposite direction of the rotor while the second MotA charges move horizontally to the top left.The protein FliG which has been moved laterally by its interactions with the first MotA can now continue to rotate with the second MotA (9) The first MotA charges move up while the second MotA charges finish their first movement to the top left. (10) The first MotA charges are back in their positions while the second MotA charges are moving down left. (11) The proton is released and a new cycle can start for the first MotA (12) The ASP32 is loaded with a proton and the first MotA charges start to move to the top left (13) while the second MotA charges finish to move to the bottom right. (14) the cycle is almost over while the first MotA finished to move to the top left, while the second MotA moves up to the top right. (15) The first MotA moves down while the second MotA is ready for a new cycle.*

The second question about the steps observed is related to the number of FliG proteins into the MS-ring. This number has been obtained by measuring the rotation of a bead grafted to the rotor with a fine control of the SMF and also with a single stator[13]. This number corresponds to the symmetry of the axis where the torque is generated and not the number of stator complex surrounding it. The number of stator has been largely discussed [14; 15; 16; 17] since the beginning of resurrection experiments to structural data about MotA and MotB. However, the exact number of stators surrounding the rotor remains unknown and only a direct observation of the assembly could definitely address

this point. Our assembly and tentative model could be integrated into the current vision of the torque delivery system. 2 protons will be needed for moving FliG one step, which could correspond to the proposed evaluation by Sowa *et al*[13] . But as we noticed before, the evaluation of protons needed for a full rotation has been subject to controversy, and should be confirmed for species like *E.Coli*. As proposed above, one of the possibilities to test our hypothesis would consist in a mathematical simulation of the behavior of a rotor with a stator system such as the one we propose. The numerous data about the torque generated by a single stator in various cases could also be envisioned. **The most critical point about our hypothesis remains the need for the structure of MotA and MotB and both assembled into the stator**. The difficulty to produce and purify MotA and MotB, as noticed in chapter 2, and also their insertion into a preformed membrane remains the big challenge ahead for the full comprehension of the BFNM. The proposed extraction protocol [18] and the arrangement [19] opened the possibility to work in vitro on the stator complex, but the work done in 2003 has not given any new results to our knowledge. AFM imaging on the extracted complex on mica surface or inserted into a preformed SPBM could address the question of MotA and MotB numbers and also spatial arrangement and dimensions. The proposed arrangement here is purely hypothetical and has not been confirmed by any experimental data. However, this hypothesis mainly finds its support in the relocation of FliG into the BFNM architecture, at an intermediary position between rotor and C-ring. The second support is related to the electron microscopy images proposed by Derosier *et al* [4]. The position of FliG at an intermediary position is more likely probable by coupling our AFM imaging data to the high resolution electronics images.

### 3. Switching

The second question about the BFNM function is related to its possibility to rotate in both direction, and its capability to alternate quickly without destroying the BFNM assembly. The role of CheY-P has been confirmed through numerous studies [20; 21; 22; 23; 24] and its binding to the FliM is the key of the switching process. Based on this observation and the new architecture we proposed, we think that the switching process could be imaged by two structural changes within the C-ring, as described in figure 11.

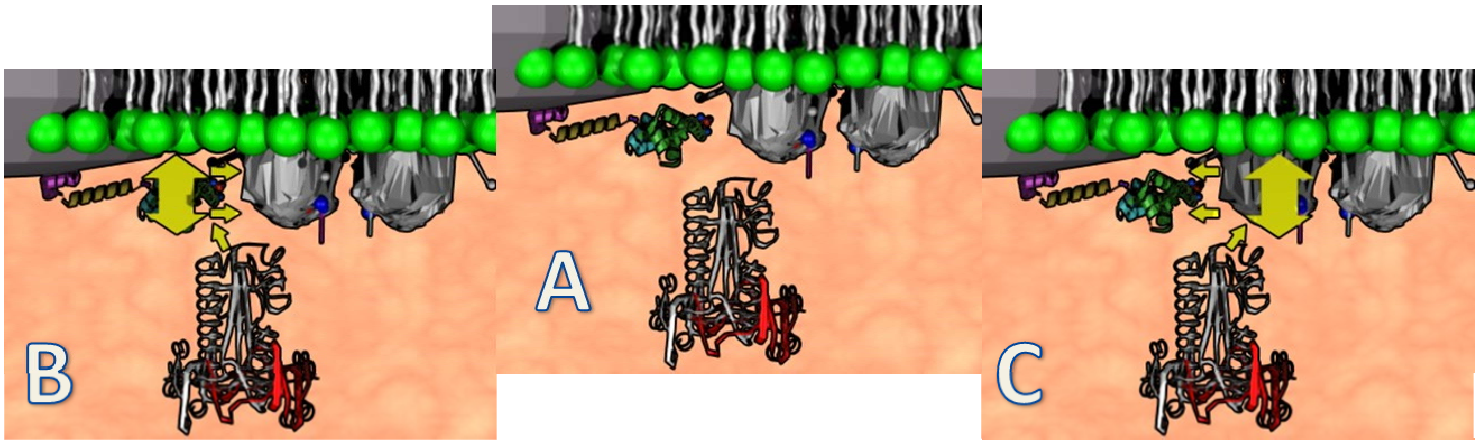


***Figure 11: the local switching mechanism****. A/ The spatial assembly of the motor units, with the inner membrane above. B/ FliM is interacting with FliG and moves up and down the FliG-C domain. This domain is interacting with the two levels of MotA, as described in the previous section. FliM is interacting and anchored to an unknown region of MotA or/and MotB as observed during the interactions studies. This link is the key for forcing and stabilizing the FliG rotation. C/ FliM is interacting with MotA and moves up and down the two levels of interactions. FliM is anchored to the MotB and meanwhile confines FliG movement. In this option, FliG is stable all the time and the two levels of interactions are moving to align to FliG level. The CheY-P is not represented here, but the sequence of events for the switching process will consist of a vertical deformation of FliM, pushing either FliG or MotA in order to change the interactions between these two proteins.*

The proposed mechanism is based on the major role played by FliM, through its interaction with the chemotaxis proteins CheY-P and with other motor elements. Two parallel processes could be imagined, both of them are supported by experimental data. These two processes mainly depend on FliM/FliG interactions. As noticed before, this interaction is the most discussed of the all motor. CryoTEM imaging has not confirmed the spatial position of FliG and the lack of symmetry between FliG and FliM numbers vanishes an allosteric interaction comparable to FliG/FliF or MotA/MotB. Two processes are possible, based on the existence of two levels on the MotA distortion, which is the source of the rotation. The two views give the same result; FliG changes its interactions with the two levels of MotA. In one way, the MotA is static and the FliG moves vertically up and down and interact alternately with the two levels of MotA, or FliG is static and the two levels of MotA are moving up and down to align with FliG. In the two

ways, FliM is vertically deformed and “pushs” either FliG or MotA to another alignment. The need for anchoring FliM to a static part is crucial in both ways, and this link has been found during the interactions studies through the FliM/MotA or FliM/MotB interactions. Based on these two options, I personnaly support the first view, with a static stator and a FliG moving vertically up and down. FliM needs to be strongly anchored to a part of the motor, here we propose the stator instead of the rotor, so FliM cannot be strongly anchored and meanwhile deforms MotA. The interaction between FliM and FliG is more a dynamical one than a bonding. FliG is rotating above a level defined by the FliM. Since this level is moving up or down, FliG ring is changing its interactions with MotA due to the above pressure of the inner membrane and the under presence of FliM.

This local phenomenon can explained also the global “1 or 0” behavior of the switching process, with an intermediate level allowing the transition between the two states. The existence of a threshold number of CheY-P bound to FliM could be envisioned in our model. Figure 12 shows a possible sequence of events for the switching process.

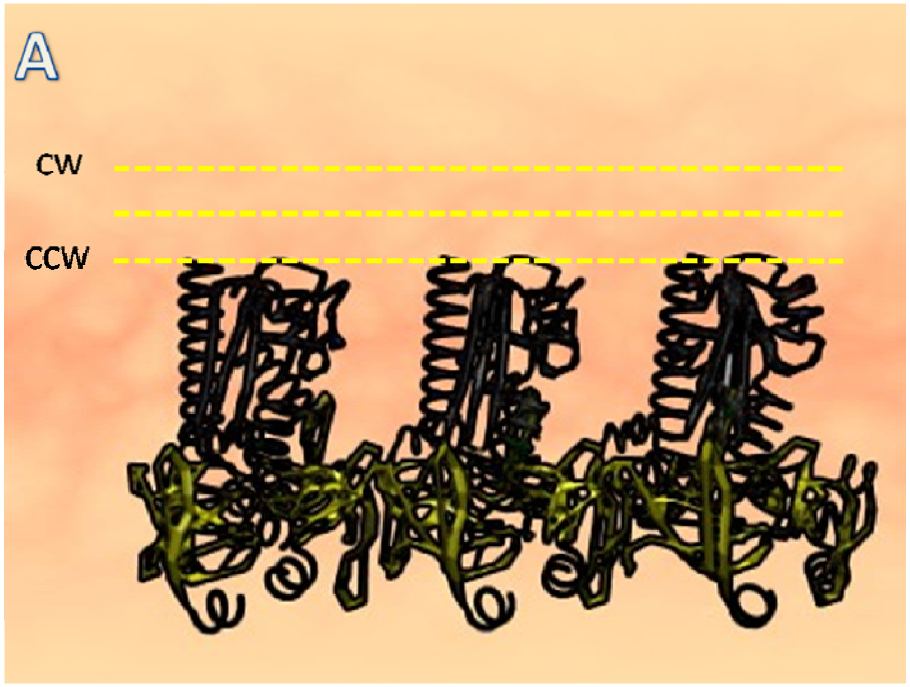


***Figure 12A: Schematic view of the switching process.*** *Three FliM are represented on the figure 12A. each of one of them has three possible deformations possible related to the states, CCW or CW, of the rotation.*

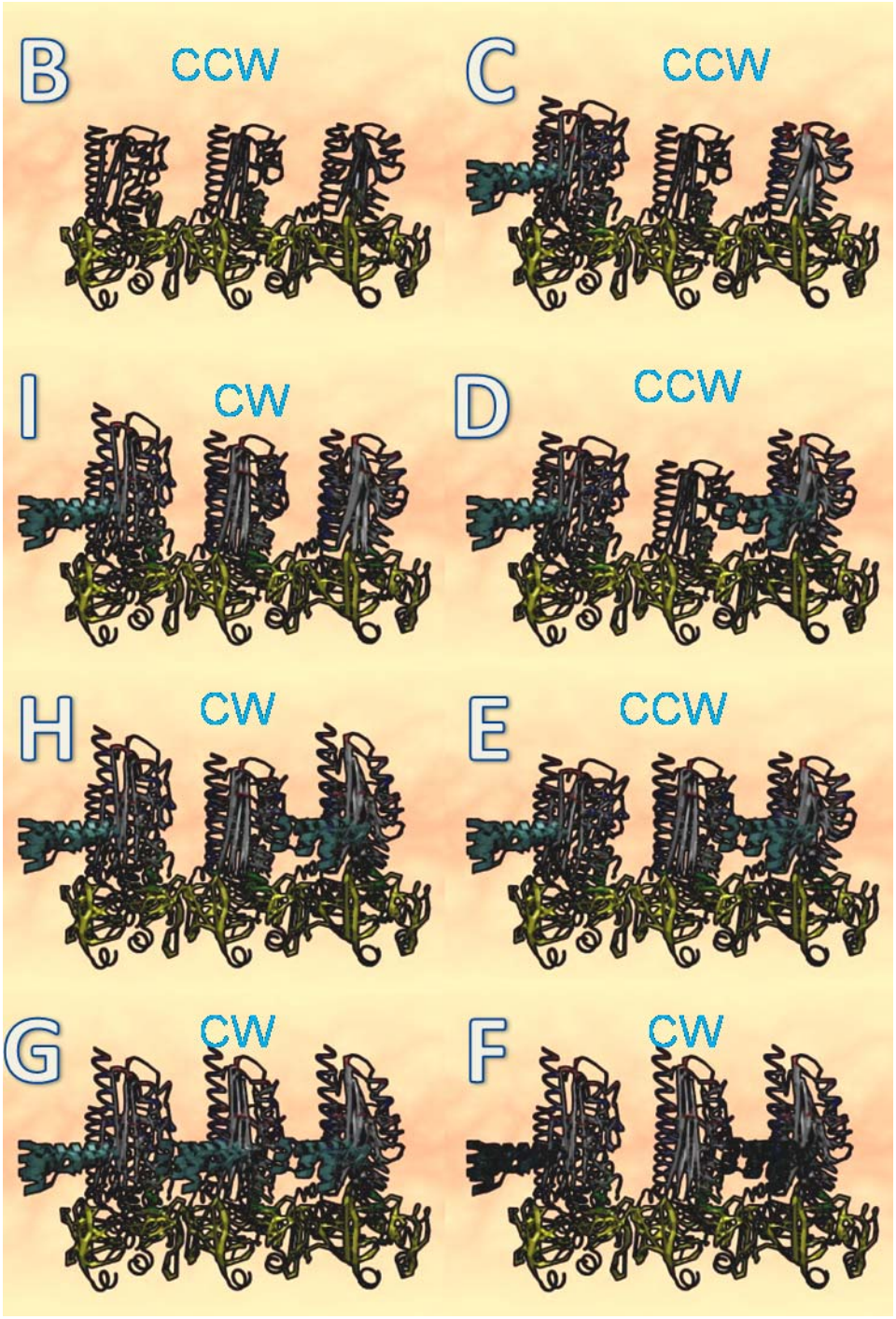


***Figure 12B: the switching process***. *B/ The three FliM are in their CCW configurations. C/ A CheY-P protein binds to the left FliM, bringing it in its intermediate configuration. This FliM can not go in its CW configuration due to the lateral interaction with two others FliM which are still in their CCW configuration. D/ A second CheY-P binds to the right FliM, which goes in its intermediate configuration. A threshold number of CheY-P is bound to the C-ring. E/ it forces now the middle FliM to go in its intermediate configuration. This situation is not stable upon time. F/ All FliM are going synchronusouly to*

*their CW configurations,whatever all FliM are interacting with CheY-P; this is the spreading event. The BFNM now rotates CW. G/All FliM are now interacting with CheY-P. H/ Some CheY-P are desphosphorilated and present no speficic affinity with FliM. The middle FliM goes back to its intermediate configuration. The BFNM still rotates CW. I/ A threshold number of CheY-P have left the C-ring. The middle and right FliM are in their intermediate configurations. This situation is not stable. The C-ring is back to its CCW configuration. A new cycle can restart.*

As proposed by Duke [25], the idea of a spreading conformation into the C-ring is elegant. Each protein in our case FliM, could have at least 2 spatial configurations, one when related to MotA FliG FliN and maybe FliM, one plus CheY-P. Each FliM will present 2 stable configurations, with an intermediate one. When a CheY-P binds to FliM, FliM starts to shifts to its second configuration. This cannot be achieved if its two neighboring FliM have not been bonded by CheY-P. the role played by the others proteins is crucial for "feeling" the FliM-CheY-P complex, and this role can be played by the FliN tetramer found at the base of the C-ring. Numerous experiments need to be done for confirming the role of FliN or other proteins as a conformational "spreader" of the switching. This basic system will allow a rapid spread of the deformation. The recent work about a plausible mechanism of switching [21] remains with FliG at the top of the C-ring. We do not support this hypothesis based on the structural data we have obtained. However, their experimental data could also be inserted in our vision of the switching process by shifting FliG to the inner side of the rotor.

## 4. Conclusion

As far as we know, the BFNM function remains unknown, despite the recent advances in structural data about FliG, FliM and FliN. Our model of the BFNM is for the moment based on two kinds of experimental data, structural coming from AFM imaging and biochemical from the QCM-D experiments. These two axes have brought to our minds a new light about the BFNM assembly and mechanism. The model we proposed is not perfect, and some established data are not going to support our vision of the BFNM. We think that most of the genetic data could be inserted into our model, despite the position of FliG and the new FliM-stator interactions we propose. Numerous

experiments, simulations will be needed to definitely confirm or declined this model, of course open to discussion and refinements.

## B) Perspectives, the return of surface patterning

### a. Introduction

As notified, my work has not addressed the issues about the BFNM function and architecture, but must be more considered as the beginning of a new series of experiments. As in my work, we can separate the future experiments into two parts, inter-connected but distinct: the structural approach and the interactions studies. The numerous interactions between motor proteins I studied could be considered as only a basis for future developments. This future work can be divided into three axes: surface imaging, interactions between proteins and 3D assembly. Working on the way to provide to a given protein suitable surface conditions for its self assembly will be the direct continuation of the current work. The structural approach, called "Surface imaging" will remain challenging. Most of my structural work has been dedicated to the study of the cytoplasmic part of the BFNM, mostly the so-called C-ring structure. All the attempts for imaging the stator within the SPBM have failed and this issue is attributed to the problem of pure proteins production and also trans-membrane insertion within a pre-formed SPBM. The approach developed can be considered as a static one, and the real major next step could be to build a set-up wherein the full motor, composed of the stator, rotor and C-ring can freely self-assemble and start the rotation. I have already addressed in chapter 3 what could be the major limits of the current approach, but taking into account these points, two future directions can be proposed: a static and a dynamic self-assembly. Static and dynamic? The first one could serve as a basis for assembling the motor at a controlled position, by mixing the Top-down and the Bottom up approach, and the second one by allowing part of the motor to spin, to reproduce a 3 dimensional environment where stator and rotor could interact, something comparable to the current approach developed for studying the F1F0-ATPase *in vitro*. In addtition, the use of altered proteins elaborated by mutagenesis will be also the direct continuation of the chapter 2. Our protocol for fixing one of the two proteins has proven to be efficient, but

others process could be envisioned, using a $SiO_2$ sensor instead of gold sensor and elaborate various protocols based on PEG chemistry which could present better control of the surface functionalization. Numerous mutant proteins are currently available within the different team around the world working on the BFNM. Comparing a same protein, for example FliG, with its mutants, could be relevant. Changing the buffer or temperature could also represent an axis of experiments. I do not want to go in more details of what could be possible for the interaction study but possibilities are relatively large, and one thesis would be probably necessary to tackle all the questions about the motor proteins interactions. On the other hand, the 3D reconstruction represents a new approach for studying the BFNM which could address the problems encountered during this work. I will describe here the first result I have obtained about the two first axes and emphasizes about the third axis, the full BFNM reconstitution in a 3D structure which represents in my mind the future of nano-bio-machines.

## b. The static view, a Multiple Surface Functionalisation Process (MSFP)

The results obtained on P-SPBM with FliG proteins were encouraging, and could be improved in a near future by a better controlled of the PEPG liposome size or by changing the patterned molecules. High resolution imaging of parts of the BFNM will not be possible if the protein density is not increased in order to create a 2D crystal of motor parts on the surface, 2D crystal comparable to those obtained with bacteriorhodopsin. Working with proteo-liposome could be a possibility, as noticed in chapter 3, but formation of a 2D crystal is not sure also by this way. The other possibility would be to fix part of the BFNM on a surface, and find the good conditions wherein the rest of the motor will self-assemble around or above the fixed part. Direct incubation of motor proteins will be the easiest way, but the direct adsorption of proteins on a surface will limit. The approach I developed based on a SPBM, mimeting the bacteria environment, remains more interesting, but the free diffusion of proteins on the surface prohibits high resolution. The mix between patterning and self-assembling render possible the generation of P-SPBM, but the presence of only one deposit molecule at the surface

limits the interest of the technique. A more complex engineering of the surface at the molecular level is required for confining the proteins around the location where the first brick of the motor has been assembled. Indeed, using conventional μCP, only one molecule using one PDMS stamp can be deposited on the surface and alignment between multiple PDMS stamp exhibiting different proteins remains technically out of reach. In order to address those points, I developed a process called One-Step-Multiple-μCP (OSM-μCP)[26]. This approach is based on a precise and controlled patterning of two different bio-molecules using only one PDMS stamp. The flexibly of the μCP has been already demonstrated[27][28; 29; 30]. By generating a highly engineered surface where one molecule could serve as a brick for the full assembly of the motor and a second one for confining SPBM and proteins self-assembly, we could build a full template for the BFNM assembly. By adjusting the medium, and the use of AFM imaging, we could learn in which conditions the BFNM self-assembles *in vitro*. I will first describe the basic idea of the process, mainly based on the deformable properties of PDMS stamps, and the process for generating a PDMS stamp dedicated to this task. In a second time, I will show how two molecules can be deposited on the surface along self aligned patterns using this special PDMS stamp and the first results obtained by mixing these surface patterns with SPBM formation.

### i. Silicon Master

The μCp is based on a replica method of a silicon master, with an elastomer (PDMS). As described in chapter 3, numerous molecules can be deposited by a simple contact between a inked PDMS stamp and a cleaned surface. In order to deposit more than one molecule in one step, the most straightforward solution consists of printing sequentially the different species which raise the problem of the alignment between the different levels[31]. Aligning elastomeric stamps made of polydimethylsiloxane-based PDMS materials is challenging due to the deformability of the stamp and its high adhesion on flat surfaces[27] limiting the use of sequential printing to large micrometric structures. Through a simplified version of this method, Inerowicz *et al[32]* successively printed two different proteins along orthogonal arrays of lines by simply rotating the stamp by 90°. The produced arrays of crossing lines enabled the immunodetection of one

specific antigene in one direction and another antigene along the orthogonal direction. The same scheme was employed recently for high resolution printing of proteins using flat stamps[27; 33]. Despite its simplicity, these later methods are restricted to specific patterns and to noninteracting molecules. Other methods enabling the printing of several molecules by μCP are based on photolithography[34], microfluidic,[35] or μCP coupled to self-assembly[36]. The use of chemical external agent,[37] the risk of contamination between patterns together with the requirement of microfluidic channels for inking the stamp, or a series of lithography levels remain crucial issues for the success of these processes. We propose an alternative method called one-step-multiple-μCP (OSM-μCP) for generating self aligned patterns of different biomolecules in one printing step, using PDMS stamps exhibiting several levels of topography. The principle described in Figure 13 takes profit from the deformability of the stamp.

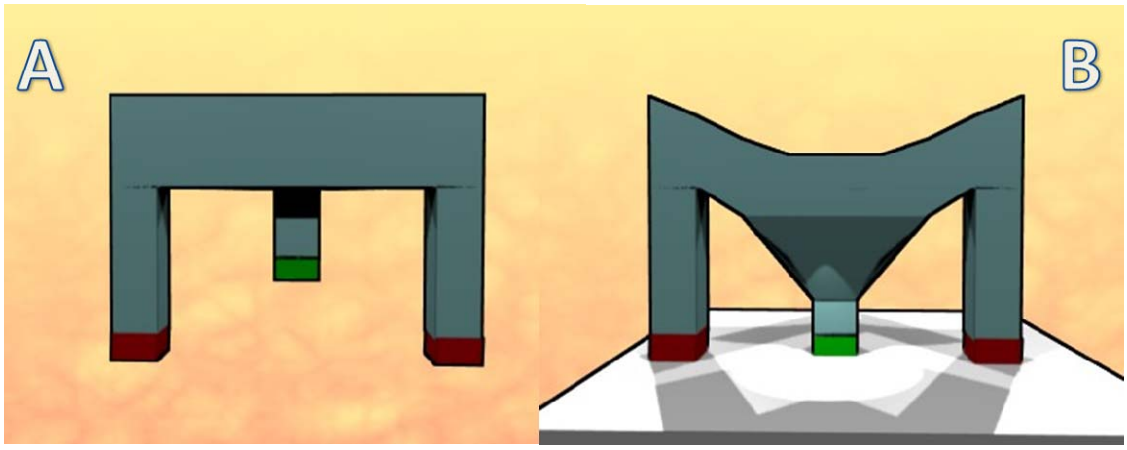


***Figure 13: Schematic view of the principle of OSM-μCP.*** *A/ a PDMS stamp with a specific topography is designed and inked locally with two different inks. B/ By applying a pressure on the top side of the stamp, the PDMS stamp deform and brought into contact with a surface the different stamp level and then transfers the different inks very specifically.*

A PDMS stamp presenting two levels of possible contact with the surface needs to be generated using nano-lithography. Figure 14 shows the technological steps for generating the silicon master.

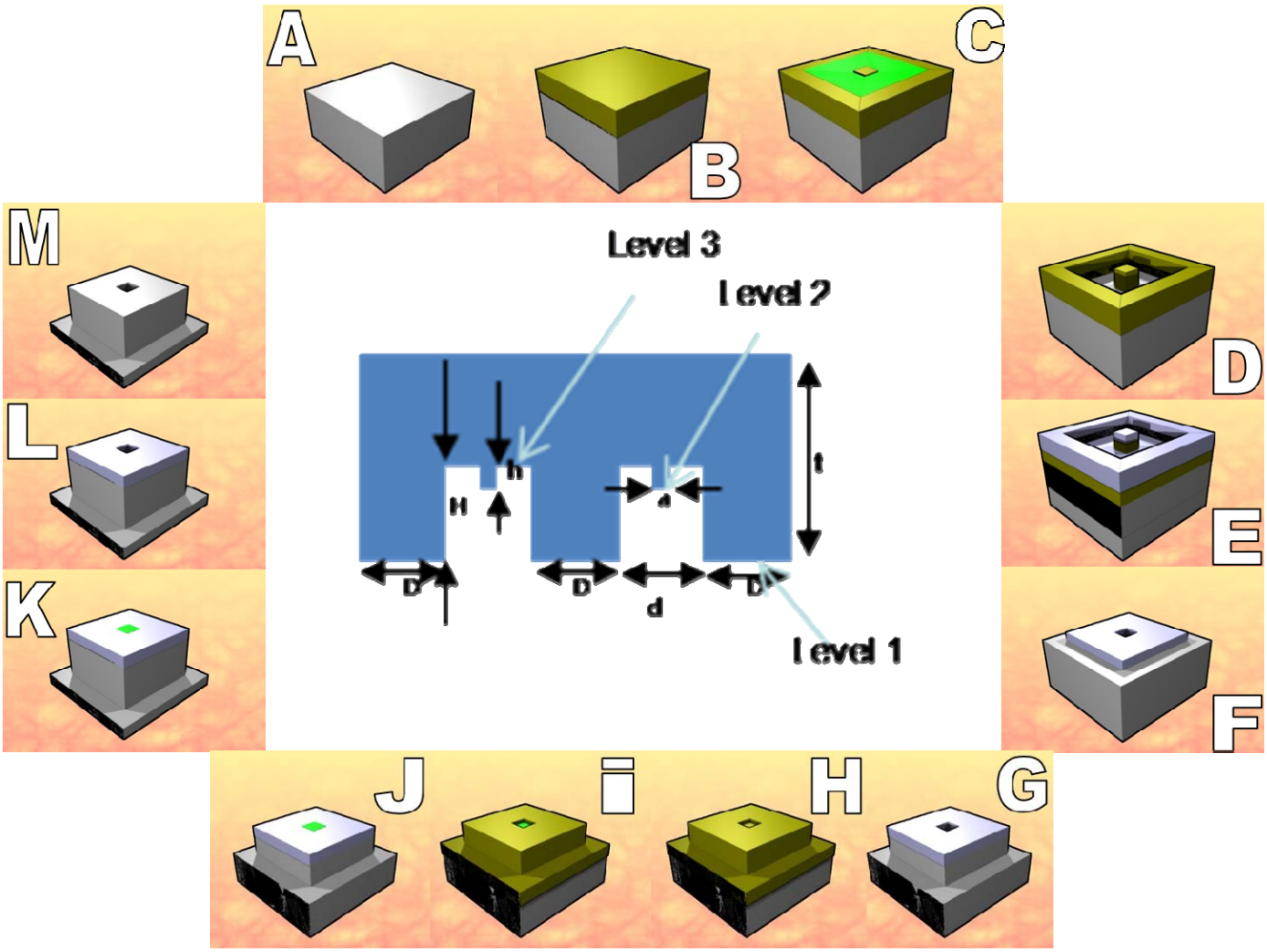


***Figure 14: The OSM-µCP master generation***. *The creation of a PDMS presenting two different levels of contact with the surface needs multiple steps. The center image shows design of the stamp. A/ a silicon wafer is cleaned .B/ A 150nm thick layer of poly(methyl)(metacrylate) resist (PMMA) is spin-coated on the cleaned silicon wafer. C/ Patterns are defined in this positive resist using EBL. D/ After resist development, E/ a 70 nm thick layer of Nickel is deposited and F/ lift-off is achieved in trichloroethylene using an ultra-sonic bath. G/ The patterns are then transferred in silicon by RIE with an etch depth of 400 nm. H/ For generating the other level of the master, a negative tone resist (maN2403-300 nm) is patterned by EBL I/ and J/ serves after development K/ as a mask for a 1000 nm deep etch of the silicon surface. The alignment of this EBL exposure on the pre-existing structures is not critical since the patterns of the negative resist together with the Ni film previously patterned act as a mask for the second RIE process. L/ The resist mask and M/ Ni film are finally removed using sequentially a tricholoroethylene bath for the resist and a mixed of Chlorohydric acid, Nitric acid and water (1/1/1) for the Ni film.*

After an anti-adhesive treatment, carried out by a well-established process using octadecyltrichlorosilane (OTS) in liquid phase, the silicon master was ready for PDMS casting. Figure 15 shows a typical silicon master.

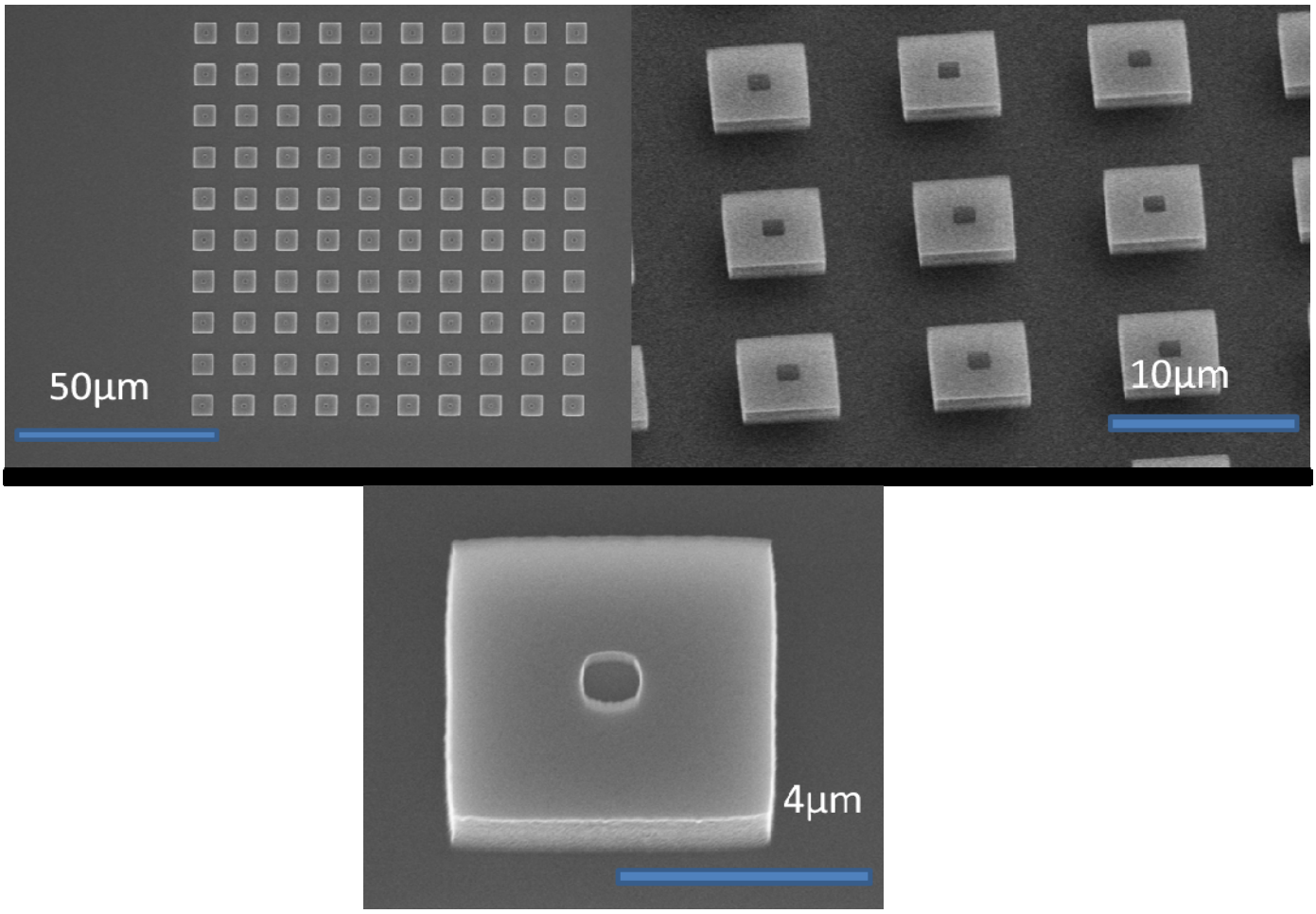


***Figure 15: SEM imaging of the silicon mold.*** *Large squares presenting a center depression correspond to the third level of the master while the bottom of the depression the second level. The first level is the surface of silicon wafe.r*

For stamp generation, we use a PDMS-based material known as Sylgard 184 (Dow Corning). We have then established a reliable technique for inking each level of the stamp with a given biomolecule.

### ii. Surface patterning with 2 molecules in one step

As a demonstrative experiment, we experimented this stamp with two couples of molecules, BSA-rhodamine and Streptavidin-FITC, Pll-g-PEG-rhodamine and antibody anti-GST-FITC. We wanted to cover a large surface with BSA-rhodamine or Pll-g-PEG-Rhodamine except into squares of 5 $\mu m^2$. Within each square, a small central spot of 1 $\mu m^2$ of streptavidin-Fluoresceine or antibody anti-GST-FITC will be deposited. I will present here the images obtained for the couple BSA/Streptavidine, but similar results were obtained with Pll-g-PEG/antibody anti-GST. Figure 16 resumes all the technological steps for generating the surface.

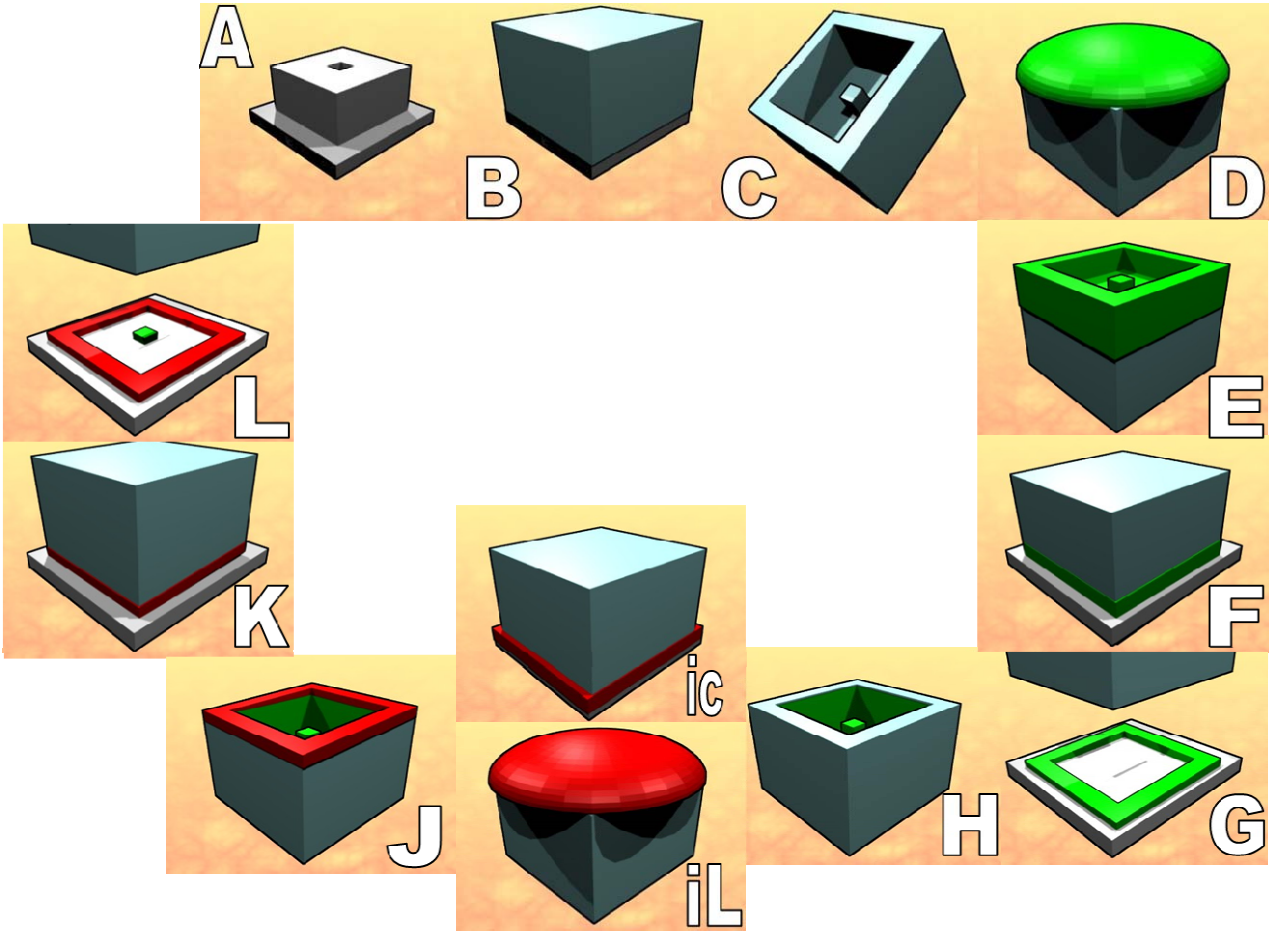


***Figure 16: the inking/printing procedure****. A/The silicon mold is treated using OTS deposited in liquid phase. B/ A PDMS pre-mixed solution is added on the mold and cured overnight at 80 °c.C/ the PDMS stamp is gently removed from the mold. It negatively replicates the mold. D/ A streptavidin-FITC solution is incubated under vacuum for removing the air bubbles trapped into the stamp. E/ the PDMS exhibit proteins covering all surfaces. F/the stamp is brought without pressure in contact with a surface. G/ and then removed. Only the first level of the stamp contacted the surface and proteins have been transferred. H/*

*After several contacts, the stamp only presents proteins on the second level. IL,IC/ a second molecule, BSA or Pll-g-PEG inks the stamp, by a direct contact with a flat PDMS stamp, or by incubation of a drop of molecule. In this second case, the presence of air bubbles inside the cavity avoids the contamination of the second level of the stamp. J/ Now, the stamp exhibits two molecules on separated level of the stamp. K/ the stamp is mechanically brought in contact with the sample, by applying a defined pressure on the top side of the stamp, each stamp level contacts the surface. L/ the stamp is removed and we obtained a self aligned patterns of two different molecules.*

To achieve this goal, the Streptavidin had to be coated on the second level of the stamp, while the BSA needed to lie on the first level. The first inking process deals with the Streptavidin molecules i.e the second level of the stamp. We inked the stamp with a droplet containing the Streptavidin proteins and brought the stamp into a vacuum chamber under primary vacuum. This pumping step enables to remove the air bubbles pinned inside the cavities of the PDMS and turned out to be mandatory for allowing the ink to cover the whole surfaces of the stamp. Then the stamp was dried with $N_2$ gas for a few seconds. We then gently put into contact the stamp without applying pressure on a cleaning substrate for transferring the streptavidin from the first level. Series of contacts are necessary for removing all the ink from the first level of the stamp. All these cleaning prints were performed carefully in order to avoid the collapse of the stamp levels with the surface.

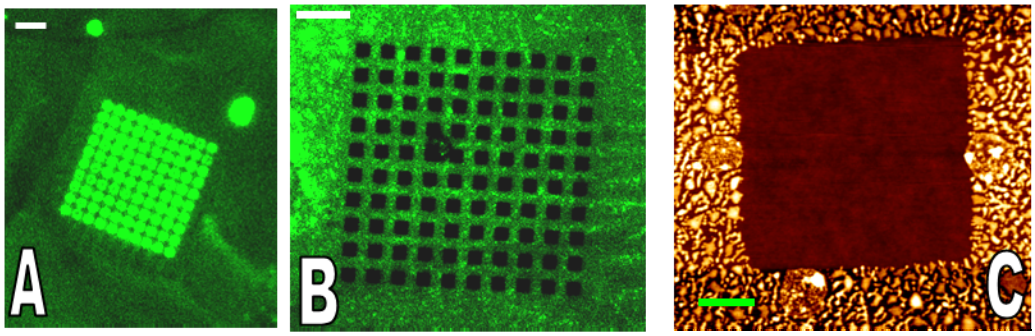


***Figure 17: the streptavidin step.*** *A/ the PDMS stamp after the cleaning procedure. Streptavidine-FITC is clearly visible within the patterns which have not contacted the surface. Scale bar 10µm. B/ the patterns generated on the surface, fluorescence imaging. Scale bar 15µm. C/ AFM imaging of a single pattern.of the cleaning surface Scale bar 1 µm.*

This is attested by the images presented in Figure 17 showing the prints produced on the cleaning substrate where no transfer of molecule from the second level of the

stamp can be observed. The absence of any trace of streptavidin after these cleaning prints on the first level of the stamp is controlled by fluorescence imaging of the stamp (see figure 17A). The multilevel stamp was then inked a second time with a drop of the second molecule (in our case BSA proteins labeled with Rhodamine fluorophores) at atmospheric pressure. In that case, the presence of air bubbles pinned into the cavities of the PDMS stamp prevent the contact of the BSA molecules with the second level of the stamp inked with the Streptavidin proteins. After stamp blow drying under $N_2$ gas, it is possible to check by fluorescence imaging of the stamp that the two inks are selectively deposited along the two levels of the stamp without contamination. A typical image is shown in Figure 18 Small green squares represented the streptavidin-FITC on the second level and large surface of BSA-Rhodamine can be seen on the first level.

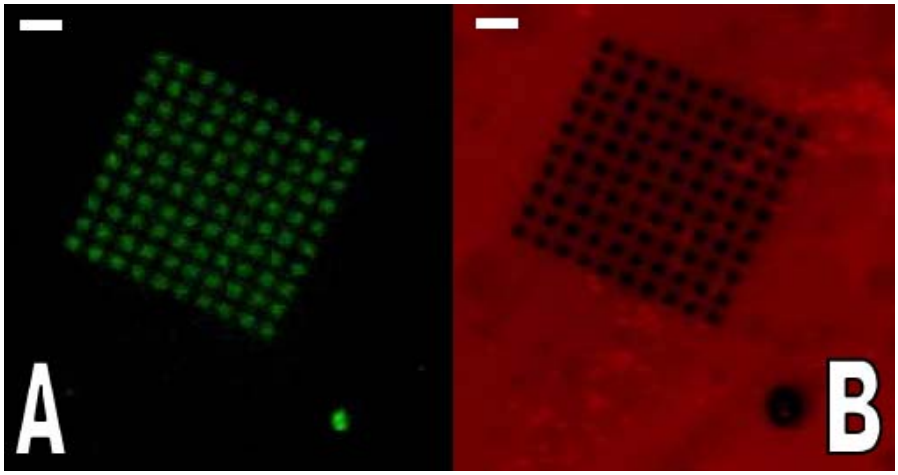


***Figure 18:PDMS stamp before the final printing****.A/ The streptavidine-FITC proteins within the patterns. B/BSA-rhodamine covering the rest of the stamp. Scale bar 15µm*

After these successive inking processes, the stamp was ready for transferring the two inks in one step by contact printing. µCP is achieved first without external pressure (the first level of the stamp delivers the BSA) and then by gently pressing homogeneously the top side of the stamp in order for the second level, inked with the Streptavidin molecule, to contact the surface. After stamp removal we obtained self-aligned patterns of two different biomolecules printed in one step. Figure 19 shows a typical result of such printed patterns using fluorescence microscopy and atomic force

microscopy (AFM) imaging in liquid environment. Controlling the pressure was a crucial point for the success of the final step.

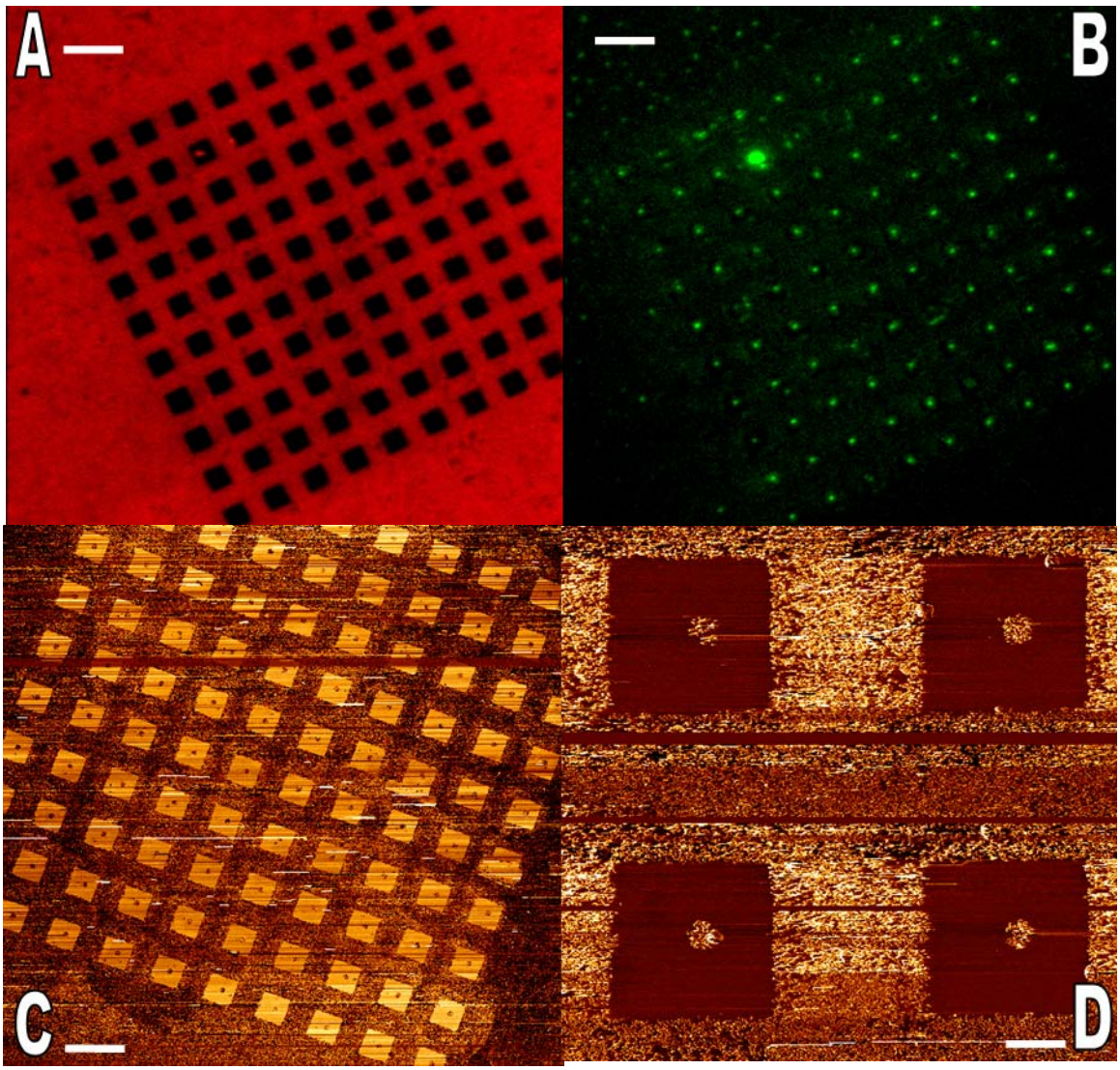


***Figure 19: fluorescence imaging and AFM imaging of the surface exhibiting two different molecules perfectly aligned.*** *Contact mode, MLCT cantilever stiffness 10mN/m, force evaluated below 50nN. A/ BSA-rhodamine, scale bar 10µm. B/ Streptavidine-FITC spots, in the middle of the patterns defined by the BSA proteins. C/ AFM imaging of the patterns generated on the surface, scale bar 10µm. D/ Zoom in on 4 patterns.*

This technique of µCP called OSM-µCP allowed, us to deposit two molecules perfectly aligned without external systems, and using a single PDMS stamp. The result obtained opened numerous applications. Others couples of molecules have been tested and especially molecules which can be used to assemble part of the BFNM on a surface,

in our case an anti body anti-GST-FITC instead of the streptavidin proteins. As demonstrated in chapter 3, BSA proteins could be used as a barrier molecules but AFM imaging remains challenging due to probe contamination. Pll-g-PEG, which has demonstrated its good properties was thus chosen to replace BSA. Final results with the couple Pll-g-PEG-rhodamine/antibody antiGST-FITC are presented in figure 20.

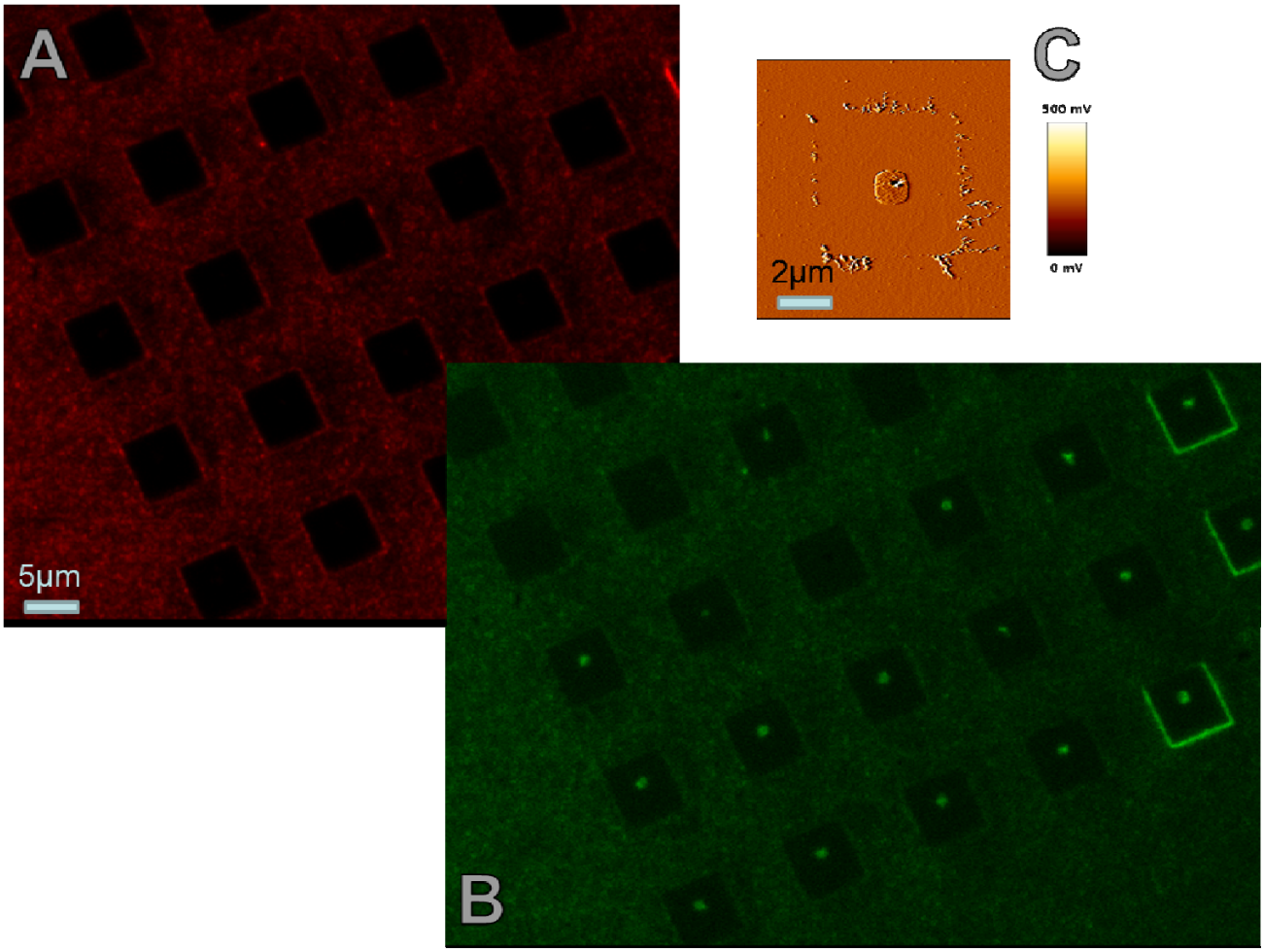


***Figure 20:OSM-µCP of Pll-g-PEG-rhodamine/antibody anti-GST-FITC*** *. A/ fluorescence imaging of the Pll-g-PEG patterns. B/ fluorescence imaging of the antibody anti-GST-FITC spots within the patterns defined by the Pll-g-PEG. C/ AFM imaging of a single pattern.*

We have developed a reliable technique which allows us to generate surface presenting two molecules, one which serves as a brick for the assembly of the BFNM, in our case antibody an anti-GST, and a second which is used as a barrier for the fusion of liposomes, here Pll-g-PEG. Two ways are now possible: we can either incubate produced

proteins directly on the surface, starting by FliF-GST and use AFM in liquid media to characterize the architecture obtained, or forms a SPBM in order to create the viable conditions for the full assembly of the BFNM. We obtained preliminary results by incubating a POPC mixture on the patterned surface. Figure 21 shows fluorescence imaging of the final surface showing the success of this method.

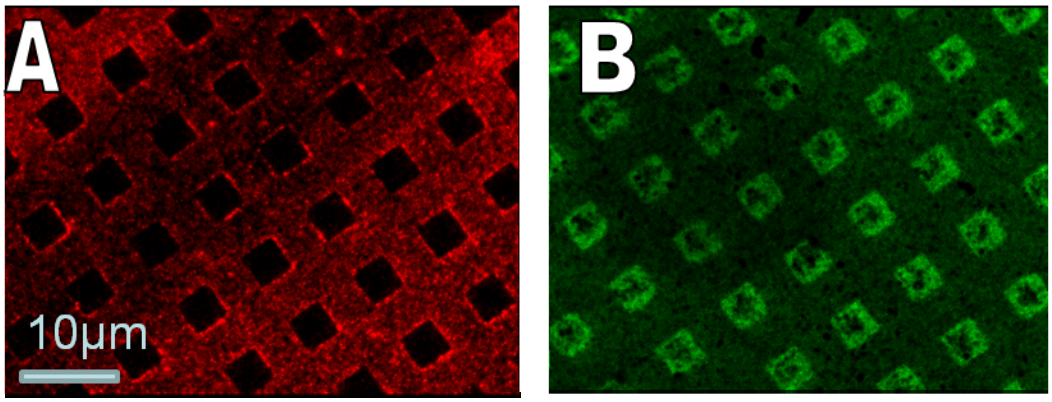


***Figure 21: OSM-µCP Pll-g-PEG, Ab-anti Gst after POPC SPBM formation.*** *A/ Fluorescence imaging of the Pll-g-PEG-Rhodamine. B/ fluorescence imaging where black spots correspond to the antibody patterns and green areas to the POPC SPBM.*

### iii. Conclusion

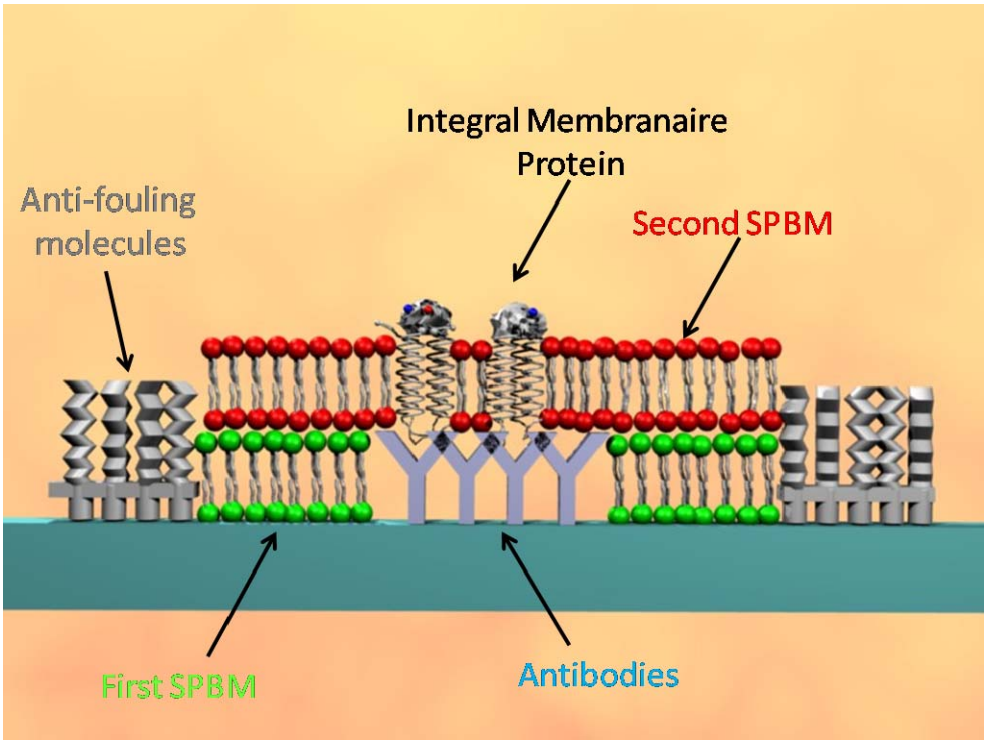


***Figure 22/ Schematic view of a complex surface architecture obtainable through OSM-µCP***

.

Figure 22 shows the final architecture we would like to reach in a near future. The primary steps are already achieved, Pll-g-PEG/antibody anti-GST patterns plus the POPC membrane. This architecture presents advantages compared to SPBM assembly and permits to graft at a desired location a trans-membrane proteins, without undesirable interactions with the support. The formation of the second layer will be the most challenging one and several ways will need to be tested. As noticed in chapter 2, the production and purification of trans-membrane proteins remains challenging, however we can use the presence of the GST tag to graft the primary brick of the BFNM on the surface , for example FliF-GST. The formation of a second bilayer covering the region of interest will mimic the inner bacteria environment. Other motors proteins will be incubated on this surface and their assembly can be investigated by AFM imaging. It will permit us to study in which conditions the BFNM self-assemble. A second approach would consist in the formation of proteoliposome presenting motor proteins. The formation of this structure remains challenging due to the insertion of pre purified

proteins into liposomes using detergent. However, we think that the feasibility of this system remains possible.

This approach represents in my mind the direction to follow in the future. The challenge encountered will require patience and skills in numerous fields: in nano-fabrication, surface chemistry and AFM imaging, but the results achievable could be applicable to a large number of bio-systems involving the assembly of different proteins.

## c. The Dynamical approach, Suspended Membrane

### i. Introduction

The second approach can be described as a dynamic approach and will have for objective to observe in vitro the movement of a reconstituted motor. This approach is tightly coupled to the static approach, where parameters which would allow the self-assembly of the motor will be defined. The major limitation of the previous approach remains the use of a SPBM as a native environment. As notified in chapter 3, only proteins of the cytoplasm side of the motor could be studied in this way, due to the difficulty to insert trans-membrane proteins. Even if we succeed to insert the trans-membrane proteins within the SPBM or into a proteo-liposome, the presence of a glass layer will reduce the possible movement of the trans-membrane proteins and constitute a major drawback. One of the possible ways to avoid that, will be to create a suspended membrane[38]. Scheuring *et al* have demonstrated through a system called "two chambers AFM" that formation of SPBM patches above a nano-hole opened the way to study trans-membrane proteins which can be free to move within a Suspended membrane. Unfortunately, this system is static. When the membrane sits on the hole there is no way for modifying the buffer in the two chambers independently. We pushed forward the idea and designed a system which couples this basic idea to a micro-fluidic device which allows the injection of different liquids on both sides of the suspended membrane. By this way, we can imagine recreate the pH gradient and observe using an attached nano-particle for example, the movement of the stator proteins. I will describe here the preliminary results about the design of this original fluidic device and the result

obtained on the formation of a PE-PG suspended membrane. Figure 23 displayed the final design including the suspended phospholipidic bilayer and trans-membrane proteins.

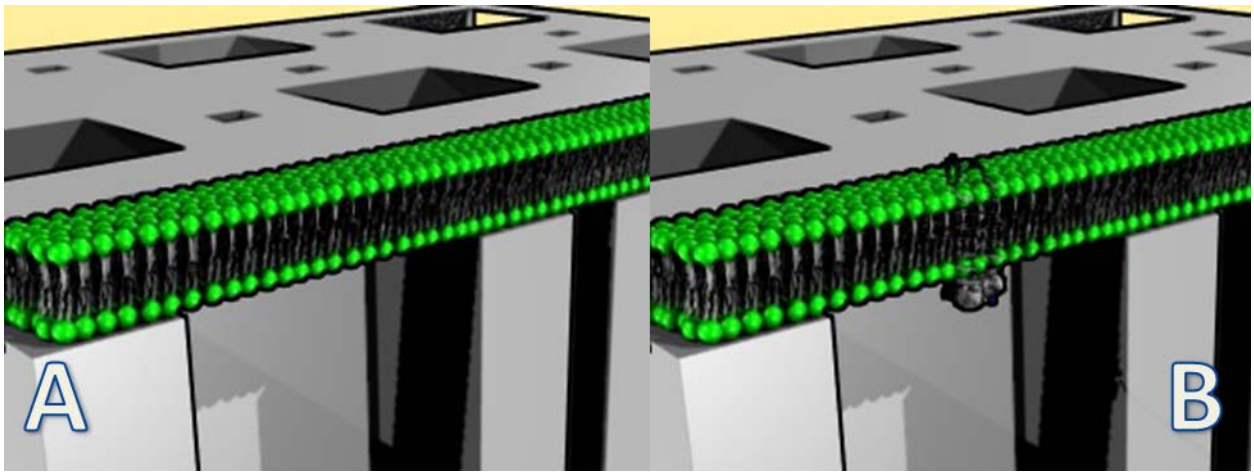


***Figure 23: Schematic view of the Suspended PBM (SUS-PBM) into the two chamber device.*** *A/ A Sus-PBM without trans-membrane proteins. B/ With a single protein, as for example MotA.*

### ii. System elaboration

The first step consists in spin-coating a 150 nm thick layer of poly (methyl metacrylate) resist (PMMA) on a cleaned Silicon On Insulator (SOI) wafer (Si: 230 nm/SiO2: 300nm/ Si: 500µm). Patterns and microchannels (300 nm holes with a step of 1µm) connecting the membrane to the reservoirs were defined in this positive resist using Electron Beam Lithography (EBL). After resist development, pattern transfer was achieved by Reactive Ion Etching (RIE). The targeted etch depth depends on the thickness of the first silicon level (~230 nm), but stops automatically on the silicon oxide due to the etching gas nature. Silicon oxide was then chemically etched by a 50% HF solution at a defined time. The principle of the formation relies on the isotropic etching of the buried Si02 layer by HF solution. The connection of neighboring cavities etched with HF will leave a Si top layer membrane, pierced with nanoholes and suspended by $SiO_2$ pillars see figure 24. To enable capillary invasion of the system a chemical treatment with Sulfochromic mixture during 5 min was carried out. Figure 24 shows the technical steps.

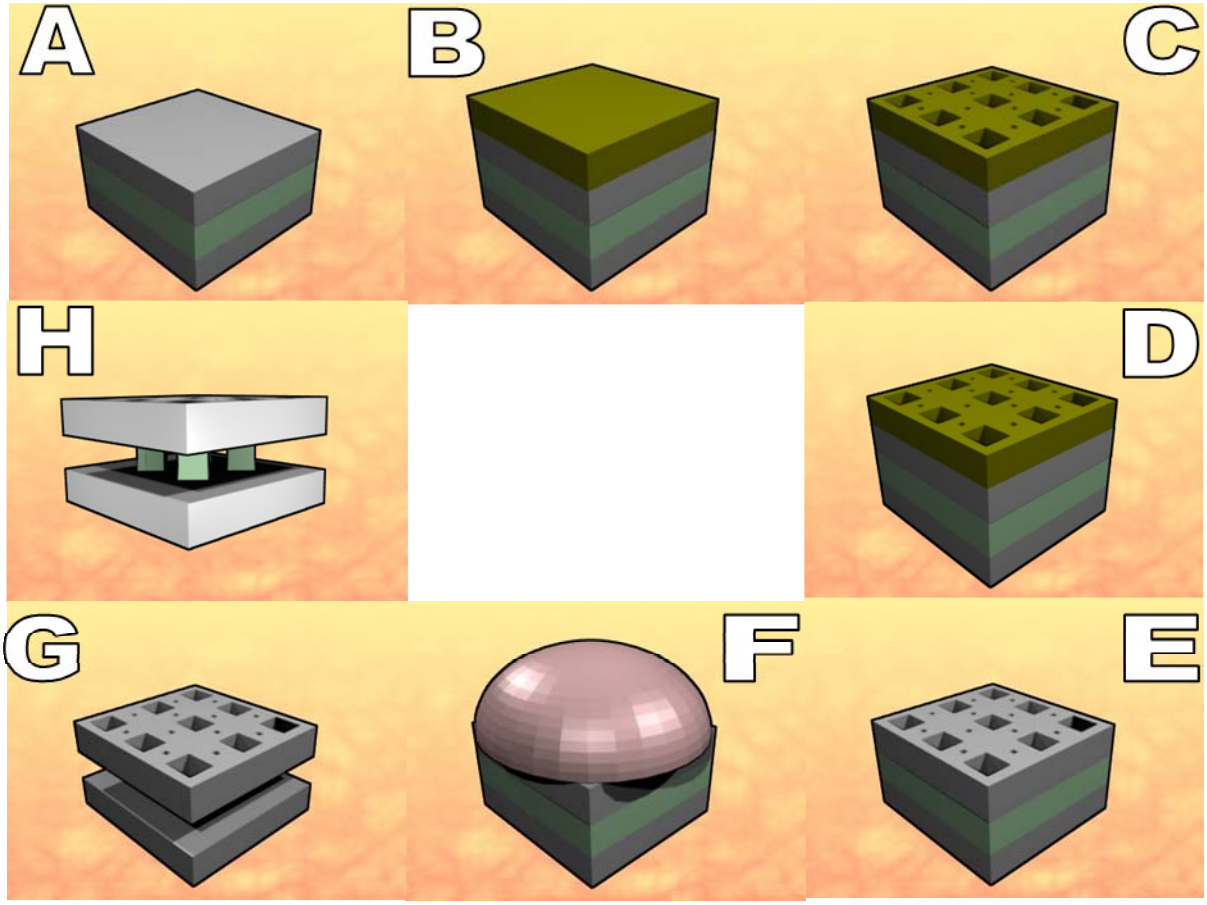


***Figure 24: technological steps****. A/ A SiO wafer composed of three layer, silicon ( grey) silicon oxide (blue) and silicon (grey), is cleaned and prepared for resist deposit in B/. C/ resist is patterned using an electron-beam lithography system, then developped using a mixture of isopropanol/MIBK Two patterns are visible on the surface, allowing later the HF to penetrate and chemically etches the under layer of SOI. D/ patterns are transferred to the silicon layer using RIE etching. E/ Resist is removed. F/ The wafer is immersed in an HF buffer during a controlled etching time. HF buffer dissolved the silicon oxide, here in blue. G/ The wafer is extensively washed using pure water. H/ From the silicon oxide layer, only pillars remain and sustain the upper silicon layer.*

The final two chamber system is shown in figure 25.

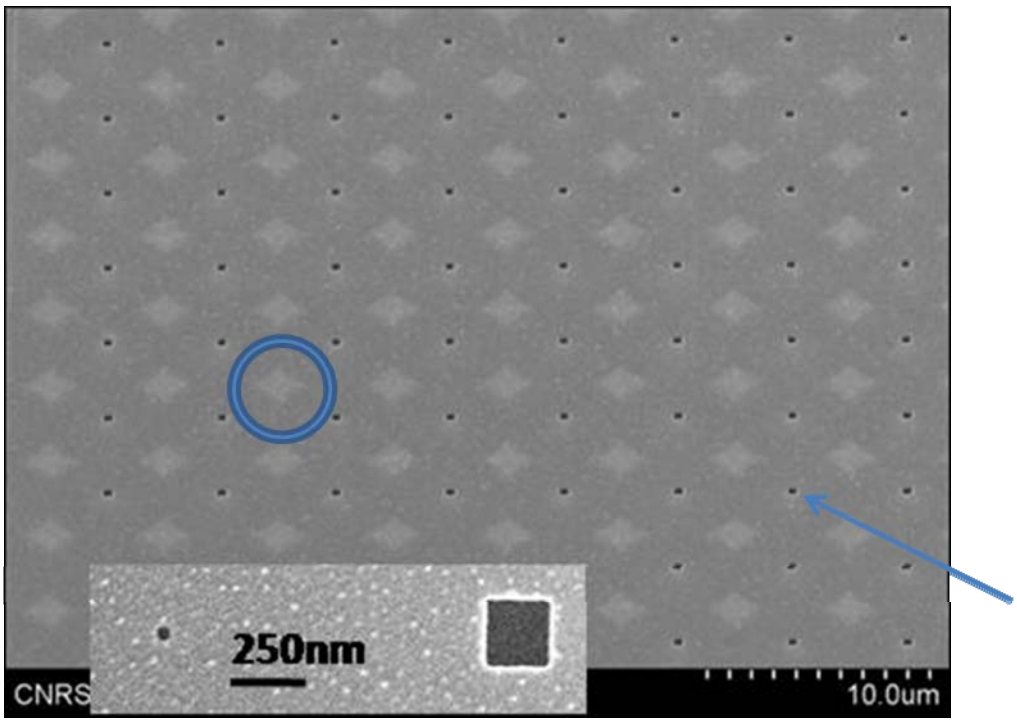


***Figure 25: SEM images of nanoholes used for etching s SOI substrate and for a suspended membrane.*** *Supporting pillars are clearly visible above the silicon surface. Blue circle/ $SiO_2$ pillars seen in transparency. Blue arrow/ cavities etched through a nanohole. An enlarged view show two nano-holes of different sizes.*

Controlling the speed of chemical etching is a key point of this technology; several issues about the chemical etching using HF were addressed during the system elaboration and are discussed largely by Thibault *et al*[39]. It turned out that two holes sizes were needed and designed at the silicon surface, a larger one of 250 nm and a second one of 50 nm. Based on their studies, etching can not occurred for hole smaller than 250 nm, probably due to an effect coming from the surface energy inside the hole which block the capillary effect and avoid the HF to etch. The etching process needed to minimize the deformation of the silicon membrane for avoiding any possible break during handling and for preserving the ability of AFM imaging at high resolution; this is why the structure was mechanically stabilized with Silicon oxide pillars as can be seen in figure 25. These pillars are formed spontaneously by the under etching. For our purpose the array of holes was then designed and the etching time calculated such as silicon oxide

pillars are formed spontaneously between the connected cavities generated below each hole.

iii. Preliminary results

Two results were achieved on this type of system, fluidic experiments and the formation of a Suspended Phospholipids Bilayer Membrane (SUS-PBM).The complete microfluidic device (figure 23) is composed of three different parts. The first one is the porous silicon membrane with an array of nanometric size holes (middle part). The size of this central region was designed for compatibility with the fluidic chamber of commercial bio AFM systems. The second part is composed of two reservoirs, one for the entrance of liquid, the other one for the exit. The last part is composed of micrometric channels, which connect the different parts of the system. A drop of water was placed in one of the reservoirs and we observed the movement of water inside the device. The filling of the cavity below the porous silicon membrane was follow, the liquid solution moved from one reservoir to the other by capillary invasion.

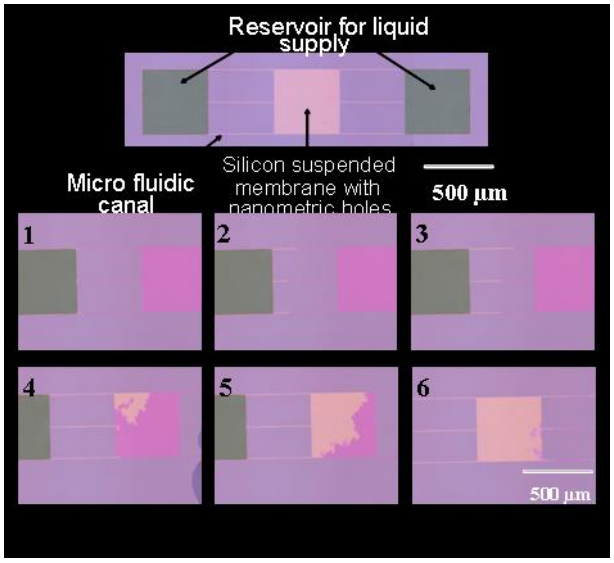


***Figure 26: Microfluidic experiments on the two chamber AFM device.*** *Top view/ the Overall system. 1 - 6,optical images of the filling of the buried channel with water.*

During these experiments we never observed any escape of water through the nanometric holes (50-200 nm) of the Silicon membrane. AFM images of figure 27 display the first result obtained on this system with a membrane called “purple

membrane" composed of bacteriorhodopsin proteins. This membrane has been widely studied and represents a validation experiment of our system.

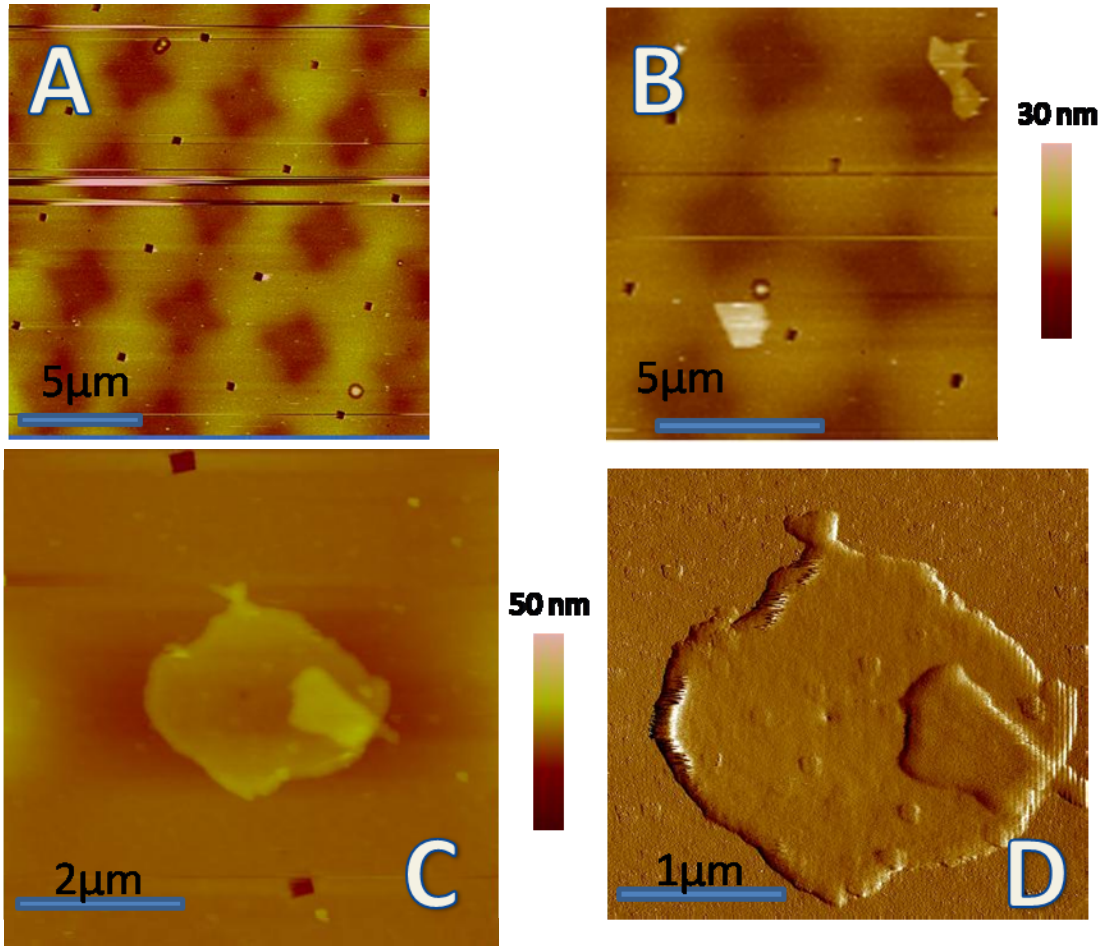


***Figure 27: BR membrane on the two chambers AFM device.*** *A/ Large view of several holes on the surface,height signal. B/ Enlarged view with few membrane patch on the surface. C/ patch located between two 250 nm holes and covering the 50 nm hole this patch forms a suspended BR membrane. D/ vertical deflection signal of the patch.*

The system developed here has shown promising results, for both technological aspects and formation of SPBM patches. Several designs will be required to fulfill all the questions about membrane activies and role. However, the next immediate steps will consist of a formation of POPC or PE-PG membrane on this surface, before insertion of trans-membrane proteins. The needs to separate both inner and top liquid will be also crucial in order to image the possible deformation of trans-membrane proteins while passing cations or others chemical elements.

### iv. Conclusions

The system is now ready and all the technological steps have been addressed. However, some points require further studies. For being sure that the system will be relevant, the SUS-PBM should form on every hole of the surface, for limiting the diffusion and mix of the different liquids, and this point remains critical using a PE-PG lipid mixture. The use of others lipids and the elaboration of a surface with a low numbers of hole could address this issue. The insertion of proteins will be the next major step of the work. Once this step will be overpassed, this system will be useful to follow dynamical change into trans-membrane systems, as for example the stator assembly. AFM could be used, for structural analysis, but also some biophysical tools such as for example the single particle tracking (SPT) could be also very interesting on these SUS-PBM.

## d. 3D reconstruction

Most of the results I have presented can be considered as the direct follow of the work presented in the second chapter of this manuscript, but these two approaches, static or dynamic will encountered the same expected problem: How to work on trans-membrane proteins? How to produce them? How to observe them in an environment as close as possible of the native one? As already noticed, the most intriguing part of the BFNM resides within the membrane, the stator complex. MotA and MotB (for its membrane part) structures remain unknown and as far as I know. I think that we can only address the question of the BFNM function by a radical change of method and tools. Until recently, working on membrane elements has been limited by the purification steps and insertion into preformed SPBM. If we think about the philosophy behind that approach, it consists of creating two separate purified elements, which do not really like to be separated and trying to re-assemble them later. As I demonstrated in chapter 3, this approach is valid for cytoplasmic elements, but it will fail for hydrophobic or membrane elements. The need for complex and non controlled chemical protocols involving detergents renders this way difficult to generalize to all membrane assembly. However, I think that this issue can be addressed by a new strategy based on one of the recent tools

developed under the term of synthetic biology. By extracting and encapsulating the bacterial cytoplasm, it is now possible to produce in a controlled way numerous proteins directly into a liposome, as demonstrated by Noireaux *et al* [40] for GFP proteins and later for a membrane element: α-hemolysin. I think that this approach will open the way to reproduce the BFNM, fully or partially, into a 3 dimensionnal structure without the needs for detergent or purification steps. The membrane, exhibiting trans-membrane proteins will be ready for analysis using various such tools as AFM or fluorescence imaging. The major impact will consist of the homogeneity of the structure assembled which reduces the problem of AFM imaging on native bacteria. By mixing this technology to the tools developed during my thesis, it will open numerous possibilities for assembling and studying nano-bio-machines of Nature.

[1]G.M. Whitesides, Nat Biotech 21 (2003) 1161.
[2]M. Stephen, Angewandte Chemie International Edition 47 (2008) 5306.
[3]S. Nakamura, N. Kami-ike, J.-i.P. Yokota, S. Kudo, T. Minamino, K. Namba, Journal of Molecular Biology 386 (2009) 332.
[4]D.R. Thomas, N.R. Francis, C. Xu, D.J. DeRosier, J. Bacteriol. 188 (2006) 7039.
[5]D.R. Thomas, D.G. Morgan, D.J. DeRosier, Proceedings of the National Academy of Sciences 96 (1999) 10134.
[6]D. Thomas, D.G. Morgan, D.J. DeRosier, J. Bacteriol. 183 (2001) 6404.
[7]G.E. Murphy, J.R. Leadbetter, G.J. Jensen, 442 (2006) 1062.
[8]J. Zhou, L.L. Sharp, H.L. Tang, S.A. Lloyd, S. Billings, T.F. Braun, D.F. Blair, J. Bacteriol. 180 (1998) 2729.
[9]T. Yorimitsu, A. Mimaki, T. Yakushi, M. Homma, Journal of Molecular Biology 334 (2003) 567.
[10]P.N. Brown, C.P. Hill, d.F. Blair, The EMBO journal 21 (2002) 3225.
[11]D.F. Blair, FEBS Letters
Protonmotive Mechanisms of Energy Transducing Enzymes 545 (2003) 86.
[12]M.C. Leake, J.H. Chandler, G.H. Wadhams, F. Bai, R.M. Berry, J.P. Armitage, Nature 443 (2006) 355.
[13]Y. Sowa, A.D. Rowe, M.C. Leake, T. Yakushi, M. Homma, A. Ishijima, R.M. Berry, Nature 437 (2005) 916.
[14]S.W. Reid, M.C. Leake, J.H. Chandler, C.-J. Lo, J.P. Armitage, R.M. Berry, Proceedings of the National Academy of Sciences 103 (2006) 8066.
[15]K. Yonekura, T. Yakushi, T. Atsumi, S. Maki-Yonekura, M. Homma, K. Namba, Journal of Molecular Biology 357 (2006) 73.
[16]E.R. Hosking, M.D. Manson, J. Bacteriol. 190 (2008) 5517.
[17]J. Yuan, H.C. Berg, Proceedings of the National Academy of Sciences 105 (2008) 1182.
[18]S. Kojima, D.F. Blair, Biochemistry 43 (2004) 26.
[19]T.F. Braun, L.Q. Al-Mawsawi, S. Kojima, D.F. Blair, Biochemistry 43 (2004) 35.
[20]Q. Wen, G. Li, J. Tang, G. Huber, Journal of Statistical Physics 128 (2007) 257.
[21]C.M. Dyer, A.S. Vartanian, H. Zhou, F.W. Dahlquist, Journal of Molecular Biology In Press, Uncorrected Proof (2009).
[22]Cohen-Ben-Lulu, et al., The EMBO Journal 27 (2008) 1134.
[23]S.-Y. Park, B. Lowder, A.M. Bilwes, D.F. Blair, B.R. Crane, Proceedings of the National Academy of Sciences 103 (2006) 11886.
[24]G.H. Wadhams, J.P. Armitage, Nat Rev Mol Cell Biol 5 (2004) 1024.
[25]T.A.J. Duke, N. Le Novere, D. Bray, Journal of Molecular Biology 308 (2001) 541.
[26]J. Chalmeau, C. Thibault, F. Carcenac, C. Vieu, Applied Physics Letters 93 (2008) 133901.
[27]A. Bietsch, B. Michel, Applied Physics Letters 88 (2000) 4310.
[28]A. Kumar, G.M. Whitesides, Applied Physics Letters 63 (1993) 2002.
[29]B.C. Wheeler, J.M. Corey, G.J. Brewer, D.W. Branch, Journal of Biomechanical Engineering 121 (1999) 73.
[30]J.P.R. A. Bernard, B. Michel, H. R. Bosshard, E. Delamarche,, Advanced Materials 12 (2000) 1067.

[31]P.F. Xiao, N.Y. He, Z.C. Liu, Q.G. He, X. X. Sun, Z.H. Lu, Nanotechnology 13 (2002) 756.
[32]H.D. Inerowicz, S. Howell, F.E. Regnier, R. Reifenberger, Langmuir 18 (2002) 5263.
[33]Andrés J.G.E.D. Sean R. Coyer, Angewandte Chemie International Edition 46 (2007) 6837.
[34]J. Tien, C.M. Nelson, C.S. Chen, Proceedings of the National Academy of Sciences 99 (2002) 1758.
[35]C. Crozatier, M.L. Berre, Y. Chen, Microelectronic Engineering
Micro- and Nano-Engineering MNE 2005 83 (2006) 910.
[36]J. Chalmeau, L. Salomé, C. Thibault, C. Severac, C. Vieu, Microelectronic Engineering 84 (2007) 1754.
[37]J. ShaikhMohammed, M.A. DeCoster, M.J. McShane, Langmuir 22 (2006) 2738.
[38]R.P. Goncalves, G. Agnus, P. Sens, C. Houssin, B. Bartenlian, S. Scheuring, Nat Meth 3 (2006) 1007.
[39]C. Thibault, F. Carcenac, E. Dague, J. Chalmeau, C. Vieu, Microelectronic Engineering In Press, Corrected Proof (2008).
[40]V. Noireaux, A. Libchaber, Proceedings of the National Academy of Sciences of the United States of America 101 (2004) 17669.

# Conclusions

The BFNM is a fabulous machine and its mechanism, as described and deciphered during this work remains a formidable subject of research. It will probably take several years to finally understand completely its mechanism. Our approach based on interactions and structural data, can be considered as a new methodology for studying such a complex system as the BFNM, and we hope that our contribution will be considered in the future. We have not answered definitely all the questions about the BFNM mechanism, and our tentative model will need now to be confronted to model data, as for example the torque speed relationship, and also data issues from crystal proteins structure. Numerous experiments can now be performed to confirm or decline our vision of the BFNM. The different tools we have developed require a mix of micro-biology, genetics and nanotechnologies even deeper than what I have done during the last three years. It represents the key for the success of this cognitive project and will require high skills in each domain. However the challenge ahead is far from being impossible and I hope that I have convinced you of the interest of our ideas and approaches.

Conference

-03/2006 France USA Workshop on NanoBio-technologies, Washington DC, USA
Poster
“Flanamo, Elucidate the mystery of the flagellum nanomotor using Nanotechnology”
J. Chalmeau, C.Thibault, F. Carcenac, C. Le Grimellec, M.C. Giocondi, L. Salomé, J.M Francois, A. Dagkessamanskaia, E. Trevisiol, J. Sternick and C .Vieu

-07/2006 Summer school “The live cell from nano to micro, mind the gap!”Cargese, Corse
Poster
“Elucidate structure of complex biological using supported bilayer membrane”
J. Chalmeau, C.Thibault, F. Carcenac, L. Salomé, and C .Vieu

-09/2006 Micro and Nano Engineering Barcelona, MNE2006, Espagne
Poster
“Elaboration of Micro domains of supported bilayer using Microcontact printing”
J. Chalmeau, C.Thibault, F. Carcenac, L. Salomé and C .Vieu

-04/2007 AFMBiomed Barcelona 2007, Espagne
Poster
“Supported bilayer membrane domains at the Nano-scale”
J. Chalmeau, C.Thibault, F. Carcenac, C. Le Grimellec. M.C. Giocondi, L. Salomé and C .Vieu

-09/2007 Doctoriale Université de Toulouse, France
Poster
« Reconstituer le petit moteur biologique du Monde, Micro et Nanotechnologies appliquées au moteur flagellaire des bacteries »
J. Chalmeau and C .Vieu

-11/2007 Micro Nano Conference, Kyoto, Japon , MNC2007
Poster
“Micro-Contact Printing of different biomolecules in one step using deformable Poly(dimethylsiloxane)-based stamps”
J. Chalmeau, C.Thibault, F. Carcenac and C .Vieu

-06/2008 International Scanning Probe Microscopy, Seattle, USA, ISPM2008
Oral presentation
“Contribution to the elucidation of the structure of the bacteria flagellum nanomotor through AFM imaging of the M-ring”
J. Chalmeau, C. Le Grimellec. M.C. Giocondi, J.M Francois, A. Dagkessamanskaia, J. Sternick and C .Vieu

-09/2008 ITAV workshop “Nanobiotechnologies une dynamique regionale, nationale et européenne”, Toulouse, France
Oral présentation
« Apport des Nanotechnologies à l’etude et a l’assemblage du nanomoteur du flagelle des bacteries »
J. Chalmeau, C.Thibault, F. Carcenac, C. Le Grimellec. M.C. Giocondi, L. Salomé, J.M Francois, A. Dagkessamanskaia, E. Trevisiol, J. Sternick and C .Vieu

-09/2008 Micro and Nano Engineering, Athenes, Greece, MNE2008
Poster
“Coupling bio-assembly and surface patterning:partial reconstitution of a biological nano-machine the flagellar nano-motor of bacteria”
J. Chalmeau, C.Thibault, F. Carcenac, C. Le Grimellec. M.C. Giocondi, J.M Francois, A. Dagkessamanskaia, J. Sternick and C .Vieu

“Porous silicon membrane, with an integrated aqueous supply, for two chamber AFM”
J. Chalmeau, C.Thibault, F. Carcenac and C .Vieu

-10/2008 JPK Nanobioviews workshop SPM in life sciences, Berlin, Allemagne
Oral presentation “Overlay for membrane-Bound protein bioship”
J. Chalmeau, C.Thibault, F. Carcenac, C. Le Grimellec. M.C. Giocondi, J.M Francois, A. Dagkessamanskaia, J. Sternick and C .Vieu

-10/2008 AFMBiomed 2008 Monterey, USA
Poster “Coupling soft nano-patterning and self-assembly for the study of membrane proteins”
J. Chalmeau, C.Thibault, F. Carcenac, J.M Francois, A. Dagkessamanskaia, J. Sternick and C .Vieu

Papers:

-“Elaboration of micro-domains of supported bilayer membranes using micro-contact printing” Microelectronic Engineering Vol 84, (5-8), 1754-1757 Proceedings of the 32nd International Conference on Micro- and Nano-Engineering
J. Chalmeau, C.Thibault, F. Carcenac, L. Salomé and C .Vieu

-“Micro-contact printing of two different biomolecules in one step using deformable poly(dimethylsiloxane)-based stamp” JAPANESE JOURNAL OF APPLIED PHYSICS vol 47 (6), 5221-5225
J. Chalmeau, C.Thibault, F. Carcenac and C .Vieu

-“Self-aligned patterns of multiple biomolecules printed in one step”, Appl Phys Lett, Vol 93 (13) applied biophysics
J. Chalmeau, C.Thibault, F. Carcenac and C .Vieu

-“Contribution to the elucidation of the structure of the bacteria flagellum nanomotor through AFM imaging of the M-ring”, Utramicroscopy special issue ISPM2008,
J. Chalmeau, C.Thibault, F. Carcenac, C. Le Grimellec, J.M Francois, A. Dagkessamanskaia, J. Sternick and C .Vieu
Under press

-“Porous silicon membrane, with an integrated aqueous supply, for two chamber AFM”, Microelectronic Engineering proceedings ,
J. Chalmeau, C.Thibault, F. Carcenac and C .Vieu
Under press

-“Micro and nanopatches of Supported phospholipidics bilayer using MicroContactPrinting of Pll-g-PEG as barriers”,
J. Chalmeau, C.Thibault, F. Carcenac, C. Le Grimellec,, L. Salomé, J. Sternick and C .Vieu
Langmuir, under correction

-“Coupling bio-assembly and surface patterning: Partial reconstitution of a biological nano-machine, the flagellar nano-motor of bacteria”,
J. Chalmeau, C.Thibault, F. Carcenac, C. Le Grimellec, J.M Francois, A. Dagkessamanskaia, , J. Sternick and C .Vieu
Lab-on-chip, under correction

-“Studying the interaction between flagellar nano motor proteins using QCM-D technology, a new insight into the motor function”,
J. Chalmeau, J.M Francois, A. Dagkessamanskaia, E. Trevisiol, J. Sternick and C .Vieu
Journal of Molecular Biology, under correction

Conference

-03/2006 France USA Workshop on NanoBio-technologies, Washington DC, USA
Poster
“Flanamo, Elucidate the mystery of the flagellum nanomotor using Nanotechnology”
J. Chalmeau, C.Thibault, F. Carcenac, C. Le Grimellec, M.C. Giocondi, L. Salomé, J.M Francois, A. Dagkessamanskaia, E. Trevisiol, J. Sternick and C .Vieu

-07/2006 Summer school “The live cell from nano to micro, mind the gap!”Cargese, Corse
Poster
“Elucidate structure of complex biological using supported bilayer membrane”
J. Chalmeau, C.Thibault, F. Carcenac, L. Salomé, and C .Vieu

-09/2006 Micro and Nano Engineering Barcelona, MNE2006, Espagne
Poster
“Elaboration of Micro domains of supported bilayer using Microcontact printing”
J. Chalmeau, C.Thibault, F. Carcenac, L. Salomé and C .Vieu

-04/2007 AFMBiomed Barcelona 2007, Espagne
Poster
“Supported bilayer membrane domains at the Nano-scale”
J. Chalmeau, C.Thibault, F. Carcenac, C. Le Grimellec. M.C. Giocondi, L. Salomé and C .Vieu

-09/2007 Doctoriale Université de Toulouse, France
Poster
« Reconstituer le petit moteur biologique du Monde, Micro et Nanotechnologies appliquées au moteur flagellaire des bacteries »
J. Chalmeau and C .Vieu

-11/2007 Micro Nano Conference, Kyoto, Japon , MNC2007
Poster
“Micro-Contact Printing of different biomolecules in one step using deformable Poly(dimethylsiloxane)-based stamps”
J. Chalmeau, C.Thibault, F. Carcenac and C .Vieu

-06/2008 International Scanning Probe Microscopy, Seattle, USA, ISPM2008
Oral presentation
“Contribution to the elucidation of the structure of the bacteria flagellum nanomotor through AFM imaging of the M-ring”
J. Chalmeau, C. Le Grimellec. M.C. Giocondi, J.M Francois, A. Dagkessamanskaia, J. Sternick and C .Vieu

-09/2008 ITAV workshop “Nanobiotechnologies une dynamique regionale, nationale et européenne”, Toulouse, France
Oral présentation
« Apport des Nanotechnologies à l’etude et a l’assemblage du nanomoteur du flagelle des bacteries »
J. Chalmeau, C.Thibault, F. Carcenac, C. Le Grimellec. M.C. Giocondi, L. Salomé, J.M Francois, A. Dagkessamanskaia, E. Trevisiol, J. Sternick and C .Vieu

-09/2008 Micro and Nano Engineering, Athenes, Greece, MNE2008
Poster
“Coupling bio-assembly and surface patterning:partial reconstitution of a biological nano-machine the flagellar nano-motor of bacteria”
J. Chalmeau, C.Thibault, F. Carcenac, C. Le Grimellec. M.C. Giocondi, J.M Francois, A. Dagkessamanskaia, J. Sternick and C .Vieu

“Porous silicon membrane, with an integrated aqueous supply, for two chamber AFM”
J. Chalmeau, C.Thibault, F. Carcenac and C .Vieu

-10/2008 JPK Nanobioviews workshop SPM in life sciences, Berlin, Allemagne
Oral presentation “Overlay for membrane-Bound protein bioship”
J. Chalmeau, C.Thibault, F. Carcenac, C. Le Grimellec. M.C. Giocondi, J.M Francois, A. Dagkessamanskaia, J. Sternick and C .Vieu

-10/2008 AFMBiomed 2008 Monterey, USA
Poster “Coupling soft nano-patterning and self-assembly for the study of membrane proteins”
J. Chalmeau, C.Thibault, F. Carcenac, J.M Francois, A. Dagkessamanskaia, J. Sternick and C .Vieu

Papers:

-“Elaboration of micro-domains of supported bilayer membranes using micro-contact printing” Microelectronic Engineering Vol 84, (5-8), 1754-1757 Proceedings of the 32nd International Conference on Micro- and Nano-Engineering
J. Chalmeau, C.Thibault, F. Carcenac, L. Salomé and C .Vieu

-“Micro-contact printing of two different biomolecules in one step using deformable poly(dimethylsiloxane)-based stamp” JAPANESE JOURNAL OF APPLIED PHYSICS vol 47 (6), 5221-5225
J. Chalmeau, C.Thibault, F. Carcenac and C .Vieu

-“Self-aligned patterns of multiple biomolecules printed in one step”, Appl Phys Lett, Vol 93 (13) applied biophysics
J. Chalmeau, C.Thibault, F. Carcenac and C .Vieu

-“Contribution to the elucidation of the structure of the bacteria flagellum nanomotor through AFM imaging of the M-ring”, Utramicroscopy special issue ISPM2008,
J. Chalmeau, C.Thibault, F. Carcenac, C. Le Grimellec, J.M Francois, A. Dagkessamanskaia, J. Sternick and C .Vieu
Under press

-“Porous silicon membrane, with an integrated aqueous supply, for two chamber AFM”, Microelectronic Engineering proceedings ,
J. Chalmeau, C.Thibault, F. Carcenac and C .Vieu
Under press

-“Micro and nanopatches of Supported phospholipidics bilayer using MicroContactPrinting of Pll-g-PEG as barriers”,
J. Chalmeau, C.Thibault, F. Carcenac, C. Le Grimellec,, L. Salomé, J. Sternick and C .Vieu
Langmuir, under correction

-“Coupling bio-assembly and surface patterning: Partial reconstitution of a biological nano-machine, the flagellar nano-motor of bacteria”,
J. Chalmeau, C.Thibault, F. Carcenac, C. Le Grimellec, J.M Francois, A. Dagkessamanskaia, , J. Sternick and C .Vieu
Lab-on-chip, under correction

-“Studying the interaction between flagellar nano motor proteins using QCM-D technology, a new insight into the motor function”,
J. Chalmeau, J.M Francois, A. Dagkessamanskaia, E. Trevisiol, J. Sternick and C .Vieu
Journal of Molecular Biology, under correction

# Annex 1: Qsense data

X/Y interactions; X is the fixed proteins and Y the injected. The concentration indicated on the figures is about the injected proteins. I just present here the raw data of the numerous couples of proteins studied and presented in chapter 2. All interactions presented here have been made in PBS buffer at different pH: 5; 6; 7,4 and 9. Proteins have been defreezing just prior experiments and pH adjusted 5 minutes before injection. Some interactions have not been presented in this document due to their negative results.

## .C-ring/ C-ring interactions

*-FliM/FliM*

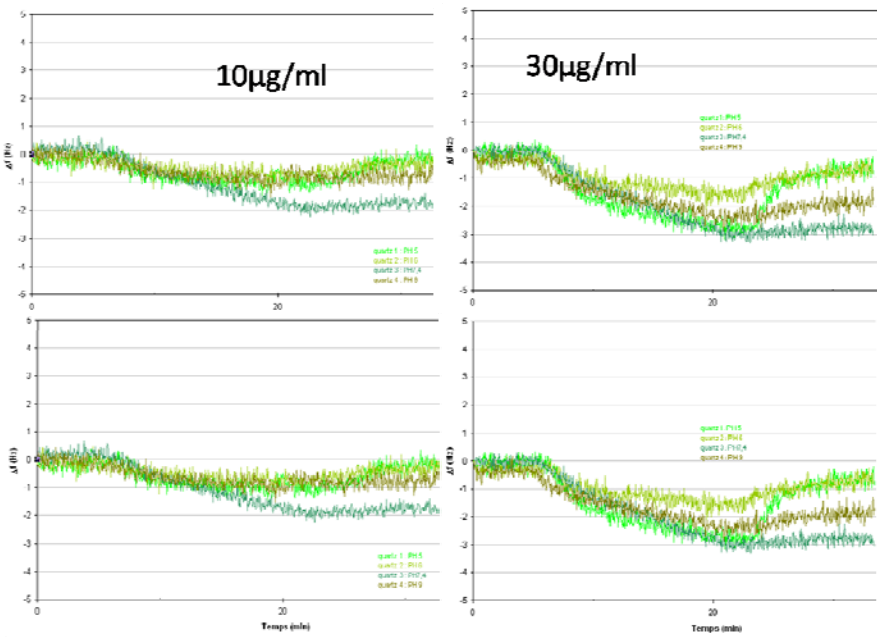


*-FliM/FliN*

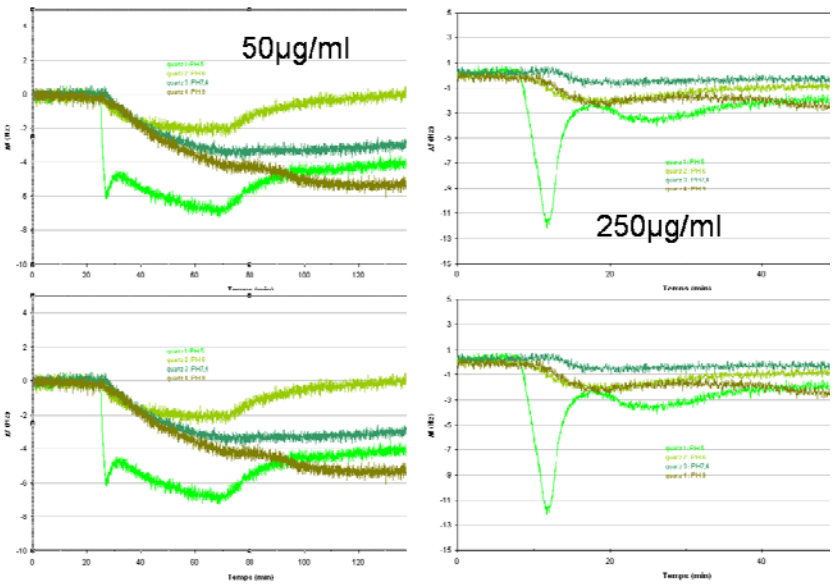

*-FliN/FliM*

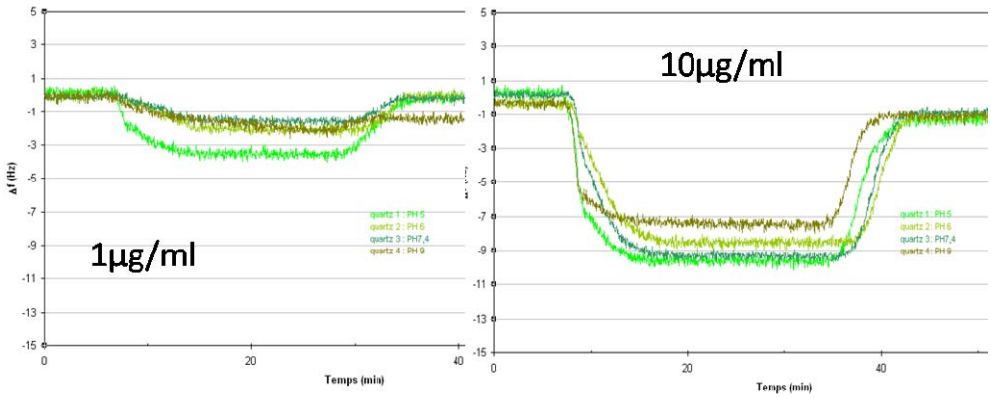


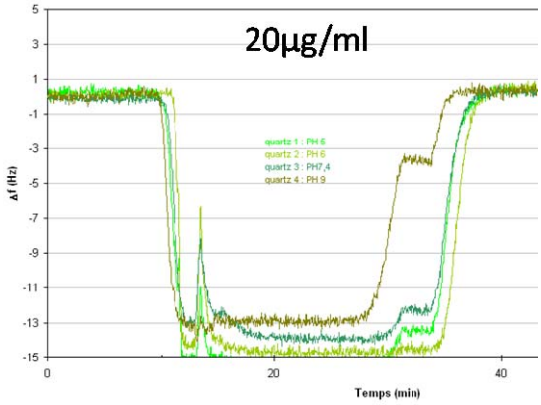


*-FliN/FliN*

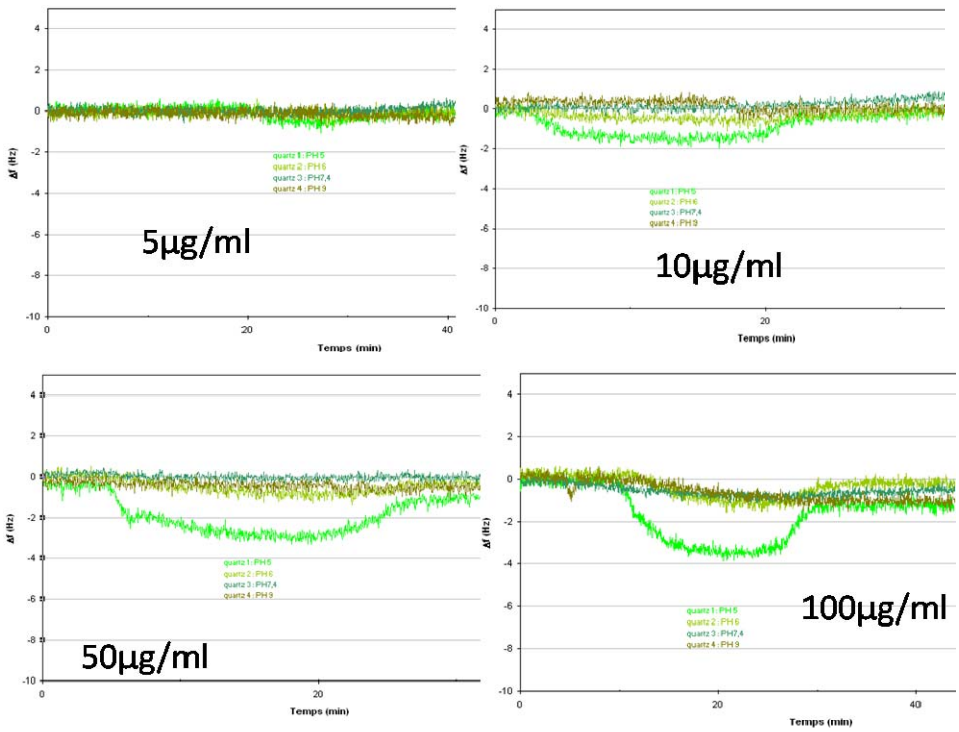

## .Rotor/ C-ring interactions

*-FliG/FliM*

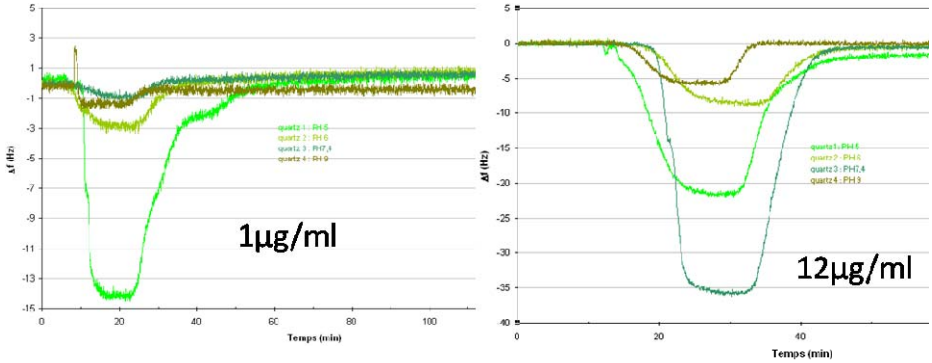


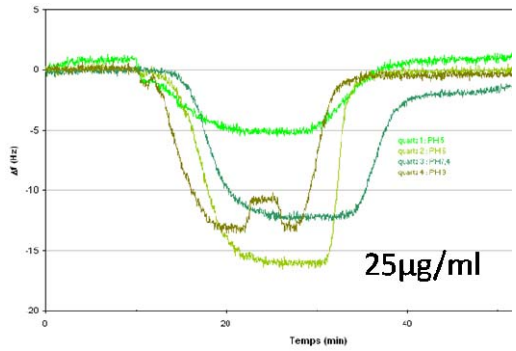


*-FliG/FliN*

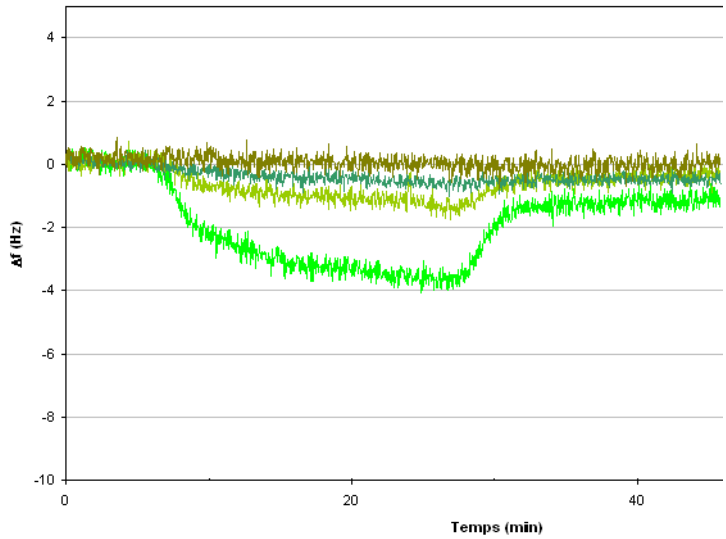

*-FliM FliG*

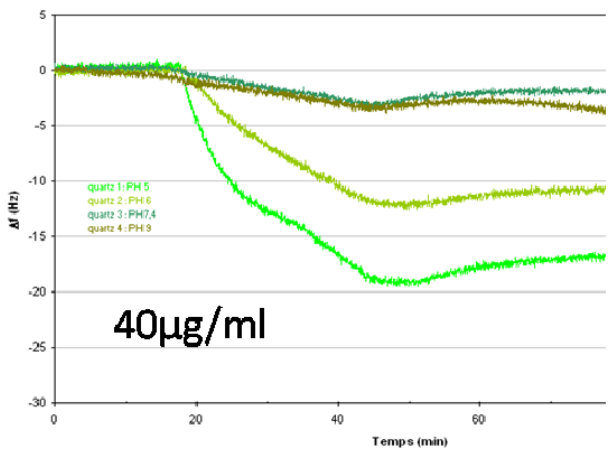


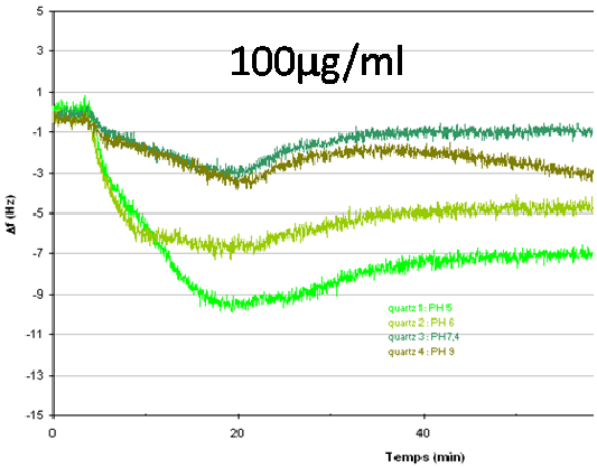


*-FliN/FliG*

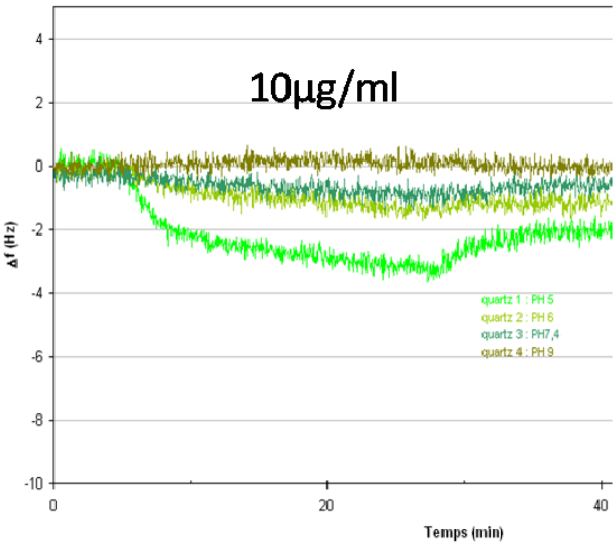


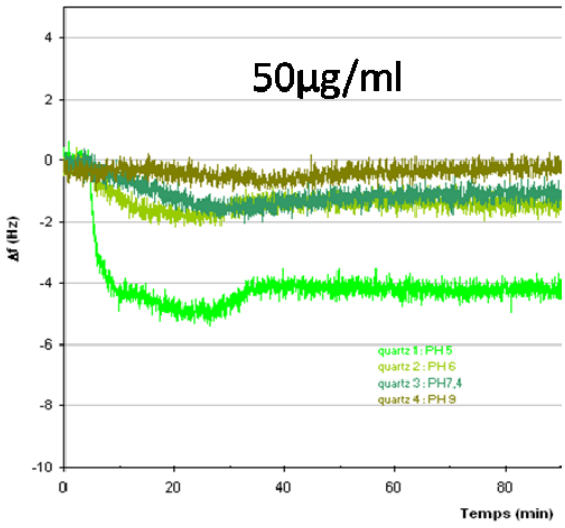


## .Stator/ C-ring interactions

*-FliM/MotB*

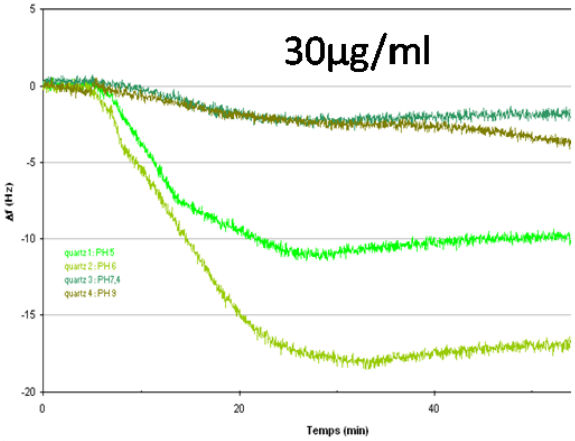


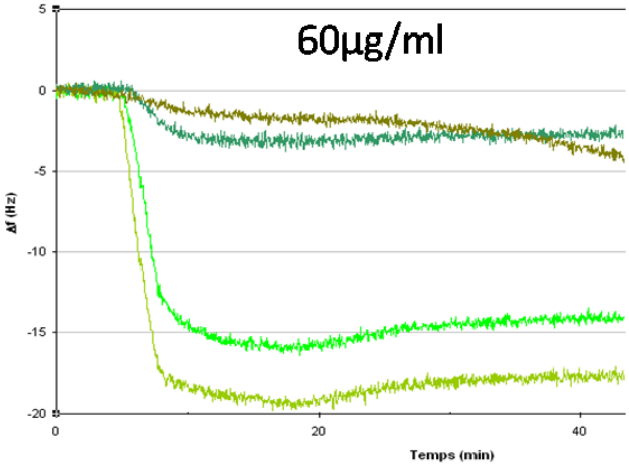

*-FliN/MotB*

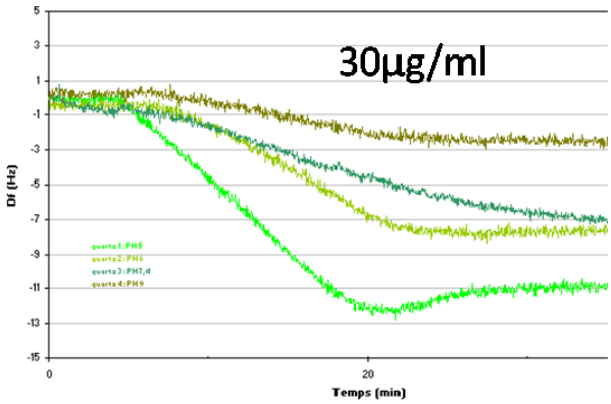


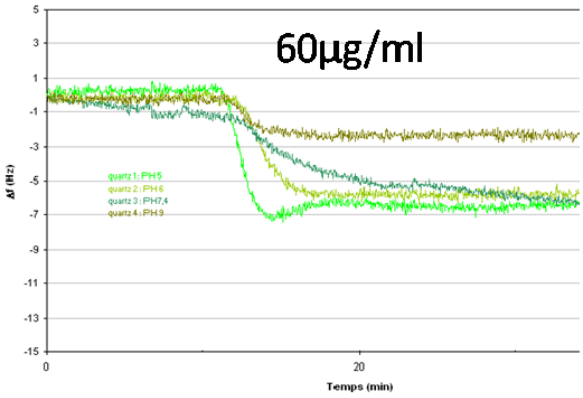


*-MotA/FliM*

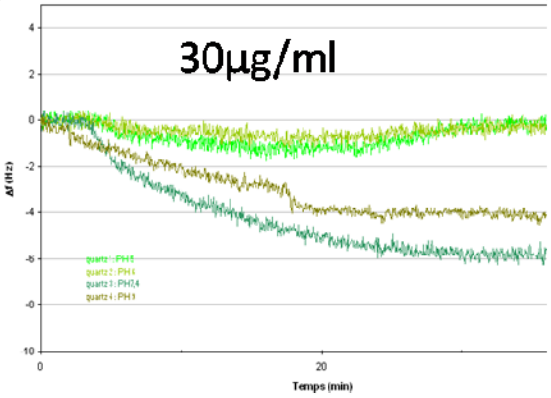


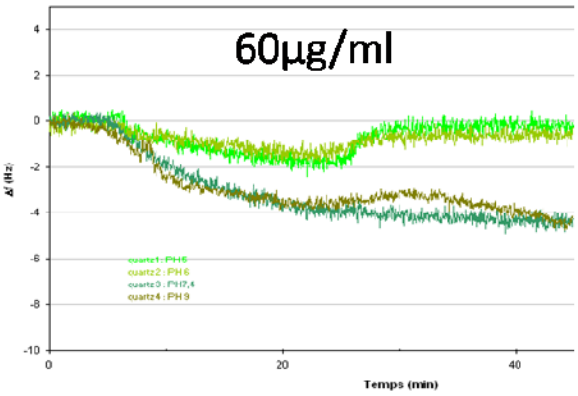


*-MotA/FliN*

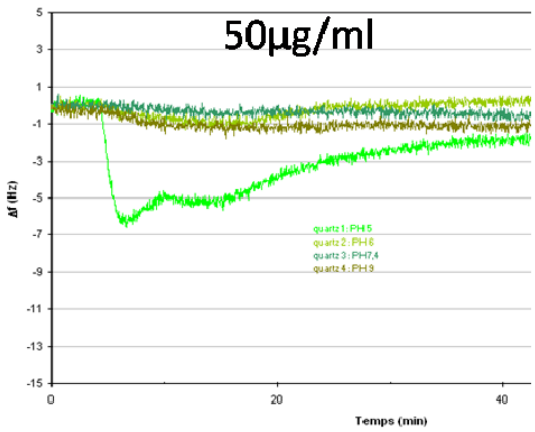


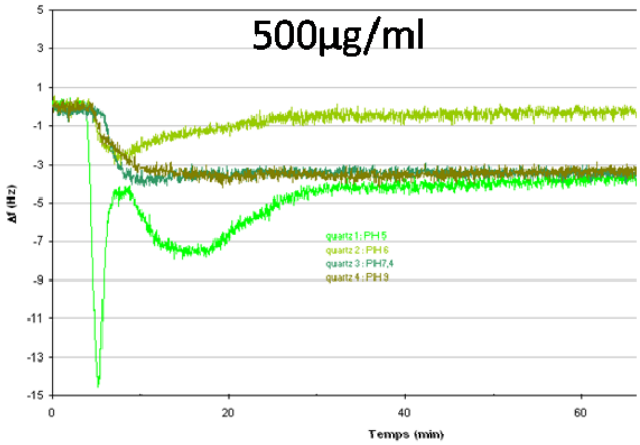

*-MotB/FliN*

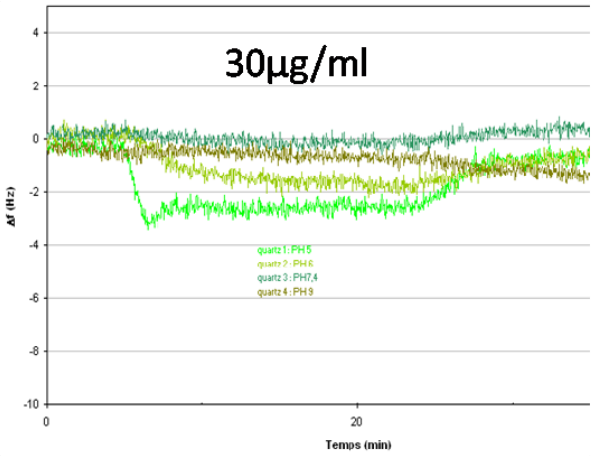


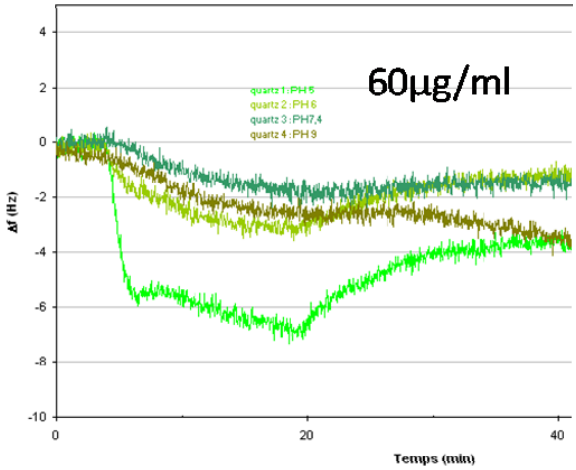


## .Stator/ Stator interactions

*-MotA/MotB*

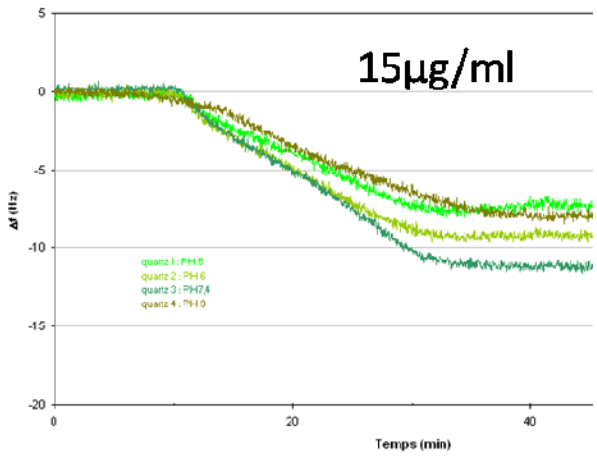


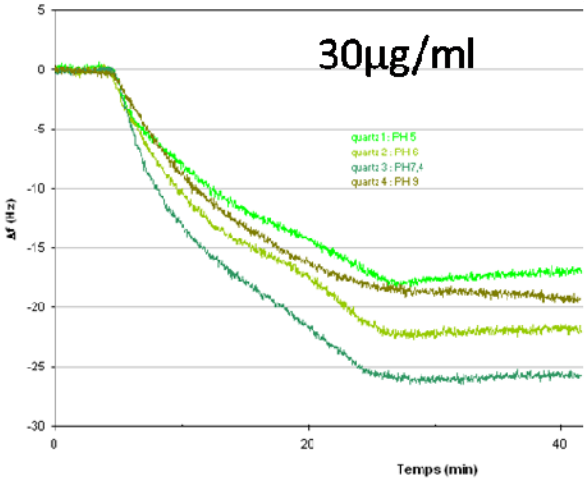


*-MotB/MotB*

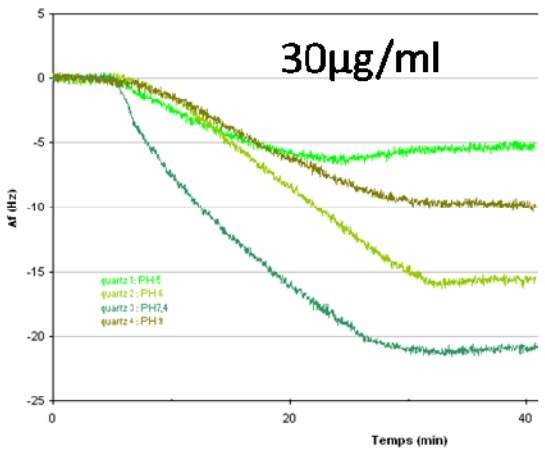


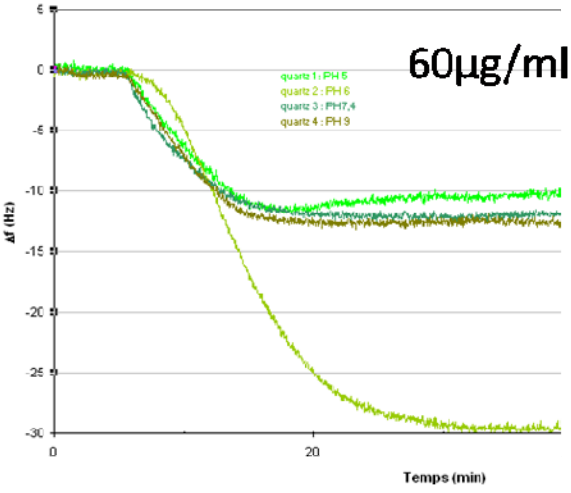

.Stator/ Rotor interactions

*-FliG/MotB*

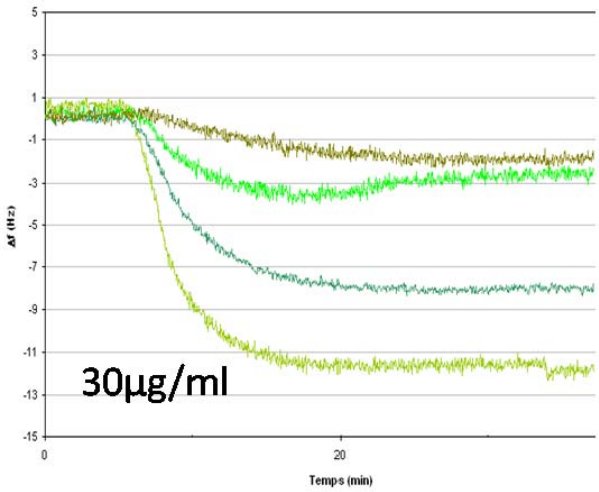


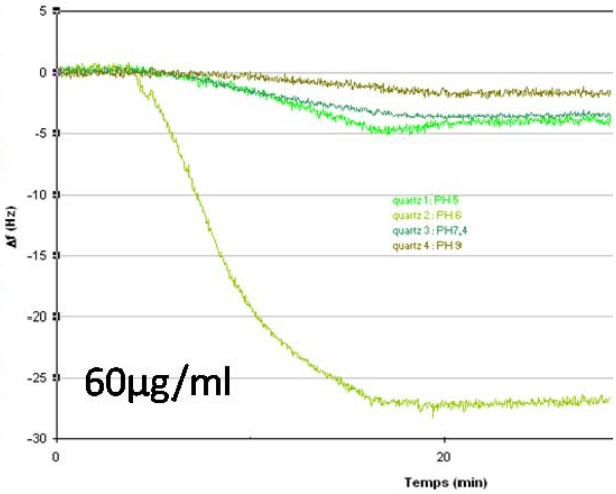


*-MotA/FliG*

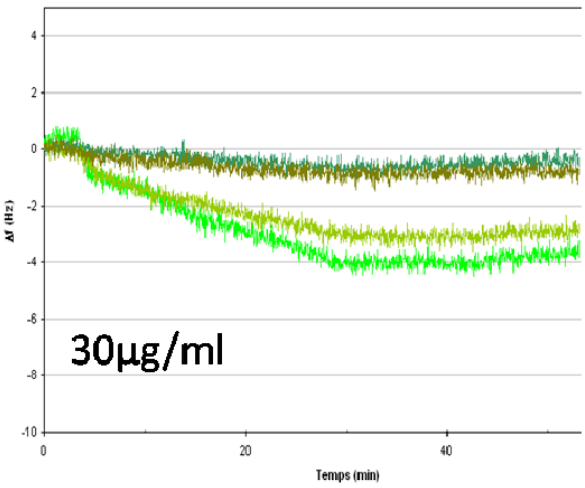


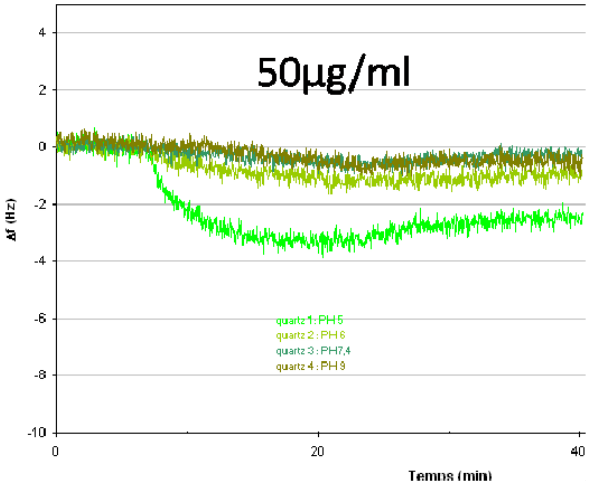


*-MotB/FliG*

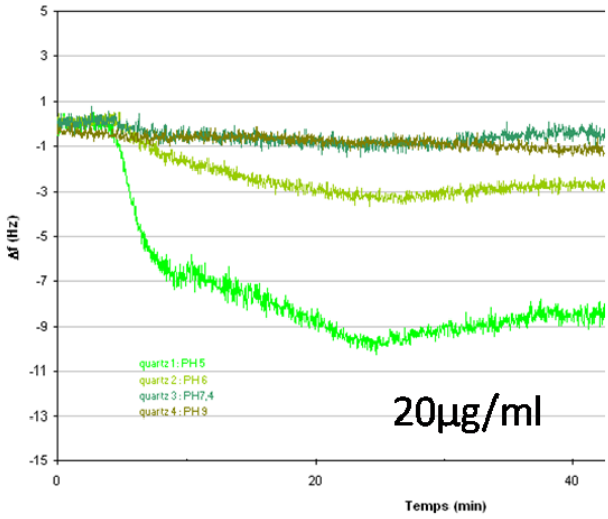


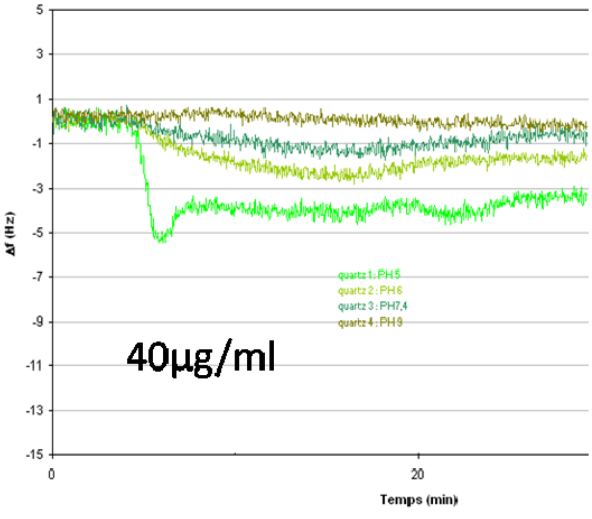

## .Rotor/ Rotor interactions

*-FliF/FliG*

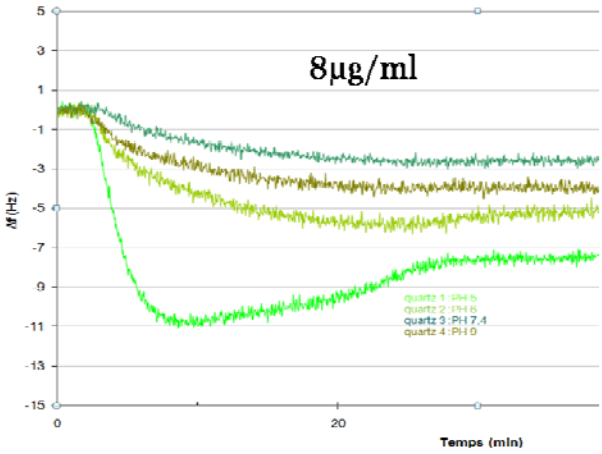


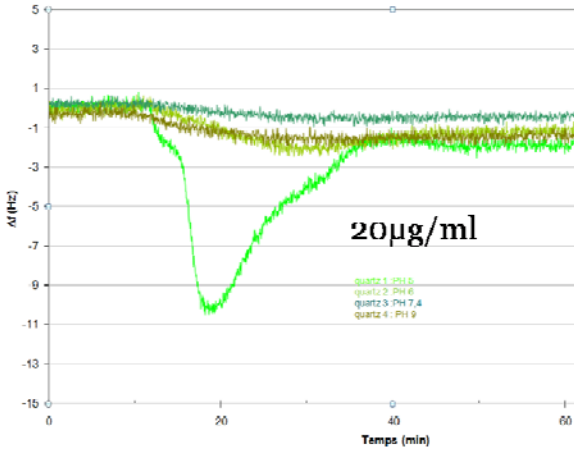


*-FliG/FliG*

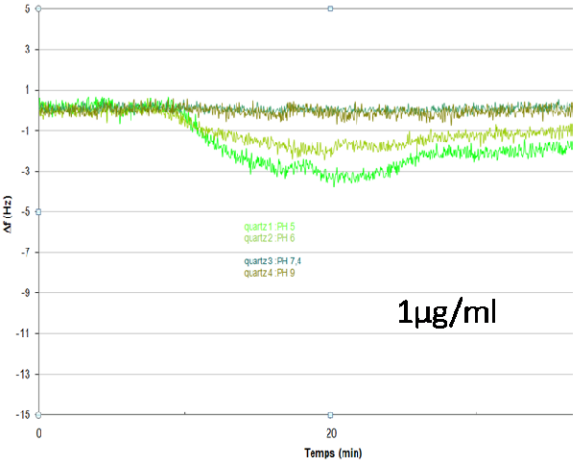


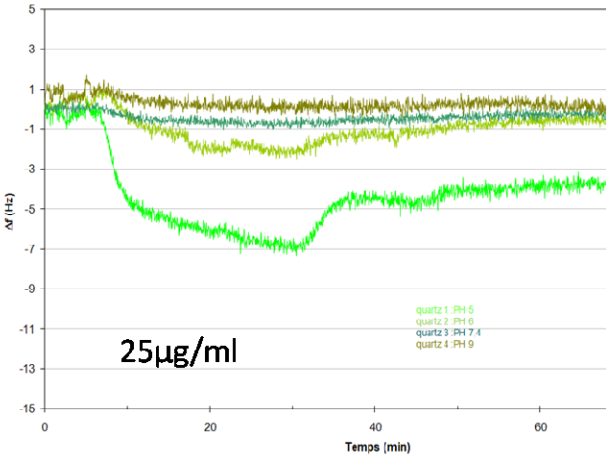


*-MotA/FliM in 4 different buffers*

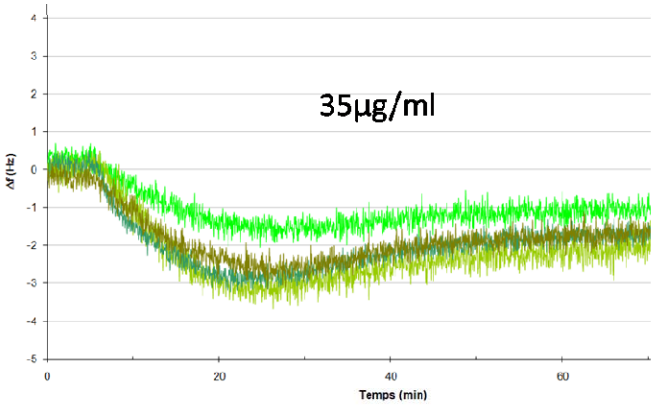


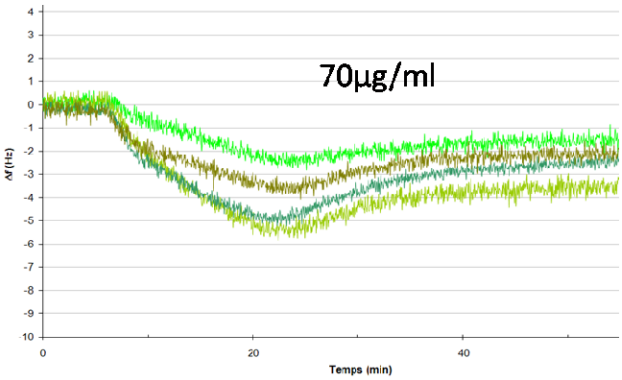


*Bright green: PBS; Green: Hepes 10mM,Nacl 150mM $CaCl_2$ 20mM; Blue Green: Tris 10 mM KCl 20 mM $MgCl_2$ 20 mM; Brown: Tris 200mM HCL. All pH buffer were adjusted to 7,4 prior experiments*

# .Negative controls

In order to validate the quality and the reproducibility of our protocol, I tested several parameters, by inversing steps, adjusting parameters and so on. I presented here several QCM traces which show the different experiments.

*-Graphic 1, passage of GST and BSA on the standard surface*

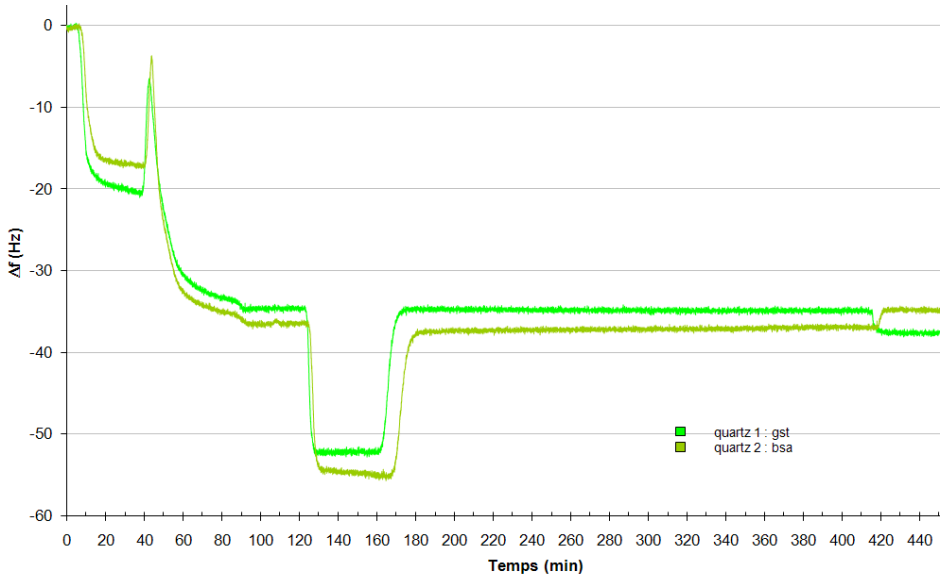


*-Graphic 2 testing parameters*

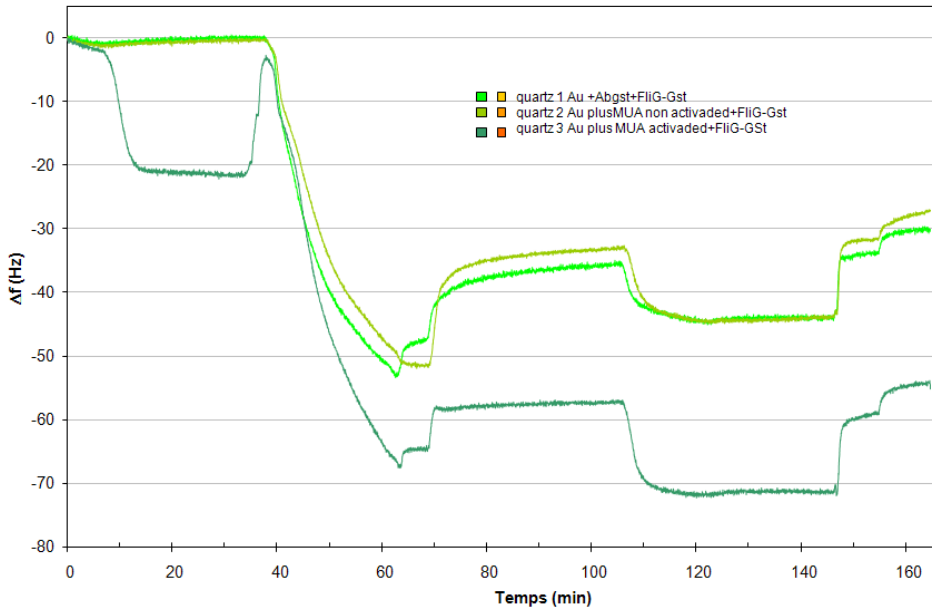


*Bright green: Au without activation+Abgst+FliG-Gst*

*Green: Au+MUA non activated+Abgst+FliG-Gst*

*BlueGreen:Au+MUA activated+FliG-Gst*

Adsorption of Ab-gst directly on gold was not stable over time. By successive washing Abgst were finally removed from the surface. Same result was found on non activated MUA. Only activated MUA layer was stable for Ab-Gst fixation.

*-Graphic 3 testing MUA activation*

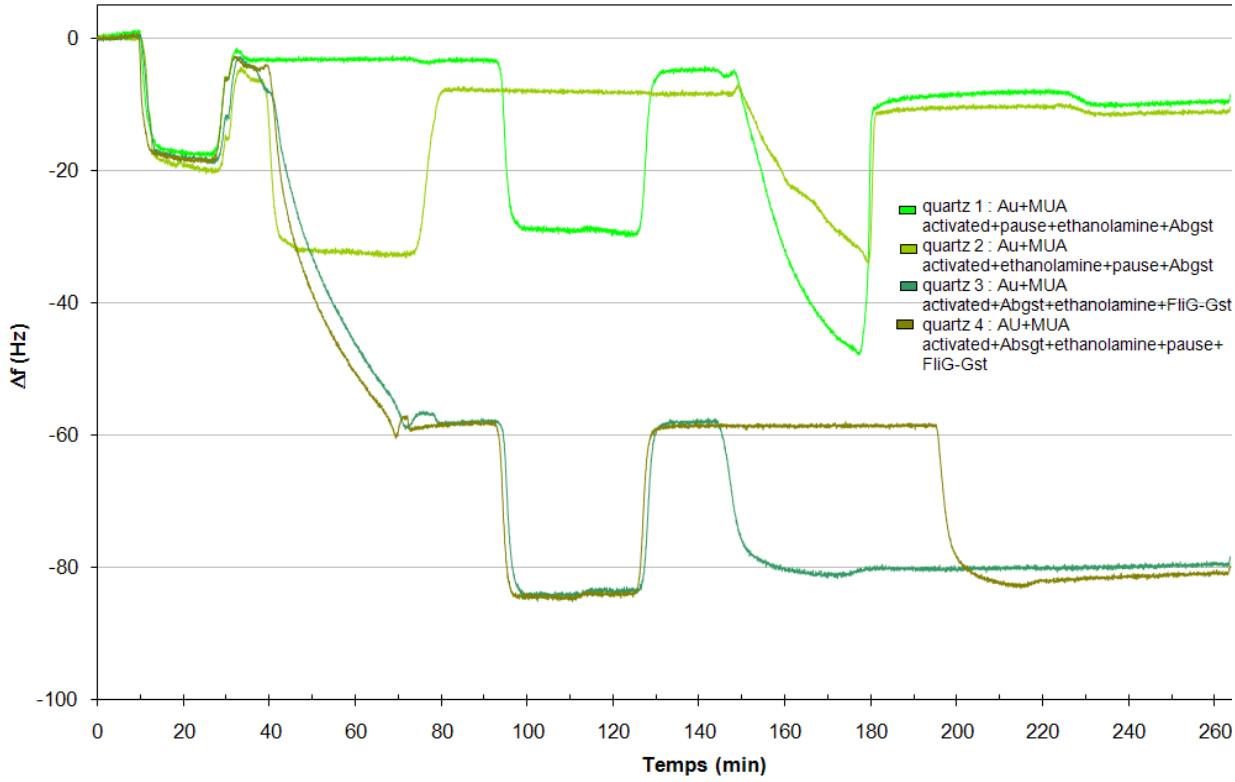


*Bright Green: Au+MUA activated+pause+ethanolamine+Abgst*

*Green: Au+MUA activated+ethanolamine+pause+Abgst*

*BlueGreen: Au+MUA activated+Abgst+ethanolamine+FliG-Gst*

*Brown: Au+MUA activated+Abgst+ethanolamine+pause+FliG-Gst*

The lifetime of the MUA activation was tested here. I activated MUA molecules on the 4 sensors and adjusted the time of injection of ethanolamine or Abgst in order to verify the activation of the MUA layer and also the quality of the anti-fouling layer of ethanolamine.

I tested the interactions between purified proteins and GSt fixed on the surface, and the observed interactions were all below 1Hz which I considered negligable. I injected also pure proteins directly on Ab-gst, and some fixations were observed but neglected compared to the fixation of the same proteins tagged Gst.

# .AFM images of the Gold sensor

In order to verify the quality of the sensor, I used AFM in PBS buffer of the Qsense Gold sensor before and after the cleaning procedure (piranha treatment). The results are clearly visible and open the question of the quality of the gold layer of the sensor sold by Qsense. Their design protocol of cleaning was even more destructive for the gold surface. More work will be needed to elaborate a reproducible surface. I tested the same interactions directly on the sensor, after 1 2 3 retreatment. Same tendency of results were found with slight change in the frequency shift, probably coming from the surface modifications. A deposition of gold using the LAAS facility will be tested in a near future in order to eliminate this problem and enhance the lifetime of the sensor, today limited to 4 experiments.

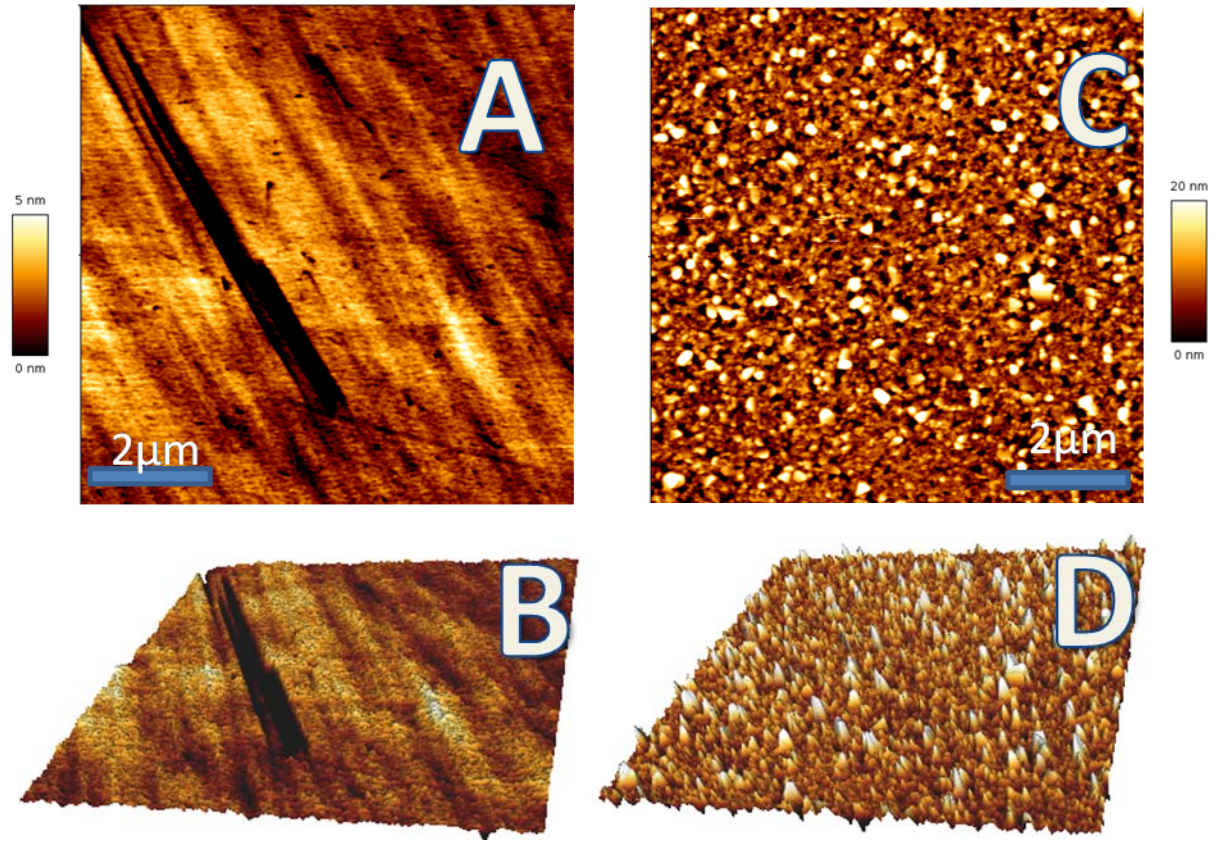


***AFM images of the gold sensor.*** *Contact mode in PBS buffer, MLCT cantilever stiffness 10mN/m; force up to 1mN. A/ Height signal of the sensor before experiments and cleaning procedure. B/ 3D software reconstruction of A. C/ Height signal of the sensor after cleaning. D/ 3D software reconstruction of C.*

# Annex 2 products

Here is the list of all chemical products, material used during this work with their references.

## .*Chemical products:*

-OTS http://www.sigmaaldrich.com/catalog/search/ProductDetail/ALDRICH/104817

-Ethanolamine hydrochloride

http://www.sigmaaldrich.com/catalog/search/ProductDetail/FLUKA/02415

-11 mercaptoundecanoic acid

http://www.sigmaaldrich.com/catalog/search/ProductDetail/ALDRICH/674427

-NHS http://www.sigmaaldrich.com/catalog/search/ProductDetail/ALDRICH/130672

-EDC http://www.sigmaaldrich.com/catalog/search/ProductDetail/FLUKA/39391

http://www.sigmaaldrich.com/catalog/search/ProductDetail/FLUKA/03450

-TRIS http://www.sigmaaldrich.com/catalog/search/ProductDetail/SIAL/252859

-MOPS http://www.sigmaaldrich.com/catalog/search/ProductDetail/FLUKA/69947

-hepes http://www.sigmaaldrich.com/catalog/search/ProductDetail/FLUKA/54457

-hellmanex http://www.sigmaaldrich.com/catalog/search/ProductDetail/FLUKA/61257

-SDS http://www.sigmaaldrich.com/catalog/search/ProductDetail/SIAL/436143

-KCL http://www.sigmaaldrich.com/catalog/search/ProductDetail/SIAL/P3911

-MgCl2 http://www.sigmaaldrich.com/catalog/search/ProductDetail/SIAL/M9272

-Cacl2 http://www.sigmaaldrich.com/catalog/search/ProductDetail/SIAL/383147

-NaCl http://www.sigmaaldrich.com/catalog/search/ProductDetail/SIAL/S9888

-sodium azide http://www.sigmaaldrich.com/catalog/search/ProductDetail/SIAL/S8032

-NaOH http://www.sigmaaldrich.com/catalog/search/ProductDetail/SIAL/221465

-PDMS sylgard 184 ref 999ES1841

*http://www.sf-composites.com/*

## .*Biological products:*

-Bovine Serum Albumine (BSA) A2289 from sigma Aldrich

http://www.sigmaaldrich.com/catalog/ProductDetail.do?N4=A2289|SIGMA&N5=SEARCH_CONCAT_PNO|BRAND_KEY&F=SPEC

-Pll-g-PEG

.Pll(20)-g[3.5]-PEG(2)FITC, PLL(20 KDa) grafted with PEG(2 KDa) having g (Lys units /PEG chains) = 3.5 with FITC attached to PLL backbone.

. PLL(20)-g[3.5]-PEG(2)/ TRITC (Red label) PLL(20 KDa) grafted with PEG(2 KDa) having g (Lys units /PEG chains)= 3.5 with TRITC attached to PLL backbone

http://www.susos.com/chemicals.php

-Antibody anti-GST

.039600-102-200 Anti GST FITC Goat pAb - (to Schistosoma japonicum)
.039600-100-200 Anti GST TRITC Anti-GST (Glutathione-STransferase) Rhodamine Conjugated Affinity Purified IgG Host: Goat

http://www.tebu-bio.com/

-phospholipids

.E. Coli PE ref 840027P
.E. Coli PG ref 841188P
.E. Coli Total extract ref 100500P
.E.Coli Polar extract ref 100600P
.EggPC ref 840051P

http://www.avantilipids.com/

## *.AFM:*

-Probes:

.MLCT from Veeco

.OTR4, OBL from Olympus

*https://www.veecoprobes.com/*

-Microscope:

.Nanowizard II from JPK

*http://www.jpk.com/nanowizard-ii-bioafm.350.html*

. BioScope SZ from veeco

*http://www.veeco.com/Products/metrology_and_instrumentation/AFM_SPM/BioScope_SZ/index.aspx?prodGroup=0*

.Multimode V

*http://www.veeco.com/Products/metrology_and_instrumentation/AFM_SPM/MultiMode_V/index.aspx?prodGroup=0*

. PicoSPM II de Molecular Imaging (Scientec, France)

## *.QCM-D:*

-System:

.Qsense E4 from Qsense

*http://q-sense.com/q_sense_e4--5.asp*

-sensors

.QX301 Gold

.QX303 $SiO_2$

*http://www.q-sense.com/sensor_crystals--27.asp*

## *.Fluorescence microscopy and imaging:*

-Inverted microscope Olympus IX70

.objectives:

UPlanFI x4/0.13

UPlanFI x20/0.40 pH

UPlanFL N x100/1.30 immersion

.fluorescence cubs

U-MWIN3

U-MWG2

UM41007

UM41008

*http://www.olympus.fr/microscopy/*

-EMCCD camera Lucas from Andor

*http://www.andor.com/scientific_cameras/luca/*

# Annex 3: technological process

Figure 1 resumes the basic principle of photo or electron-beam lithography. Two kinds of resist have been developed, positive and negative. I will describe the process for a positive resist but negative resist present the exact opposite behavior Briefly, a positive resist, in our case PMMA (polyméthacrylate de methyl) which is photo or electro sensible, was spread on a silicon 4 inch wafer using a spin coater at defined up to a defined thickness. This resist was then exposed on precise location, respecting a mask for photo-lithography or a specific path for electron beam lithography. The exposure cut bonds between the resist chemical chains, which diminish its molecular weight and increased its solubility into a buffer, here MIBK/IPA for MethylIsoButhyl Ketone/IsoPropanol Alcool(1:2). Due its lower weight, the exposured areas dissolved naturally into the solvent and are removed from the surface, this is the development step. Then surface was etched using a Reactive Ion etching system (fluorine based chemistry) for transferring the patterns into the silicon, the remained resist played the role of mask at the wafer's surface. After patterns transfer, were transferred to the silicon, the remained resist was finally removed using a chemical buffer, often the trichloroethylene which attacked the resist chains and dissolved them in solution.

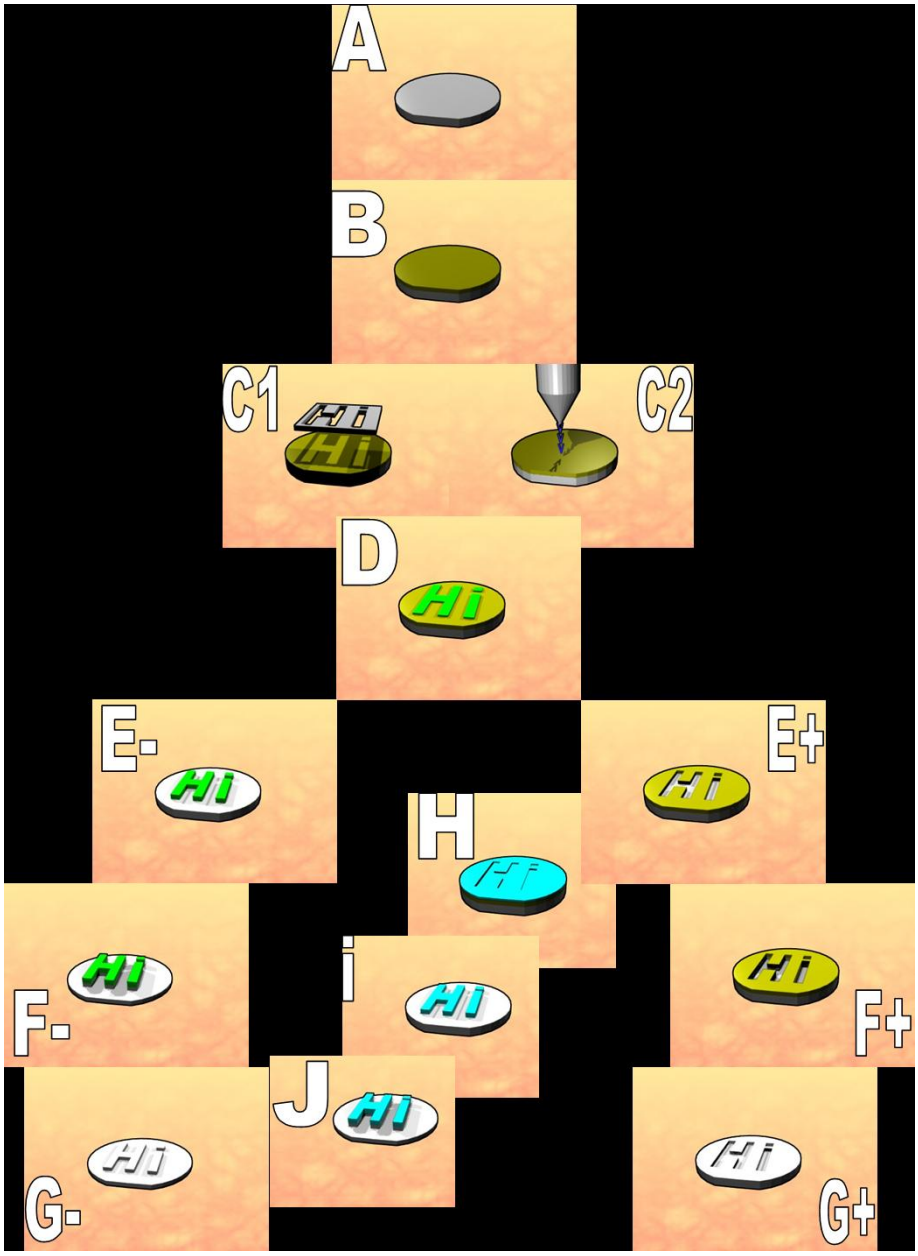


***Figure 1: lithography principle.*** *A/ a silicon wafer is prepared to receive a resist in step B/. C1 and C2/ Insolation of the resist through desired patterns, using a mask for photo-lithography in C1 (micrometric patterns) or through the displacement of an electron beam in C2 (nano patterns). D/ the resist are chemically changed by the photo or electron exposure. I will split here in two ways, for the positive resist ( X+) or the negative resist (X-).E+/The exposed resist are removed using a specific solvent. F+/ The sample was then etched using a RIE system for Reactive Ion Plasma for transferring the pattern into the silicon. G+/ And finally the remained resist is removed and the wafer treated with an anti-adhesive molecule, here the OTS we obtained by this way hole and depression in the wafer. E-/ The non-exposed resist is removed from the wafer. F-/ The sample was then etched using a RIE system for Reactive Ion Plasma for transferring the pattern into the silicon. G-/ And finally the remained resist is removed and the wafer treated with an anti-adhesive molecule, here the OTS we obtained by this way pillars and protuberance on the wafer. An alternative way for creating pillar using a positive resist is described, the lift off approach. Starting from E+, H/ a thin metal layer is deposited on the wafer. I/ resist are removed and let only on the wafer metal in the previous insolated place. J/ The sample were*

*then etched using a RIE system for Reactive Ion Plasma for transferring the pattern into the silicon and gave the same result as G-. The lift off process generates in J the negative patterns obtained in G.*

After silicium etching the Si wafer exhibits the desired. For the casting process, it is therefore necessary to coat the silicul wafer with an anti-adhesive film. We have selected a simple approach consisting in grafting layer of OTS ( octadecyltrichlorosilane) at the silicium surface. In order to achieve that, the surface is activated using plasma oxygen treatement and then immersed into an Octa-trichloro-silane solution (OTS) diluted 1% in trichoroethylen for 5 minutes under a nitrogen flow. The OTS molecules self-assembled on the surface on a homogenous layer which exhibited a hydrophobic head, see figure 2.

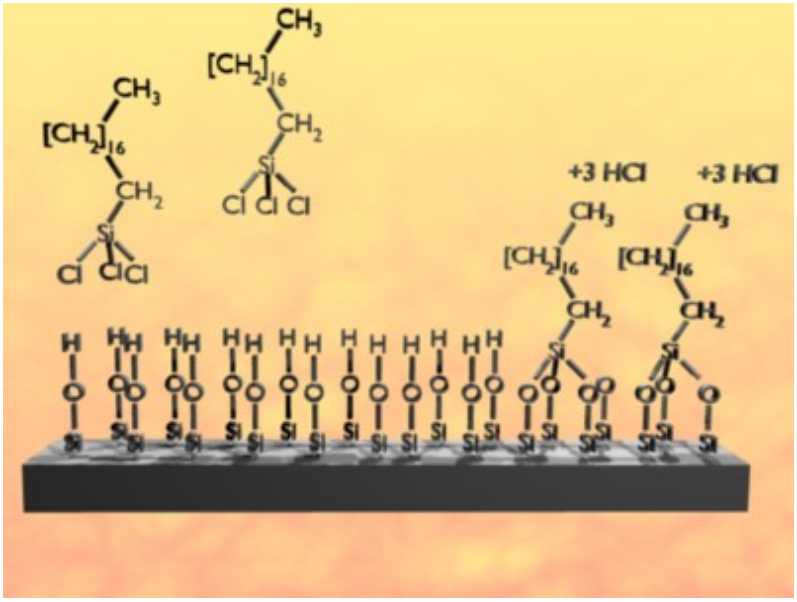


*Figure 2: Silanisation of the silicon master. OTS molecules are freely to move on an activated silicon surface, which exhibit numerous Si-O-H bonds. Formation of covalent bonds between the Si and the O presented on the surface are possible*